DOKUZ EYLÜL UNIVERSITY

GRADUATE SCHOOL OF NATURAL AND APPLIED SCIENCES

EFFECT OF CURING PROCESS OF ON DYNAMIC PROPERTIES OF COMPOSITE PRESSURE VESSEL

by

Şeyma İNCE

July, 2023

İZMİR

EFFECT OF CURING PROCESS OF ON DYNAMIC PROPERTIES OF COMPOSITE PRESSURE VESSEL

A Thesis Submitted to the

Graduate School of Natural, and Applied Sciences of Dokuz Eylül University

In Partial Fulfillment of the Requirements for the Degree of Master of Science in Mechanical Engineering

by

Şeyma İNCE

July, 2023

İZMİR

M.Sc THESIS EXAMINATION RESULT FORM

We have read the thesis entitled "**EFFECT OF CURING PROCESS OF ON DYNAMIC PROPERTIES OF COMPOSITE PRESSURE VESSEL**" completed by **ŞEYMA İNCE** under supervision of **PROF. DR. HASAN ÖZTÜRK** and **DR. OĞUZHAN DAŞ** and we certify that in our opinion it is fully adequate, in scope and in quality, as a thesis for the degree of Master of Science.

Prof. Dr. Hasan ÖZTÜRK	Assist. Prof. Dr. Oğuzhan DAŞ
Supervisor	Supervisor
Prof. Dr. Binnur GÖREN KIRAL	Assist. Prof. Dr. Aysun BALTACI
Jury Member	Jury Member

Assoc. Prof. Şahin YAVUZ

Jury Member

Prof. Dr. Okan FISTIKOĞLU

Director
Graduate School of Natural and Applied Sciences

ACKNOWLEDGEMENTS

My thesis advisor, who guided me with his wisdom, and encouraged me, and whose student I will always be proud to be, I would like to thank Prof. Dr. Hasan ÖZTÜRK.

I would like to thank the second thesis advisor, Assist. Prof. Dr. Oğuzhan Daş, for his valuable opinions, and contributions.

I am truly grateful to my manager Dr. Rahmi AKIN, and Mrs. Beril AKIN, who guided me in deciding on the thesis topic, and did not hesitate to share all their knowledge with me in my first work experience.

I also thank all my colleagues in IZOREEL COMPOSITE, including my manager Murat EROĞLU, who made the production of the samples, subject to the thesis take place.

Finally, I heartedly thank my parents Mrs. Ferruh İNCE, and Mr. Mehmet İNCE, and my brother Sinan İNCE. They always encouraged and inspired me during my education.

Şeyma İNCE

EFFECT OF CURING PROCESS OF ON DYNAMIC PROPERTIES OF COMPOSITE PRESSURE VESSEL

ABSTRACT

Fiber-reinforced polymer composite materials are frequently preferred in aerospace, aerospace and defense industries. Vibration analysis of structures exposed to dynamic loads under operating conditions is important. In this study, the effect of fiber-reinforced polymer composites on the dynamic properties of the structure as a result of production at different curing temperatures was investigated. The cylindrical structures that are the subject of the study were produced by filament winding technique using glass fiber and epoxy resin. There are different recommended temperature and time for the curing of the resin and fiber mixture that makes up fiber-reinforced polymer composites. For the curing temperature parameter, the manufacturer's recommended temperature and time are used as reference. Three different temperature curing processes were carried out, including the reference temperature and above and below this temperature. Filament angles, one of the production parameters of fiber-reinforced polymer composite materials, affect the engineering properties of the structure. In this study, the effect of different filament angles on the dynamic properties of the structure was investigated. Delamination structural defect was created in the production process of the samples and its effects is included in the research. Natural frequencies are determined by measuring the response of a given unit pulse. The natural frequency of the products cured at a higher temperature than the reference temperature determined by the manufacturer is lower than the samples cured at the reference temperature.

Keywords: Cylindric composite, curing, delamination, vibration analysis, damping ratio

KÜRLENME İŞLEMİNİN KOMPOZİT BASINÇLI TANKLARIN DİNAMİK ÖZELLİKLERİNE ETKİSİ

ÖZ

Fiber takviyeli polimer kompozit malzemeler havacılık, uzay ve savunma sanayinde sıklıkla tercih edilmektedir. Çalışma şartlarında dinamik yüklere maruz kalan yapıların titreşim analizi önem taşımaktadır. Bu çalışmada fiber takviyeli polimer kompozitlerin farklı kürlenme sıcaklıklarında üretilmesi sonucunda yapının dinamik özelliklerine etkisini incelenmiştir. Çalışmaya konu olan silindirik yapılar cam elyaf ve epoksi reçine kullanılarak filament sarma tekniği ile üretilmiştir. Fiber takviyeli polimer kompozitleri oluşturan reçine ve elyaf karışımının kürlenmesi için önerilen farklı sıcaklık ve zaman değerleri vardır. Kürlenme sıcaklığı parametresi için üreticinin tavsiye ettiği sıcaklık ve zaman değerleri referans olarak kullanılmıştır. Referans sıcaklık değeri ve bu değerin altında ve üstünde olmak üzere üç farklı sıcaklık kürlenme işlemi yapılmıştır. Fiber takviyeli polimer kompozit malzemelerin üretim parametrelerinden biri olan filament açıları, yapının mühendislik özelliklerini etkiler. Bu çalışmada, farklı filament açılarının yapının dinamik özelliklerine etkisi incelenmiştir. Numunelerin üretim sürecinde delaminasyon yapısal kusuru oluşturulup etkileri araştırmaya dahil edilmiştir. Doğal frekanslar, belirli bir birim darbenin yanıtı ölçülerek belirlenmiştir. Üretici firma tarafından belirlenen referans sıcaklıktan daha yüksek sıcaklıkta kürlenen ürünlerin doğal frekansının referans sıcaklıkta kürlenen numunelere göre daha düşük olduğu gözlemlenmiştir.

Anahtar kelimeler: Silindirik kompozitler, kürlenme, delaminasyon, titreşim analizi, sönüm oranı

CONTENTS

Page

LIST OF FIGURES

Page

LIST OF TABLES

Page

CHAPTER ONE

INTRODUCTION AND LITERATURE REVIEW

1.1 Introduction

The history of fiber-reinforced polymers (FRP) composites are relatively recent. The lightness and stiffness of fiber-reinforced polymer composite materials make them competitive with conventional materials. In terms of fuel, and energy consumption of structures, relatively light products consume less power. They provide ergonomics for handling.

The production of FRP composite materials in different geometric shapes has emerged in different areas of use. Plates, tubes, and pressure vessels are examples of different geometries. The cylindrical structures examined in this study and the pressure tanks analyzed are frequently used in the defense and space industries. Cylindrical FRP composites are used as launch tubes for missiles. FRP composite pressure vessels are often preferred because they can contain low weight and high pressure. Figure 1.1 shows composite overwrapped pressure vessel.

Figure 1.1 Composite overwrapped pressure vessel (McLaughlan, Forth & Grimes-Ledesma 2011)

The concept of natural frequency is significant for systems composed of parts working together. When a structure operates at its natural frequency, it may face the phenomenon called resonance where damage may occur due the excessive oscillations. As a design criterion, it is expected that this phenomenon should not occur during the operation of structure. In the defense, and space industry, the products are qualified by putting the systems to the test regarding the worst-case conditions that they may face. The resonance phenomenon can be observed in these tests.

The production of composite materials is far from being standardized. The components added to the composite are not isotropic. Some of their features are more convenient in direction, and they should be oriented according to the direction in which the load should be transported. The products produced in this study were made by means of semi-automated machines to eliminate the human factor in production which brings along some production defects. In the filament winding method, the part where the human is involved is the resin stripping process. Performing this process homogeneously causes air gap formation defect in the sample in micro dimension, and dimensional irregularities, and mass differences in macro dimension. These differences cause the results obtained from the study to be different than those obtained by the 3D finite element analysis.

1.2 Importance of Study

FRP composite production is an emerging production method and it is important to optimize production parameters. In this study, it is aimed to determine the effects of choosing the temperature parameter used in the curing process below or above the reference temperatures. Thus, the selection of the curing temperature according to the dynamic property desired to be obtained can be interpreted according to the results of the tests.

In addition to the main parameters, the effect of the filament degree used in the production method and the delamination concept, which is a production defect, on

the dynamic properties of FRP composite structures were investigated under different curing temperatures.

1.3 Literature Review

In order to produce filament-added resin composites, delamination, curing temperature, and filament laying angles were the key research areas in this thesis. Separate analyses of the impact of manufacturing parameters on the mechanical and dynamic characteristics of the structure were carried out, along with a literature review on the topic.

1.3.1 Effects of Winding Angles on Mechanical Properties

Three different winding angles were used to test samples made by the filament winding technique employing epoxy glue and E-glass filament fiber. To investigate how the winding angle affects the sample's strength in three different loading scenarios, experimental data were collected. Biaxial compression (mode III), hoop pressure loading (mode I), biaxial compression loading (mode II), and axial compression loading were all used to test the samples. Three alternative winding angles were tested for stress/strain under various loading scenarios.

According to the test results, winding angle has an impact on elastic constants and nonlinear stress-strain behavior. The outcomes demonstrated a direct relationship between loading modes and the ideal winding angle for filament winding samples. Those optimum winding angles were found to be 55° for loading mode I, 75° for loading mode II, and 85° for loading mode III (Hamed et al.,2007).

The optimum winding angle, and stress/strain response for filament-winded samples depend on the loading conditions as well. Besides, winding angles, and layer arrangements directly impact the stress-strain curve (Rosenow,1984). In this study, it has been determined that the most suitable angle for biaxial compression loading is 55°, and a 75° winding angle is for pressure loading.

1.3.2 Effects of Winding Angles on Dynamic Properties

In a composite structure, the natural frequency is mostly determined by the stiffness of the structure. Fiber orientation during manufacture affects this natural frequency by influencing the stiffness of the composite material in different directions. When the fibers align with the direction of the applied load, the composite material has a higher stiffness in that direction than in other directions. On the other hand, when the fibers are misaligned or randomly oriented, the stiffness of the composite in that direction is reduced. This difference in stiffness is a factor that results from fiber orientation and affects the natural frequency of the composite structure (Reddy,2003).

The damping ratio in a composite structure is an important parameter that determines how quickly vibration energy is dissipated from the system. Fiber orientation in the structure is effective on the internal friction and energy distribution of the composite material. When the fibers are aligned correctly, they can transfer energy effectively and dissipate vibrations, resulting in higher damping rates. However, the energy dissipation ability decreases, and the damping ratio decreases when the fibers are dispersedly aligned or randomly oriented (Barbero, 2017).

For laminated pipes has been observed that the optimal fundamental frequency is highest for the two fixed-end pipes. The effect of changing the ratios of L/r, where L is the length of the sample, and r is the diameters of the sample, is less than the effect of changing the boundary conditions, either fixed or free (Hu & Tsai,1999).

1.3.3 Effects of Delamination on Mechanical Properties

In the composite production, the resin-infused fiber layers contain cavities that affect the mechanical properties of the part. The ratio of saturation also depends on the amount of resin flow in the laminate during the manufacturing process and the manufacturing method used (Carlone & Palazzo, 2015).

Composites cured by the conventional method at 70°C for 80 minutes have higher tensile and bending moduli than those cured by the microwave heated curing method (Chaowasakoo & Sombatsompop, 2007). If composite pipes made of carbon fiber reinforced polymer (CFRP), and glass fiber reinforced polymer (GFRP) materials are exposed to high temperatures, their strength decreases and increases as this temperature increases (Al-Salloum, Elsanadedy & Abadel, 2011).

GFRP materials are more vulnerable under high-temperature shear and compression than they usually are under stress. When they are operating under 200°C, the strength of the material reduces to 54% of its original strength that it had at ambient temperature. When this comparison is made for shear and compression strengths, it provides an 11% decrease in shear strength and a 5% decrease in compressive strength when exposed to curing at high temperatures compared to curing at ambient temperature (Bazli & Abolfazli, 2020). The increase in temperature and curing time create brittleness in the material. The optimum temperature and time must be determined depending on the resin type to ensure maximum tensile strength (Czaderski et al., 2012). The damage mode in the fiber may change from fiber pullout to fiber breakage with the increase in temperature. A cure cycle can be chosen according to the type of resin to reach maximum tensile strength (Badawy, 2021). As the fiber/resin ratio increases, the strength of the composites approaches the characteristic properties of the fiber, and since the increase in temperature will increase this ratio, an increase in the flexural strength and modulus of the composites is observed after exposure to temperature (Furtos et al., 2012).

The decrease in hardness and strength in the laminates that make up the composite is due to the lack of load sharing between the fibers as the resin softens at a temperature near the glass transition temperature (Chowdhury et al., 2011).

In structures made of all FRP materials, cavities facilitate moisture absorption, oxidize the fibers, and disrupt the fiber matrix interfaces, which reduces the strength of the structure (Costa, 2006).

1.3.4 Effects of Delamination on Dynamic Properties

In the tests made for the composite beam, the natural frequency of the structure decreased as the delamination thickness of the specimen and length of specimen ratio of the beam increased. Since the increase in the delamination rate will decrease the stiffness of the beam, it is inevitable that the natural frequency will decrease. The results showed that the delamination at the edge of the structure reduced the natural frequency more than the delamination occurring at the interior. In addition, it has been observed that the natural frequency changes with the change in the laying angles of the lamination layers. The highest natural frequency is observed in the [0/90] layered beam, where the fibers are parallel to the beam axis (Campanelli & Engblom, 1995).

Gadelrab et al. (1996) observed that for composite beams, delamination reduces the natural frequency of the structure, and the percent deviation of delamination occurring near the fixation point increases compared to the non-delamination.

1.3.5 Effects of Curing on Mechanical Properties

The saturation and unsaturation of the fiber layers with the resin in their cavities in the composite production affects the mechanical properties of the part. The ratio of saturation also depends on the amount of resin flow in the laminate during the manufacturing process and the manufacturing method used (Carlone & Palazzo, 2015).

Composites cured by conventional method at 70°C for 80 minutes have higher tensile and bending modulus than microwave heated curing method (Chaowasakoo & Sombatsompop, 2007). If composite pipes made of carbon fiber reinforced polymer (CFRP) and glass fiber reinforced polymer (GFRP) materials are exposed to high temperatures, their strength decreases and increases as this temperature increases (Al-Salloum et al.,2011). GFRP materials are more vulnerable under high temperature shear and compression than they are under stress. When they are under

200°C, the strength of the material is 54% of the strength it has at ambient temperature. When this comparison is made for shear and compressive strengths, it decreases by 11% for shear strength and 5% for compression strength compared to ambient temperature in case of exposure to high temperatures (Bazli & Abolfazli, 2020). The increase in temperature and time creates brittleness in the material. The optimum temperature time cycle must be determined depending on the resin type to ensure maximum tensile strength Czaderski et al.,2012). The damage mode in the fiber can change from fiber pull out to fiber breakage with temperature increase. Cure cycle can be chosen according to the type of the resin to reach maximum tensile strength (Badawy,2012). As the fiber resin ratio increases, the strength of the composites approaches the characteristic properties of the fiber, since the increase in temperature will increase this ratio, an increase in the flexural strength and modulus of the composites is observed after exposure to temperature (Furtos et al., 2012).

The decrease in hardness and strength in the laminates that make up the composite is due to the lack of load sharing between the fibers as the resin softens at a temperature near the glass transition temperature (Chowdhury et al.,2011). In structures made of all FRP materials, cavities facilitate moisture absorption, oxidize the fibers, and disrupt the fiber matrix interfaces, which reduces the strength of the structure (Costa et al, 2006).

1.3.6 Effects of Curing on Dynamic Properties

The curing temperature of a composite material can have a significant impact on its dynamic characteristics, including its natural frequency and damping ratio. This is because curing temperature affects the molecular structure of the polymer matrix and the fiber-matrix interface, which can influence the stiffness and damping properties of the composite material.

Generally, an increase in curing temperature results in a higher degree of crosslinking and a more tightly packed polymer network, which can lead to increased stiffness and a higher natural frequency. This effect is due to the increased strength

of the chemical bonds formed between the polymer chains and the reduction of free volume within the material (Koushyar et al., 2012).

It is crucial to keep in mind, though, that high curing temperatures can also result in thermal deterioration of the matrix and fibers, which can lessen the stiffness and strength of the composite material. High curing temperatures can also cause a material's residual stresses to increase, which can change a composite's ability to dampen vibrations (Russo et al., 2016).

The impact of the temperature of cure can be complexities in regard to the damping ratio. A higher curing temperature can result in a lower damping ratio while the material becomes more rigid. However, other factors, including as the type of matrix and fiber material utilized, as well as the curing procedure used, may also have an impact on the effect of curing temperature on damping ratio (Singh et al., 2018).

Overall, the impact of curing temperature on the dynamic properties of composite materials, such as natural frequency and damping ratio, is a complex topic that may depend on numerous aspects. While higher curing temperatures can lead to increased stiffness and natural frequency, they can also cause thermal degradation and residual stresses, which can affect the damping properties of the material.

1.4 Layout of Thesis

In Chapter 1, presents a comprehensive survey of the topic. It contains the study results that contribute to the determination of the parameters to be selected to produce the samples to be used in the tests. It provides a basis for the comments to be made in the following sections.

In Chapter 2, the products and methods used in the production of composite materials are explained. The production method used in this thesis is discussed.

In Chapter 3, calculation methods of basic engineering properties used for composite materials are explained for macro and micro dimensions.

In Chapter 4, methods for calculating the vibration responses of materials are explained. The Logarithmic Decrement method, which is used to determine damping ratio, is also explained in this section.

In Chapter 5, the production of the samples and the tests performed are shown. The results of the tests are included in this section. The determination of natural frequencies and damping ratios of samples using free vibration analysis is also included in this section.

In Chapter 6, test results for pressurized and non-pressurized boundary conditions using ANSYS program for composite pressure vessels are examined.

In Chapter 7, the outputs of all tests and calculations for this thesis are comprehensively commented. The results obtained from these analyzes are presented in detail and the conclusions of the findings in the context of the research problem are made. The extensive comments made in this section contribute to the overall understanding of the thesis by providing information on the importance and relevance of the results.

In addition, Chapter 7 includes suggestions for future research similar to this research. These recommendations are designed to guide future researchers who may be interested in exploring the topic further. This section offers suggestions on how to extend the existing work, highlighting possible avenues for further research.

CHAPTER TWO
COMPOSITE MATERIALS

2.1 Introduction

Composites are defined as the combination of multiple materials to achieve superior material properties. They are composed of two main parts called the matrix and reinforcement. The matrix transfers the force acting on the structure to the reinforcements to carry the load.

The reinforcement mentioned in this thesis is fiberglass. Glass fibers form rovings, which are frequently used as engineering materials. Regarding the fiber form, the diameter is always smaller than the length. Aspect ratio, which has a wide variety, is the ratio of the fiber length to the diameter of the fiber. Continuous fibers have longer aspect ratios compared to discontinuous fibers.

Continuous fibers are stacked with different angle orientations, and desired strength properties are achieved when the fiber volume ratio is kept between 60, and 70 percent.

The matrix, on the other hand, not only transmits the load to the fibers but also keeps the fibers in the determined angle orientation and keeps them away from environmental effects.

In this thesis, polymer matrix composites were discussed. Two types of polymer matrices are commonly used. Thermoset resins are low-viscosity resins that react during use. Another type of resin is thermoplastic resin. These resins have a high viscosity and can be used by bringing them to the melting temperature. Since thermoplastic resins harden during composite production, they cannot be reheated and used.

2.2 Fiber Reinforced Polymer (FRP) Materials

FRP materials consist of a macro-level combination of resin, and fibers. Here, the fibers carry the load, while the resin provides load transmission and the integrity of the structure.

2.2.1 Fibers

Fiber materials for composites are synthetic fibers. Products belonging to this category include aramid, glass fiber, carbon fiber, nylon, etc., as examples.

Aramid fibers are especially preferred in the production of products that require high temperature resistance, and bulletproof properties. Carbon fibers are quite frequently used in the fields of defense and space because they are stronger than steel, and relatively lighter. It is difficult to process due to its high electrical conductivity. Glass fibers, meanwhile, are utilized in a wide range of applications in industry due to their superior insulation qualities. The mentioned fiber types show superior engineering properties with the appropriate resin system and laying angle orientation. There are varied sizes, and shapes of fibers according to their production methods. The smallest unit of fiber is the filament. The filaments combine to form fibers. Wicks, and twists are available. Roving has higher strength than twists. The classification of glass fiber is shown in Figure 2.1.

Woven fabrics are two-dimensional assemblies formed by the weaving of fibers. In woven fabrics, the fibers are held together by mechanical interlocking. They are sewn with cotton-like fibers to form a woven fabric by angling the fibers (Maxineasa & Taranu, 2018).

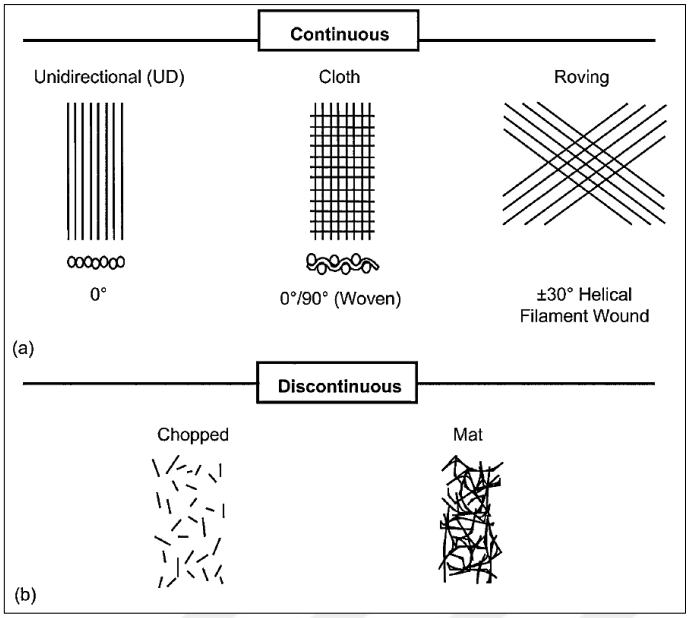

Figure 2.1 a) Continuous fiber b) Discontinuous fiber (Campbell, 2010)

2.2.2 Resin

Resins are viscous polymers that harden by curing. Resins are divided into two categories: organic and synthetic resins. Synthetic resins are frequently used in industry. There are different types of resins according to their chemical properties.

Polyester resins are not employed for high-performance structures because, compared to other resins, they have a poor capacity for moisture absorption. In terms of mechanical performance and price, vinyl esters often lie between polyesters and epoxies. While these resins are used in production, they are more tolerant than epoxy resins to changes in catalyst/resin mixture ratios. They are also chosen more than polyester because of their enhanced resilience to harsh chemicals and environmental deterioration. Vinyl esters are preferred when it is necessary to avoid chemical and moisture effects. Vinyl esters are treated and cured like polyesters. The high temperature curing brings the high toughness resistance.

Epoxies are available in liquid, solid, and semi-solid forms, and they usually react and harden when used with amines or anhydrides. Unlike polyester resins, epoxies are not cured by means of a catalyst; instead, a hardener (another name for a curing

agent) is used for curing. Among the resin types, epoxy resins have the highest performance. Due to their superior mechanical qualities and excellent resilience to environmental conditions, epoxy resins have been chosen in proficient technical applications. Epoxy resins exhibit better mechanical properties compared to vinyl ester or polyester, so they are used in applications requiring high mechanical properties. It has a low tolerance for deviations from the hardener/resin mix ratios and is therefore more difficult to process than other resins. Despite this epoxy resins are commonly utilized this due to the show superior environmental resilience (Fiore & Valenza, 2013).

Epoxies are suitable for working at room temperature. High-temperature, high-performing types are also available. These resins have particularly good chemical and corrosion resistance (Park & Seo, 2011).

2.3 Manufacturing of Composite Materials

The manufacturing process provides a means of combining the resin matrix and reinforcing fiber mat into the desired shape of the target part, ensuring minimum voids, and maximum resin fiber wetting. Therefore, the goal of any hybrid machining method is to achieve maximum wetting while meeting the performance requirements of the part at the desired production rate. Resin impregnation is influenced by the process parameters of the manufacturing process used, such as the pressure used, and curing temperature. Regardless of the manufacturing technique chosen, factors such as raw material properties, including reinforcement permeability, fiber volume fraction, resin cure kinetics, viscosity, and product size, and complexity, will affect finished part results. Classification of composite processing techniques is shown in Figure 2.2.

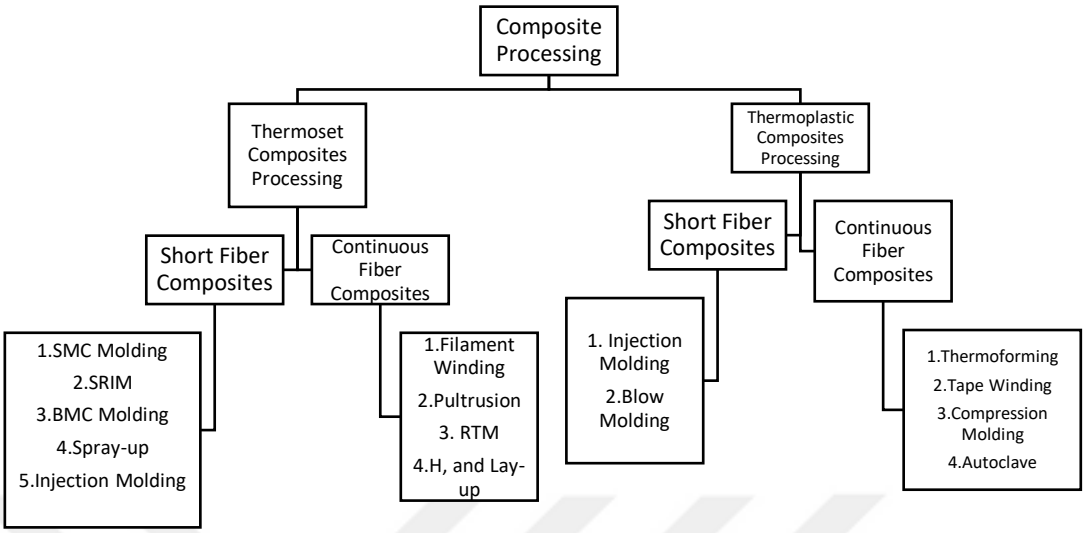

Figure 2.2 Classification of composite processing techniques

2.3.1 Hand Lay-up

Composite material production with the hand lay-up method is the easiest, and least expensive. There is no dimensional restriction for the parts to be produced. A suitable mold is produced according to the surface geometry of the product to be produced. The hand lay-up technique is shown in Figure 2.3.

In general, polyester resins with a short curing time and low curing temperatures are used in hand layup. Mold release chemicals are used to prevent the polyester from sticking to the surface. These chemicals also protect the mold's surface. When the surface of the product is to be glossy or when the final version is to be used as it comes out of the mold, gelcoat is applied to the mold surface. The fiber used can be woven fabric or shredded fabric. It is also seen that core materials are used in some applications. Before starting the polyester resin process, it is mixed with its hardener at the appropriate rate in a separate container. The fiber is laid on the surface. It is applied to the resin fiber with the help of rollers, and brushes. Resin is impregnated with the help of brush strokes. Inhomogeneous structures that may be formed by air

spaces are eliminated. After the determined fiber fabric orientation is placed in the mold in sequence, it is left to cure. The increase in the viscosity of the resin mixture prepared in this process is a factor limiting the processing time. Before the resin hardens, the fibers should be laid, and the structure should take its final form. In this production method, there is 40% fiber and 60% resin in the structure. Manufactured parts are not expected to carry dynamic loads.

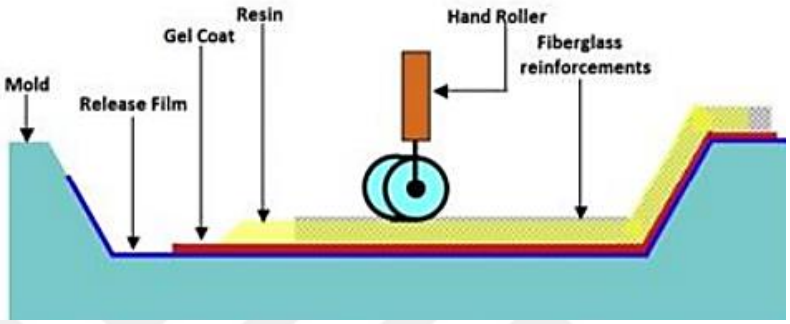

Figure 2.3 Hand lay-up (Abdurohman et al, 2018)

2.3.2 Spray-Up

The spraying method is very similar to hand laying. Application is made with molds. The laminate formed by a chopped fiber can be easily shaped thanks to the spraying method. It takes less time to produce a product with the same geometry by the spraying method than by the hand-laying method. This method is more dependent on the operator, as the thickness must be constantly controlled during production. It allows on-site production as portable equipment is used. Equipment costs are low. There is no geometric dimension that limits production. For production, glass fiber is a reinforcing agent, and polyester is primarily a matrix.

The application begins with the application of mold release agents, followed by the application of gelcoat. Combines continuous fiber, roving, and a resin application gun. After the mixture coming out of the gun falls on the mold, it is passed over with roller brushes to saturate the fiber parts with the resin. At the end of the process, it is cured at atmospheric temperature. Spray-up technique is shown in Figure 2.4.

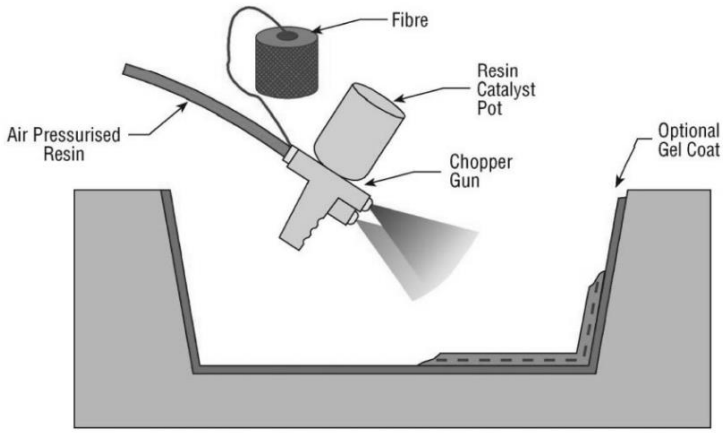

Figure 2.4 Spray-up technique (Cripps, 1999)

2.3.3 Bag Molding

In this method, the excess resin in the structure is removed with the vacuum applied to the vacuum bag laid on the laminate. An excess of resin is generally undesirable, as the increase in the fiber-to-resin ratio improves the mechanical properties of the structure. The pressure to the bag takes the air in the uncured structure. Molds are also used in vacuum bagging method. Mold release and gelcoat application are available.

2.3.4 Vacuum Bagging

The vacuum bagging process can be used to produce a wide variety of composite parts in different sizes. The vacuum bagging process helps to ensure that the resin and reinforcement materials are properly distributed and saturated during the curing process, leading to a strong and uniform final product. The process involves placing the matrix and reinforcement materials in a mold and covering them with an impermeable film (vacuum bag), which is then sealed to the edges of the part. By drawing out the air between the vacuum bag and the mold using a vacuum pump, the resin can cure more quickly and efficiently. Once the curing is complete, the equipment can be removed, leaving behind a well-formed composite structure.

The advantages of this method are that it can be used in the production of exceptionally large parts and allows for homogeneous curing of the part due to the equal distribution of atmospheric pressure in all directions. Since the applied pressure is lower than other methods, the fiber-to-resin ratio is low. This reduces the strength of the part. Since the vacuum bag, ventilation fabric, and peeling layer fabric cannot be recycled and reused after production, waste material production is high. Since one side of the part contacts the mold and the other side contacts the bag, the face that contacts the mold will have a good surface quality. Vacuum bagging technique is shown in Figure 2.5.

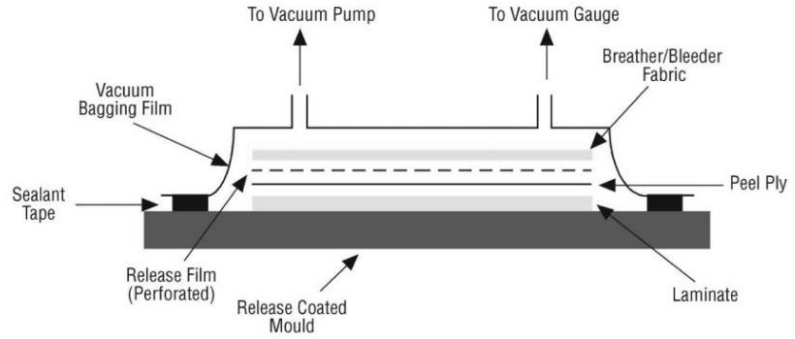

Figure 2.5 Vacuum bagging technique (Cripps, 1999)

2.3.5 Prepreg Resin Transfer Molding (RTM)

A technique called resin transfer molding (RTM) was created to address the issue of unmanageable extra resin in hand lay-up. Unlike hand layup, RTM molds are closed molds with male and female molds. Manual corrections are made to the RTM fiber laid on the female mold to take the shape of the mold. The male mold is closed on the female mold. Resin injection and vacuum support are provided through the ports on the mold. The resin spreads in the mold until it leaves no dry surface. When the resin starts to flow into the resin collection chamber, the resin inlet channels are closed, and the vacuum channels are opened. Excess resin is deposited in the resin collection chamber by a vacuum. The mold is opened and the component is taken out once it has had time to cure. The resin transfer molding technique is shown in Figure 2.6.

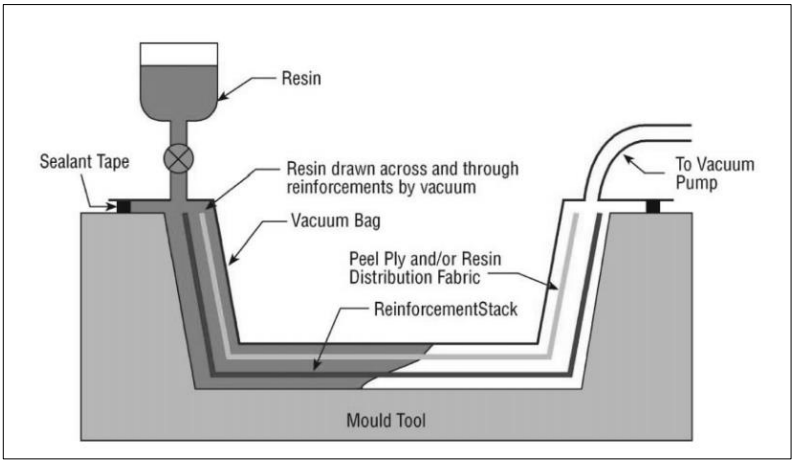

Figure 2.6 Resin transfer molding (RTM) method (Cripps, 1999)

2.3.6 Pultrusion

The pultrusion method is a method used to produce composites with a certain cross-section. Fibers impregnated with resin are extruded to form the determined cross-sectional area, then cured. The pultrusion technique is shown in Figure 2.7.

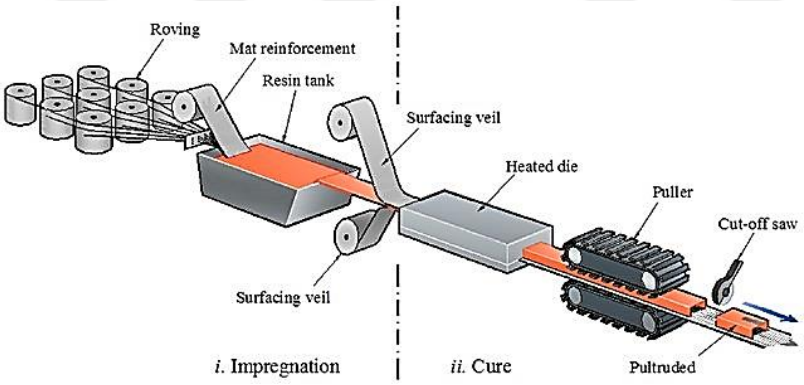

Figure 2.7 Pultrusion method (Landesmann et al.,2015)

2.3.7 Compression Molding

In the compression molding technique, the molds are pressurized. The fiber-reinforced resin laid in the mold is pressurized and heated. In this way, curing takes place. After the curing process is finished, the molds are opened. In the compression molding method, high-volume products are produced. Since the fiber-to-resin ratio is

high, it allows for the production of high-strength products. It is not suitable for its complex structure.

2.3.8 Autoclave Processing

In the production of composite materials, the ventilation of the material is the biggest factor that reduces the strength of the structure. The autoclave method takes its name from the curing method. Vacuum bags are placed on the resin-impregnated fibers deposited in the mold. Until this part, the same processes are conducted with the vacuum bagging method. The prepared system is taken to autoclave ovens. It is connected to the autoclave through the vacuum ports. With this piping system, the pressure of the structure during curing is adjusted. The distinctive feature of the method is that the pressure and temperature during curing can be adjusted. This method allows the production of high-strength structures. The autoclave processing technique is shown in Figure 2.8.

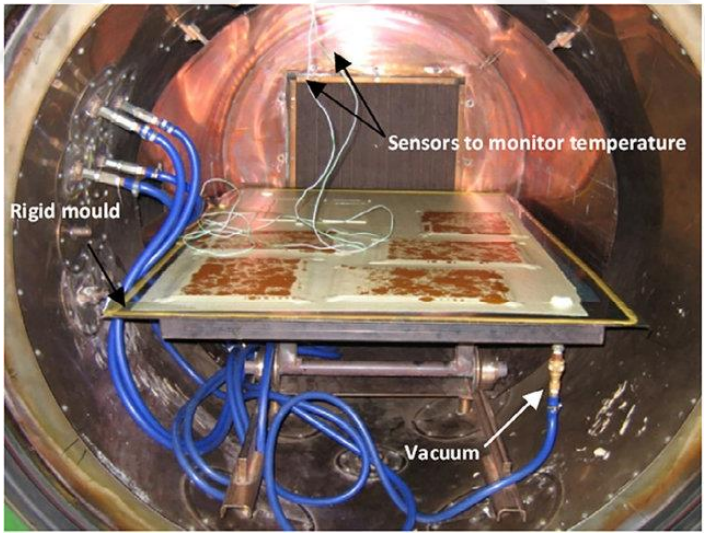

Figure 2.8 Autoclave processing (Nguyen-Dinh et al.,2019)

2.3.9 Filament Winding Technology

A manufacturing technique known as filament winding is used to create continuous fiber-reinforced resins spread out in specific directions. The structures

produced by this method are axisymmetric shells that stand as fibers wound at + θ, and –θ angles with respect to the symmetry axis. The production technique has excellent engineering qualities, including excellent strength, low weight, and resistance to corrosion thanks to its high fiber-resin ratio. Winding angle, which is also a production parameter, significantly changes the mechanical performance (Soden et al., 1993).

The process of filament winding involves passing a continuous roving through a resin impregnation bath and winding it onto a revolving mandrel. The wick can be wound spirally or polarly (in a circle). When the fibers are coiled in polar winding, they do not cross. Up until the desired thickness is obtained, successive layers are laid down at fixed or variable angles. The mandrel is removed after the thermoset resin has finished curing, which takes place at a high temperature. Epoxy, polyester, and vinyl ester resins are frequently combined with glass, carbon, and aramid fibers to create filament wound shapes. Wet winding and pre-impregnated winding are the two types of filament winding. Roving transitions and areas between layers with various fiber orientations are where gaps in filament winding are most likely to occur (Boon et al., 2021). The filament winding technique is shown in Figure 2.9.

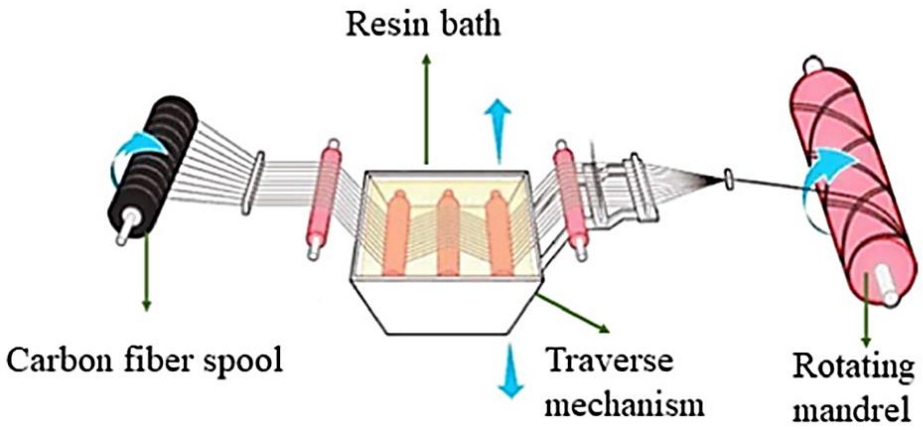

Figure 2.9 Filament winding technique (Quanjin et al.,2018)

2.4 Winding Patterns

There are three types of winding patterns that can be created by the filament winding method. The windings formed according to the α winding angle with the longitudinal axis as in Figure 2.10, are called helical, and polar windings.

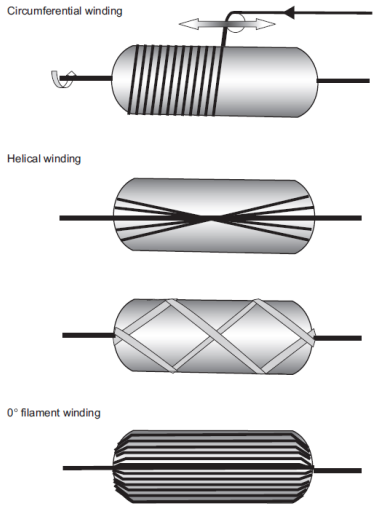

Figure 2.10 Principle of filament or tape winding (Böhlke et al, 2019)

Manufacturing with a winding angle approaching 90° is called a circle or circumferential winding process. The helical winding has constant mandrel rotation as the carrier unit moves back and forth in a linear motion. Polar winding is often used in the manufacture of high-pressure vessels because the fiber is wound directly from one end to the other on the mandrel. Angles close to 0° are required in this pattern (Peters, 2011) Winding pattern is shown in Figure 2.11.

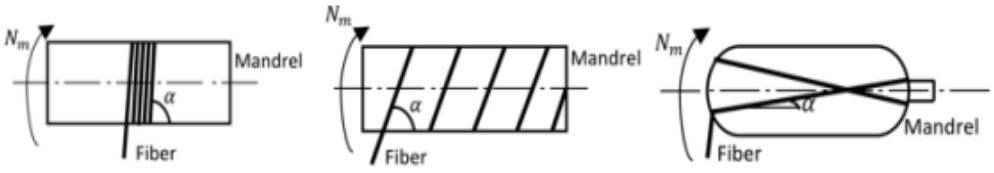

Figure 2.11 Winding patterns (Advani & Sozer, 2002)

Winding the fibers perpendicular to the mandrel's axis is referred to as circumferential winding, while winding the fibers either parallel to the axis or at an angle to it is referred to as helical winding (Abdalla et al.,2007).

CHAPTER THREE
MECHANICAL PROPERTIES OF COMPOSITE MATERIALS

3.1 Introduction

Planes formed by resin-impregnated fibers are laminates. Laminates are formed by laying the laminae on top of each other at predetermined angles. The part on the macro-mechanical properties of composites discusses the mechanical properties of laminates, whereas the section on the micro-mechanical properties of composites discusses the mechanical characteristics of laminates.

3.2 Micromechanical Behavior of Composites

The fiber-resin volume ratio is a result of the formulas created to determine the strength and stiffness characteristics of the lamina. The composite must be specified in terms of density and mass fraction in order to ascertain the fiber volume ratio.

3.2.1 Volume Fractions

The fibers contained in the laminate contribute more to the strength of the structure than the resin. The fiber/resin ratio is kept high to achieve the highest strength at the lowest weight. The direct result of the chosen technique in the production methods determines the fiber/resin ratio. Ratios of 50% can be achieved with wet-laid production methods without reducing resin. In processes such as vacuum bagging and resin stripping, where the resin is drawn, this ratio allows for high-strength products with 60% fiber dominance.

Vacuum pressure, resin viscosity, resin curing time (time before gelation under vacuum), apertured film pattern, and hole size affect the fiber-resin ratio. High vacuum pressure is a risky operation as it can pull low-viscosity resins more than necessary. Perforated film allows you to restrict the epoxy flow through the laminate and use a higher vacuum pressure (Kaw, 2005).

Now define the fiber volume fraction V_f , and the matrix volume fraction V_m as

$$V_f = \frac{v_f}{v_c} \quad V_m = \frac{v_m}{v_c} \tag{3.1}$$

The variation of volume fractions is

$$V_f + V_m = 1 \tag{3.2}$$

Also, composite volume fraction υ_c describe as;

$$\upsilon_f + \upsilon_m = \upsilon_c \tag{3.3}$$

3.2.2 Mass Fractions

The mass of the composite is the combination of the mass of the fiber, and the matrix that composes it. w_c, $f_{,m}$ represents the mass of composite, fiber, and matrix, respectively. W_f is ratio of mass of fiber/mass of composite, and W_m is ratio of mass of matrix/mass of composite.

$$\begin{gathered} W_f = \frac{w_f}{w_c} \text{ , and } W_m = \frac{w_m}{w_c} \\ W_f + W_m = 1 \\ w_f + w_m = w_c \end{gathered} \tag{3.4}$$

From the definition of the density of a single material, and

$$\begin{aligned} w_c &= r_c \upsilon_c, \\ w_f &= r_f \upsilon_f, \\ w_m &= r_m \upsilon_m, \end{aligned} \tag{3.5}$$

where r_c is density ratio of composite, r_f is density ratio of fiber, and r_m is density ratio of matrix.

The mass fraction, and volume fractions are related as,

$$W_f = \frac{\rho_f}{\rho_c} V_f$$
$$W_m = \frac{\rho_m}{\rho_c} V_m \tag{3.6}$$

where ρ_c is density of composite, ρ_f is density of fiber, and ρ_m is density of matrix.

In terms of the fiber, and matrix volume fractions. The mass fractions in terms of density, and volume can be denoted as,

$$W_f = \frac{\rho_f}{\frac{\rho_f}{\rho_m} V_f + V_f} V_f$$
$$W_m = \frac{1}{\frac{\rho_f}{\rho_m}(1 - V_m) + V_m} V_m \tag{3.7}$$

3.2.3 Density

Since the mass of the composite is the product of the volume, and density of the composite, mass is written in terms of volume, and density. The density function is derived from the equation.

$$w_c = w_f + w_m$$
$$\rho_c \upsilon_c = \rho_f \upsilon_f + \rho_m \upsilon_m \tag{3.8}$$
$$\rho_c = \rho_f \frac{\upsilon_f}{\upsilon_c} + \rho_m \frac{\upsilon_m}{\upsilon_c}$$

Using the definitions of fiber, and matrix volume fractions,

$$\rho_c = \rho_f V_f + \rho_m V_m \tag{3.9}$$

The volume of a composite v_c is the sum of the volumes of the fiber (v_f), and matrix (v_m),

$$v_c = v_f + v_m \tag{3.10}$$

The density of the composite in terms of mass fractions can be found as,

$$\frac{1}{\rho_c} = \frac{W_f}{\rho_f} + \frac{W_m}{\rho_m} \tag{3.11}$$

3.2.4 Void Content

The voids contained in composite structures will reduce their physical and mechanical properties. When the resins in FRP structures cannot get rid of the gas that occurs during the chemical reactions that occur while passing from the liquid state to the solid state, air gaps occur in the structure (Yahaya et al., 2015).

Due to the matrix's insufficient wetting of the fibers, there are more voids present. Additionally, moisture that was present in the fiber throughout manufacturing is another factor that contributes to the formation of void content. The fiber has hollow interiors that the resin cannot enter. In addition, air entrapment during the resin manufacturing process for the epoxy resin and hardening agent could result in a void (De Albuquerque et al., 2000).

The autoclave curing process is used to obtain high-performance products because this method allows simultaneous control of pressure and temperature during curing, but even if this method is used, it is inevitable that there will be voids near the surface of FRP materials. (Nele et al., 2016).

The amount of curing pressures and the timing of applying pressure will significantly affect the laminates' void content. If those two elements are carefully chosen, the laminates' trapped air, water vapor, and extra resin will be forced out, resulting in laminates with low porosity and good performance. Due to the extremely high acceptance criteria for design performance requirements, it could have negative

economic effects. The void content is very important for several composite applications, and values exceeding 1% are not acceptable, as in the case of advanced composite dynamic aircraft structures. Levels of 5% and greater can be tolerated in other applications (Liu et al., 2006). Gaps develop between the layers as composite materials are created. The volume grows as a result, which is why the density computed theoretically differs from the actual density. Additionally, the composite's mechanical properties deteriorate due to the imperfect structure and void formation. Voids between the laminates is shown in Figure 3.1.

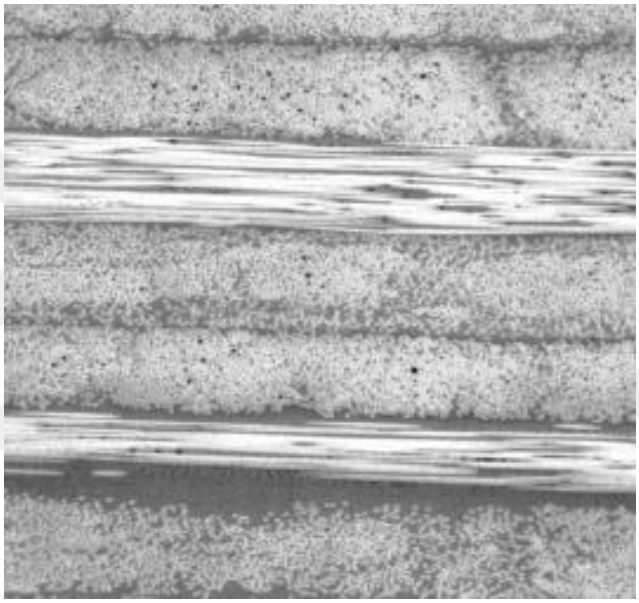

Figure 3.1 Void content (Kaw, 2005)

The damages that gaps can cause are:

• Compressive, and transverse tensile strengths

• Shear stiffness, and strength

• Fatigue, and moisture resistance

A certain volume of voids $v_{v,}$ and the volume fraction of voids V_v is defined as

$$V_v = \frac{v_v}{v_c} \tag{3.12}$$

Then, the total volume of a composite (v_c) with voids is given by

$$V_c = \frac{v_c}{v_v} \tag{3.13}$$

Regarding the experimental density ρ_{ce} of a composite, the actual volume of the composite is

$$v_c = \frac{w_c}{\rho_{ce}} \tag{3.14}$$

and the theoretical density ρ_{ct} of the composite, the theoretical volume of the composite is

$$\begin{aligned} v_f + v_m &= \frac{w_c}{\rho_{ct}} \\ \frac{w_c}{\rho_{ce}} &= \frac{w_c}{\rho_{ct}} + v_v \end{aligned} \tag{3.15}$$

The volume of void is given by

$$\begin{aligned} v_v &= \frac{w_c}{\rho_{ce}}\left(\frac{\rho_{ct} - \rho_{ce}}{\rho_{ct}}\right) \\ V_v &= \frac{v_v}{v_c}\left(\frac{\rho_{ct} - \rho_{ce}}{\rho_{ct}}\right) \end{aligned} \tag{3.16}$$

The void content was calculated by using following Equations (3.16) – (3.19).

$$R = w_F / w_B \times 100 \tag{3.17}$$

$$R = 100 - r \tag{3.18}$$

$$\rho t = 100/(R/\rho_f + r/\rho_r) \tag{3.19}$$

$$\text{Void Content} = 100/(\rho t - \rho_m)/\rho t \tag{3.20}$$

Where, the resin in the composite denoted by R is given in percentage, and r is the weight % of the reinforcement in the composite. w_F is the mass of fiber, and w_B is mass of composite, ρ_r is the density of the resin, ρ_f is the density of the fiber, ρ_t is theoretical density, and ρ_m is measured density (de Almeida et al., 1994).

There is an exponentially decreasing relationship between the number of voids, and the curing pressure. The number of voids formed in composite structures can be optimized with the applied pressure. For this reason, higher yields in mechanical properties are expected from pressure-cured composites in autoclave ovens (Liu et al., 2016).

3.3 Macromechanical Behavior of a Lamina

3.3.1 Orthotropic Material

The stiffness matrix of the material with three perpendicular planes of material symmetry is found as follows

$$[C] = \begin{bmatrix} C_{11} & C_{12} & C_{13} & 0 & 0 & C_{16} \\ C_{12} & C_{22} & C_{23} & 0 & 0 & C_{26} \\ C_{13} & C_{23} & C_{33} & 0 & 0 & C_{36} \\ 0 & 0 & 0 & C_{44} & C_{45} & 0 \\ 0 & 0 & 0 & 0 & C_{55} & 0 \\ 0 & 0 & 0 & 0 & 0 & C_{66} \end{bmatrix} \quad (3.21)$$

The stiffness matrix given in equation (3.20) can be derived by utilizing the stiffness matrix [C] for the monoclinic material. With two more planes of symmetry, the following constants are reset.

$$C_{16} = 0,\ C_{26} = 0,\ C_{36} = 0,\ C_{45} = 0 \quad (3.22)$$

The structure, which has three symmetry planes perpendicular to each other, also has nine elastic constants. While there is material symmetry in traditional structures, there is no symmetry in composite structures because it has dominant features in a certain direction. The compliance matrix reduces to

$$[S] = \begin{bmatrix} S_{11} & S_{12} & S_{13} & 0 & 0 & 0 \\ S_{12} & S_{22} & S_{23} & 0 & 0 & 0 \\ S_{13} & S_{23} & S_{33} & 0 & 0 & 0 \\ 0 & 0 & 0 & S_{44} & 0 & 0 \\ 0 & 0 & 0 & 0 & S_{55} & 0 \\ 0 & 0 & 0 & 0 & 0 & S_{66} \end{bmatrix} \tag{3.23}$$

Unidirectional laminates are orthographic materials, and if these laminates are low-layered, and do not carry out-of-plane loads at the same time, plane stress assumptions are acceptable for these materials. Where σ is stress, and τ is the shear stress, assuming $\sigma_3 = 0$, $\tau_{23} = 0$, and $\tau_{31} = 0$, then

$$\varepsilon_3 = S_{13}\sigma_1 + S_{23}\sigma_2 \tag{3.24}$$

$$\gamma_{23} = \gamma_{31} = 0 \tag{3.25}$$

The normal strain, ε_3, is a property that is interdependent as it is a function of the other two normal strains, ε_1, and ε_2. This normal strain, ε_3, can be derived from the stress-strain relationship. Also, shear stresses γ_{23}, and γ_{31} are close to zero, and are neglected. An orthotropic plane stress can be written as:

$$\begin{bmatrix} \varepsilon_1 \\ \varepsilon_2 \\ \gamma_{12} \end{bmatrix} = \begin{bmatrix} S_{11} & S_{12} & 0 \\ S_{12} & S_{22} & 0 \\ 0 & 0 & S_{66} \end{bmatrix} \begin{bmatrix} \sigma_1 \\ \sigma_2 \\ \tau_{12} \end{bmatrix} \tag{3.26}$$

The stress–strain relationship can be expressed as

$$\begin{bmatrix} \sigma_1 \\ \sigma_2 \\ \tau_{12} \end{bmatrix} = \begin{bmatrix} \mathrm{Q}_{11} & \mathrm{Q}_{12} & 0 \\ \mathrm{Q}_{12} & \mathrm{Q}_{22} & 0 \\ 0 & 0 & \mathrm{Q}_{66} \end{bmatrix} \begin{bmatrix} \varepsilon_1 \\ \varepsilon_2 \\ \gamma_{12} \end{bmatrix} \tag{3.27}$$

The reduced stiffness coefficients are,

$$Q_{11} = \frac{S_{22}}{S_{11}S_{22} - S_{11}^2}$$

$$Q_{12} = -\frac{S_{22}}{S_{11}S_{22} - S_{12}^2} \tag{3.28}$$

$$Q_{22} = \frac{S_{11}}{S_{11}S_{22} - S_{12}^2}$$

$$Q_{66} = \frac{1}{S_{66}}$$

3.3.2 Hooke's Law for a Two-Dimensional Angle Lamina

Since laminates have strengthened mechanical properties according to direction, a structure is generally not created by laying in one direction. This lay is determined by shaped angles. For this reason, the stress-strain relationship of a particular angle lamina must be determined separately. The coordinate system of laminates can be shown in Figure 3.1. Directions (1-2) in the coordinate system are in the direction of the fibers. Direction 1 is parallel to the fiber, direction 2 is perpendicular to the fiber. The angle between the axes, and the fiber direction is denoted by the angle θ is shown in Figure 3.2.

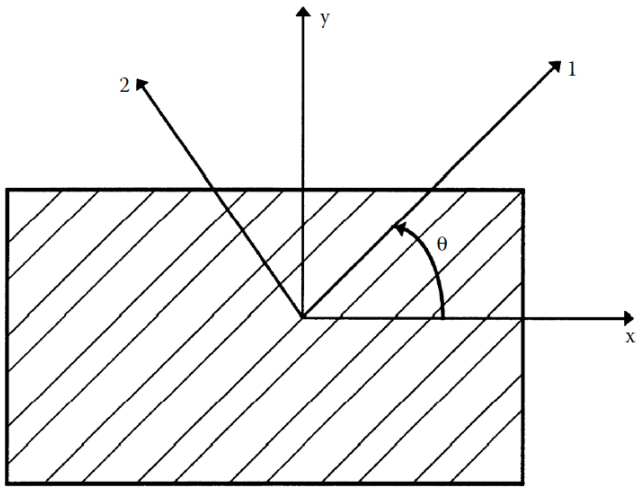

Figure 3.2 Local, and global axes of an angle lamina

The global, and local stresses in an angle lamina are related to each other through the angle of the lamina, θ;

$$\begin{bmatrix} \sigma_x \\ \sigma_y \\ \tau_{xy}/2 \end{bmatrix} = [T]^{-1} \begin{bmatrix} \sigma_1 \\ \sigma_2 \\ \tau_{12} \end{bmatrix} \tag{3.29}$$

where [T] is called the transformation matrix, and is defined as

$$[T]^{-1} = \begin{bmatrix} c^2 & s^2 & -2sc \\ s^2 & c^2 & 2sc \\ sc & -sc & c^2 - s^2 \end{bmatrix} \text{ c=Cos(θ), s=Sin(θ)} \tag{3.30}$$

Using the stress–strain equation (3.7) in the local axes, Equation (3.10) can be written as;

$$\begin{bmatrix} \sigma_x \\ \sigma_y \\ \tau_{xy} \end{bmatrix} = [T]^{-1}.[Q] \begin{bmatrix} \varepsilon_1 \\ \varepsilon_2 \\ \gamma_{12} \end{bmatrix} \tag{3.31}$$

where $[\overline{Q_{ij}}]$are called the elements of the transformed reduced stiffness matrix $[\bar{Q}]$, and are given by

$$\begin{bmatrix} \sigma_x \\ \sigma_y \\ \tau_{xy} \end{bmatrix} = \begin{bmatrix} \bar{Q}_{11} & \bar{Q}_{12} & \bar{Q}_{13} \\ \bar{Q}_{21} & \bar{Q}_{22} & \bar{Q}_{23} \\ \bar{Q}_{31} & \bar{Q}_{32} & \bar{Q}_{33} \end{bmatrix} \begin{bmatrix} \varepsilon_x \\ \varepsilon_y \\ \gamma_{xy} \end{bmatrix} \tag{3.32}$$

$$\begin{aligned} \bar{Q}_{11} &= Q_{11}.c^4 + Q_{22}.s^4 + 2(Q_{12} + 2Q_{66})s^2c^2 \\ \bar{Q}_{12} &= (Q_{11} + Q_{22} - 4.Q_{66})s^2c^2 + Q_{12}(c^4 + s^2) \\ \bar{Q}_{22} &= Q_{11}.s^4 + Q_{22}.c^4 + 2(Q_{12} + 2Q_{66})s^2c^2 \\ \bar{Q}_{16} &= (Q_{11} - Q_{12} - 2.Q_{66})c^3s\text{-}(Q_{22} - Q_{12} - 2.Q_{66})\, s^3c \\ \bar{Q}_{26} &= (Q_{11} - Q_{12} - 2.Q_{66})s^3c - (Q_{22} - Q_{12} - 2.Q_{66})\, c^3s \\ \bar{Q}_{66} &= (Q_{11} + Q_{22} - 2Q_{12} - 2Q_{66})s^2c^2 + Q_{66}(s^4 + c^4) \end{aligned} \tag{3.33}$$

Inverting Equation 3.13 gives;

$$\begin{bmatrix} \varepsilon_x \\ \varepsilon_y \\ \gamma_{xy} \end{bmatrix} = \begin{bmatrix} \bar{S}_{11} & \bar{S}_{12} & \bar{S}_{13} \\ \bar{S}_{21} & \bar{S}_{22} & \bar{S}_{23} \\ \bar{S}_{31} & \bar{S}_{32} & \bar{S}_{33} \end{bmatrix} \begin{bmatrix} \sigma_x \\ \sigma_y \\ \sigma_{xy} \end{bmatrix} \tag{3.34}$$

where $[\overline{S_{ij}}]$ are called the elements of the transformed reduced stiffness matrix $[\bar{S}]$, and are given by

$$\begin{aligned} \bar{S}_{11} &= S_{11}.c^4 + S_{22}.s^4 + (2S_{12} + S_{66})s^2c^2 \\ \bar{S}_{12} &= (S_{11} + S_{22} - 4.S_{66})s^2c^2 + S_{12}(c^4 + s^2) \\ \bar{S}_{22} &= S_{11}.s^4 + S_{22}.c^4 + (2S_{12} + S_{66})s^2c^2 \\ \bar{S}_{16} &= (2S_{11} - 2S_{12} - S_{66})c^3s - (2S_{22} - 2S_{12} - S_{66})\, s^3c \\ \bar{S}_{26} &= (2S_{11} - 2S_{12} - S_{66})s^3c - (2S_{22} - 2S_{12} - S_{66})\, c^3s \\ \bar{S}_{66} &= 2(2S_{11} + 2S_{22} - 4S_{12} - S_{66})s^2c^2 - S_{66}(s^4 + c^4) \end{aligned} \tag{3.35}$$

3.3.3 Engineering Constants of an Angle Lamina

To find the engineering elastic moduli in direction x;

$$\sigma_x \neq 0\ ,\ \sigma_y = 0\ ,\ \tau_{xy} = 0, \tag{3.36}$$

Then, from Equation 3.36,

$$\begin{aligned} \varepsilon_x &= \bar{S}_{11}\sigma_x \\ \varepsilon_y &= \bar{S}_{12}\sigma_x \\ \gamma_{xy} &= \bar{S}_{16}\sigma_x \end{aligned} \tag{3.37}$$

E_x, the elastic moduli x is defined as,

$$E_x \equiv \frac{\sigma_x}{\varepsilon_x} = \frac{1}{\bar{S}_{11}}$$
$$\nu_{xy} = -\frac{\varepsilon_y}{\varepsilon_x} = \frac{\bar{S}_{12}}{\bar{S}_{11}} \tag{3.38}$$

E_y, the elastic moduli y is defined as,

$$\sigma_x = 0\ ,\ \sigma_y \neq 0\ ,\ \tau_{xy} = 0,$$
$$E_y = \frac{1}{\bar{S}_{22}} \tag{3.39}$$
$$\nu_{xy} = -\frac{\bar{S}_{12}}{\bar{S}_{22}}$$

Also, by applying the stresses can be found the shear moduli (G_{xy})

$$\sigma_x = 0\ ,\ \sigma_y = 0\ ,\ \tau_{xy} \neq 0,$$
$$G_{xy} = \frac{1}{\bar{S}_{66}} \tag{3.40}$$

CHAPTER FOUR
VIBRATION OF FILAMENT WOUND COMPOSITES

4.1 Vibration of Composite Structure

The concept of vibration can be briefly expressed as the oscillation from the equilibrium state. Vibration testing allows the measurements of the natural frequency, damping ratio, and mode shape parameters of the structure in a non-destructive manner according to the classical test methods. Modal parameters are structure-specific and express the characteristic features of the structure. It changes the static and dynamic properties of the structure depending on the size of the damage and its location. A dynamic system is a whole with masses that can move relative to each other. Vibration is avoided in designs, but there are applications where vibration is beneficial.

The object's degree of freedom is taken into consideration when classifying vibrations. Systems with one degree of freedom are referred to as single degrees of freedom systems (SDOF), systems with several degrees of freedom are referred to as multiple degrees of freedom systems (MDOF), and systems with infinitely many degrees of freedom are referred to as continuous systems when discretizing the systems with a finite number of degrees of freedom. Assuming that the energy from the vibration does not spread or get damped, it is known as random vibration if the duration and magnitude of the applied force are not in a specific order. When a vibration is expected to propagate and become dampened, its damping form is used to categorize the vibration.

The system can be activated with the inputs that disrupt the equilibrium state given at the initial moment. A vibration that takes place without any disturbing input from the starting moment is called a free vibration. Therefore, free vibrations are characteristic vibrations that define the vibration modes of the system and the natural behavior of the system. The initial condition is to load energy into the system. The type of energy in this object can be kinetic or potential. If there is nothing in the system to absorb the energy, the system is undamped and can vibrate indefinitely. If

there is a damper in the system, the energy will be transformed, and vibration will not occur after a certain period (Tse et al., 1963).

4.2 The Method of Analysis Frequency, and Mode Shape

4.2.1 Modal Analysis

Modal analysis is a method that includes both theoretical and experimental techniques. In theoretical modal analysis, mass, stiffness and damping parameters are specified in the system model. The system model can be expressed in the form of partial differential equations. In solving this equation, the truth relations between the eigenvectors in the system are used. Thanks to these relations, the system mathematical model equation is transformed into independent differential equations. By solving this equation, natural frequency, mode shapes and forced vibration information are obtained. In the experimental method, the data of the measured structure is tried to be harmonized with an existing mathematical model. In this mathematical model, assumptions are made regarding factors such as the number of degrees of freedom in the structure, damping type, and the number of vibration modes in the measured frequency range (Thomsen, 2003).

4.2.2 Mode Shapes

The mode shape is the deviation of the modal frequency of the structure from the pole position. While the modes do not depend on the forces acting on the structure, they depend on the material properties or boundary conditions of the structure. Mode shapes are unique between points of the build. It is a dynamic property of the structure in terms of free vibration. Displacement in a harmonically excited system depends on the mode shapes. In random vibration, the displacement includes contributions from all mode shapes.

4.2.3 Single Degree of Freedom Systems Formulation of The Equation of Motion

Newton's second law (The Principle of Least Action) is;

$$F = \frac{dI}{dt} = \frac{d}{dt}(m\dot{u}) = m\ddot{u} \tag{4.1}$$

where I is impulse.

The force corresponds to the change of impulse over time. Hence,

$$-f_k(t)-f_c(t)+F(t)= m\ddot{u}(t) \tag{4.2}$$

Introducing the spring force, and the damping force becomes;

$$m\ddot{u}(t)+ c\dot{u}(t)+ku(t)=F(t) \tag{4.3}$$

(Thomson, 2018).

4.3 Free Vibrations Analysis

When a structure is forced out of its static equilibrium, free vibrations occur. It can then oscillate without any dynamic stimulation from outside.

4.3.1 Undamped free vibrations

$$m\ddot{u}\,(t) + ku\,(t) = 0 \tag{4.4}$$

Formulation 1: Amplitude, and phase angle

$$\begin{gathered} u(t)= A\cos(\omega_n t - \phi) \\ \ddot{u}\,(t) = -A\omega_n^2 \cos(\omega_n t - \phi) \end{gathered} \tag{4.5}$$

By substituting equations (4.5)

$$\text{A } (-\omega_n^2 m + k)\cos(\omega_n t - \phi) = 0$$

$$(-\omega_n^2 m + k) = 0 \tag{4.6}$$

$$\omega_n = \sqrt{k/m}$$

The relationship among the angular frequency, ordinary frequency, , and period can be expressed as

$$\omega_n = \sqrt{k/m}$$

$$f_n = \frac{w_n}{2\pi} \tag{4.7}$$

$$T_n = \frac{2\pi}{w_n}$$

The angular frequency unit is rad/s, ordinary frequency is the number of revolutions per time, and its unit is hertz. The period is time required per revolution, and its unit is second.

Arranging equation (4.4) considering the angular frequency given in equation (4.7) gives

$$\ddot{u}\,(t) + w_n^2 u(t) = 0 \tag{4.8}$$

The static equilibrium is disturbed by the initial displacement u(0)=u_0 , and initial velocity $\dot{u}(0) = v_0$. Determination of the unknowns A, and ϕ:

$$A = \sqrt{u_0^2 + \left(\frac{v_0}{w_n}\right)^2},\ tan\phi = \frac{v_0}{u_0 w_n} \tag{4.9}$$

Trigonometric function

$$m\ddot{u}\,(t) + ku\,(t) = 0$$

$$\text{u(t)}=A_1\cos(\,\omega_n t - \phi) + sin\omega_n t) \tag{4.10}$$

$$\ddot{u}\,(t) = -A_1 w_n^2\cos(w_n t) - A_2 w_n^2\sin(w_n t)$$

By substituting equations

$$A_1 w_n^2\cos(w_n t) + A_2 w_n^2\sin(w_n t) = 0$$

$$-w_n^2 m + k = 0 \tag{4.11}$$

$$\omega_n = \sqrt{k/m}$$

The static equilibrium is disturbed by the initial displacement $u(0)=u_0$, and the initial velocity $\dot{u}(0) = v_0$. Determination of the unknowns A_1, and A_2:

$$A_1=u_0,\ A_2=\frac{v_0}{w_n} \tag{4.12}$$

Motion equation is explained by;

$$[M]\ddot{u}\,(t) + [K]u\,(t) = 0$$

$$\text{u(t)}=e^{\lambda t} \tag{4.13}$$

$$\ddot{u}(t) = \lambda^2 e^{\lambda t}$$

By substituting equations (4.13)

$$m\lambda^2 + k = 0$$

$$\lambda^2 = -\frac{k}{m} \tag{4.14}$$

$$\lambda = \pm\text{i}\sqrt{\frac{k}{m}} = \pm\text{i}\omega_n$$

The complete solution is:

$$u(t)= C_1 e^{iw_n t} + C_2 e^{-iw_n t} \tag{4.15}$$

and by means of Euler's formulas, equation (4.15) can be re-arranged as

$$\cos \alpha=\frac{e^{i\alpha}+e^{-i\alpha}}{2}, \sin \alpha=\frac{e^{i\alpha}-e^{-i\alpha}}{2i}$$

$$e^{i\alpha} = \cos(\alpha) + isin(\alpha), e^{-i\alpha} = \cos(\alpha) - isin(\alpha)$$

$$u(t)= (C_1 + C_2)\cos (w_n t)+i(C_1 - C_2)\sin (w_n t) \tag{4.16}$$

$$u(t)= A_1 \cos (w_n t)+ A_2 \sin (w_n t)$$

Damped free vibration is explained by;

$$m\ddot{u}\ (t) + c\dot{u}(t) + ku\ (t) = 0 \tag{4.17}$$

where c represents the damping factor. In practice, damping occurs, vibrations are attenuated, and it is essentially impossible to mathematically characterize damping precisely. Damping constant: c [N.$\frac{s}{m}$]. The displacement function given in equation 4.17, and its derivatives can be denoted as;

$$u(t)=e^{\lambda\tau},\dot{u}(t) = \lambda e^{\lambda\tau},\ddot{u}(t) = \lambda^2 e^{\lambda\tau} \tag{4.18}$$

By substituting equations (4.18)

$$(\lambda^2 m + \lambda c + k)\, e^{\lambda\tau} = 0$$

$$\lambda^2 m + \lambda c + k = 0 \tag{4.19}$$

$$\lambda = -\frac{c}{2m} \pm \frac{1}{2m}\sqrt{c^2 - 4km}$$

If critical damping exists;

$$c^2 - 4km = 0,\ c_{cr}=2\sqrt{km} = 2w_n m \tag{4.20}$$

Damping ratio can be calculated as

$$\zeta = \frac{c}{c_{cr}} = \frac{c}{2\sqrt{km}} = \frac{c}{2w_n m} \tag{4.21}$$

Transforming of the equation of motion given in equation (4.17)

$$\begin{gathered} m\ddot{u}\,(t) + c\dot{u}(t) + ku\,(t) = 0 \\ \ddot{u}\,(t) + \frac{c}{m}\dot{u}(t) + \frac{k}{m}u\,(t) = 0 \\ \ddot{u}\,(t) + 2\zeta w_n \dot{u}(t) + {w_n}^2 u\,(t) = 0 \end{gathered} \tag{4.22}$$

Depending on the damping ratio, the type of vibration changes. Types of vibrations;

$\zeta = \frac{c}{c_{cr}} < 1$: Underdamped free vibrations

$\zeta = \frac{c}{c_{cr}} = 1$: Critically damped vibrations

$\zeta = \frac{c}{c_{cr}} > 1$: Overdamped free vibrations

Underdamped free vibrations $\zeta < 1$

By substituting equations (4.22)

$$\zeta = \frac{c}{c_{cr}} = \frac{c}{2\sqrt{km}} = \frac{c}{2w_n m}\text{ , and } \omega_n = \sqrt{k/m}$$

$$\lambda = -\frac{c}{2m} \pm \frac{1}{2m}\sqrt{c^2 - 4km} = -\frac{c}{2m} \pm \sqrt{\left(\frac{c}{2m}\right)^2 - \frac{k}{m}} \tag{4.23}$$

It is obtained by using equations (4.23);

$$\lambda = \zeta\omega_n \pm \sqrt{\omega_n^2\zeta^2 - \omega_n^2} = -\zeta\omega_n \pm \omega_n\sqrt{\zeta^2 - 1} = -\zeta\omega_n \pm i\omega_n\sqrt{1 - \zeta^2}$$

$$\omega_d = \omega_n\sqrt{1 - \zeta^2} \tag{4.24}$$

$$\lambda = -\zeta\omega_n \pm i\omega_d$$

Hence, the complete solution is;

$$u(t) = C_1 e^{(-\zeta\omega_n + i\omega_d)t} + C_2 e^{(-\zeta\omega_n - i\omega_d)t}$$

$$u(t) = e^{-\zeta\omega_n t}(C_1 e^{i\omega_d t} + C_2 e^{-i\omega_d t}) \tag{4.25}$$

$$u(t) = e^{-\zeta\omega_n t}((A_1 \cos(\omega_d t) + (A_2 \sin(\omega_d t))$$

The calculation A_1, and A_2 is carried out as usual by means of the initial conditions for displacement u (0) = u_0, and velocity $\dot{u}(0) = v_0$. Hence,

$$A_1 = u_0,\ A_2 = \frac{v_0 + \xi w_n u_0}{w_d} \tag{4.26}$$

This equation (4.25) can be rewritten, the amplitude, and phase angle;

$$u(t) = Ae^{-\zeta w_n t}\cos(w_d t - \phi) \text{ with}$$

$$A = \sqrt{u_0^2 + \left(\frac{v_0 + \zeta w_n u_0}{w_d}\right)^2},\ \tan\phi = \frac{v_0 + \zeta w_n u_0}{w_d u_0} \tag{4.27}$$

The motion is a sinusoidal vibration with circular frequency w_d , and decreasing amplitude;

$$Ae^{-\zeta w_n t} \tag{4.28}$$

4.4 Logarithmic Decrement

The natural logarithm of the ratio of the vibrational amplitudes of succeeding cycles is the definition of the logarithmic decrement for underdamped free vibrations (Thomson, 2018).

Logarithmic decrement is a criterion used in oscillation analysis to determine the damping degree of a system. The natural logarithm is obtained by dividing the ratio of two consecutive oscillations by the number of oscillations between them. In other words, the amplitude of an oscillation refers to how much it decreases in each cycle. In equation (4.28) describe logarithmic decrement. Where δ is logarithmic decrement, T_d is period, ω_n is natural frequency, and ζ is damping ratio. In Figure 4.1, x (t) can be chosen as X_1, X_2 or X_n.

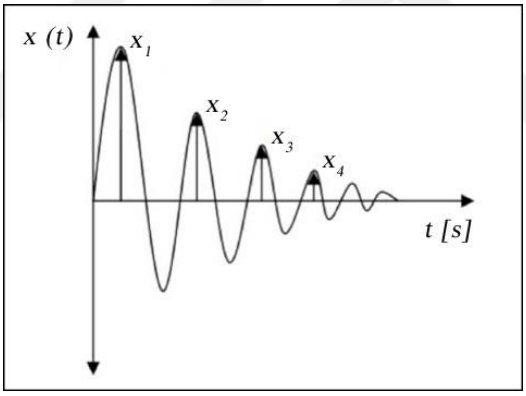

Figure 4.1 Logarithmic Decrement

$$\delta = ln\left(\frac{x(t)}{x(t+T_d)}\right) = \zeta\omega_n T_d = \frac{2\pi\zeta}{\sqrt{1-\zeta}} \tag{4.29}$$

The logarithmic decrement value is determined by the system's damping. A highly damped system usually has a small logarithmic decrement, showing that the amplitude decreases slowly over time. On the other hand, a less damped system indicates that the logarithmic decrement value is larger, and the amplitude decreases rapidly. Logarithmic decrement is commonly used in analysis of mechanical and electrical systems, earthquake science, and other fields where oscillations are important.

CHAPTER FIVE
EXPERIMENTAL STUDY

5.1 Production of Filament Wound Composite Tube

The material of the samples to be used in the experiments to be carried out in this section was chosen as glass/fiber composites. The production method is the filament winding method. Since the production of composite pressure vessels, which is the subject of the thesis, is costly, cylindrical composite pipes with the closest geometry were produced and tested. The difference between composite pressure vessels and composite pipes is the absence of domes that close the two open ends of the cylinder. Composite pipes are often used commercially in reverse osmosis water purification systems.

Polymer composites consist of fiber, and matrix. Fiber production was made with 8 glass fiber rovings. There are 1200 fibers in each roving wire. Huntsman Araldite MY740 resin, Aradur HY918 hardener, and DY062 hardener were used for the resin system. Epoxy impregnated glass fiber is shown in Figure 5.1.

The prepared resin mixture is added to the resin bath and heated continuously to keep the viscosity of this mixture at a suitable level for use. A resin bath is used to mix and process glass rovings. The filament winding technique is used to wind fibers that have been resin-impregnated on a mandrel. The mandrel acts as a mold for the composite part to take its final shape. The product, whose winding process is complete, is placed in the ovens for curing. The structure matures in the determined curing. The products, which are cooled in open air, are separated from the mandrel with the help of a press.

Cylindrical geometries are produced on the filament winding machine. Its working principle is similar to that of a lathe. While the mandrel rotates on its own axis, the head with the fibers moves in the axis of the mandrel and performs the winding process. Bands shown in Figure 5.1 are consisted of glass fiber that is

impregnated with epoxy. Bandwidth is dependent on the winding angle and shown in Figure 5.2.

Figure 5.1 Filament winding process

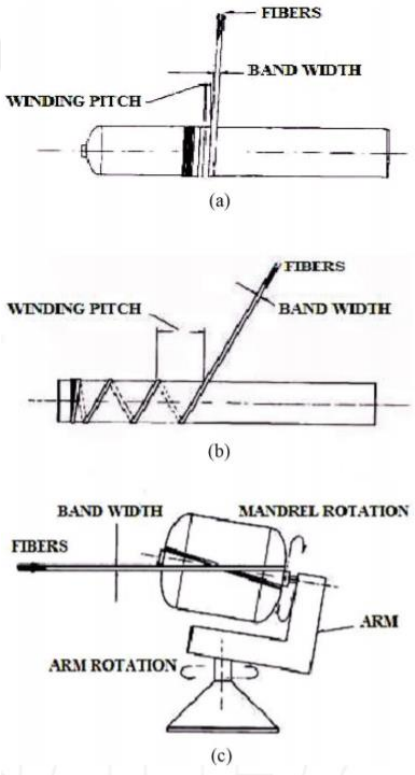

Figure 5.2 Filament winding terms (Peters, 2011)

Pressure vessels can also be produced with these machines. In this study, samples produced by the filament winding process with fiber winding angles of 55, 75, and 85 degrees were produced. As seen in Figure 5.3, the plane on which the angle is referenced is considered the axis of the mandrel.

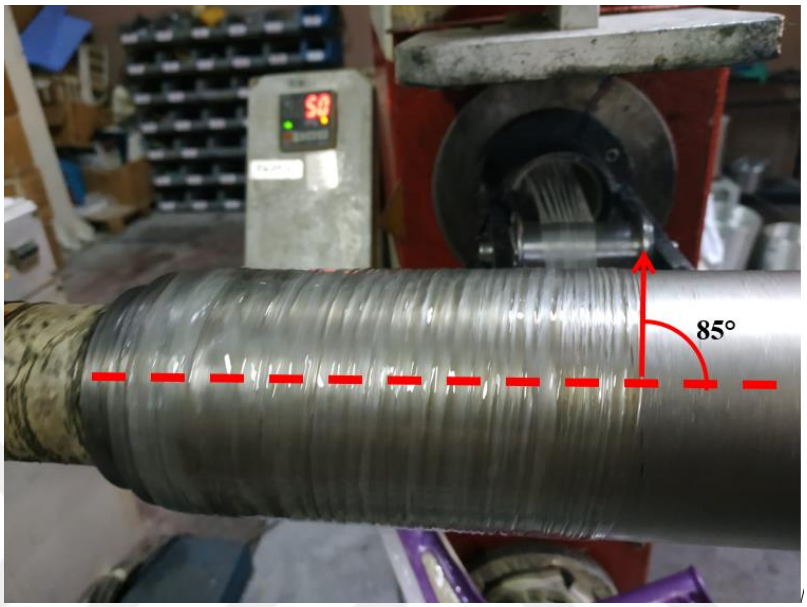

Figure 5.3 Filament winding, and winding angle

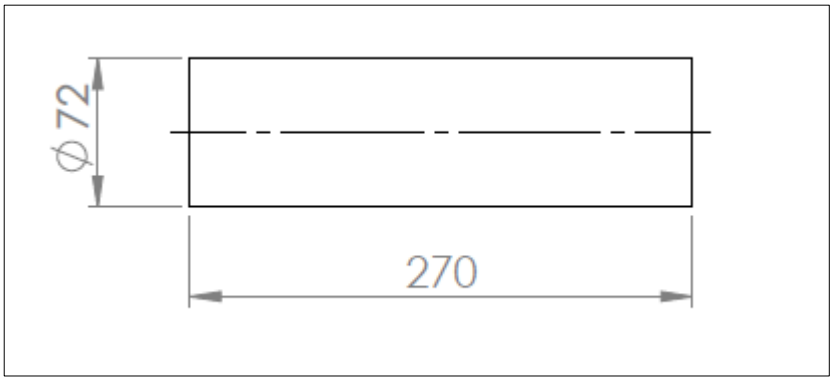

Figure 5.4 Dimensions of test specimens

The test specimens were wound on a ∅72 mm diameter mandrel as seen in Figure 5.4. [55/-55/55], [75/-75/75], and [85/-85/85] degree angle configurations, and samples with a length of 270 mm were obtained. Curing temperatures of 90°C, 120°C, and 140°C were applied separately for the study. The curing temperature recommended by the resin manufacturers is 120°C. The cured at 120°C for 3 hours

was taken as the reference product. A temperature of 90°C was considered under-cured, and 140°C was considered over-cured. Figure 5.5 shows the composite curing oven.

Figure 5.5 Curing oven

In order to deliberately create delamination in the products, 1/3 of the length of the product was covered with Teflon fabric, which was laid between the second and third layers, which are close to the surface. The position of the delamination was placed in line with the edge of the part and in the middle of the part, and the test results were contrasted with those of a healthy product made in the same factory. Samples wound at 55 winding angles were measured as 280±2 gr, samples wrapped at 75 winding angles were measured as 400±2 gr and samples wrapped at 85 winding angles were measured as 280±2 gr. As shown in Figure 5.6-Figure 5.17, a total of 27 were produced for natural frequency testing.

Figure 5.6 85-degree filament wound at all curing temperatures

Figure 5.7 55-degree filament wound at all curing temperatures

Figure 5.8 75-degree filament wound at all curing temperatures

Figure 5.9 85-degree filament wound at 140°C curing temperature, and delamination

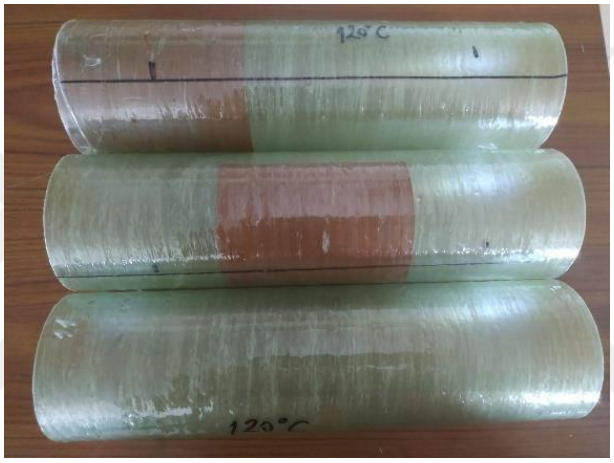

Figure 5.10 85-degree filament wound at 120°C curing temperature, and delamination

Figure 5.11 85-degree filament wound at 90°C curing temperature, and delamination

Figure 5.12 75-degree filament wound at 140°C curing temperature, and delamination

Figure 5.13 75-degree filament wound at 120°C curing temperature, and delamination

Figure 5.14 75-degree filament wound at 90°C curing temperature, and delamination

Figure 5.15 55-degree filament wound at 140°C curing temperature, and delamination

Figure 5.16 55-degree filament wound at 120°C curing temperature, and delamination

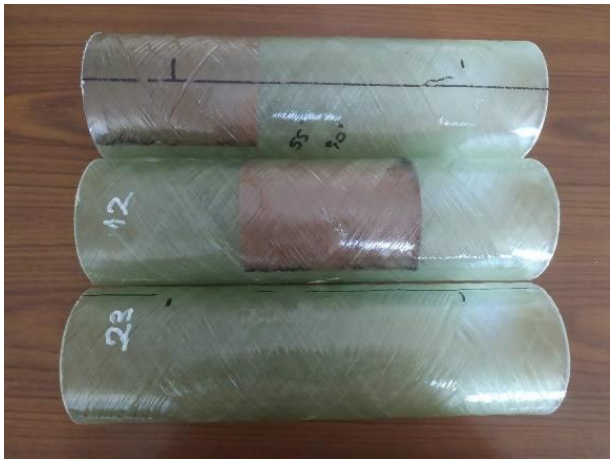

Figure 5.17 55-degree filament wound at 90°C curing temperature, and delamination

5.2 Setting Experimental Equipment

The test arrangement allowed for free hanging of the samples. Using the test setup shown in Figure 5.18, the cylindrical composite part's free vibration response was assessed. Three PCB 352A24 type accelerometers were used to monitor the vibration signals produced by a percussive hammer of type PCB 086C01, as shown in Figure 5.18. Each accelerometer weighs 0.8 g and has a sensitivity of 100 mV/g. It is appropriate for vibration measurements in the 0.4–12,000 Hz range. All vibration signals acquired from the accelerometers were recorded on a computer using NI PXI 4496, a National Instruments device, at a frequency of 15,000 Hz. Data acquisition system, and LabVIEW software, as seen in Figure 5.18-Figure 5.20.

5.2.1 Free-Free Boundary Conditions

Since free-edge circumstances can be very easily approximated experimentally, free-free samples were chosen for these testing. The samples were hung on flexible strings in order to accomplish this, and an unconnected loudspeaker that was only activated through acoustic means served as the excitation source. A tiny piezoelectric strain gauge attached to the sample was used to measure the response. The strain gauge's mass and wires weight were sufficiently negligible to be regarded.

Figure 5.18 Test setup

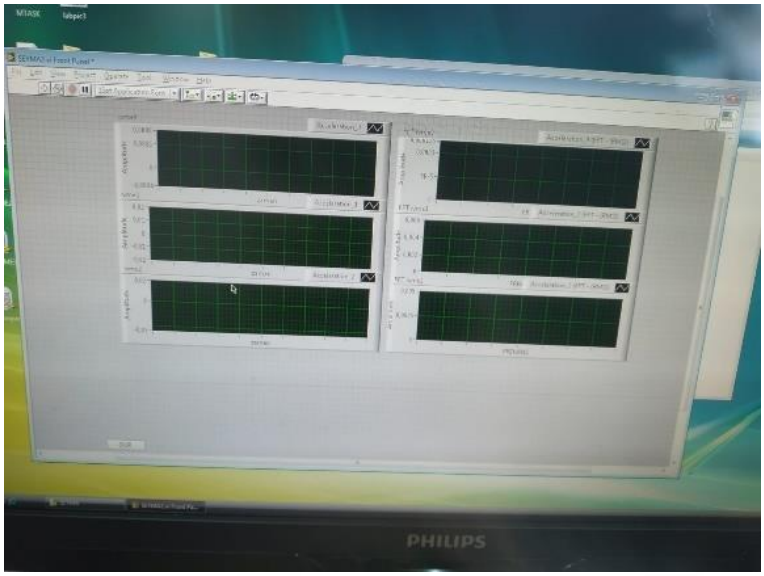

Figure 5.19 LabVIEW software

Figure 5.20 Delaminated sample testing

5.2.2 Fixed-Free Boundary Conditions

Boundary condition with fixed and free end was provided by clamping one end of the sample to the vise. An unconnected loudspeaker that was only activated through acoustic means served as the excitation source. A tiny piezoelectric strain gauge attached to the sample was used to measure the response. The strain gauge's mass was sufficiently negligible to be regarded.

5.3 Experimental Results for Free-Free Boundary Condition

The results from the LabView program were processed in MATLAB. In Figure 5.21-Figure 5.29 show samples wound at 85 degrees.

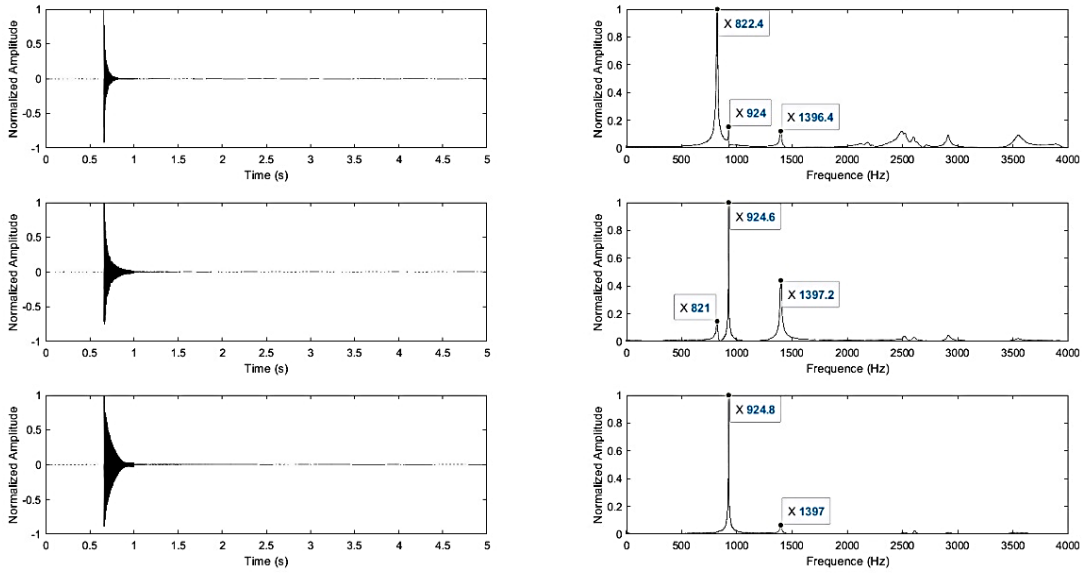

Figure 5.21 Vibration analysis results of the sample having 85-degrees filament wound, cured at 90°C and delamination at edge

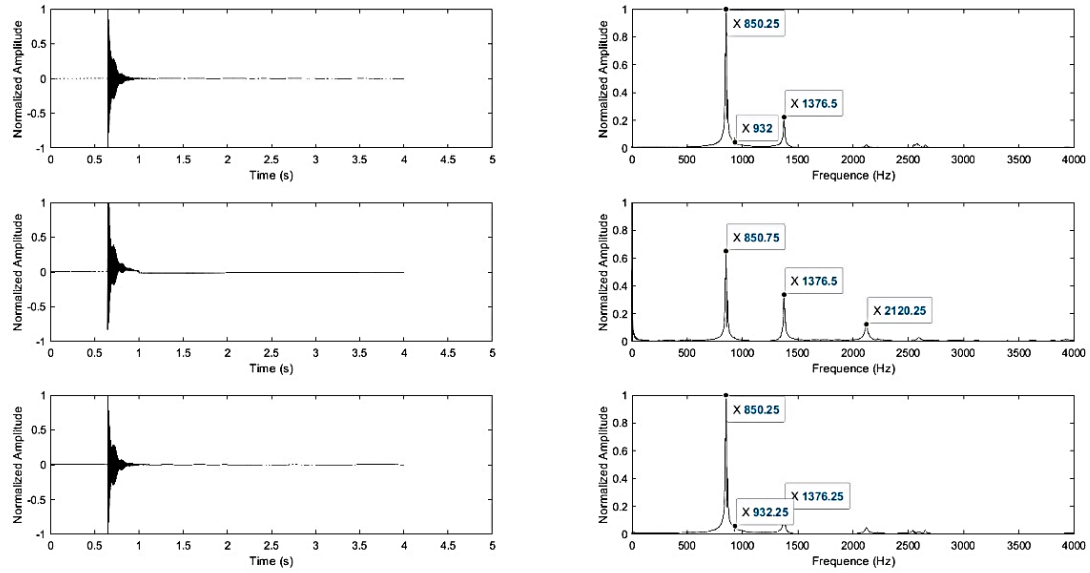

Figure 5.22 Vibration analysis results of the sample having 85-degrees filament wound, cured at 90°C and delamination in the middle

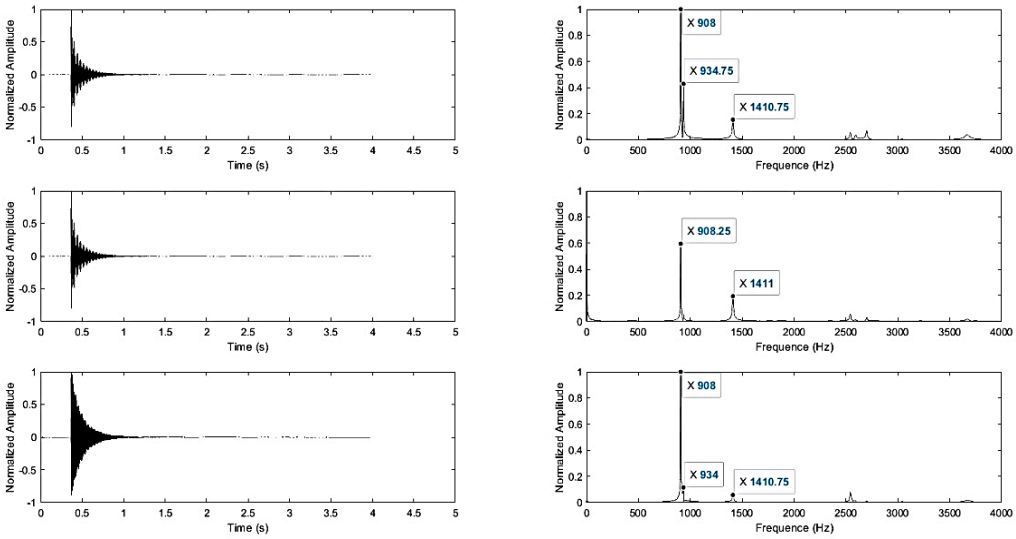

Figure 5.23 Vibration analysis results of the sample having 85-degrees filament wound, cured at 90°C and without delamination

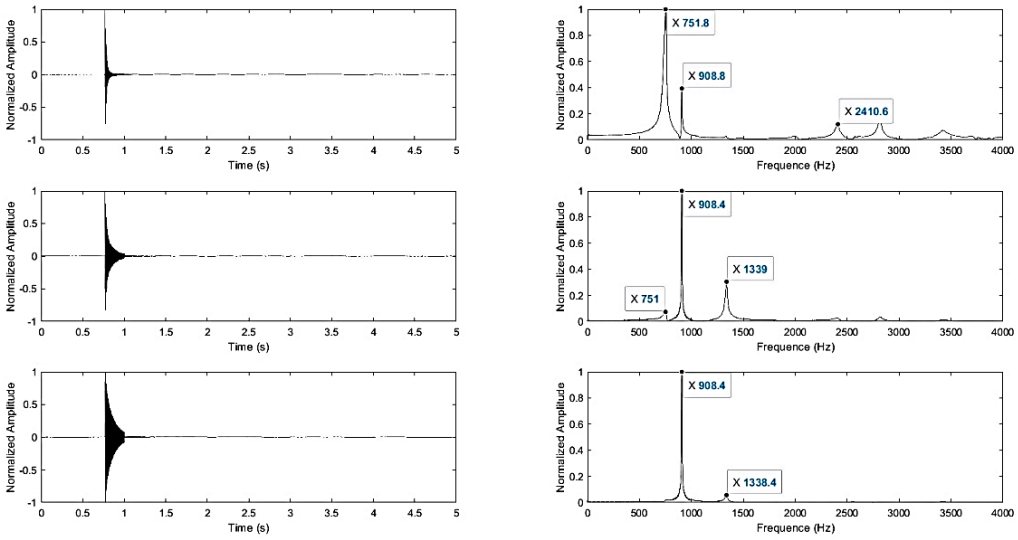

Figure 5.24 Vibration analysis results of the sample having 85-degrees filament wound, cured at 120°C and delamination at edge

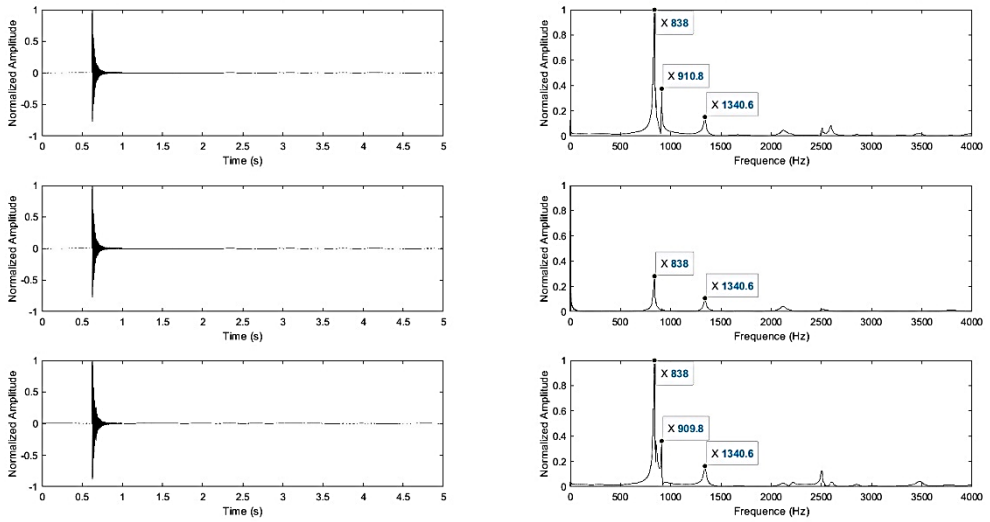

Figure 5.25 Vibration analysis results of the sample having 85-degrees filament wound, cured at 120°C and delamination in the middle

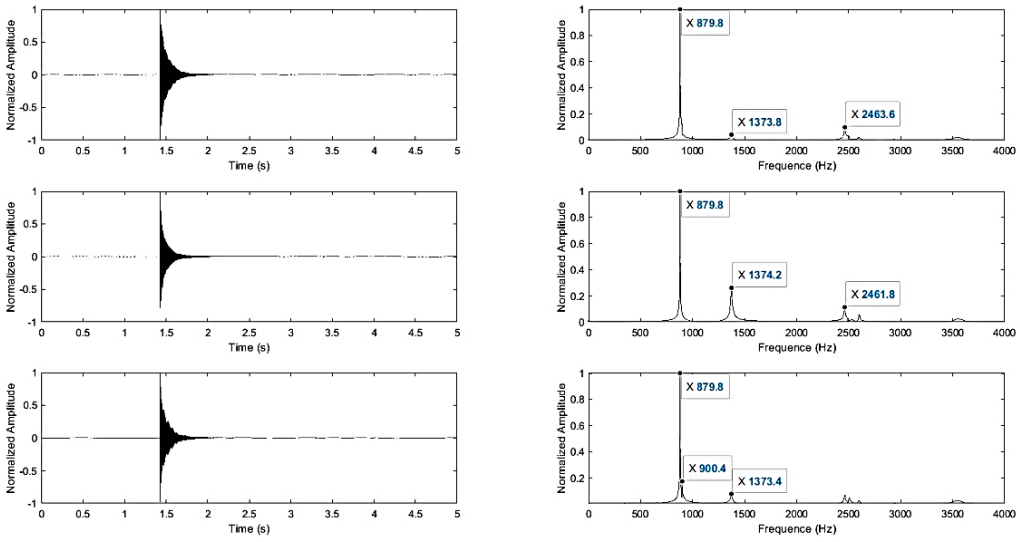

Figure 5.26 Vibration analysis results of the sample having 85-degrees filament wound, cured at 120°C and without delamination

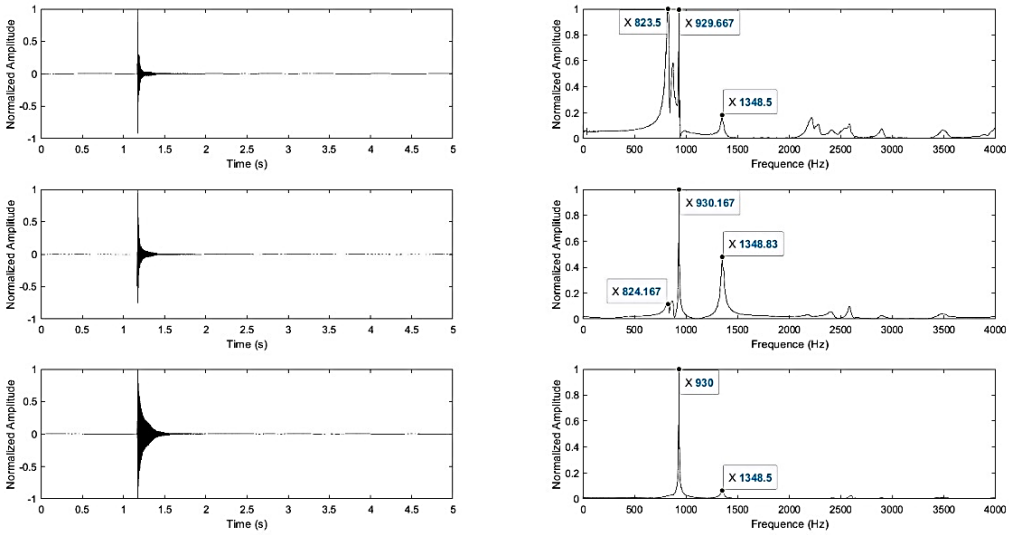

Figure 5.27 Vibration analysis results of the sample having 85-degrees filament wound, cured at 140°C and delamination at edge

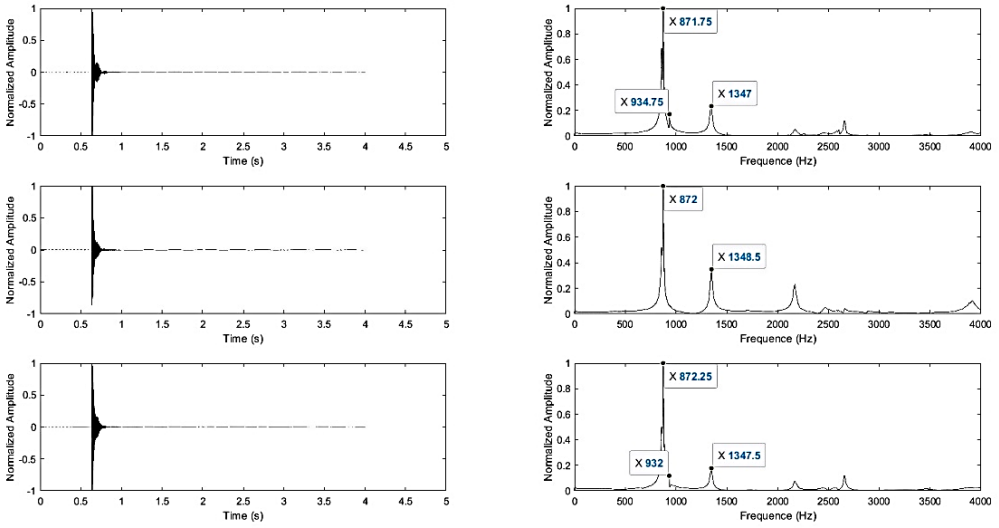

Figure 5.28 Vibration analysis results of the sample having 85-degrees filament wound, cured at 140°C and delamination in the middle

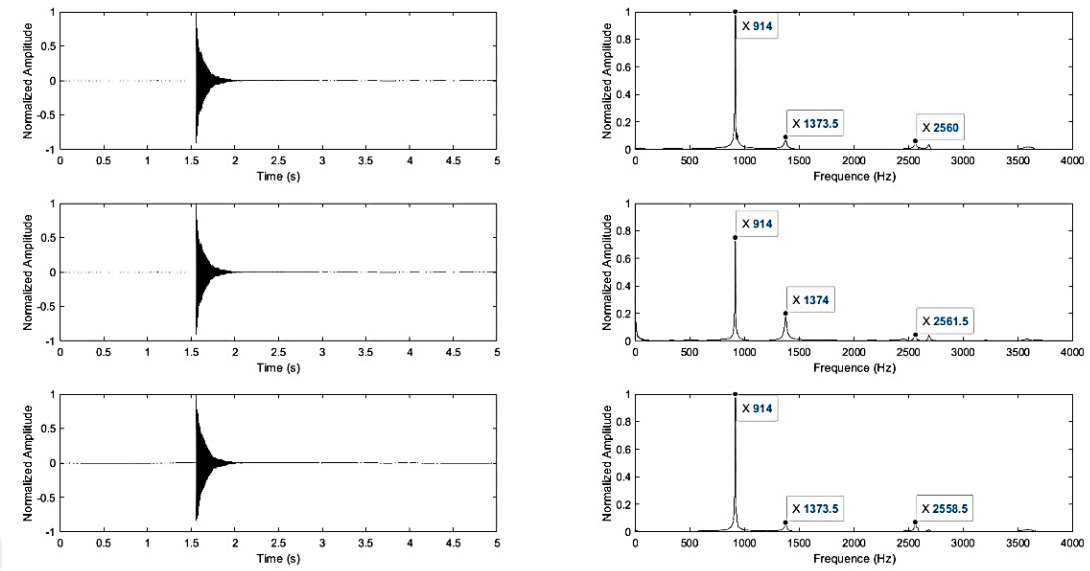

Figure 5.29 Vibration analysis results of the sample having 85-degrees filament wound, cured at 140°C and without delamination

In Figure 5.30-Figure 5.38 the variation of the first, second, and third natural frequencies regarding different 85 degrees, curing temperature, delamination positions, and are shown.

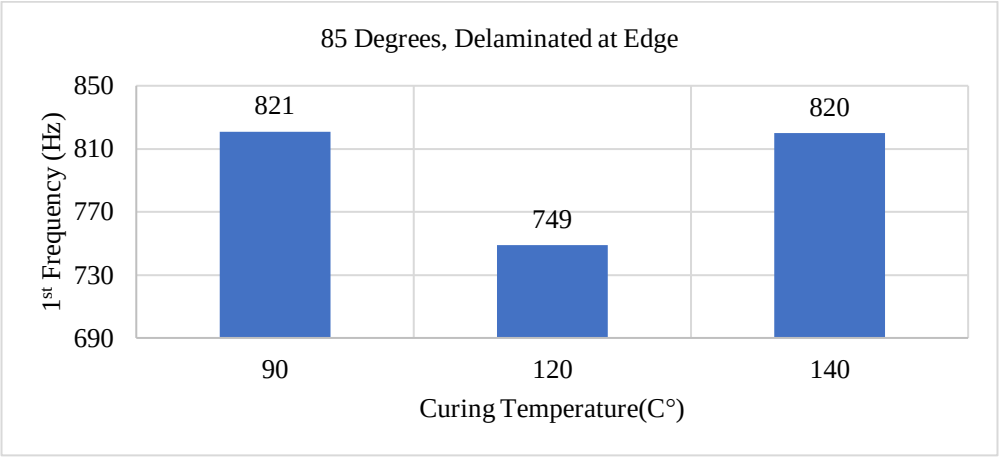

Figure 5.30 85 degrees filament wound, D++, for 1st natural frequency

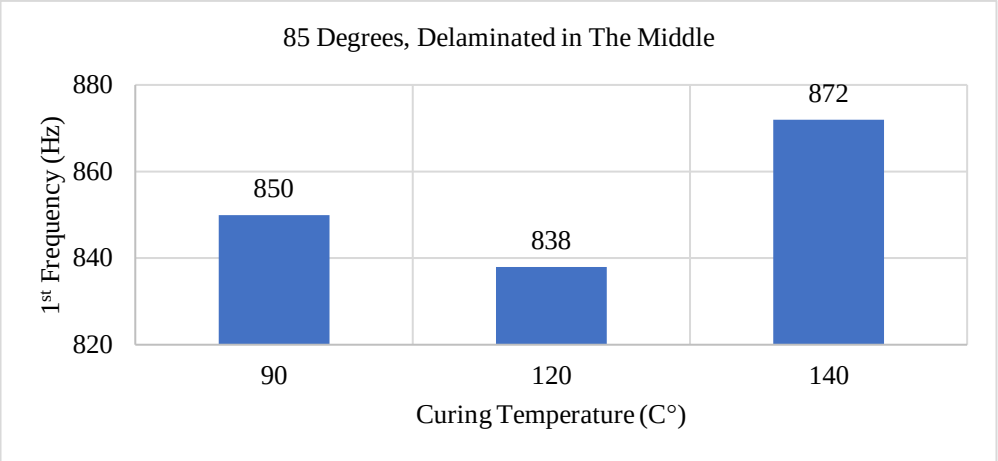

Figure 5.31 85 degrees filament wound, D+, for 1st natural frequency

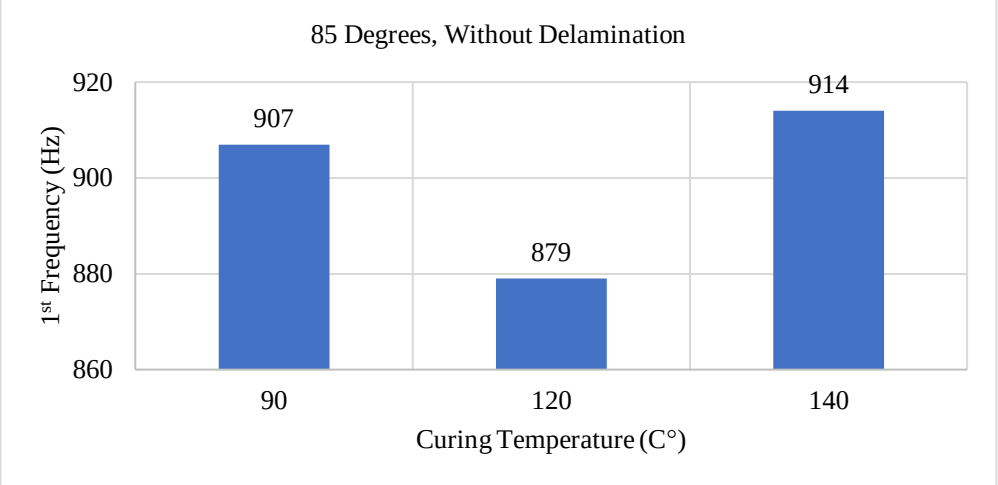

Figure 5.32 85 degrees filament wound, D-, for 1st Natural Frequency

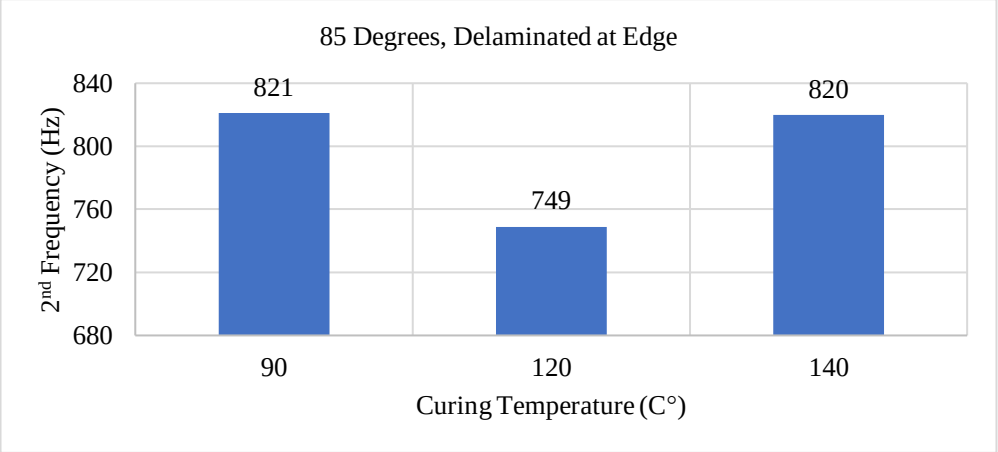

Figure 5.33 85 degrees filament wound, D++, for 2nd natural frequency

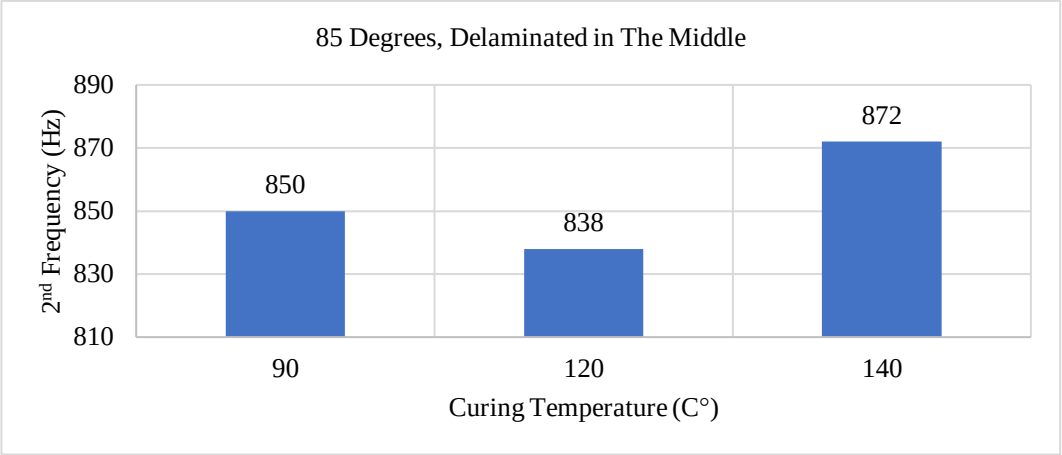

Figure 5.34 85 degrees filament wound, D+, for 2nd natural frequency

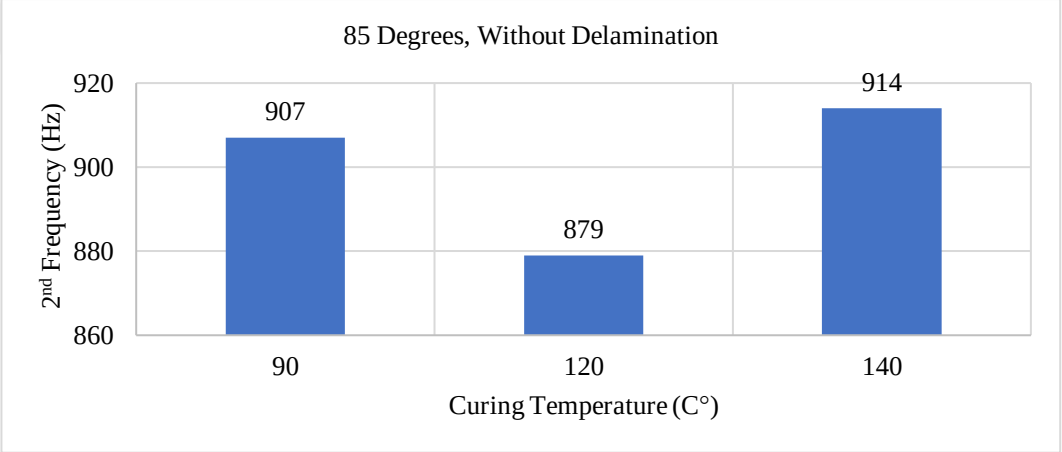

Figure 5.35 85 degrees filament wound, D-, for 2nd natural frequency

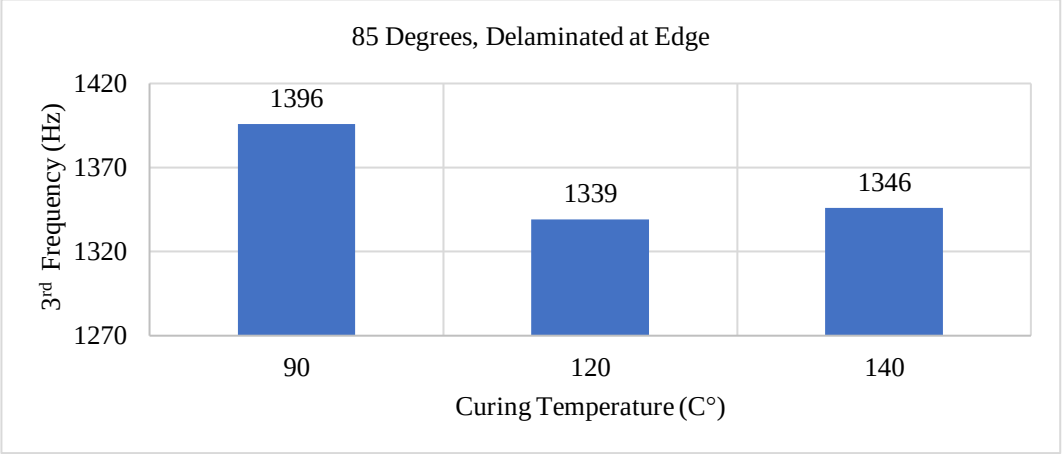

Figure 5.36 85 degrees filament wound, D++, for 3rd natural frequency

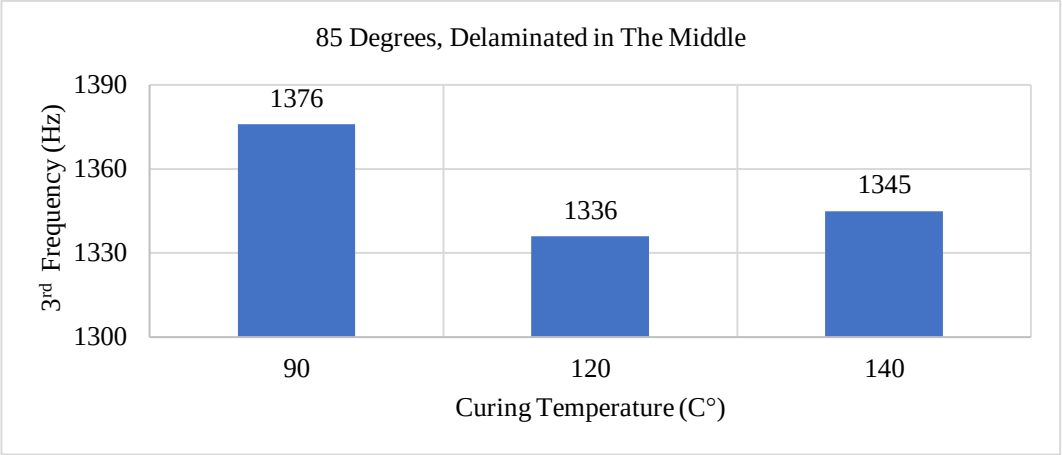

Figure 5.37 85 degrees filament wound, D+, for 3rd natural frequency

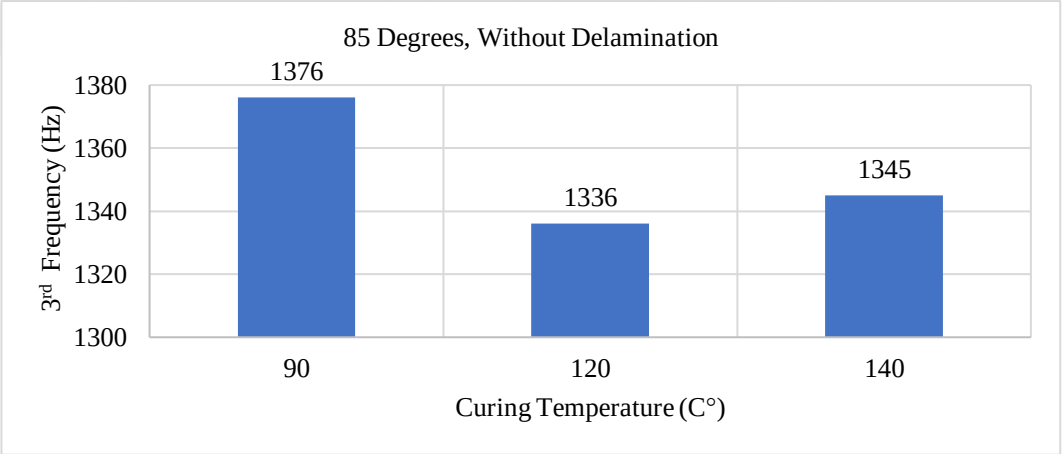

Figure 5.38 85 degrees filament wound, D-, for 3rd natural frequency

In Figure 5.39-Figure 5.47 are shown samples wound at 75 degrees.

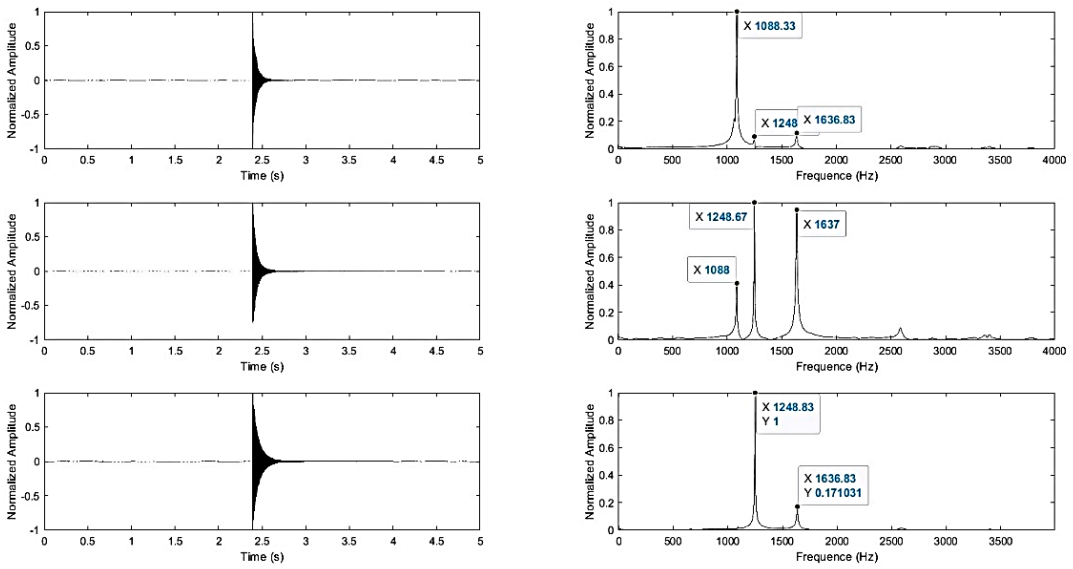

Figure 5.39 Vibration analysis results of the sample having 75- degrees filament wound, cured at 90°C and delamination at edge

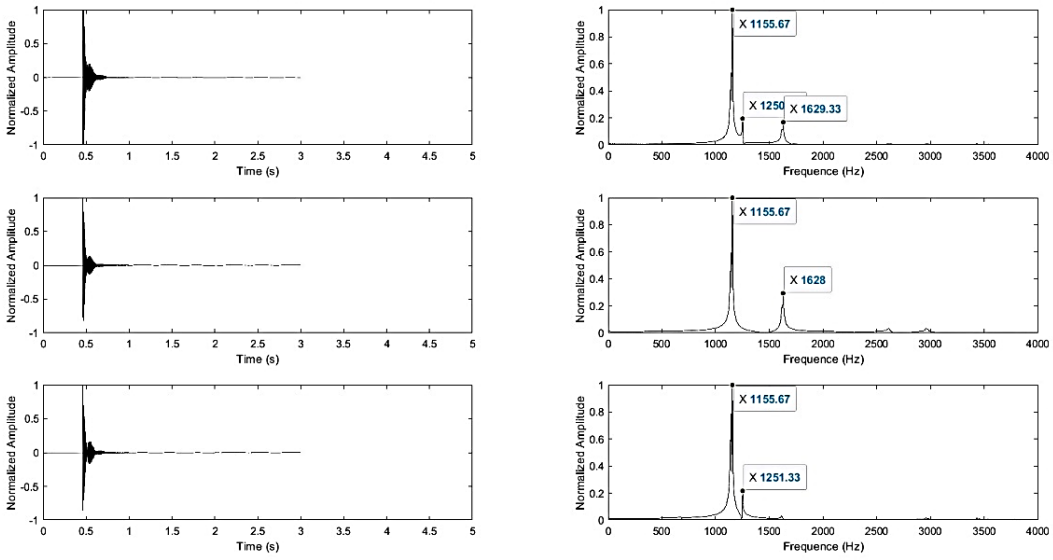

Figure 5.40 Vibration analysis results of the sample having 75- degrees filament wound, cured at 90°C and delamination in the middle

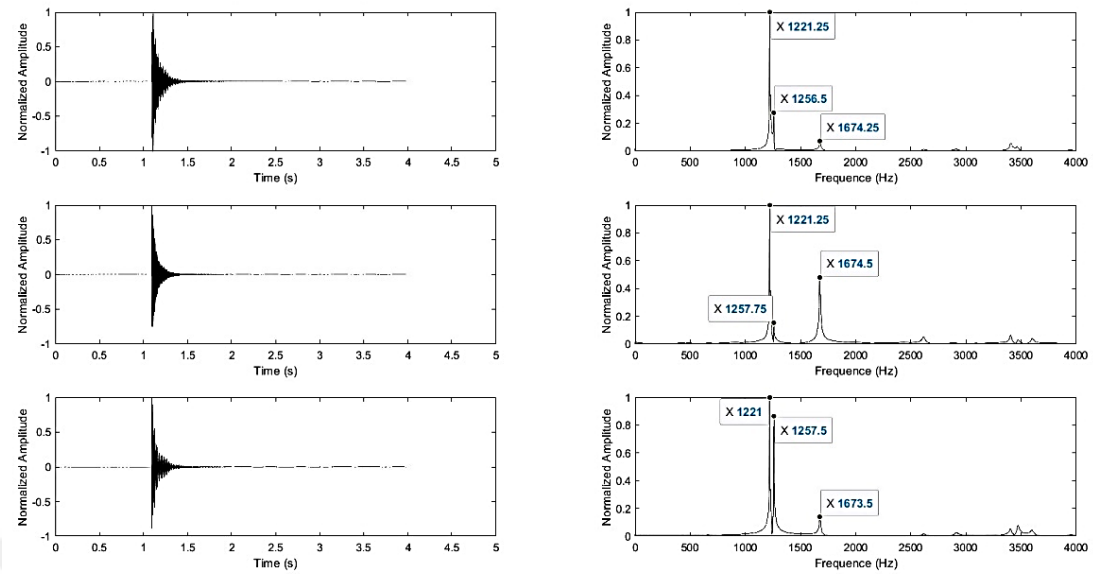

Figure 5.41 Vibration analysis results of the sample having 75- degrees filament wound, cured at 90°C and without delamination

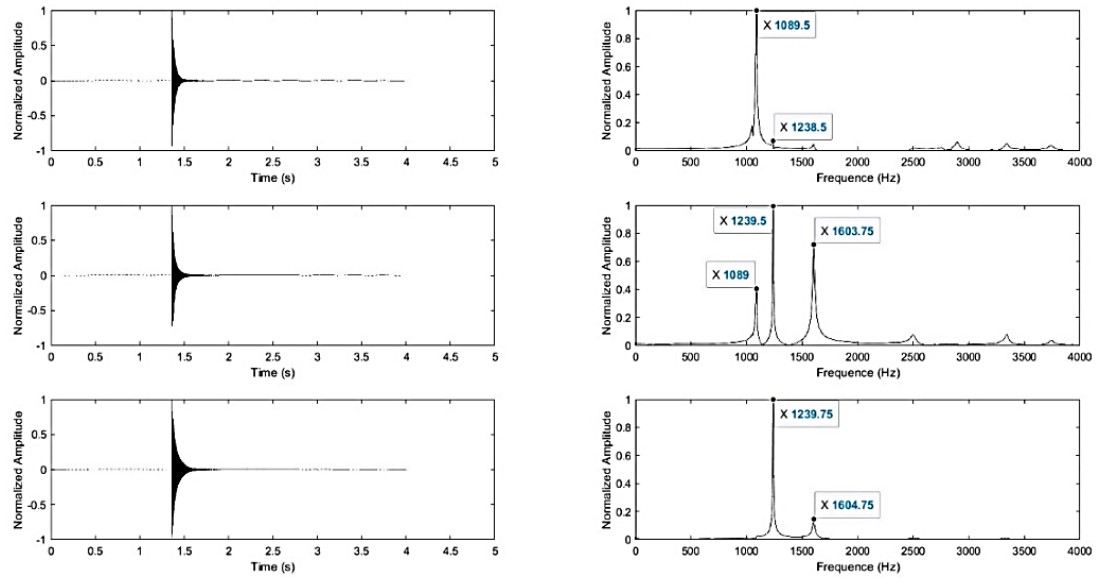

Figure 5.42 Vibration analysis results of the sample having 75- degrees filament wound, cured at 120°C and delamination at edge

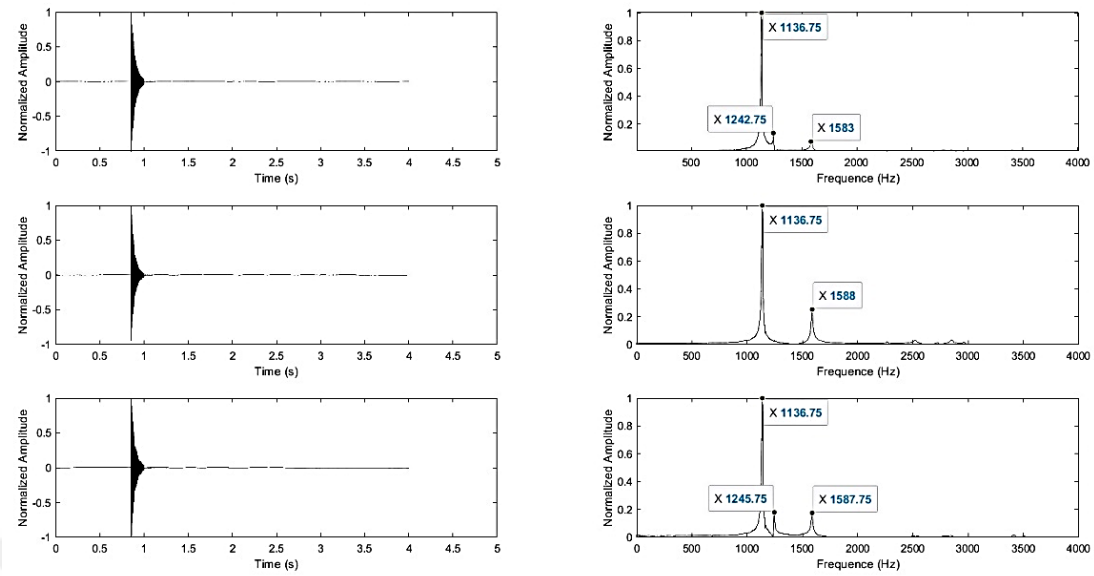

Figure 5.43 Vibration analysis results of the sample having 75- degrees filament wound, cured at 120°C and delamination in the middle

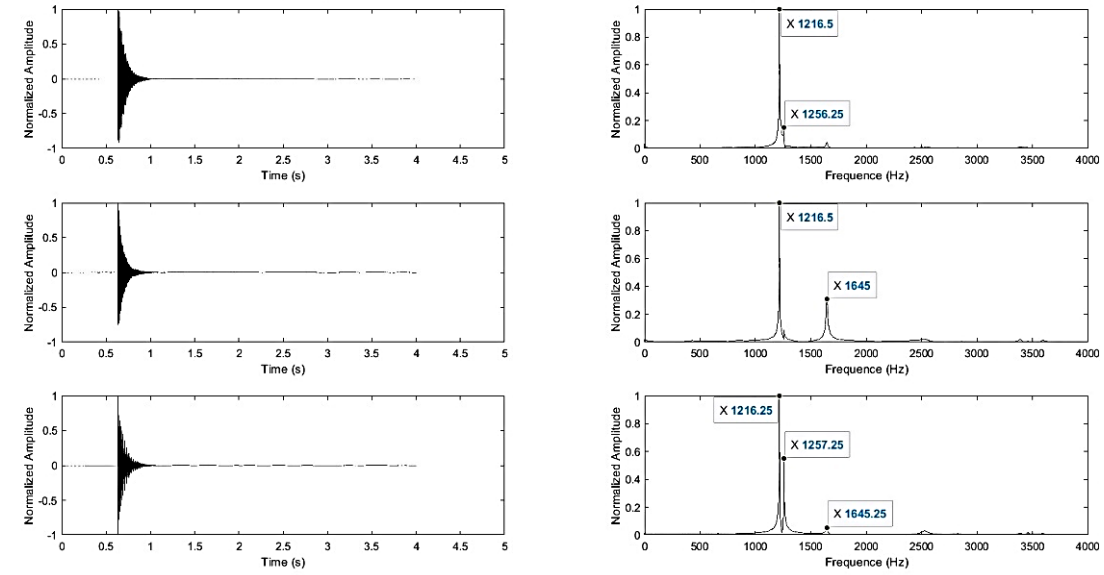

Figure 5.44 Vibration analysis results of the sample having 75- degrees filament wound, cured at 120°C and without delamination

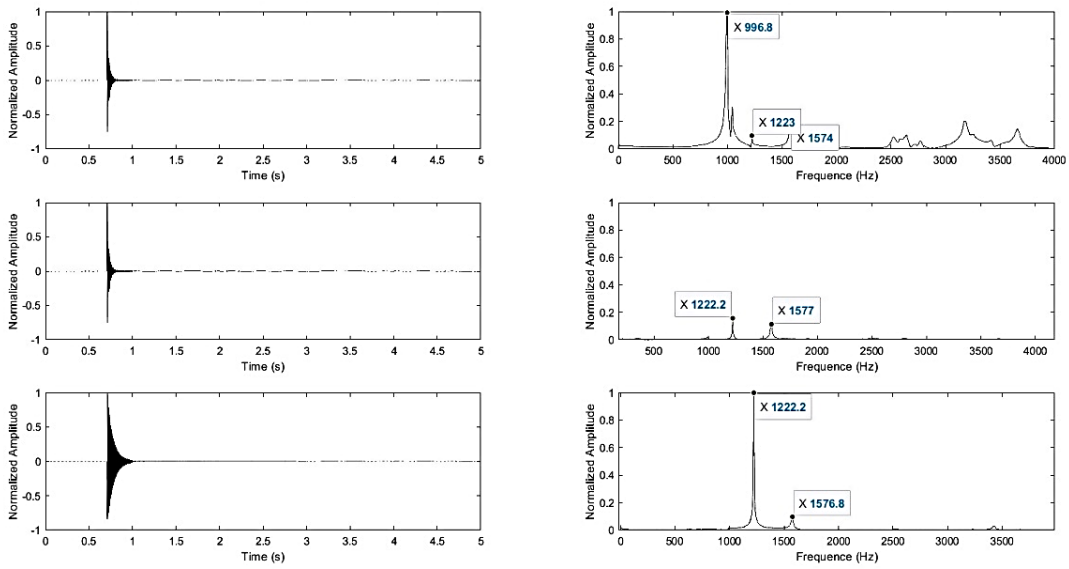

Figure 5.45 Vibration analysis results of the sample having 75- degrees filament wound, cured at 140°C and delamination at edge

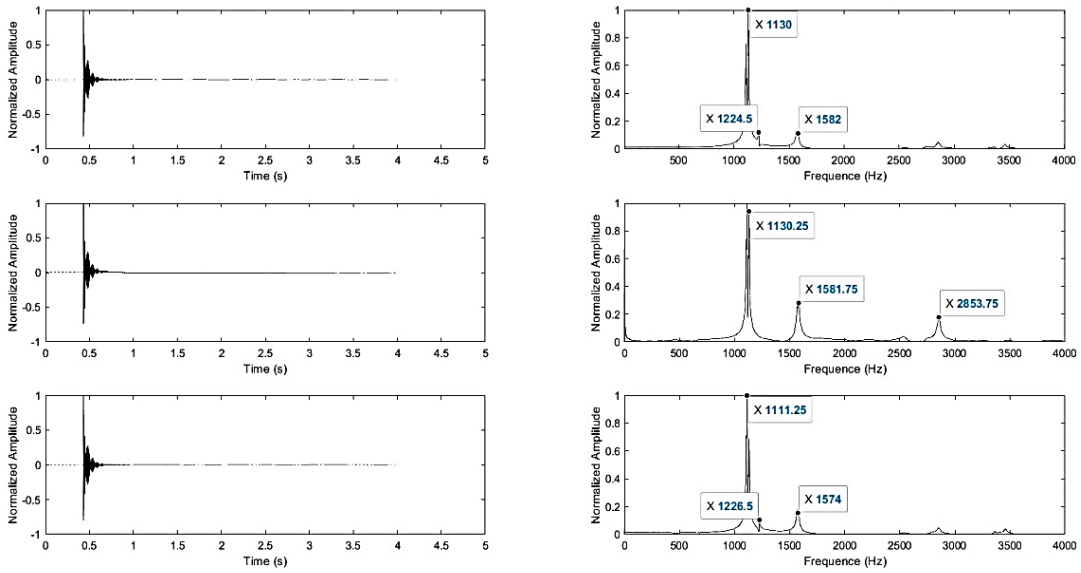

Figure 5.46 Vibration analysis results of the sample having 75- degrees filament wound, cured at 140°C and delamination in the middle

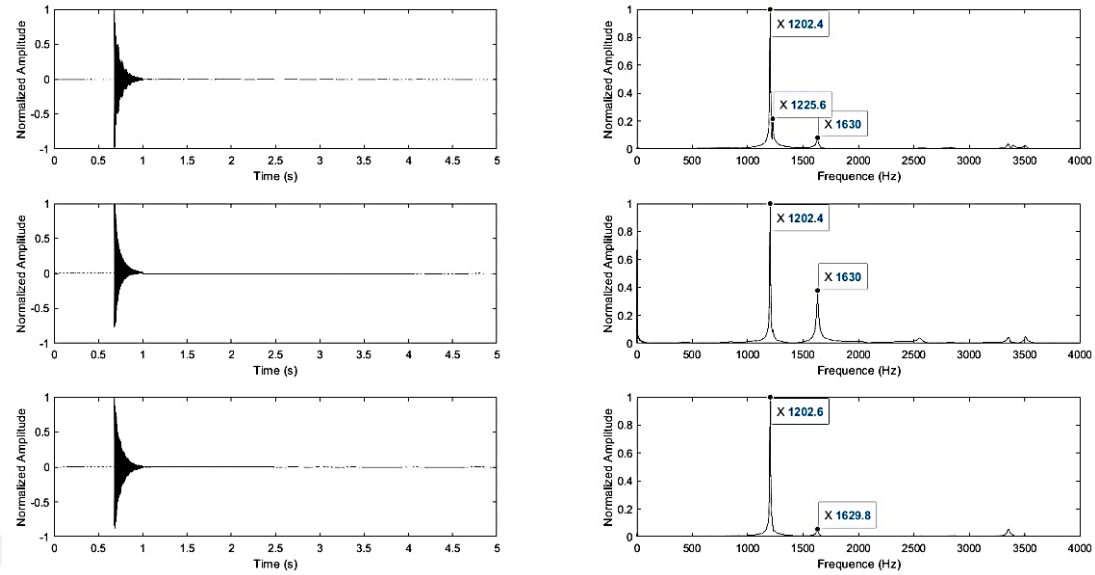

Figure 5.47 Vibration analysis results of the sample having 75- degrees filament wound, cured at 140°C and without delamination

In Figure 5.48-Figure 5.56, the variation of the first, second, and third natural frequencies regarding different 75 degrees filament wound, curing temperature, delamination positions, and are shown.

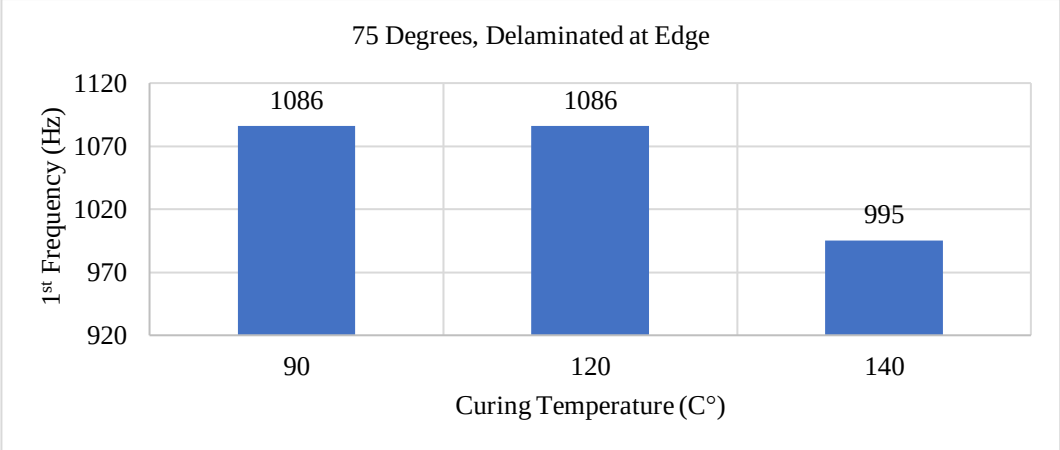

Figure 5.48 75 degrees filament wound, D++, for 1st natural frequency

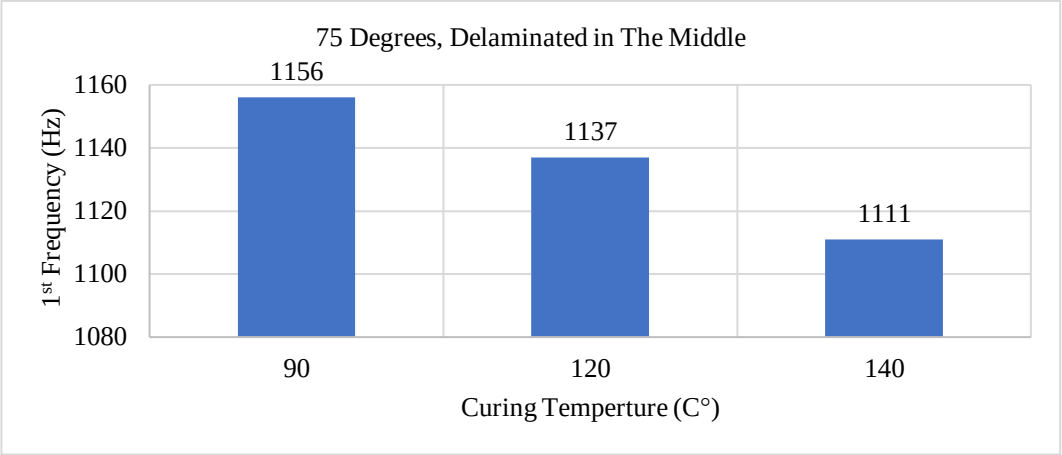

Figure 5.49 75 degrees filament wound, D+, for 1st natural frequency

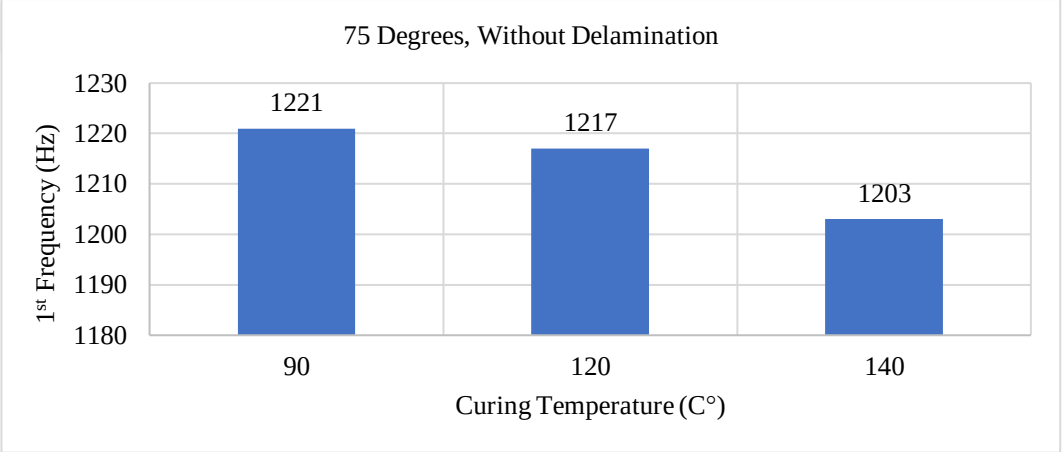

Figure 5.50 75 degrees filament wound, D-, for 1st natural frequency

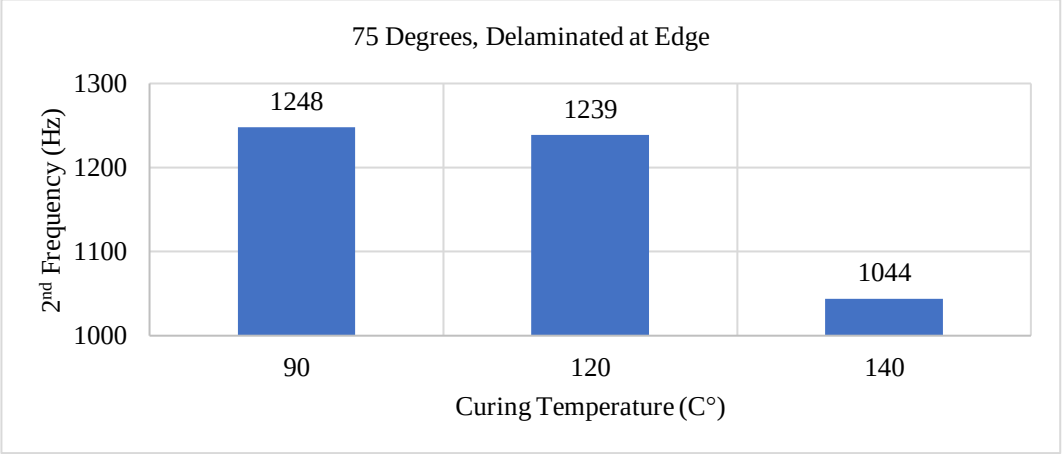

Figure 5.51 75 degrees filament wound, D++, for 2nd natural frequency

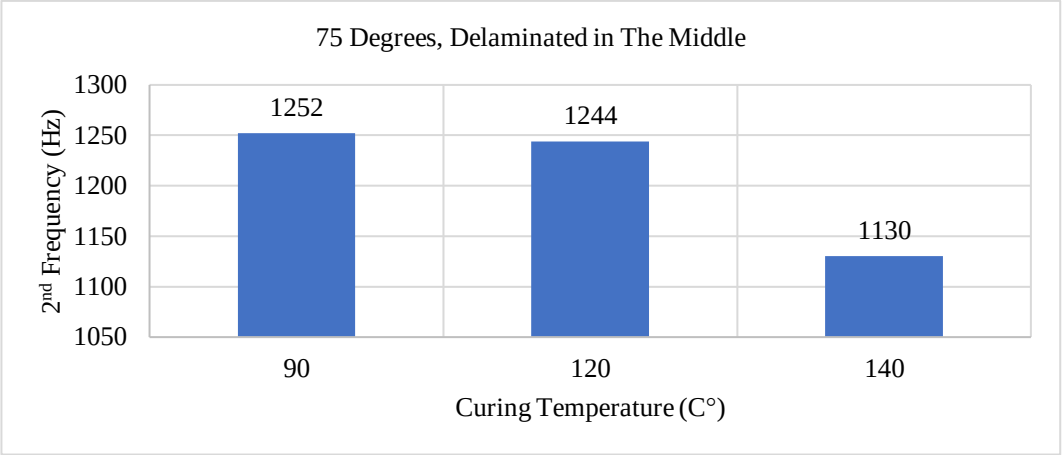

Figure 5.52 75 degrees filament wound, D+, for 2nd natural frequency

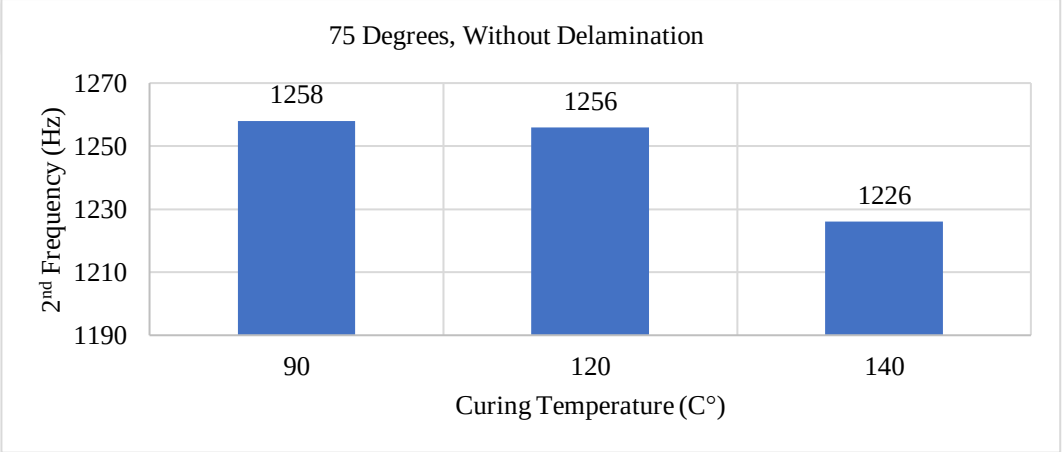

Figure 5.53 75 degrees filament wound, D-, for 2nd natural frequency

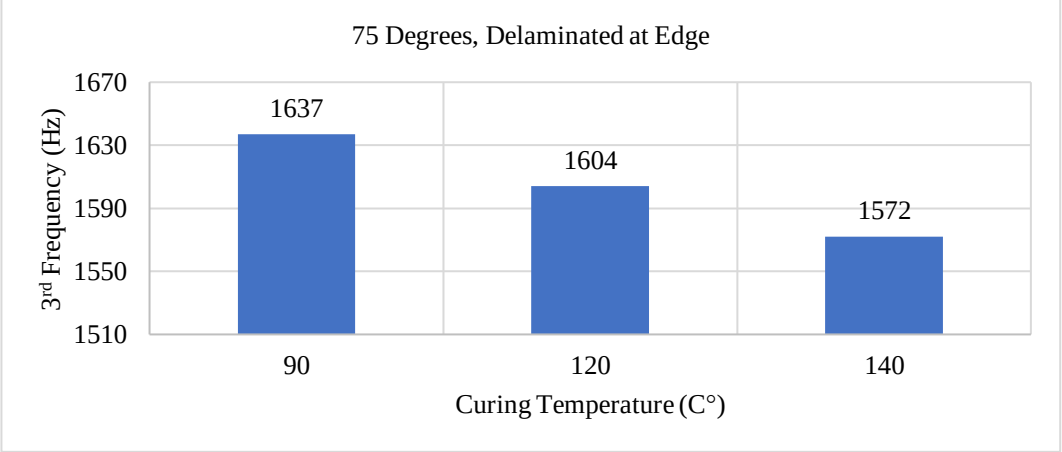

Figure 5.54 75 degrees filament wound, D++, for 3rd natural frequency

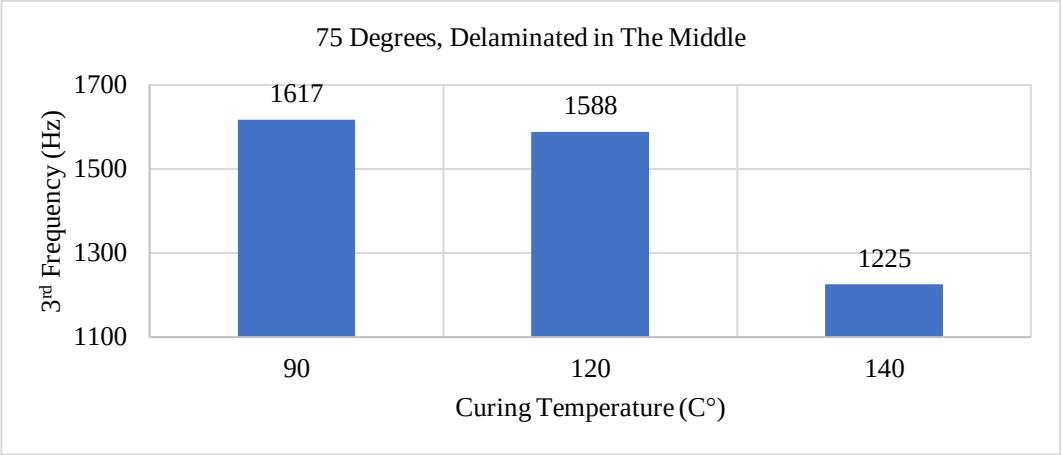

Figure 5.55 75 degrees filament wound, D+, for 3rd natural frequency

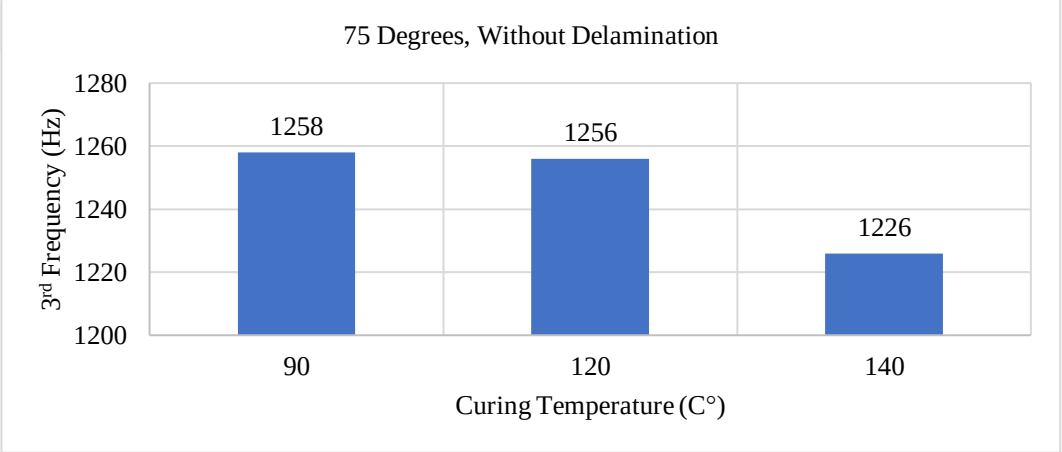

Figure 5.56 75 degrees filament wound, D-, for 3rd natural frequency

In Figure 5.57-Figure 5.65 are shown samples wound at 55 degrees.

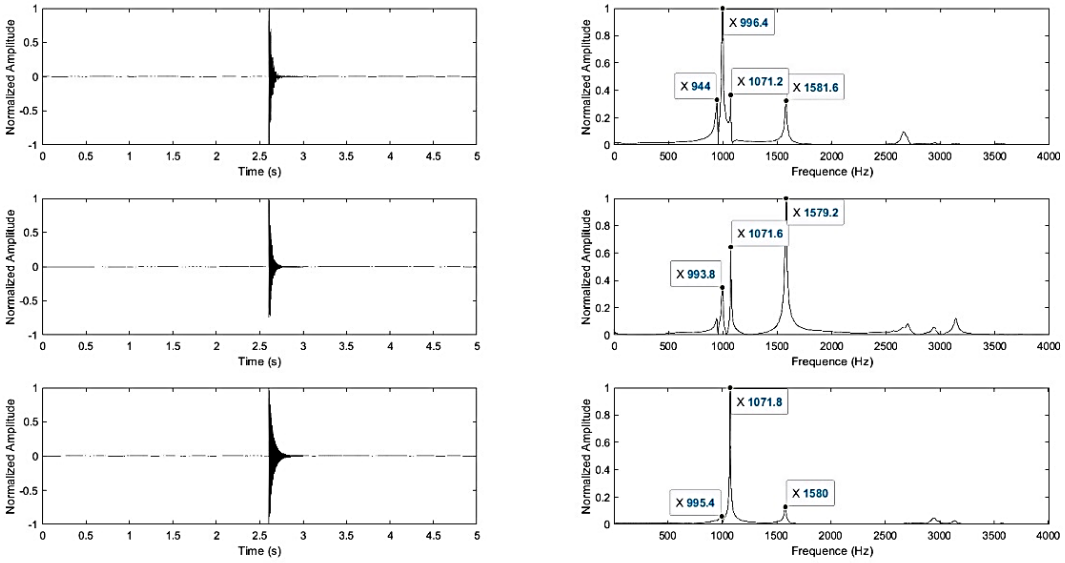

Figure 5.57 Vibration analysis results of the sample having 55- degrees filament wound, cured at 90°C and delamination at edge

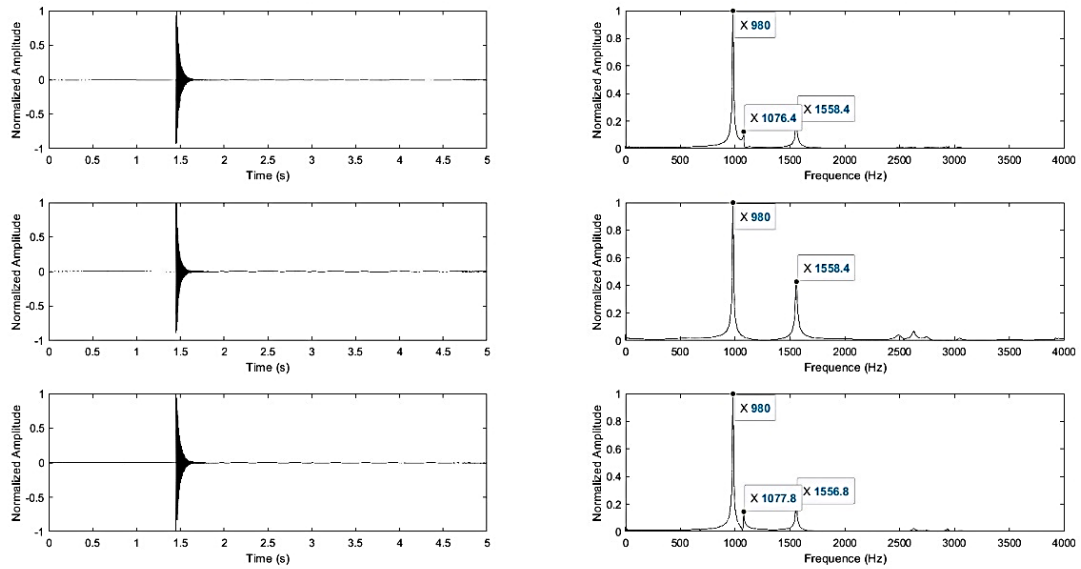

Figure 5.58 Vibration analysis results of the sample having 55- degrees filament wound, cured at 90°C and delamination in the middle

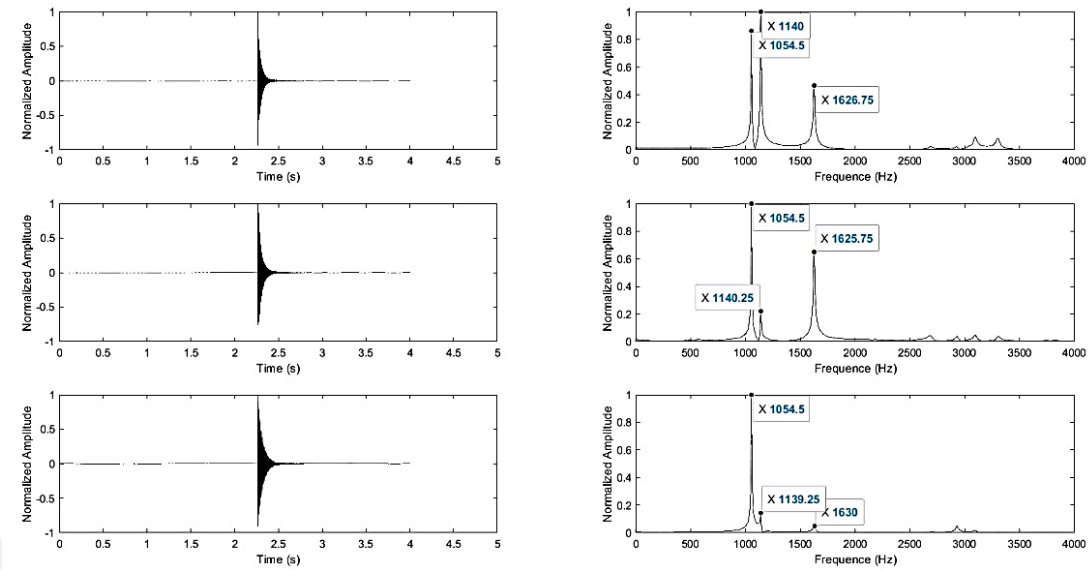

Figure 5.59 Vibration analysis results of the sample having 55 degrees filament wound, cured at 90°C and without delamination

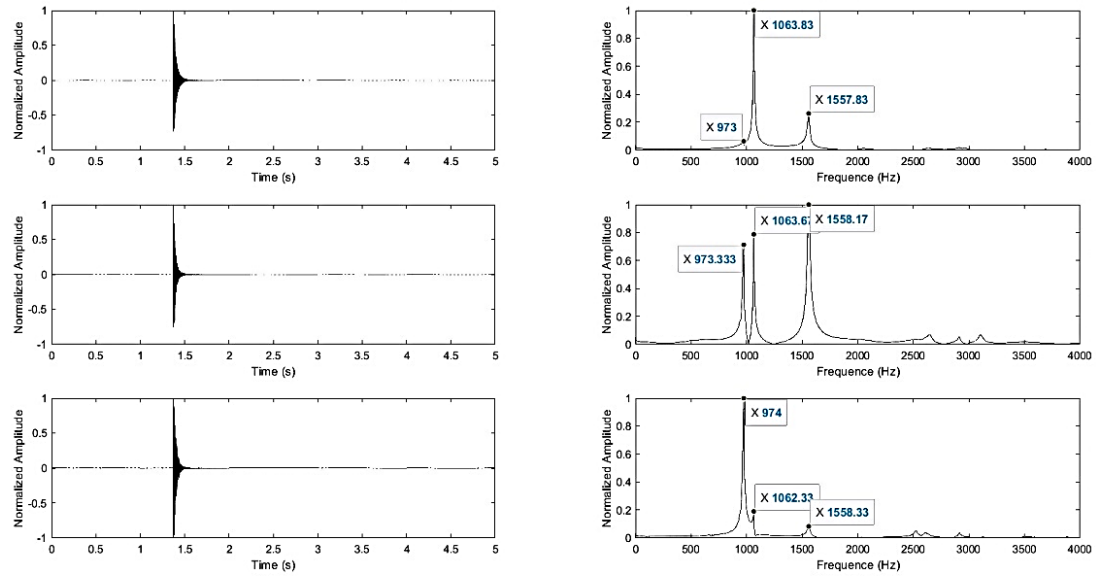

Figure 5.60 Vibration analysis results of the sample having 55- degrees filament wound, cured at 120°C and delamination at edge

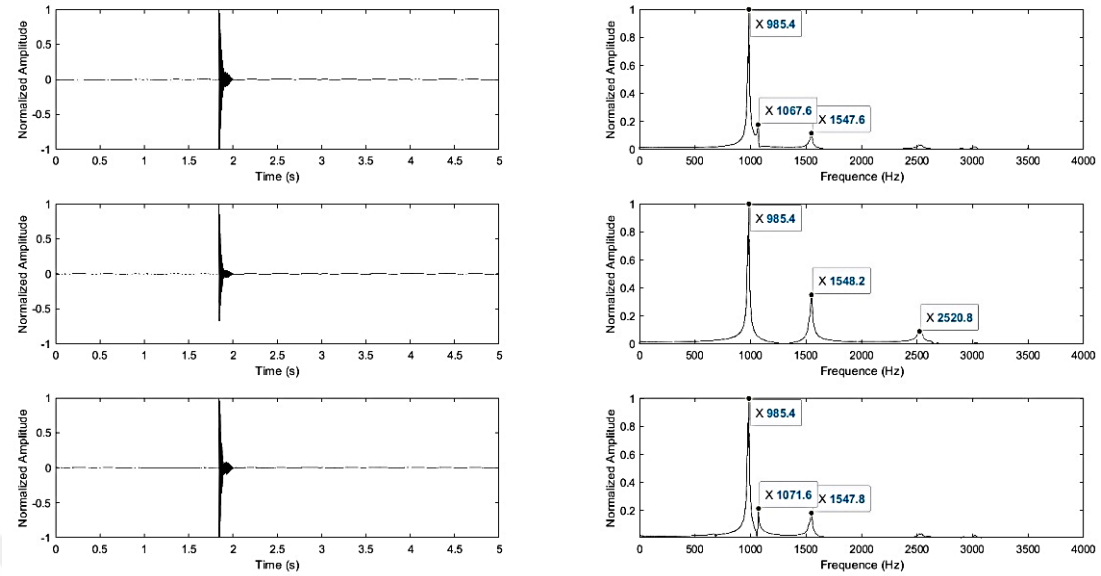

Figure 5.61 Vibration analysis results of the sample having 55- degrees filament wound, cured at 120°C and delamination in the middle

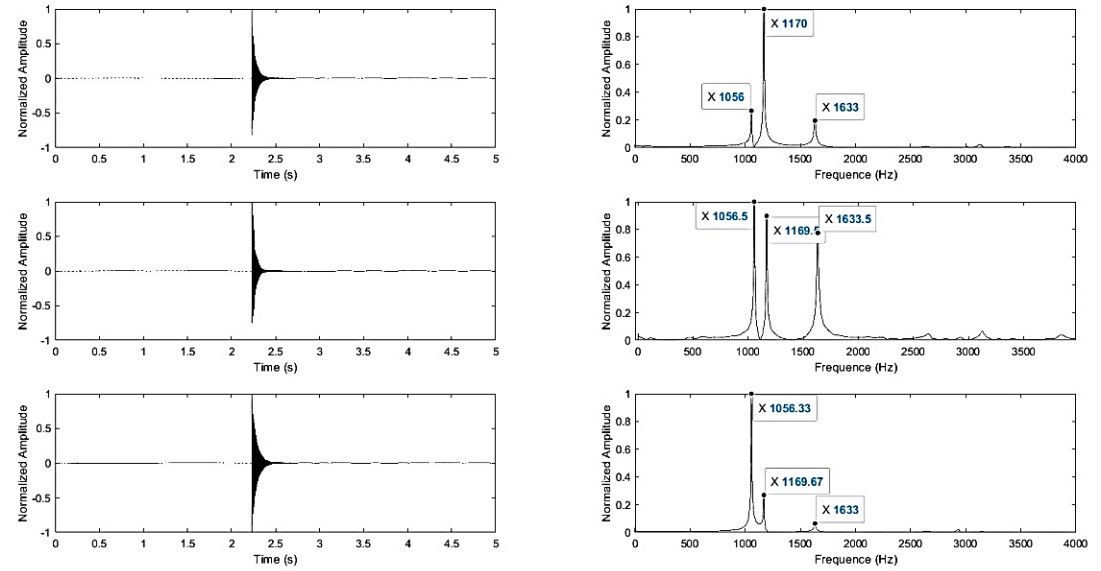

Figure 5.62 Vibration analysis results of the sample having 55- degrees filament wound, cured at 120°C and without delamination

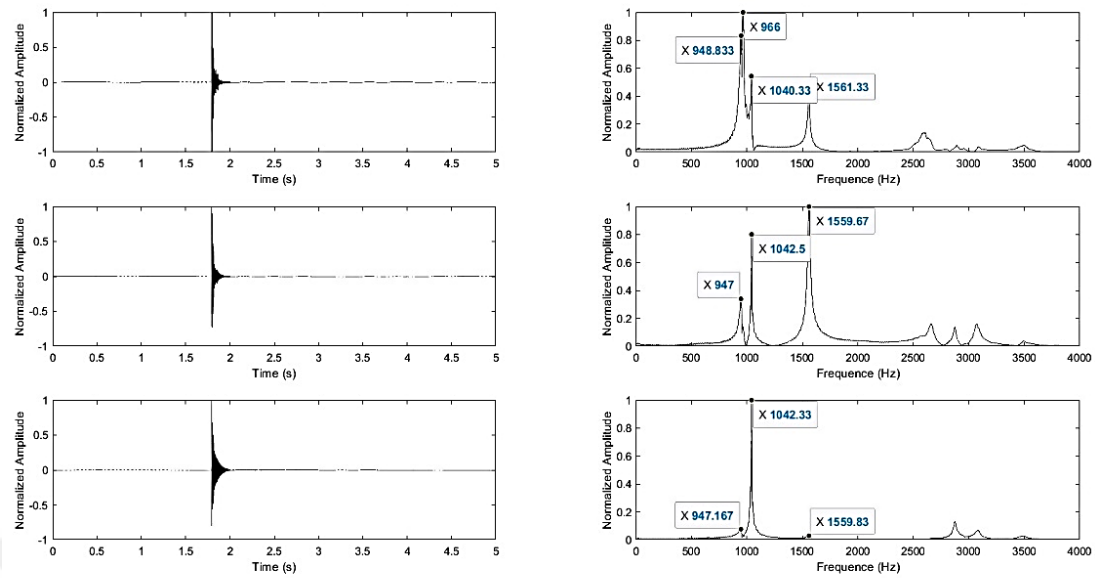

Figure 5.63 Vibration analysis results of the sample having 55- degrees filament wound, cured at 140°C and delamination at edge

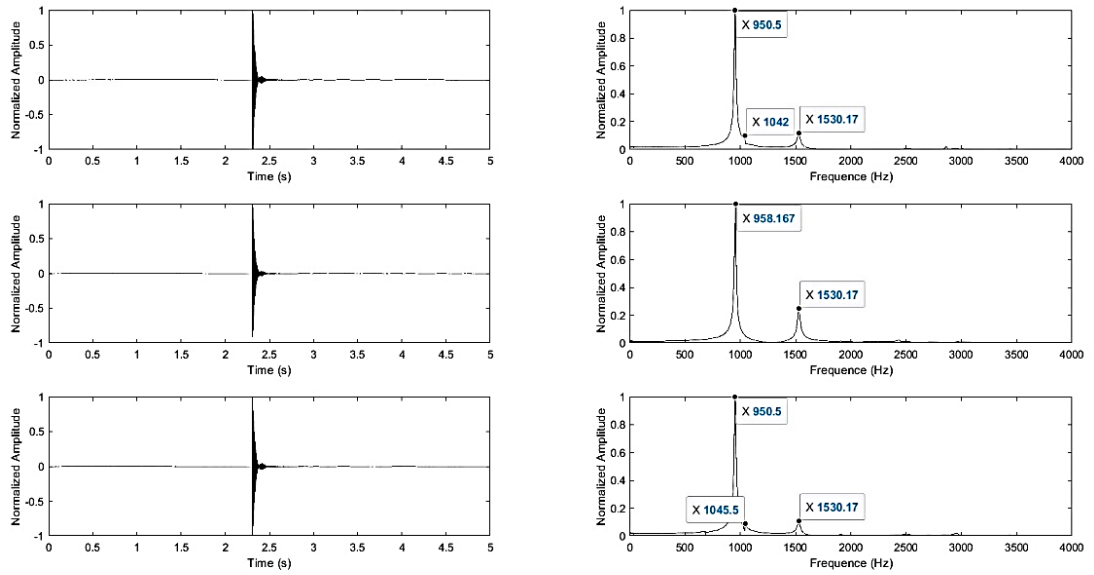

Figure 5.64 Vibration analysis results of the sample having 55- degrees filament wound, cured at 140°C and delamination in the middle

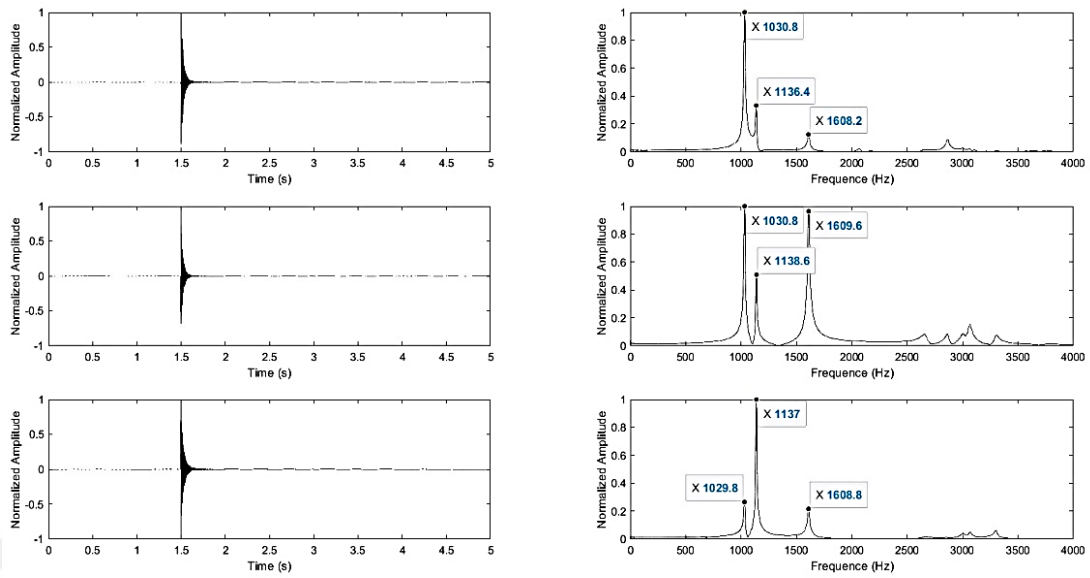

Figure 5.65 Vibration analysis results of the sample having 55- degrees filament wound, cured at 140°C and without delamination

In Figure 5.66-Figure 5.74, the variation of the first, second, and third natural frequencies regarding different 55 degrees, curing temperature, delamination positions, and are shown.

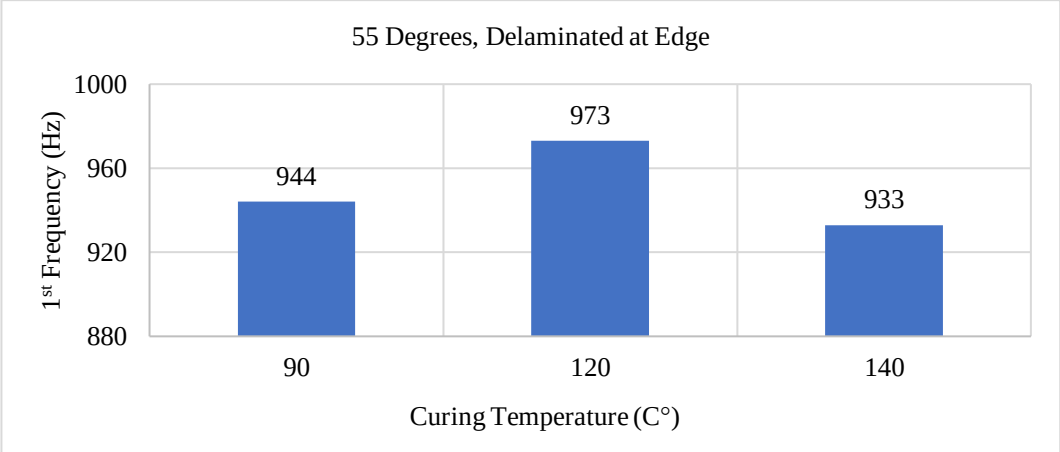

Figure 5.66 55 degrees filament wound, D++, for 1st natural frequency

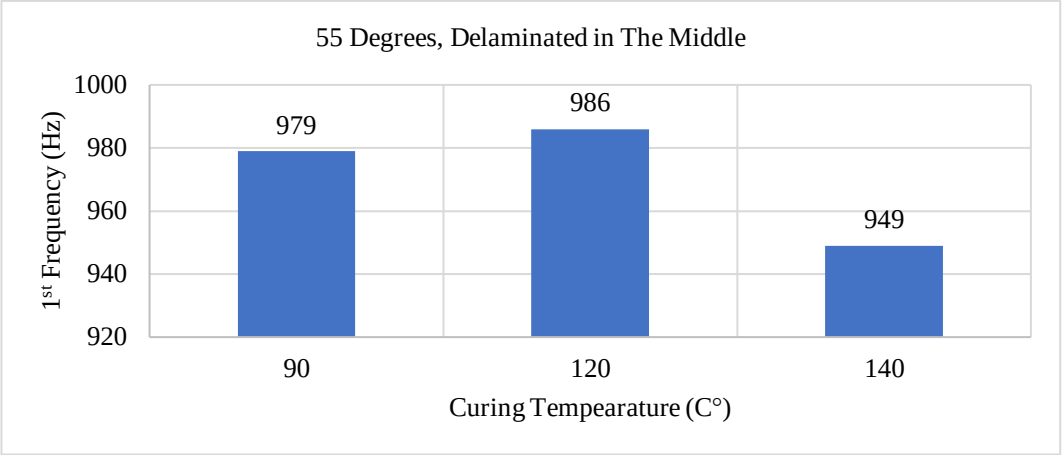

Figure 5.67 55 degrees filament wound, D+, for 1st natural frequency

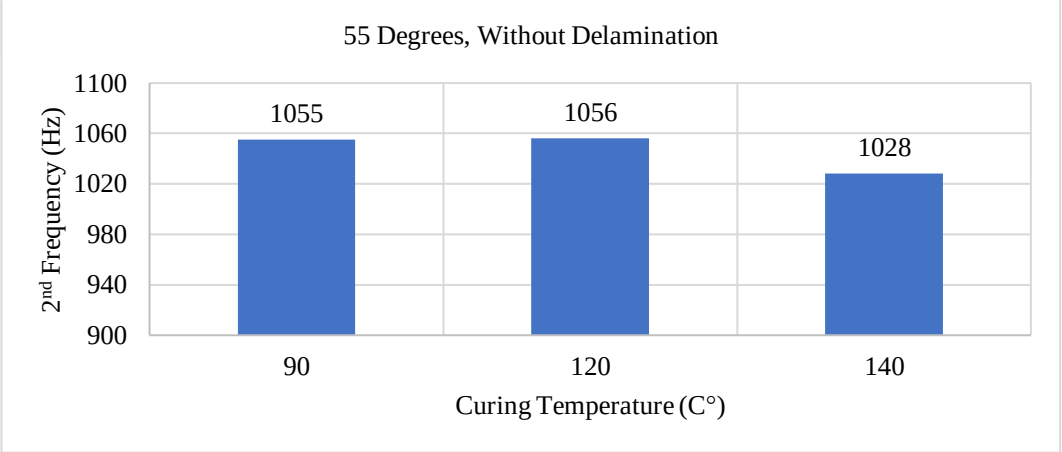

Figure 5.68 55 degrees filament wound, D-, for 1st natural frequency

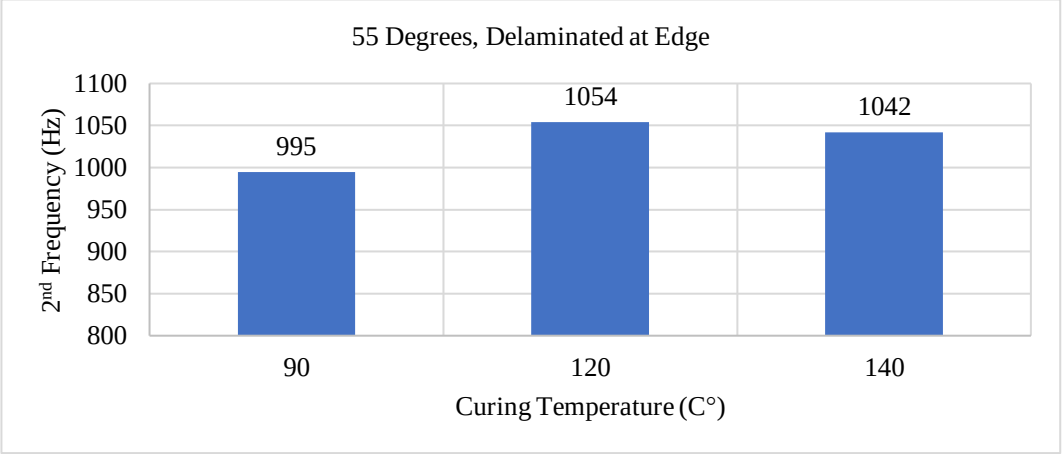

Figure 5.69 55 degrees filament wound, D++, for 2nd natural frequency

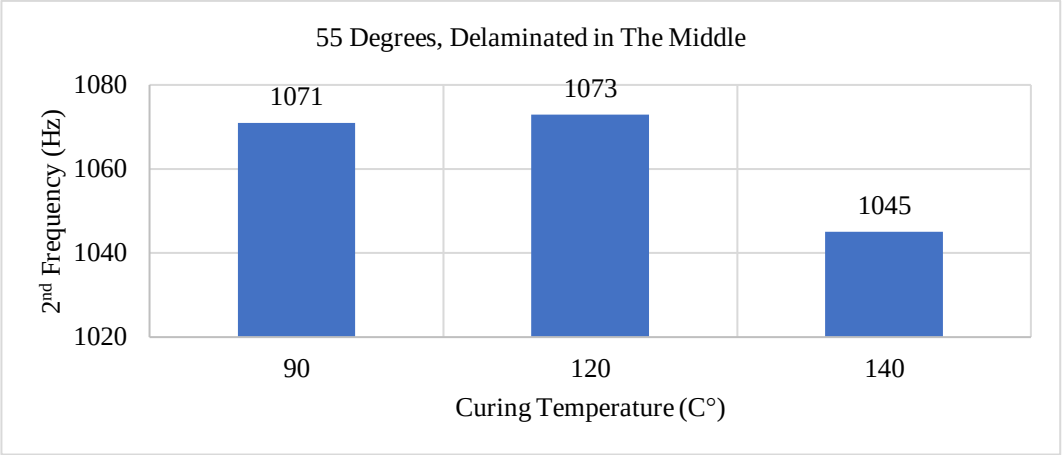

Figure 5.70 55 degrees filament wound, D+, for 2nd natural frequency

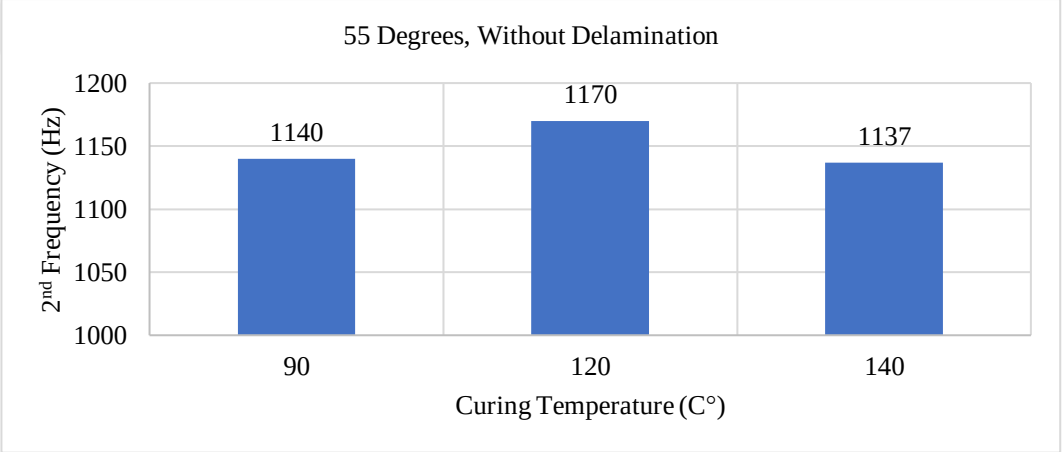

Figure 5.71 55 degrees filament wound, D-, for 2nd natural frequency

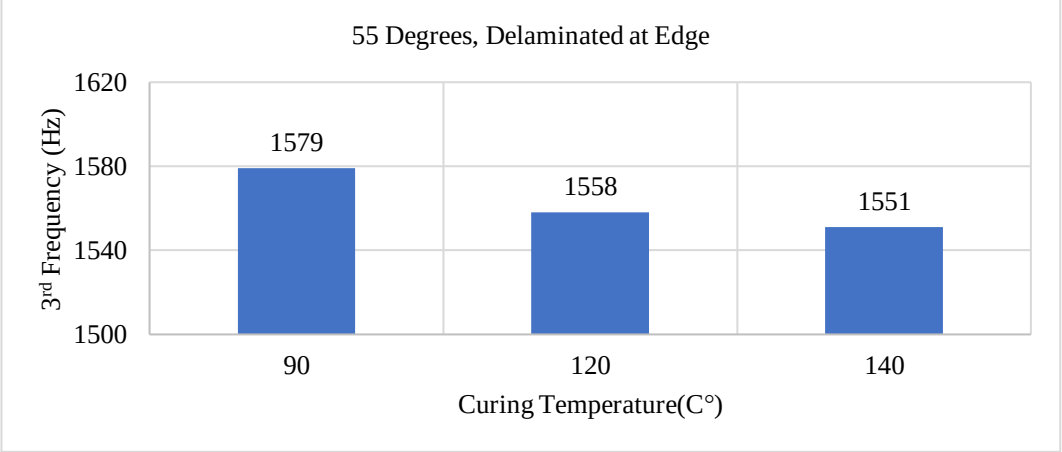

Figure 5.72 55 degrees filament wound, D++, for 3rd natural frequency

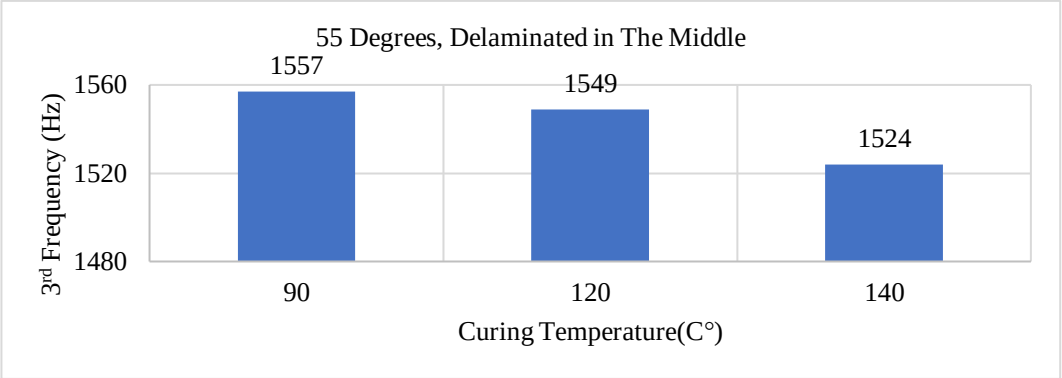

Figure 5.73 55 degrees filament wound, D+, for 3rd natural frequency

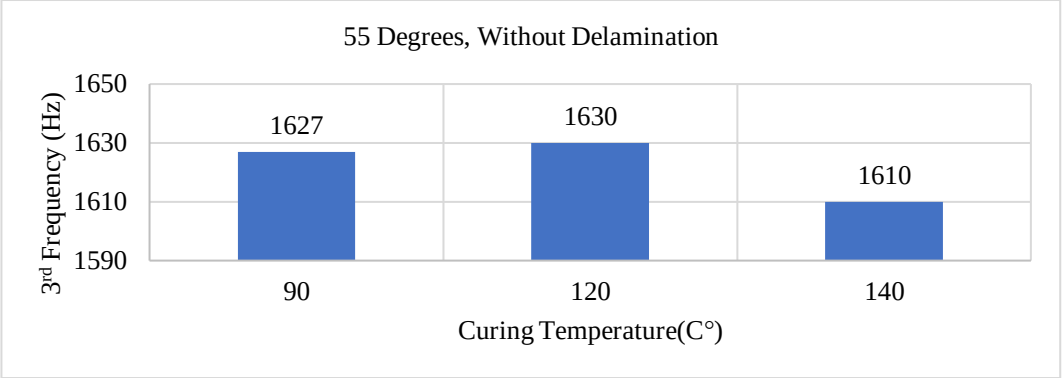

Figure 5.74 55 degrees filament wound, D-, for 3rd natural frequency

In Figure 5.75 the variation of natural frequency according to degrees of angle, and degrees of temperature for first natural frequency is shown. The highest natural frequency for all curing temperatures was obtained for specimens wound at 75 degrees.

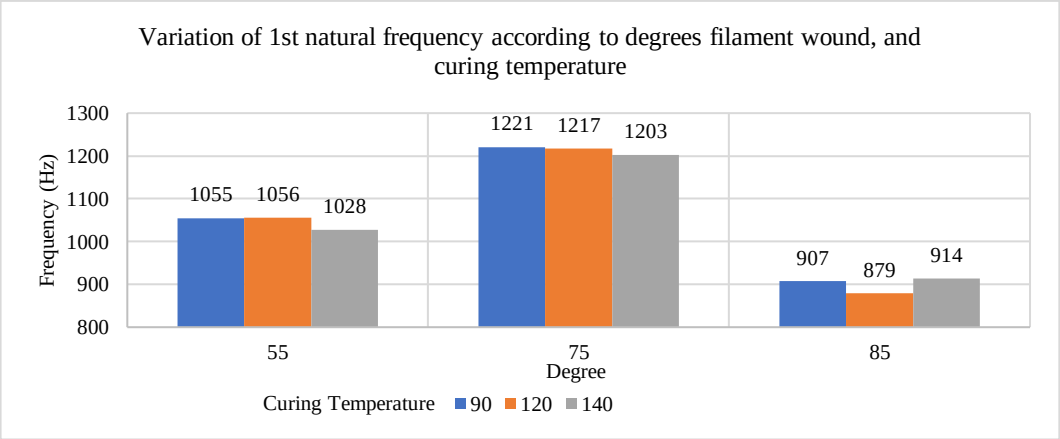

Figure 5.75 Variation of first natural frequency according to degrees filament wound, and curing temperature

5.4 Damping Ratio Results for Free-Free Boundary Condition

The damping ratio can be calculated using the logarithmic decrement method. In Figure 5.76-Figure 5.93, the variation of the damping ratio regarding different degrees, curing temperature, and delamination positions are shown.

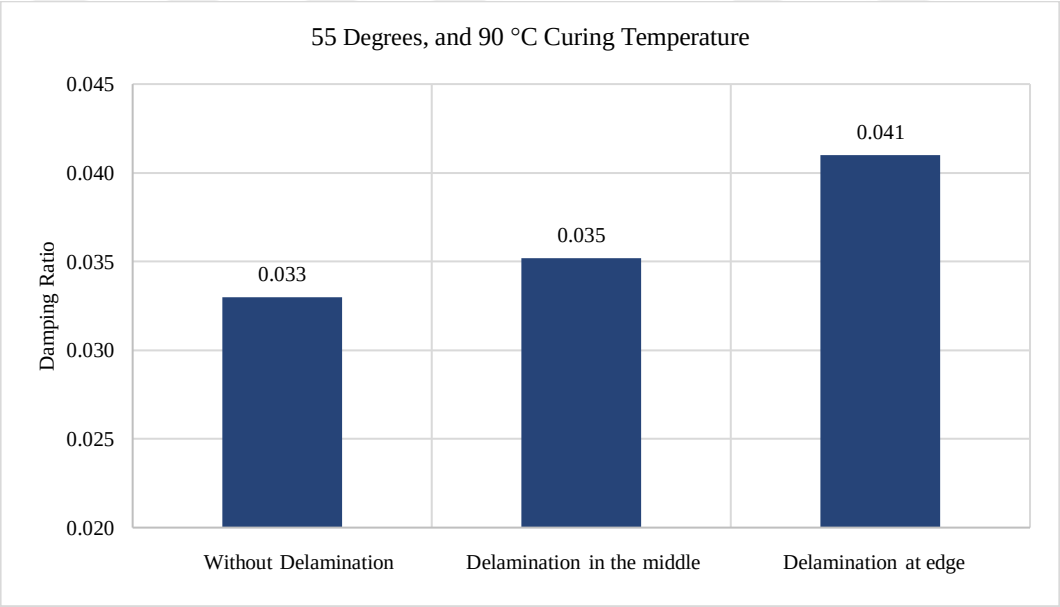

Figure 5.76 Damping ratio for 55 degrees filament wound, and 90 °C curing temperature

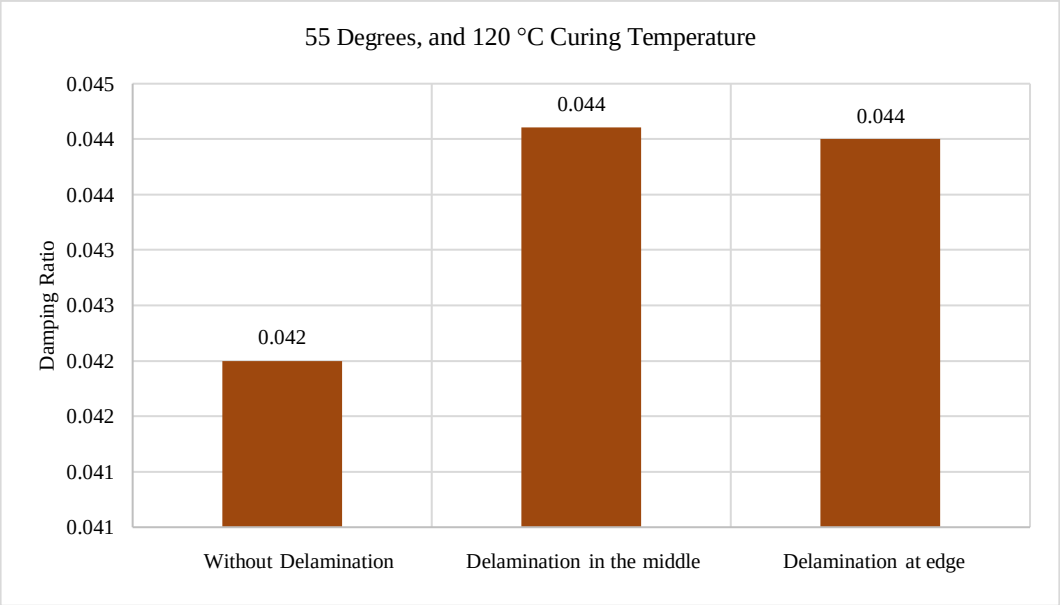

Figure 5.77 Damping ratio for 55 degrees filament wound, and 120 °C curing temperature

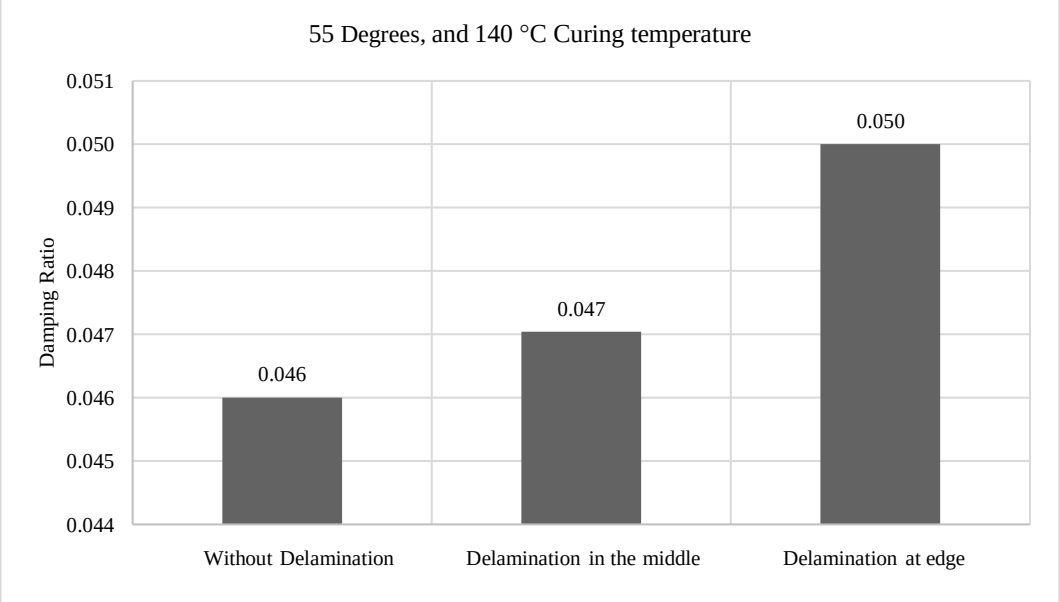

Figure 5.78 Damping ratio for 55 degrees filament wound, and 140 °C curing temperature

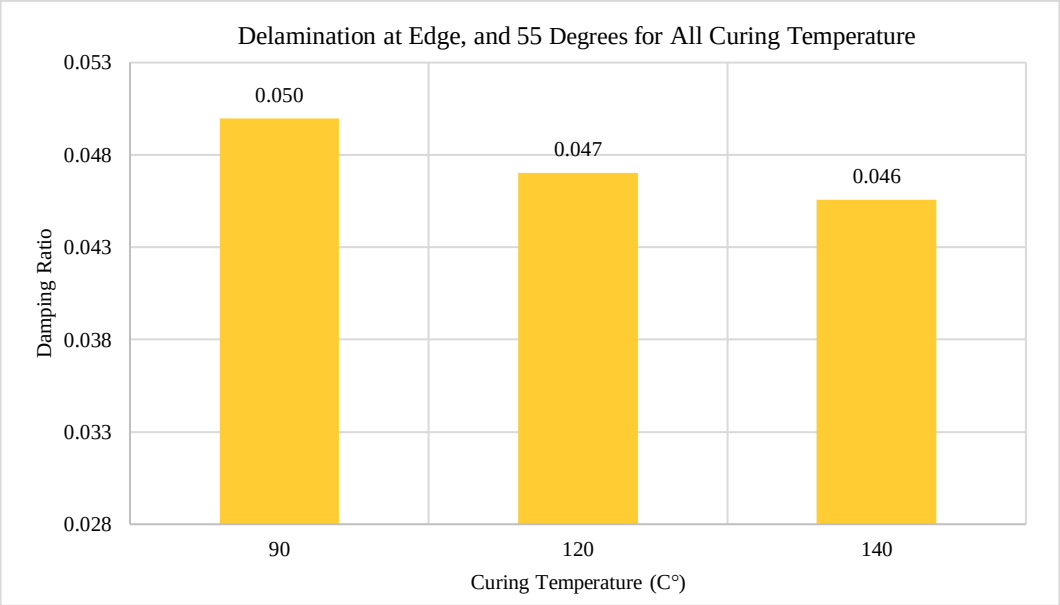

Figure 5.79 Damping ratio of the structure delamination at edge , and 55 degrees filament wound for all curing temperature

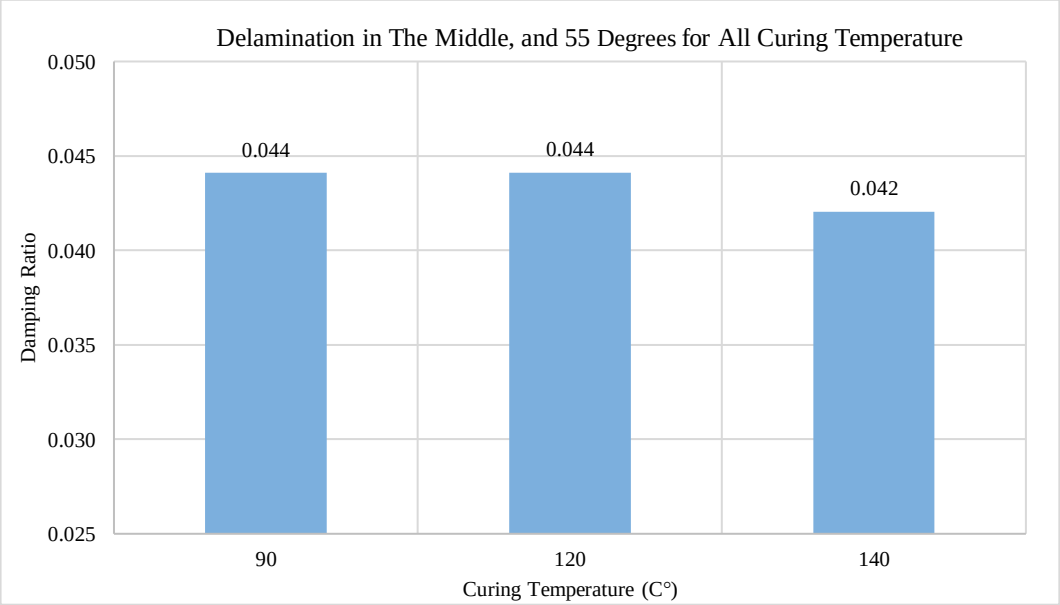

Figure 5.80 Damping ratio of the structure delamination in the middle, and 55 degrees filament wound for all curing temperature

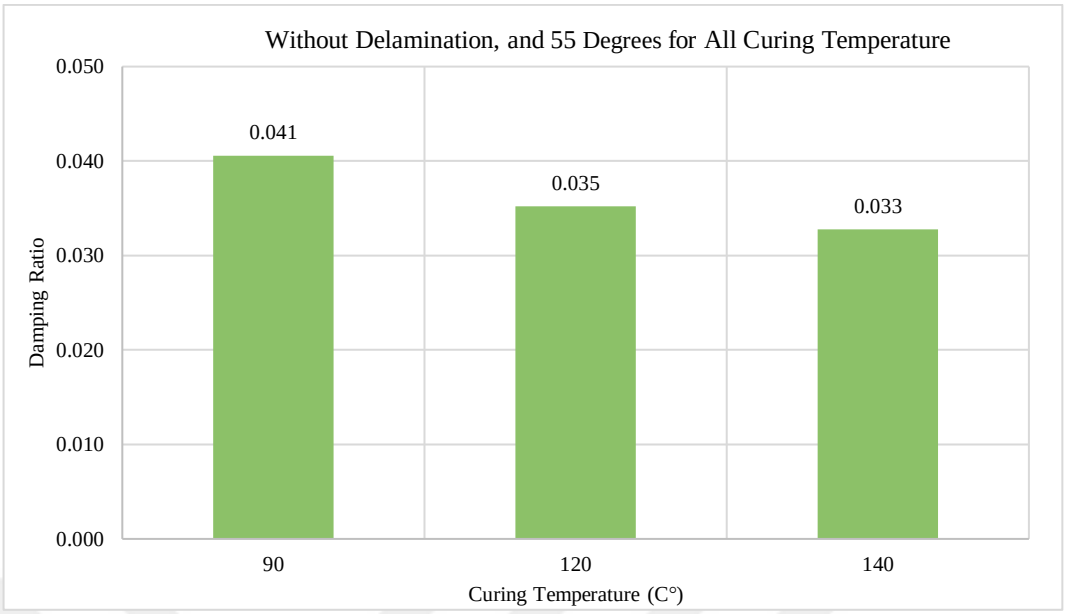

Figure 5.81 Damping ratio of the structure without delamination, and 55 degrees filament wound for all curing temperature

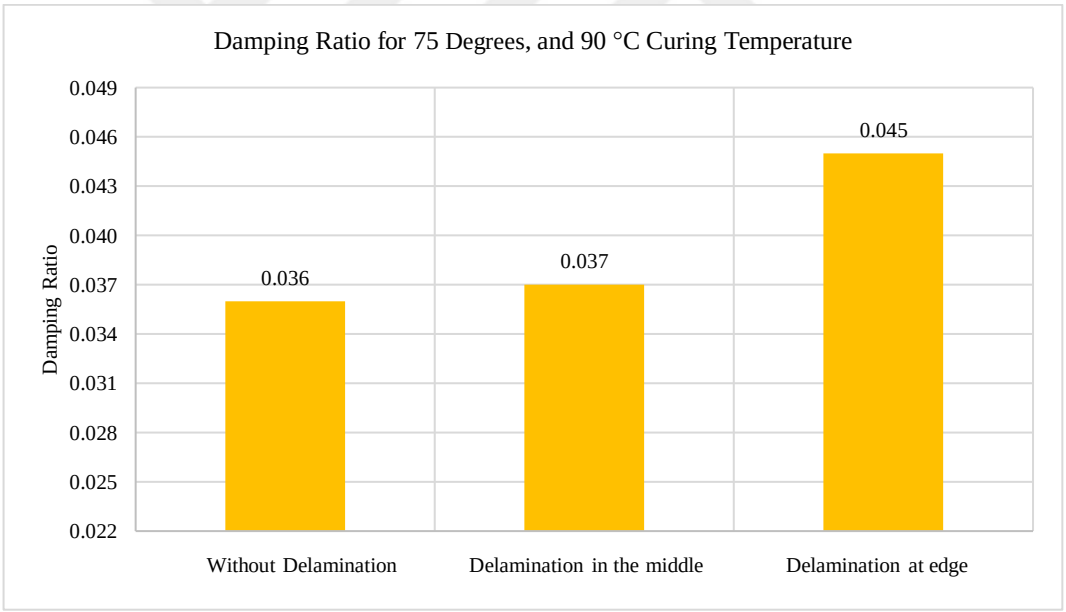

Figure 5.82 Damping ratio for 75 degrees filament wound, and 90 °C curing temperature

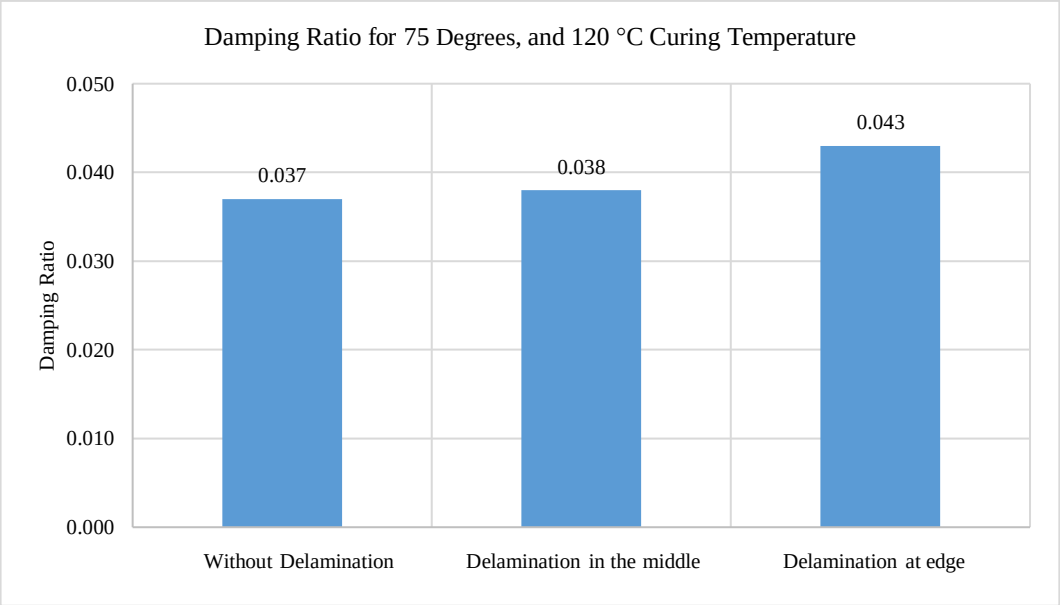

Figure 5.83 Damping ratio for 75 degrees filament wound, and 120 °C curing temperature

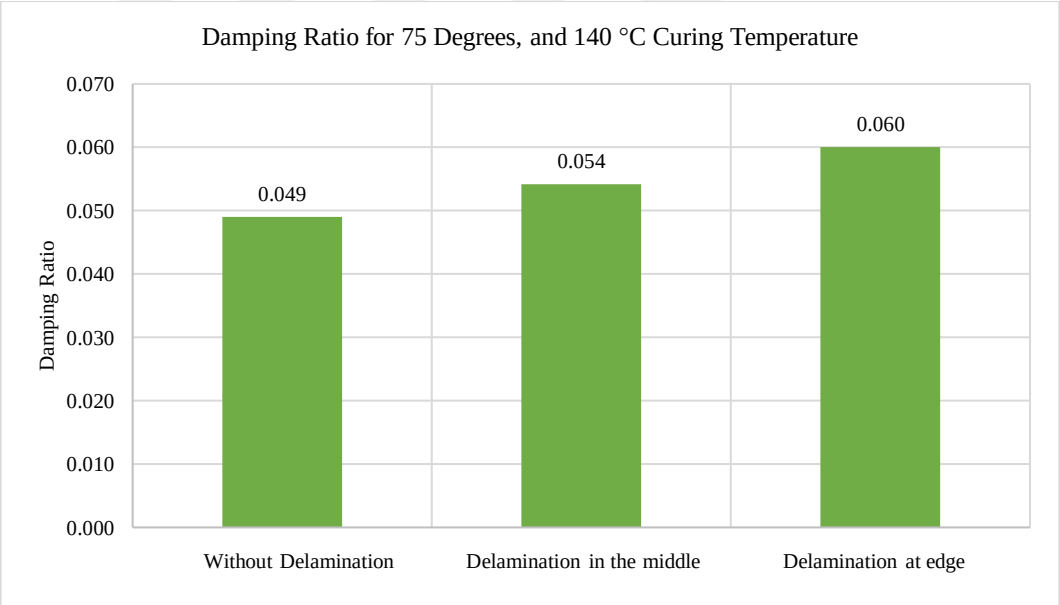

Figure 5.84 Damping ratio for 75 degrees filament wound, and 140 °C curing temperature

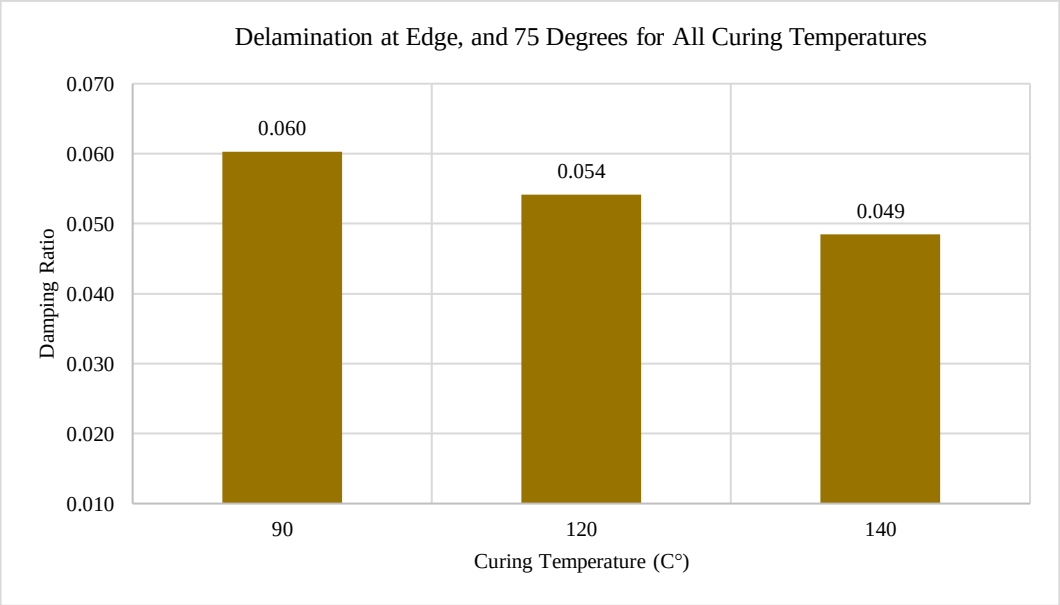

Figure 5.85 Damping ratio of the structure delamination at edge, and 75 degrees filament wound for all curing temperature

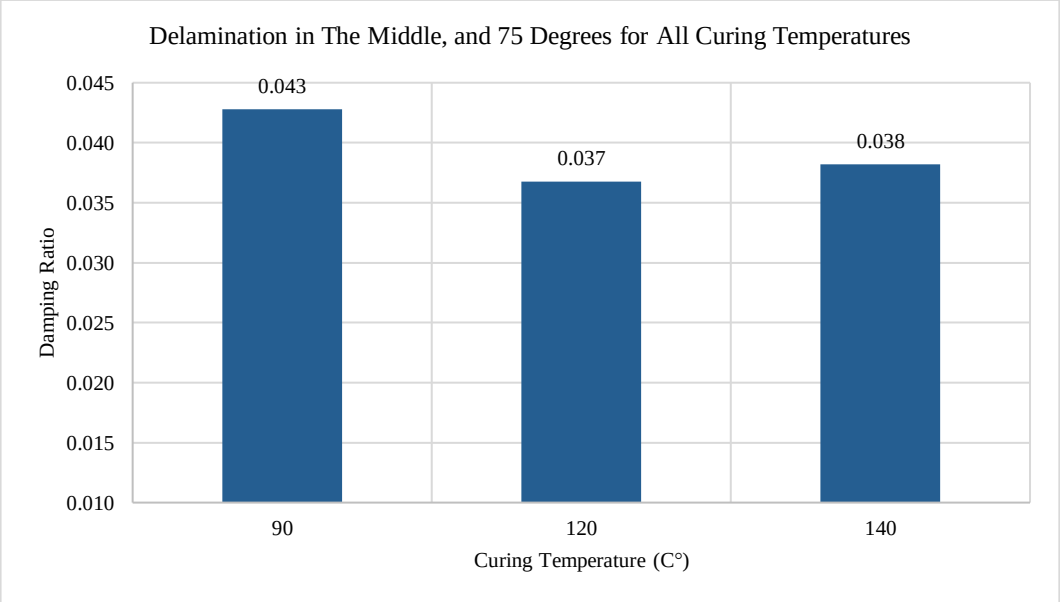

Figure 5.86 Damping ratio of the structure delamination in the middle, and 75 degrees filament wound for all curing temperatures

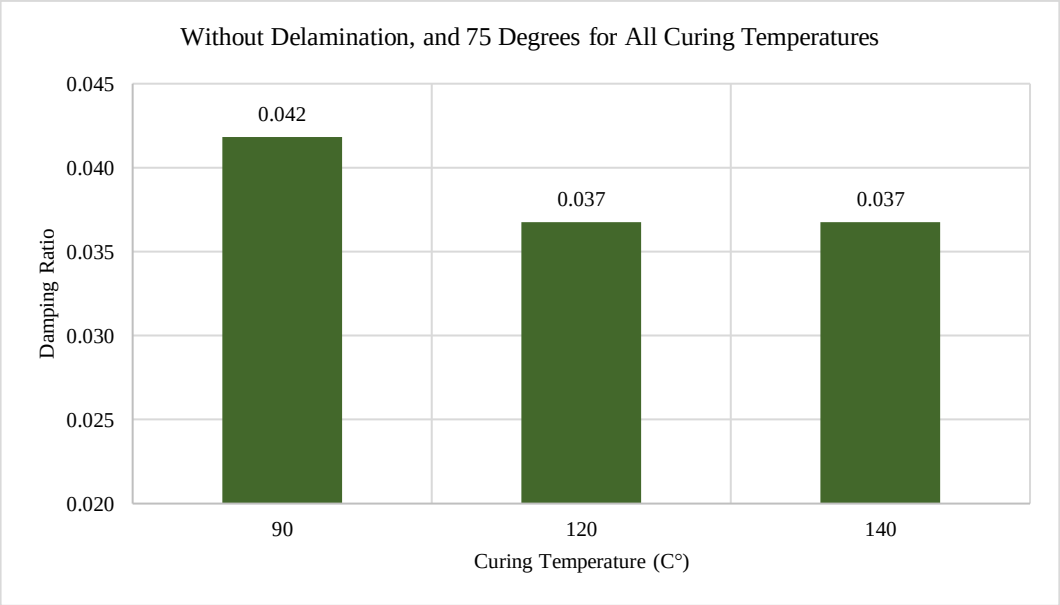

Figure 5.87 Damping ratio of the structure without delamination, and 75 degrees filament wound for all curing temperatures

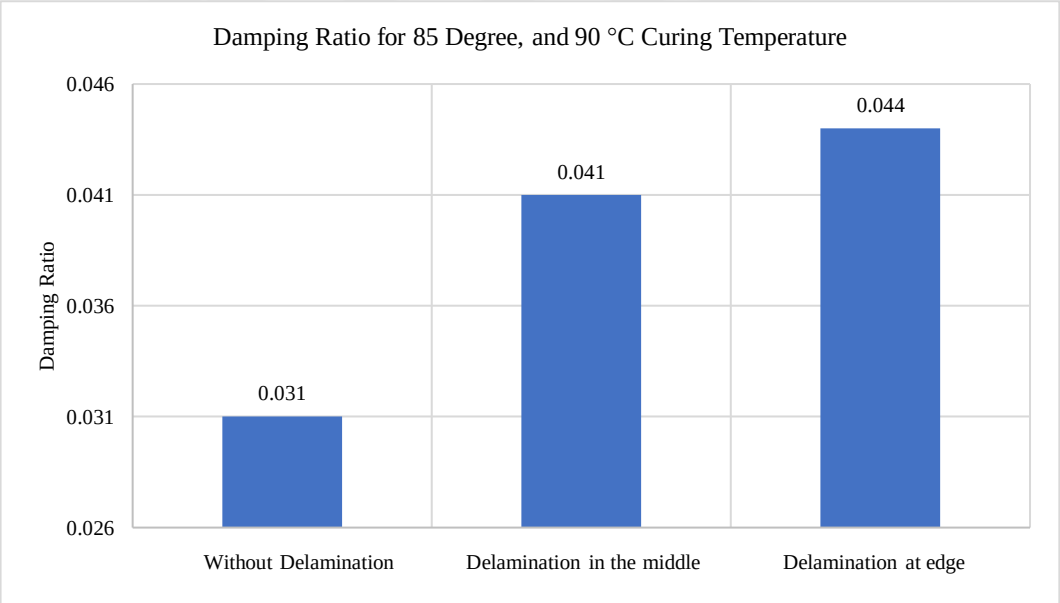

Figure 5.88 Damping ratio for 85 degrees filament wound, and 90 °C curing temperature

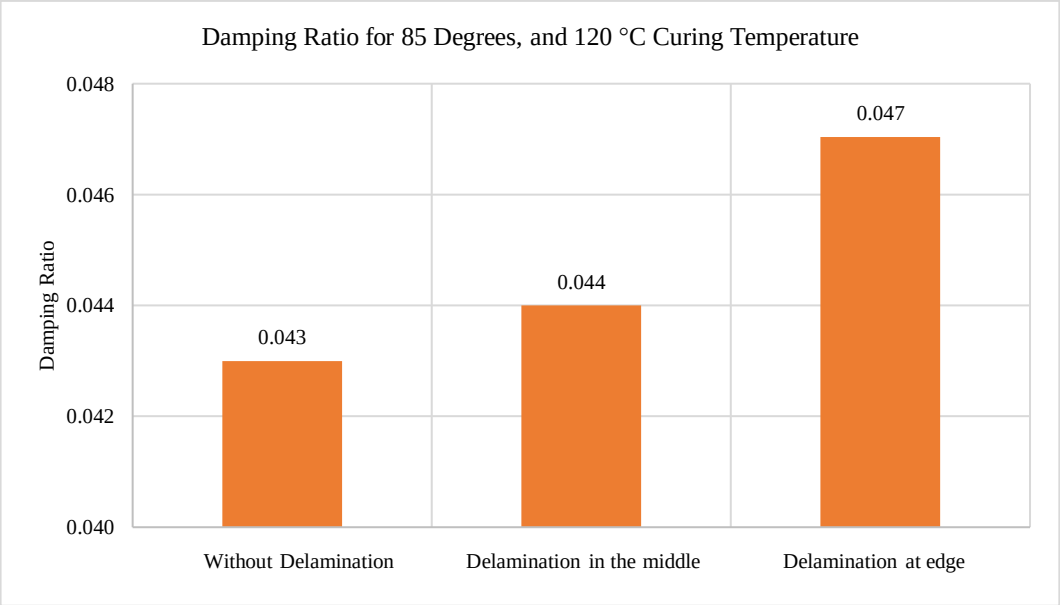

Figure 5.89 Damping ratio for 85 degrees filament wound, and 120 °C curing temperature

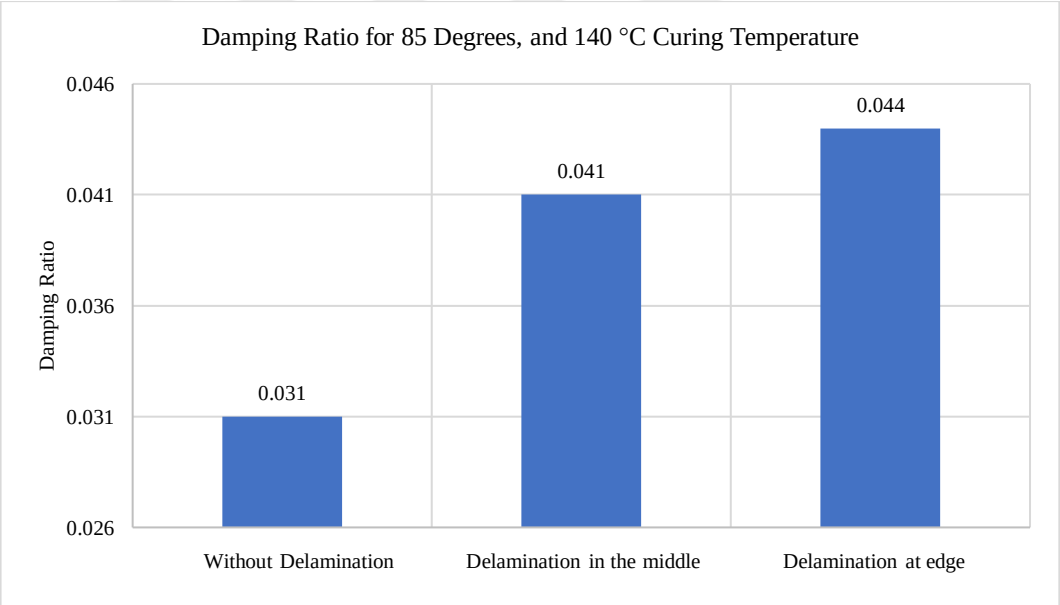

Figure 5.90 Damping ratio for 85 degrees filament wound, and 140 °C curing temperature

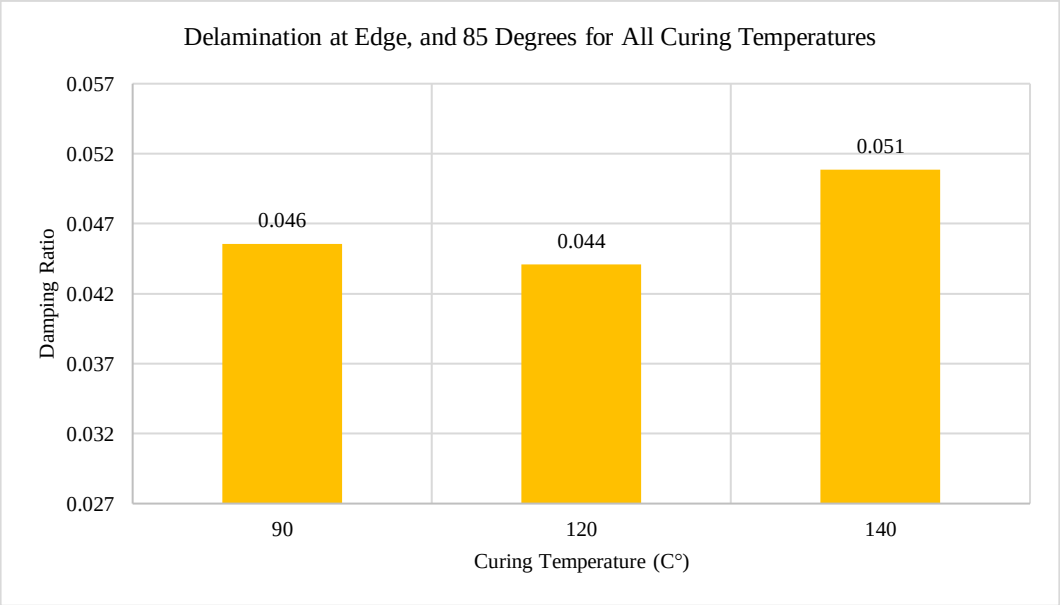

Figure 5.91 Damping ratio of the structure delamination at edge and 85 degrees filament wound for all curing temperature

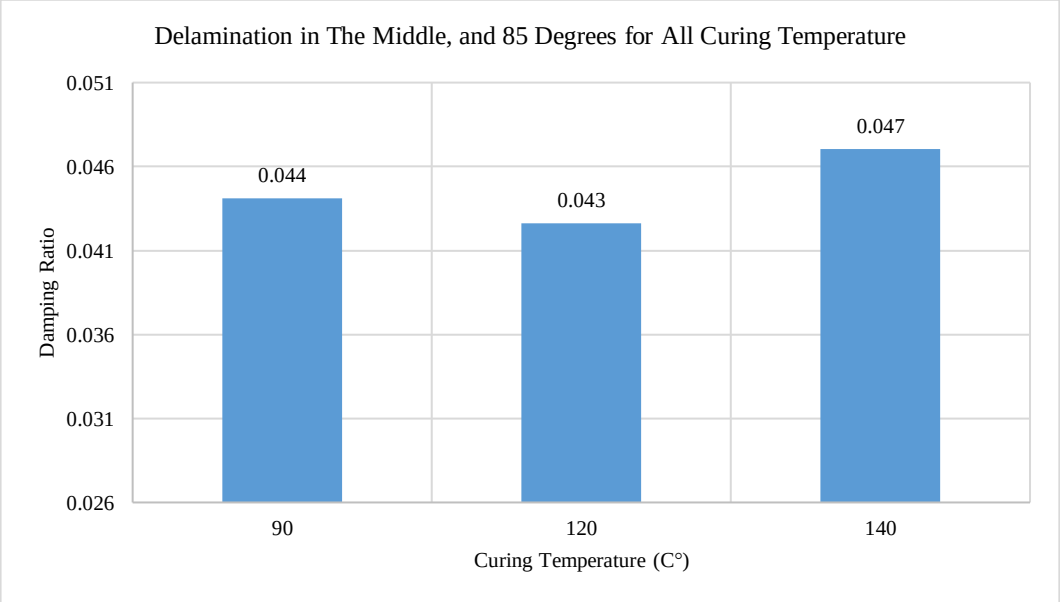

Figure 5.92 Damping ratio of the structure delamination in the middle, and 85 degrees filament wound for all curing temperature

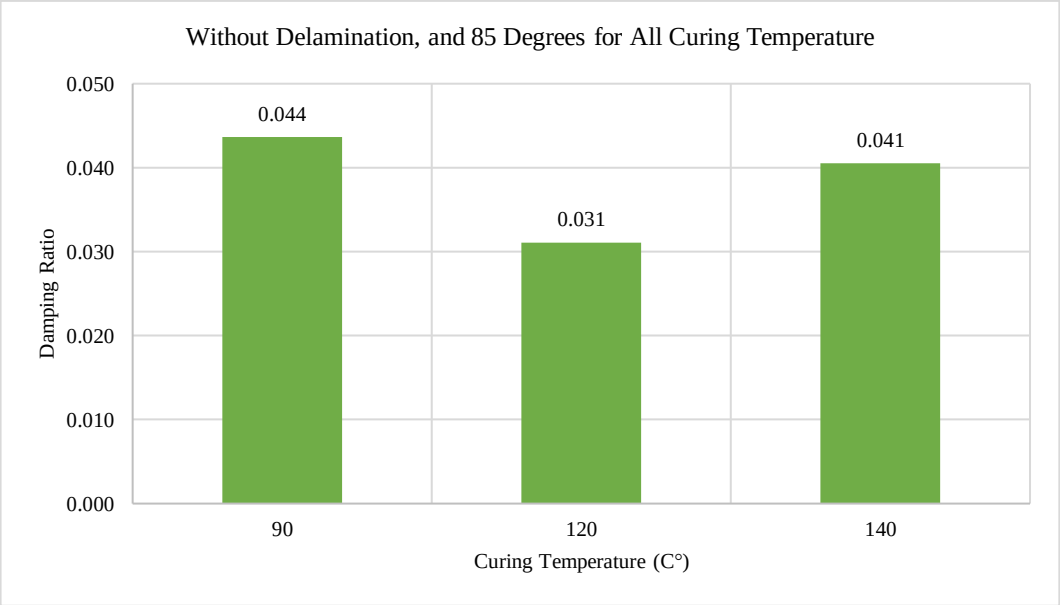

Figure 5.93 Damping ratio of the structure without delamination, and 85 degrees filament wound for all curing temperatures

5.5 Experimental Results for Fixed-Free Boundary Condition

The results from the LabView program were processed in MATLAB. In Figure 5.93-Figure 5.102 show samples wound at 85 degrees filament angle.

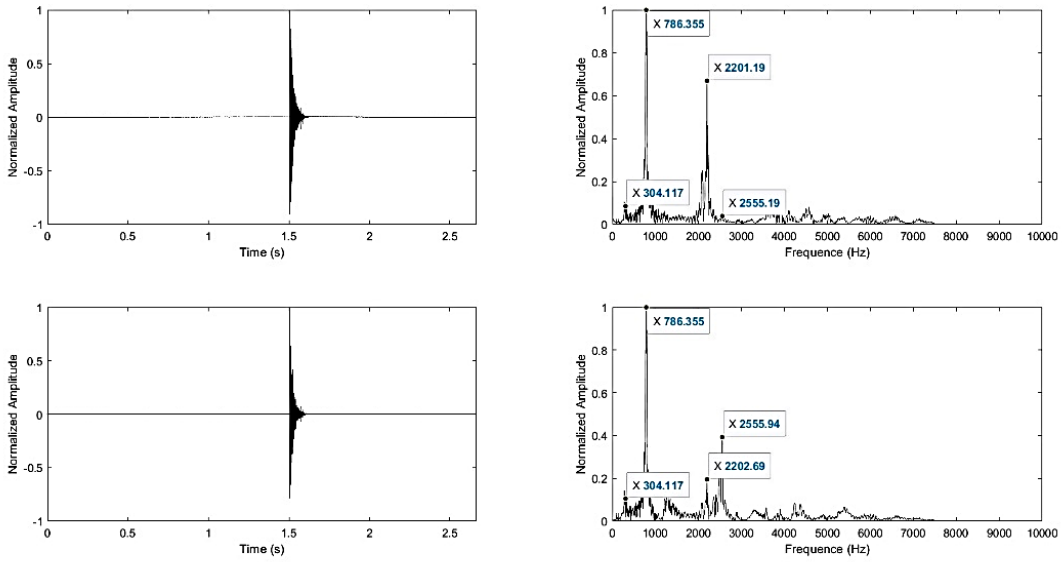

Figure 5.94 Vibration analysis results of the sample having 85- degrees filament wound, cured at 90°C and delamination at edge

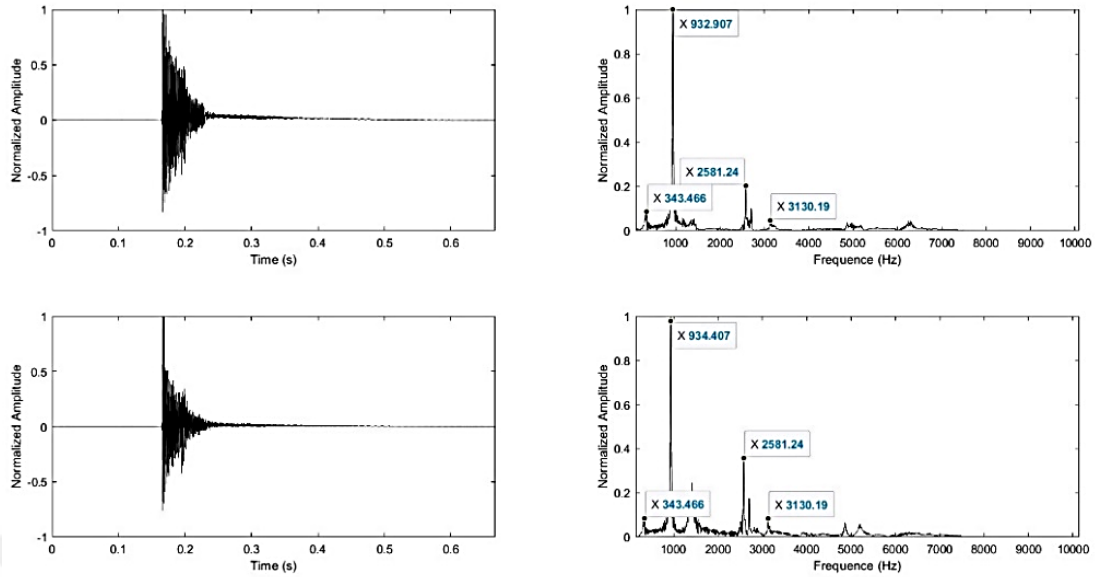

Figure 5.95 Vibration analysis results of the sample having 85- degrees filament wound, cured at 90°C and delamination in the middle

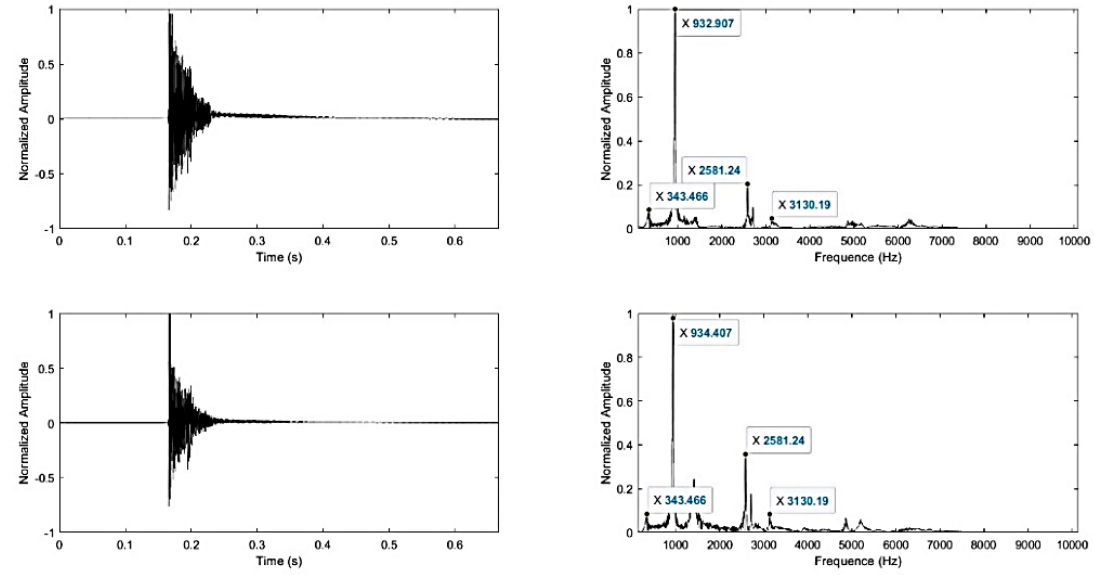

Figure 5.96 Vibration analysis results of the sample having 85- degrees filament wound, cured at 90°C and without delamination

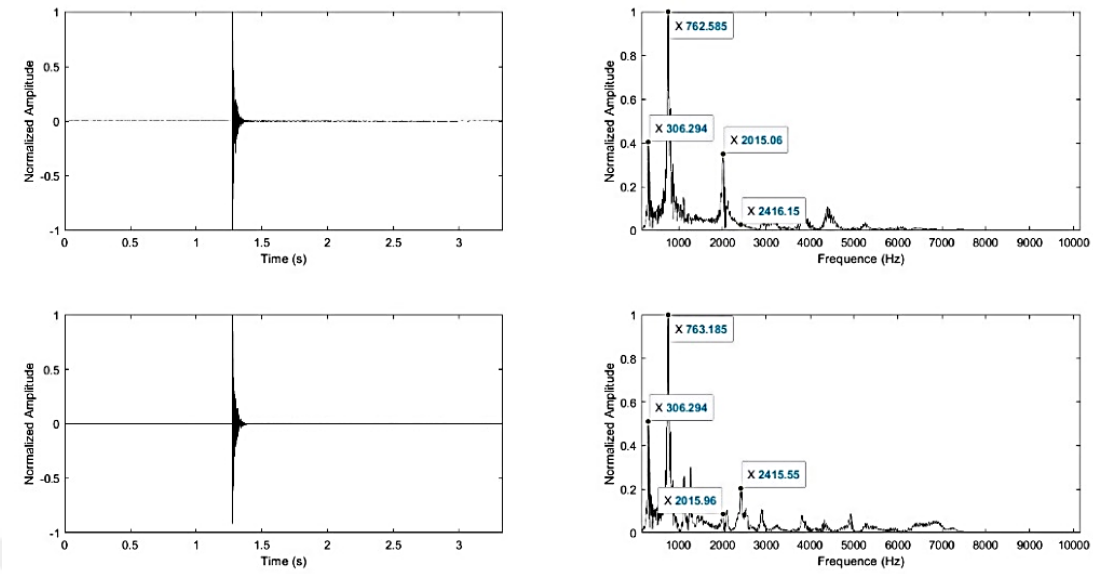

Figure 5.97 Vibration analysis results of the sample having 85- degrees filament wound, cured at 120°C and delamination at edge

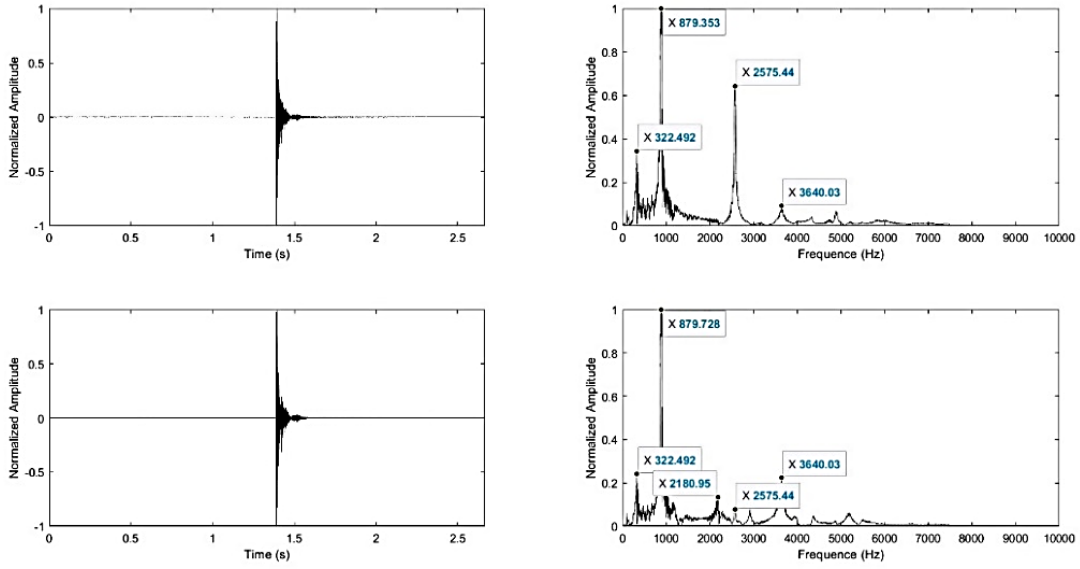

Figure 5.98 Vibration analysis results of the sample having 85- degrees filament wound, cured at 120°C and delamination in the middle

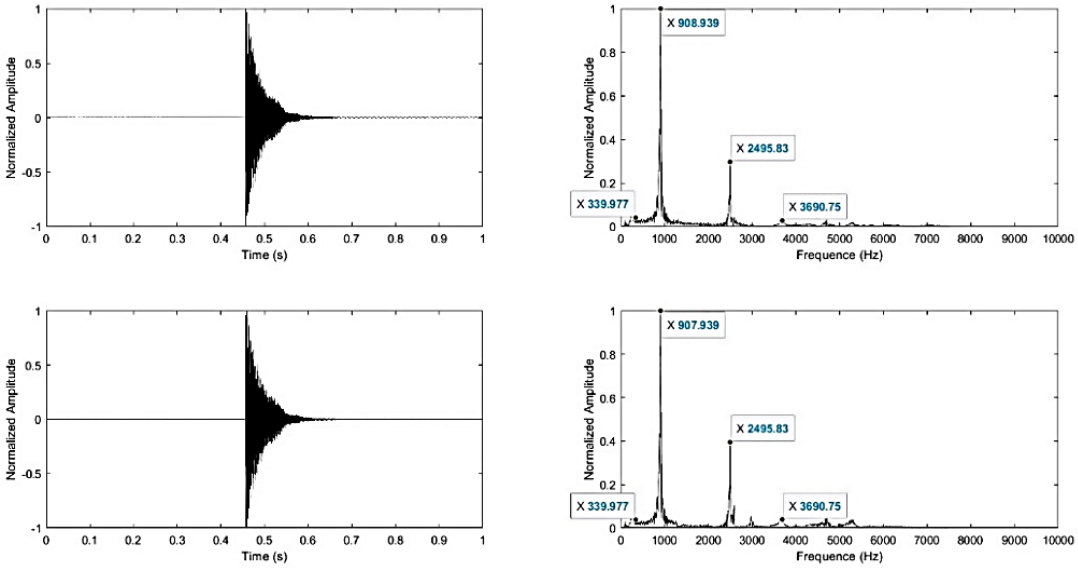

Figure 5.99 Vibration analysis results of the sample having 85- degrees filament wound, cured at 120°C and without delamination

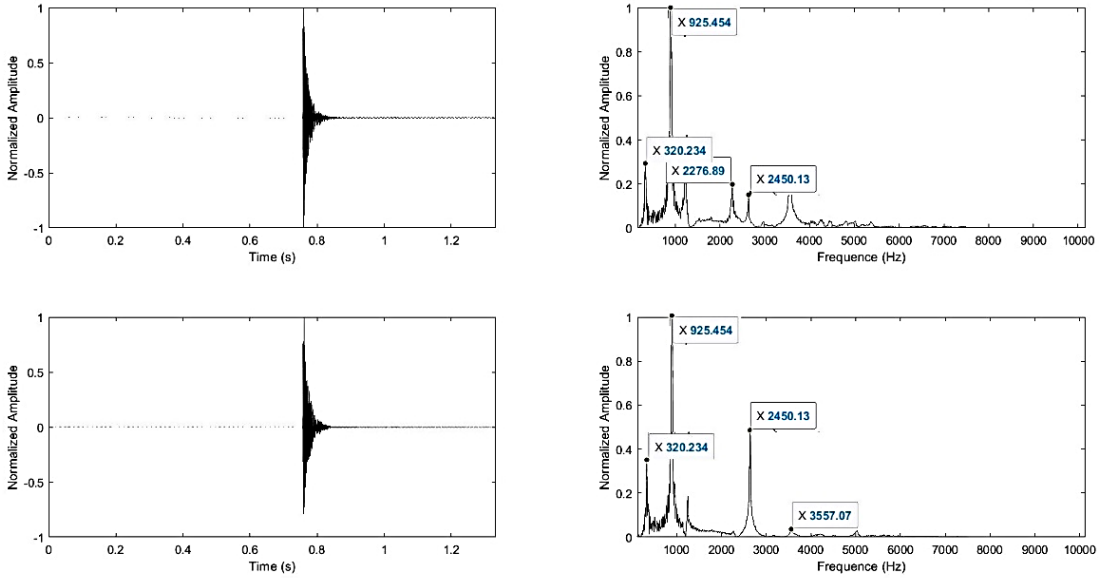

Figure 5.100 Vibration analysis results of the sample having 85- degrees filament wound, cured at 140°C and delamination at edge

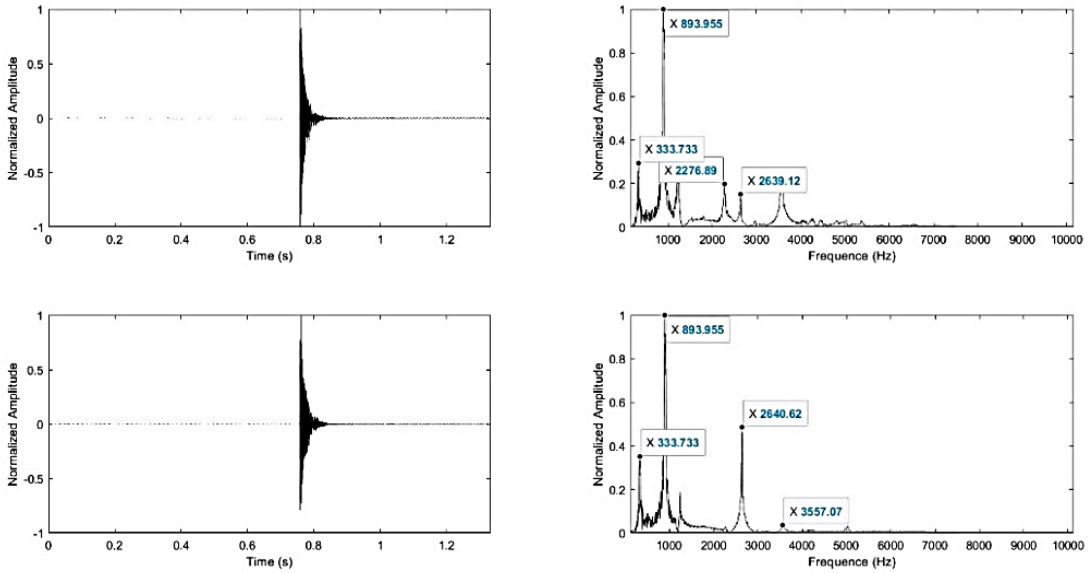

Figure 5.101 Vibration analysis results of the sample having 85- degrees filament wound, cured at 140°C and delamination in the middle

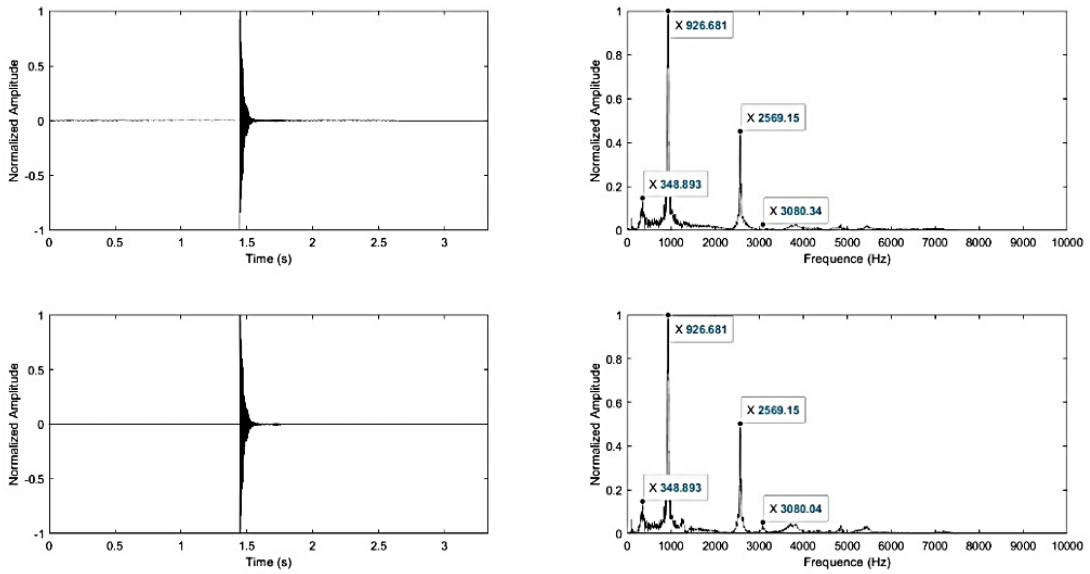

Figure 5.102 Vibration analysis results of the sample having 85- degrees filament wound, cured at 140°C and without delamination

In Figure 5.103-Figure 5.111, the variation of the first, second, and third natural frequencies regarding different 85 degrees filament wound, curing temperatures, delamination positions, and are shown.

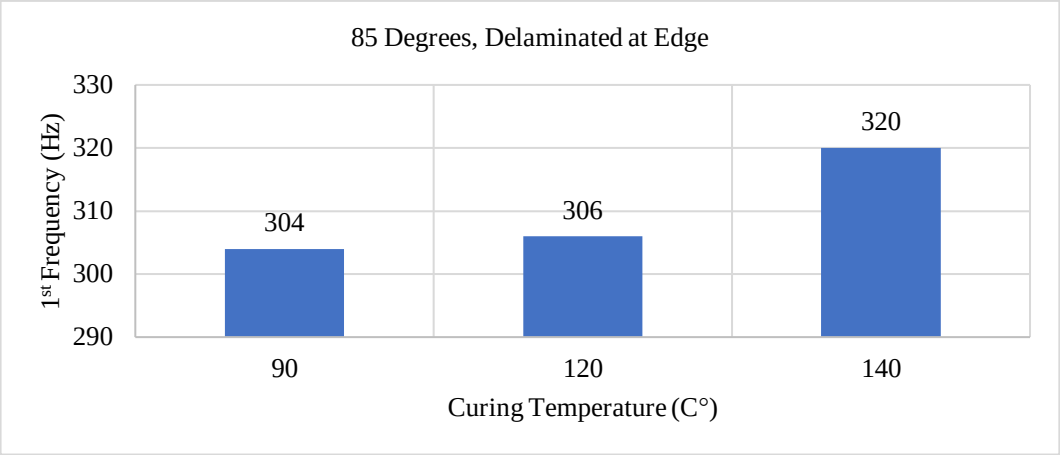

Figure 5.103 85 degrees filament wound, D++, for 1st natural frequency

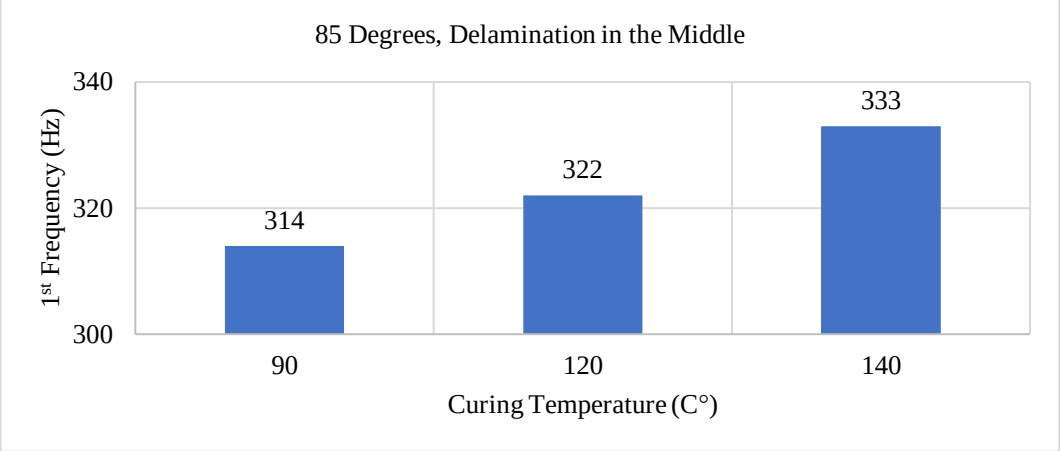

Figure 5.104 85 degrees filament wound, D+, for 1st natural frequency

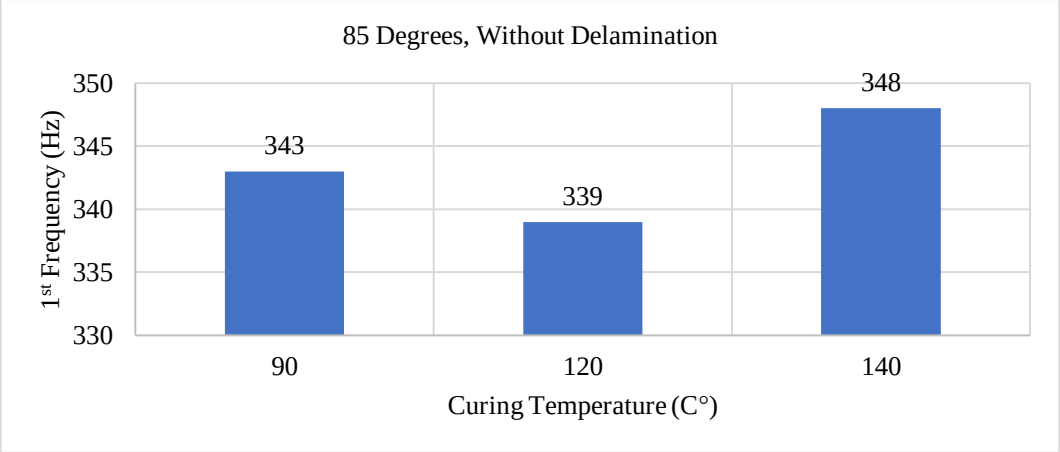

Figure 5.105 85 degrees filament wound, D-, for 1st Natural Frequency

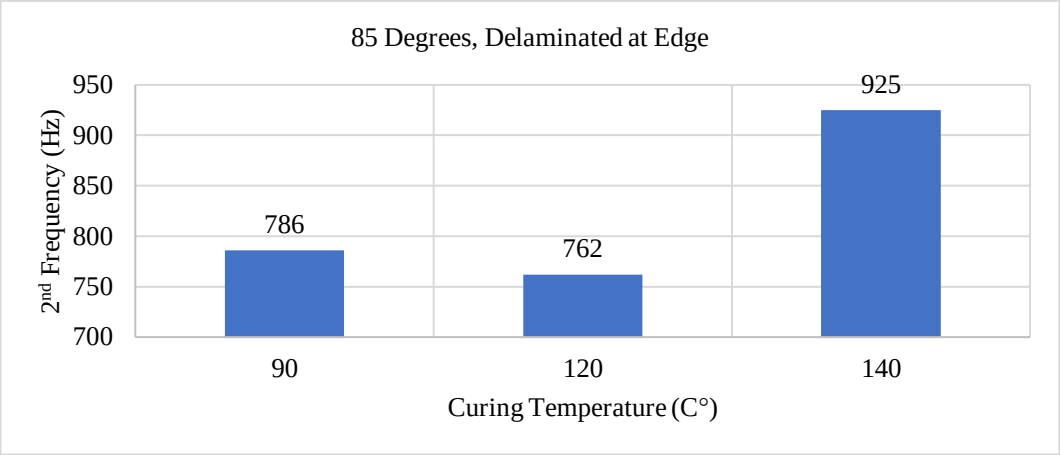

Figure 5.106 85 degrees filament wound, D++, for 2nd natural frequency

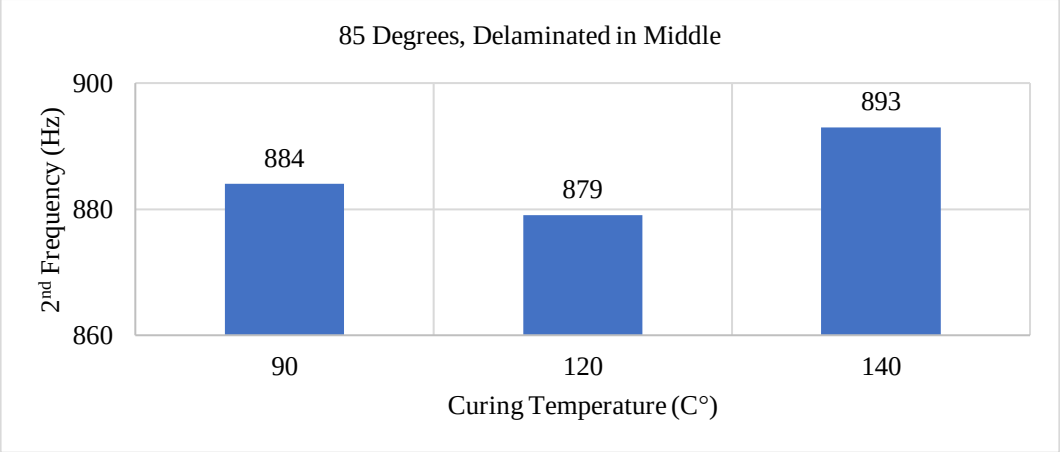

Figure 5.107 85 degrees filament wound, D+, for 2nd natural frequency

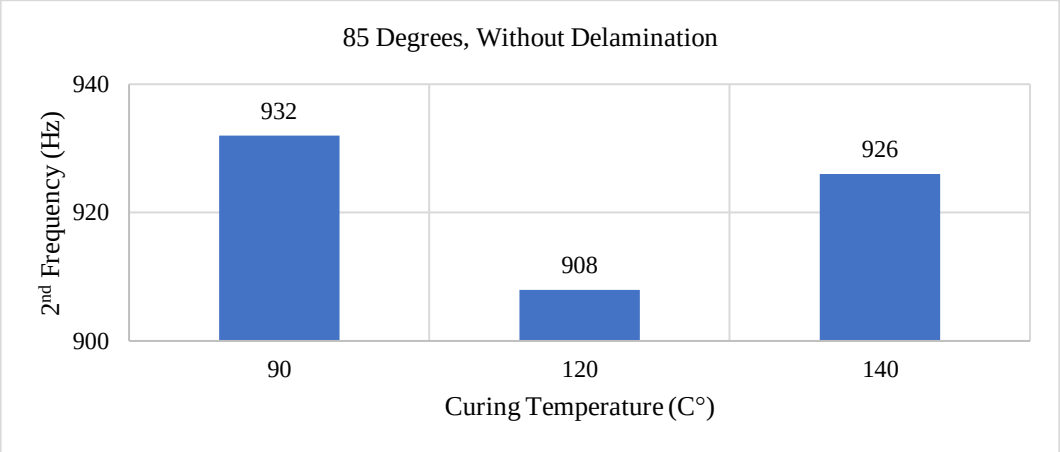

Figure 5.108 85 degrees filament wound, D-, for 2nd natural frequency

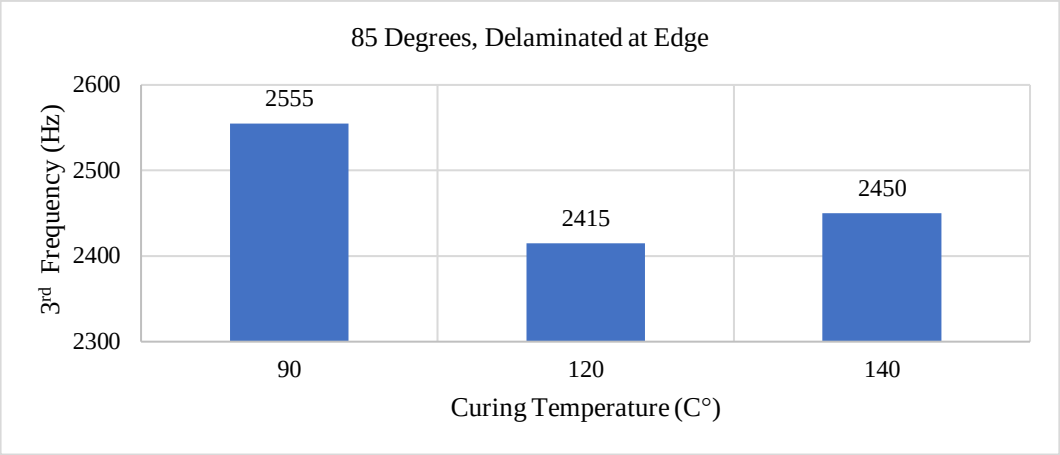

Figure 5.109 85 degrees filament wound, D++, for 3rd natural frequency

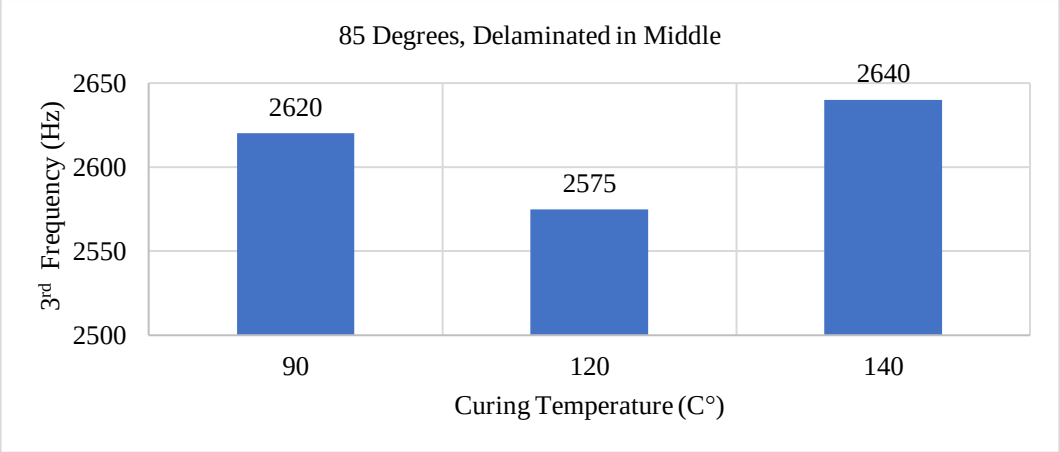

Figure 5.110 85 degrees filament wound, D+, for 3rd natural frequency

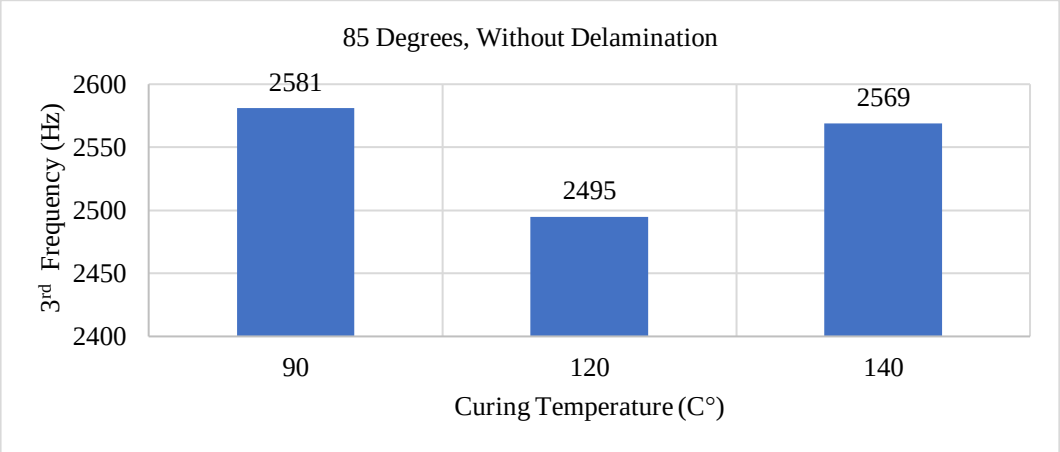

Figure 5.111 85 degrees filament wound, D-, for 3rd natural frequency

In Figure 5.112- Figure 5.120 show samples wound at 75 degrees.

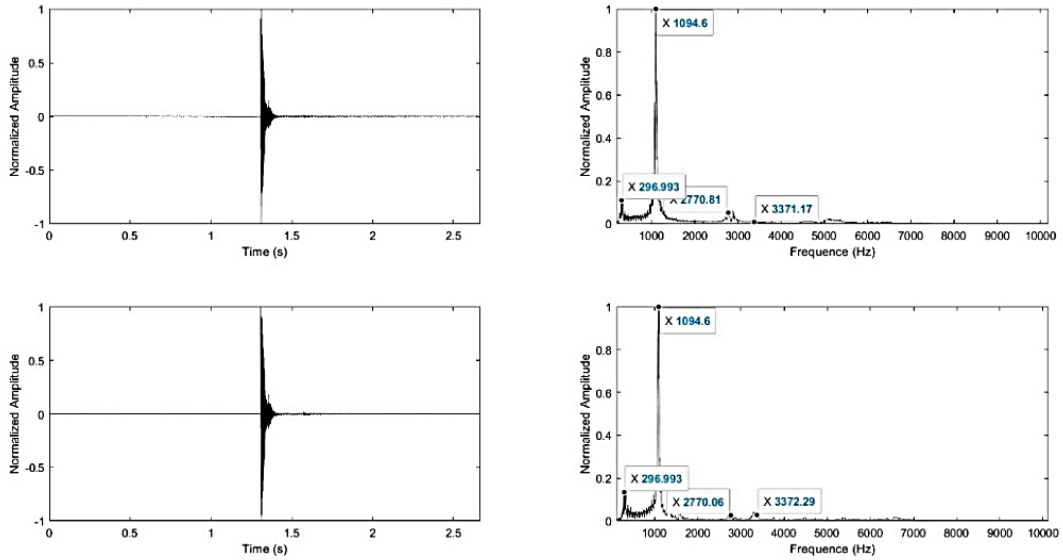

Figure 5.112 Vibration analysis results of the sample having 75- degrees filament wound, cured at 90°C and delamination at edge

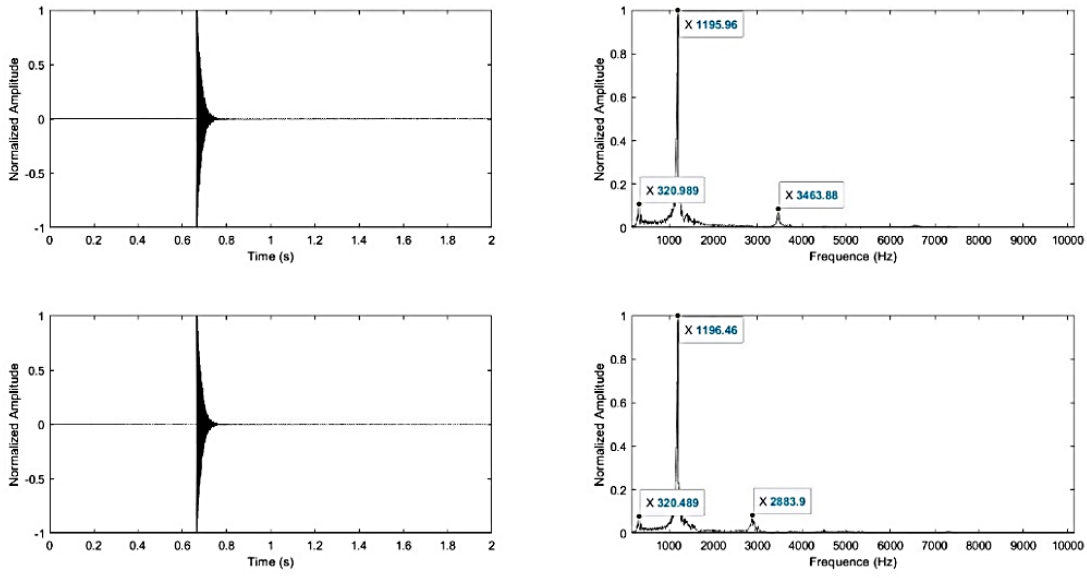

Figure 5.113 Vibration analysis results of the sample having 75- degrees filament wound, cured at 90°C and delamination in the middle

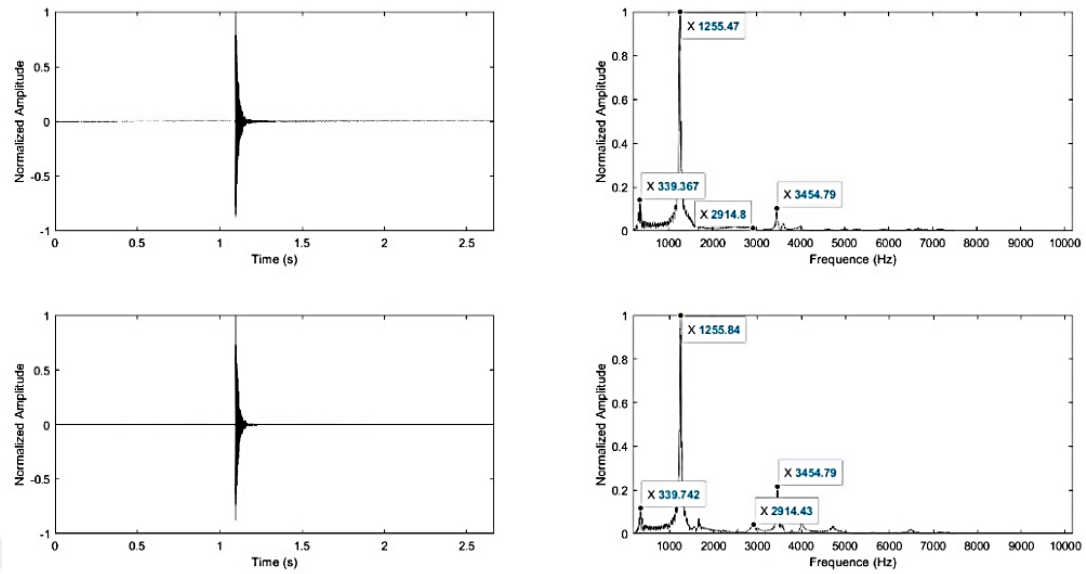

Figure 5.114 Vibration analysis results of the sample having 75- degrees filament wound, cured at 90°C and without delamination

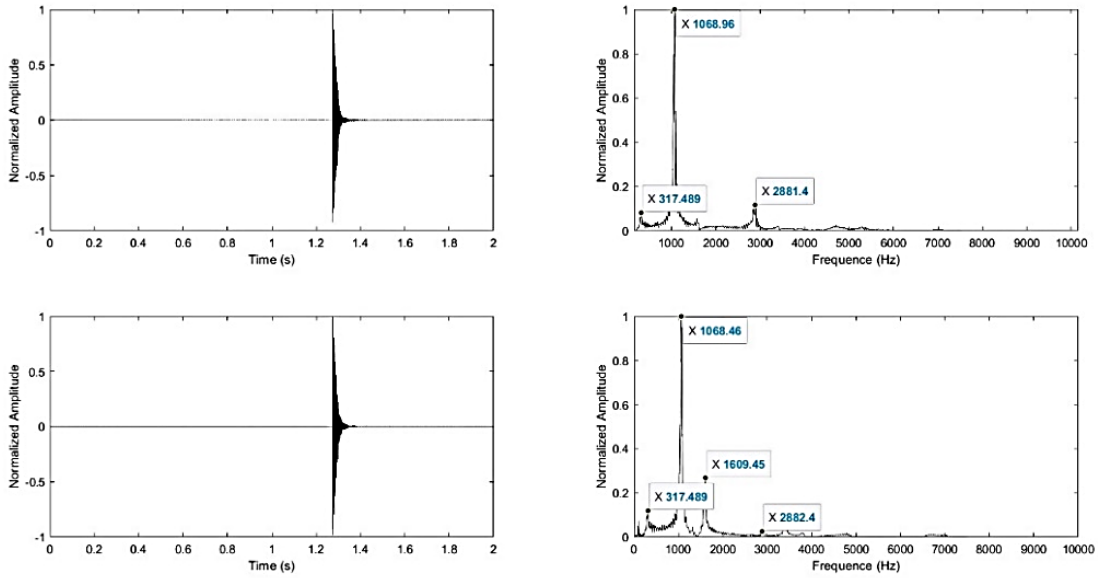

Figure 5.115 Vibration analysis results of the sample having 75- degrees filament a wound, cured at 120°C and delamination at edge

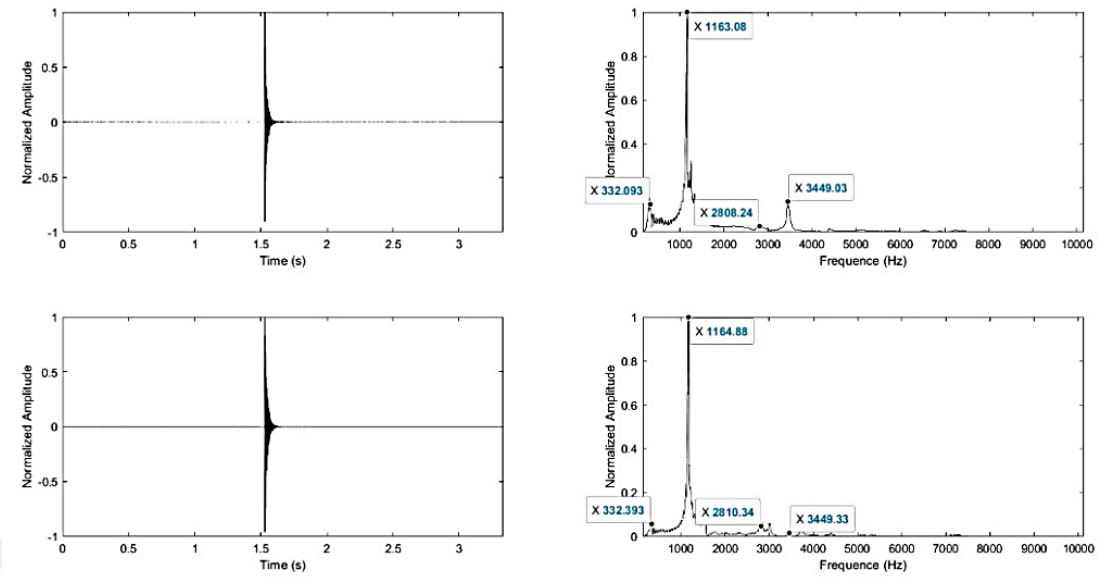

Figure 5.116 Vibration analysis results of the sample having 75- degrees filament wound, cured at 120°C and delamination in the middle

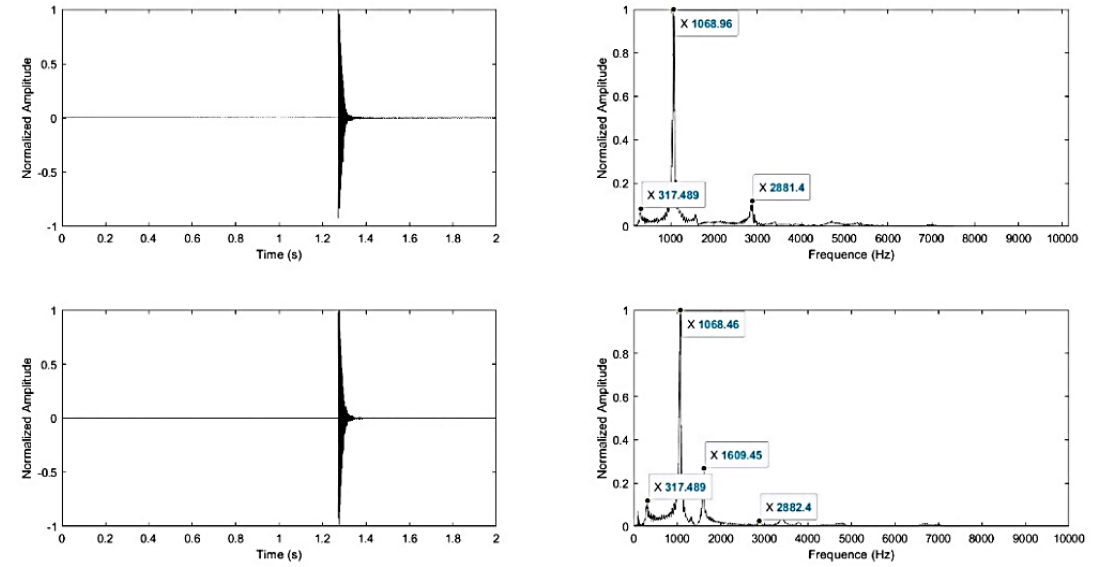

Figure 5.117 Vibration analysis results of the sample having 75- degrees filament wound, cured at 120°C and without delamination

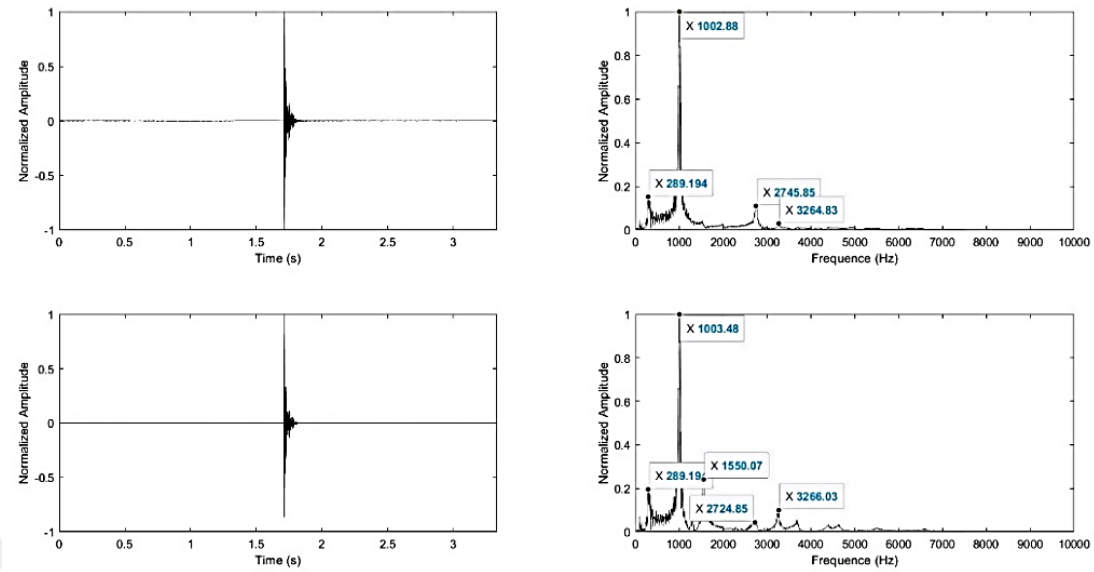

Figure 5.118 Vibration analysis results of the sample having 75- degrees filament wound, cured at 140°C and delamination at edge

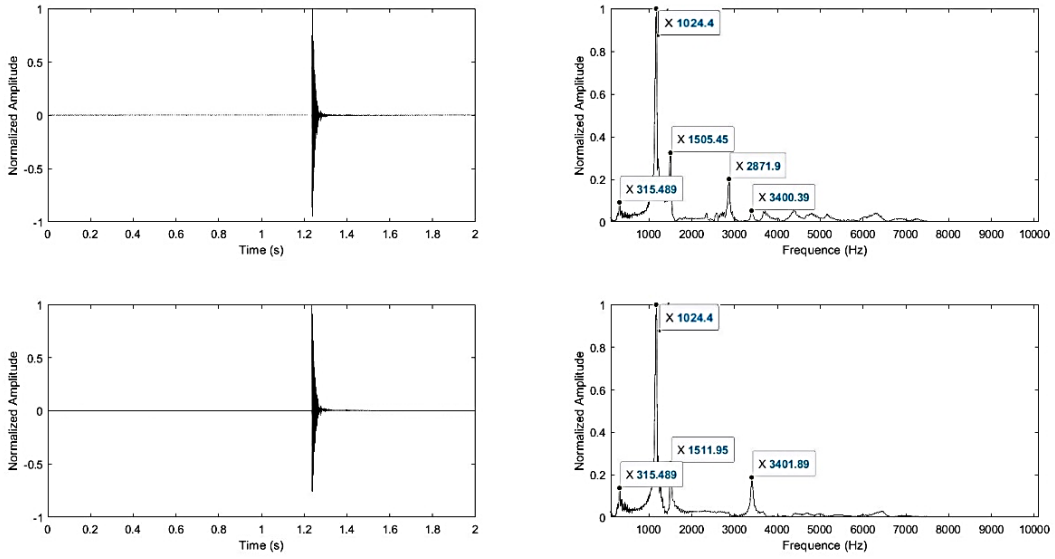

Figure 5.119 Vibration analysis results of the sample having 75- degrees filament wound, cured at 140°C and delamination in the middle

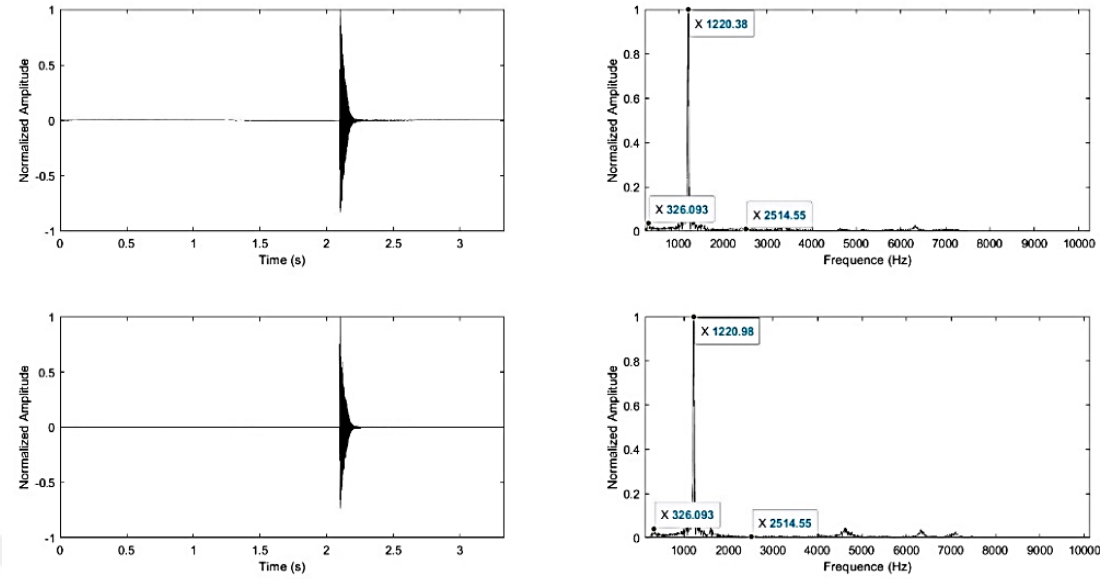

Figure 5.120 Vibration analysis results of the sample having 75- degrees filament wound, cured at 140°C and without delamination

In Figure 5.121-Figure 5.129, the variation of the first, second, and third natural frequencies regarding different 75 degrees filament wound, curing temperatures, delamination positions, and are shown.

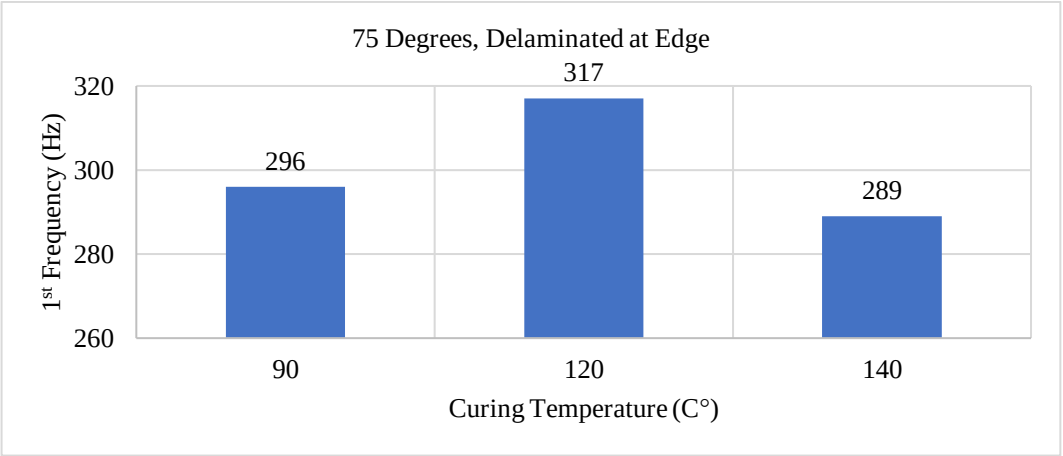

Figure 5.121 75 degrees filament wound, D++, for 1st natural frequency

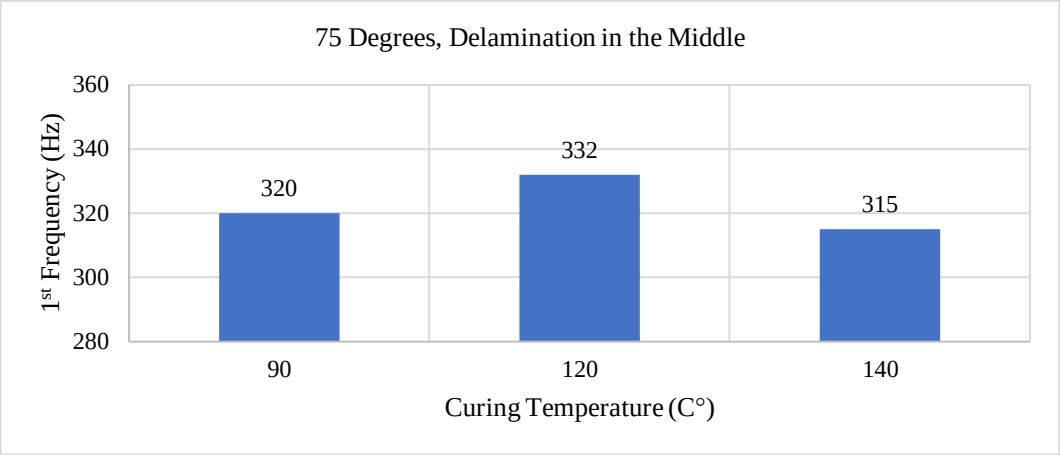

Figure 5.122 75 degrees filament wound, D+, for 1st natural frequency

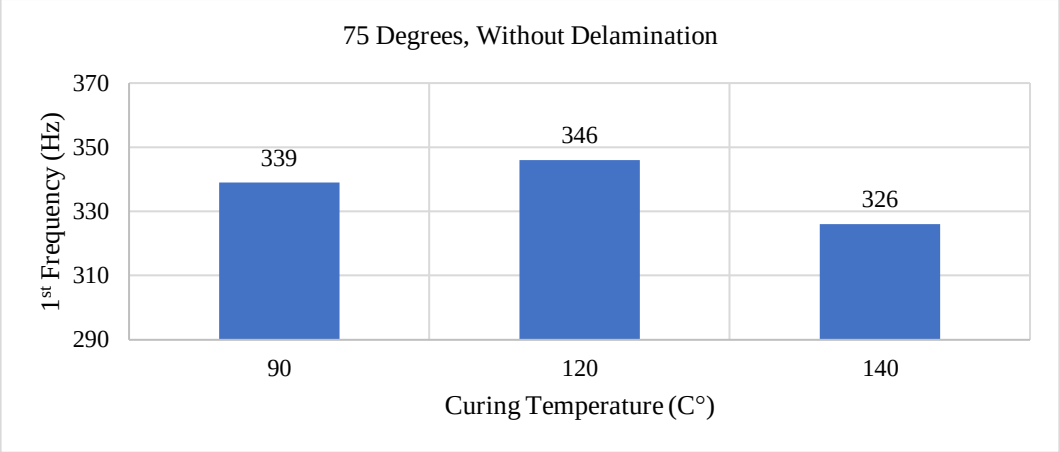

Figure 5.123 75 degrees filament wound, D-, for 1st natural frequency

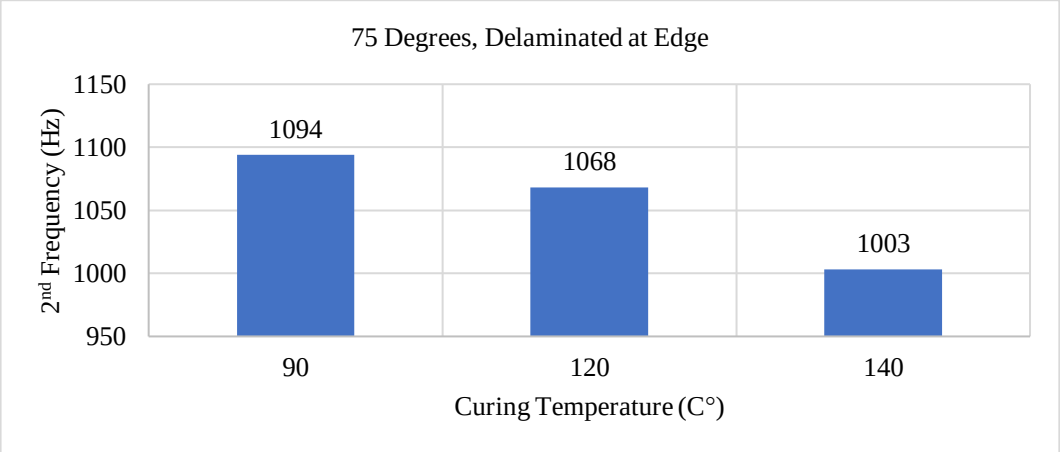

Figure 5.124 75 degrees filament wound, D++, for 2nd natural frequency

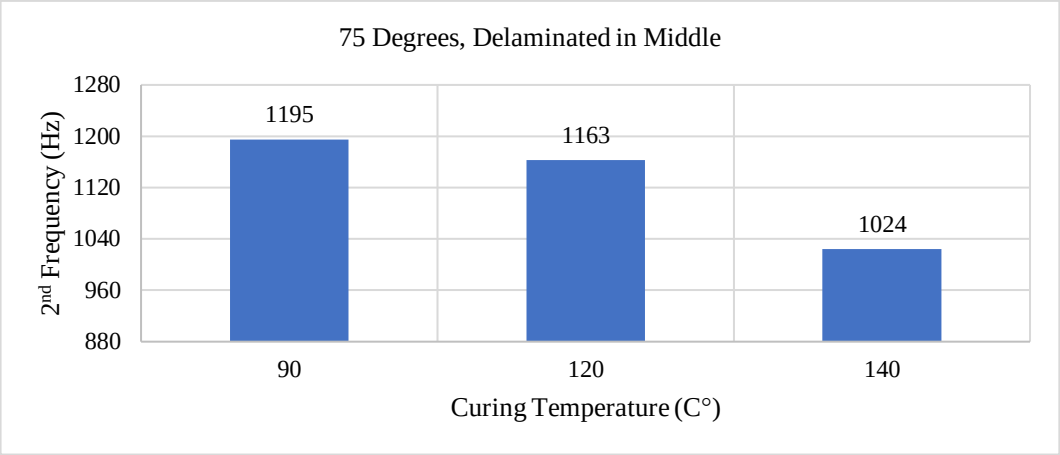

Figure 5.125 75 degrees filament wound, D+, for 2nd natural frequency

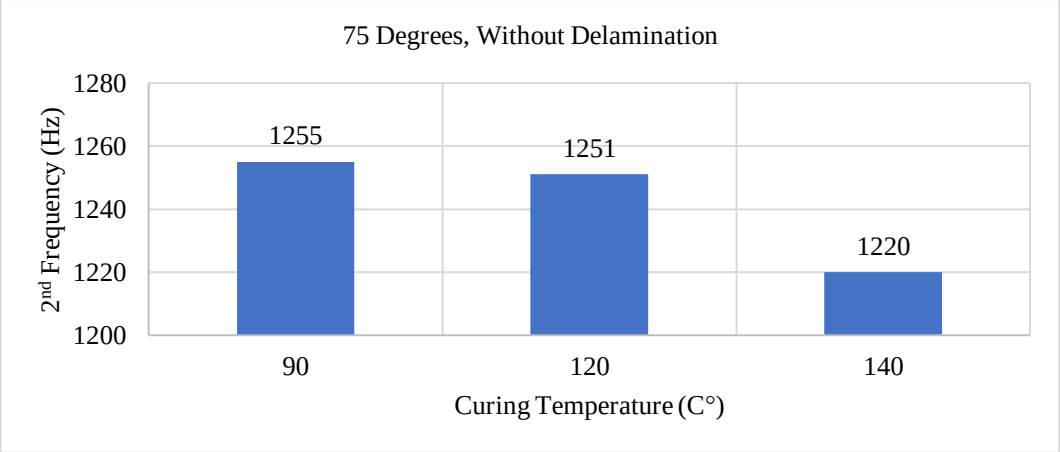

Figure 5.126 75 degrees filament angle, D-, for 2nd natural frequency

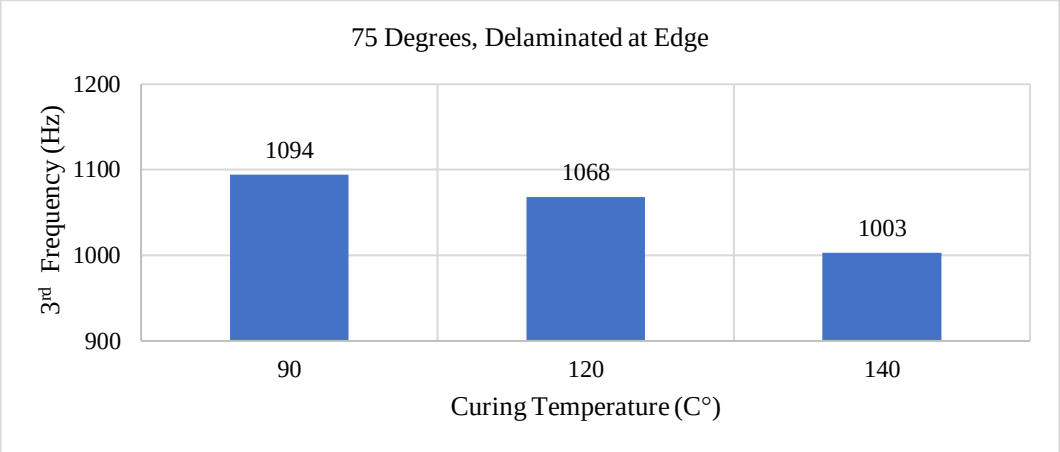

Figure 5.127 75 degrees filament wound, D++, for 3rd natural frequency

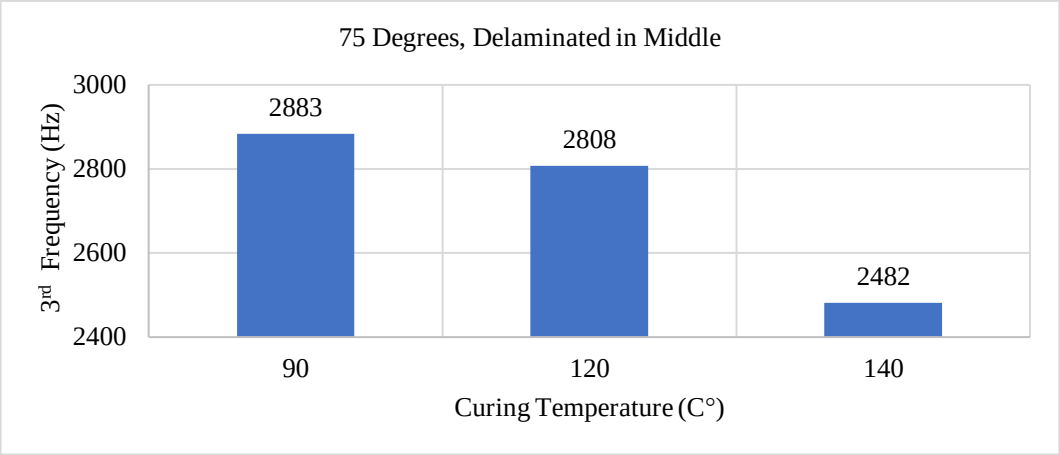

Figure 5.128 75 degrees filament wound, D+, for 3rd natural frequency

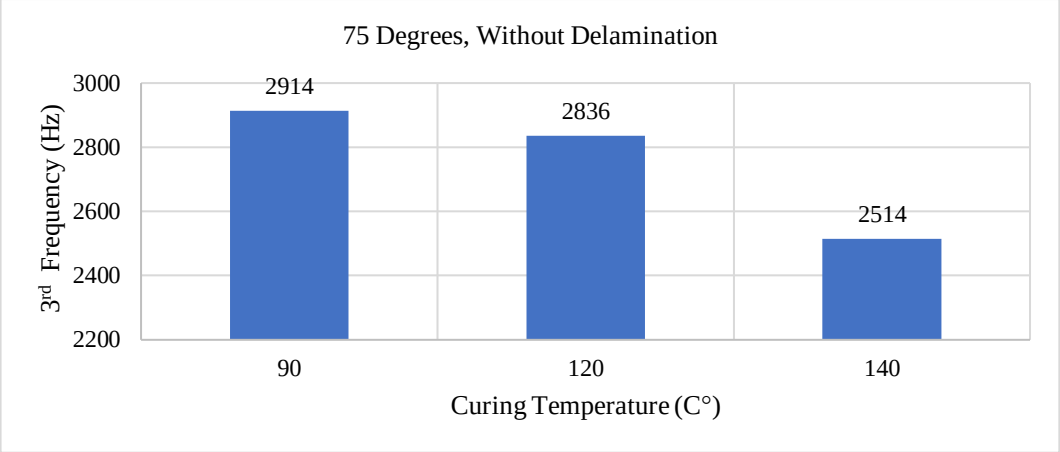

Figure 5.129 75 degrees filament wound, D-, for 3rd natural frequency

In Figure 5.130-Figure 5.138 shows samples wound at 55 degrees filament angle.

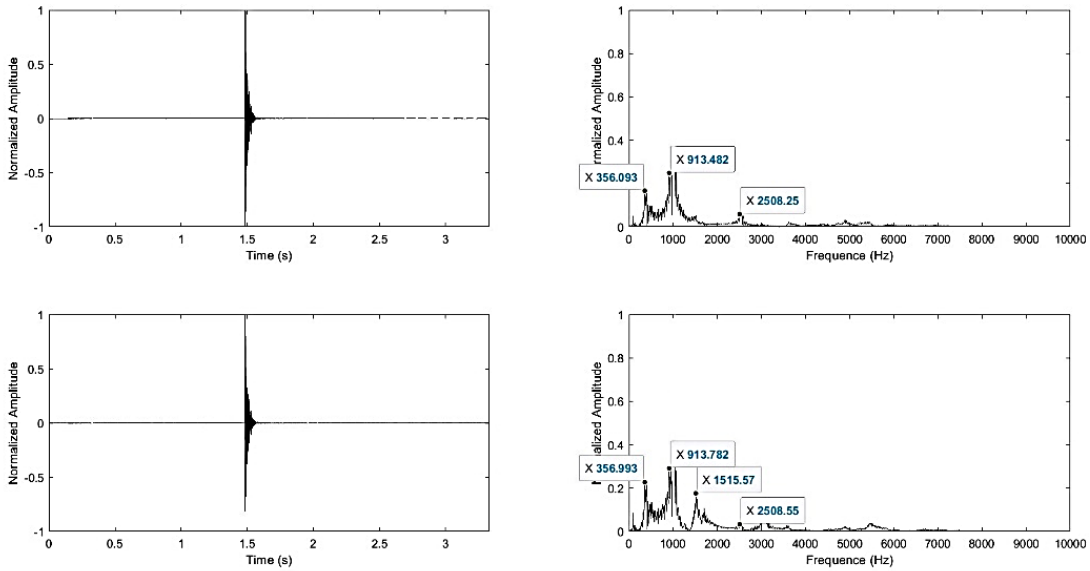

Figure 5.130 Vibration analysis results of the sample having 55- degrees filament wound, cured at 90°C and delamination at edge

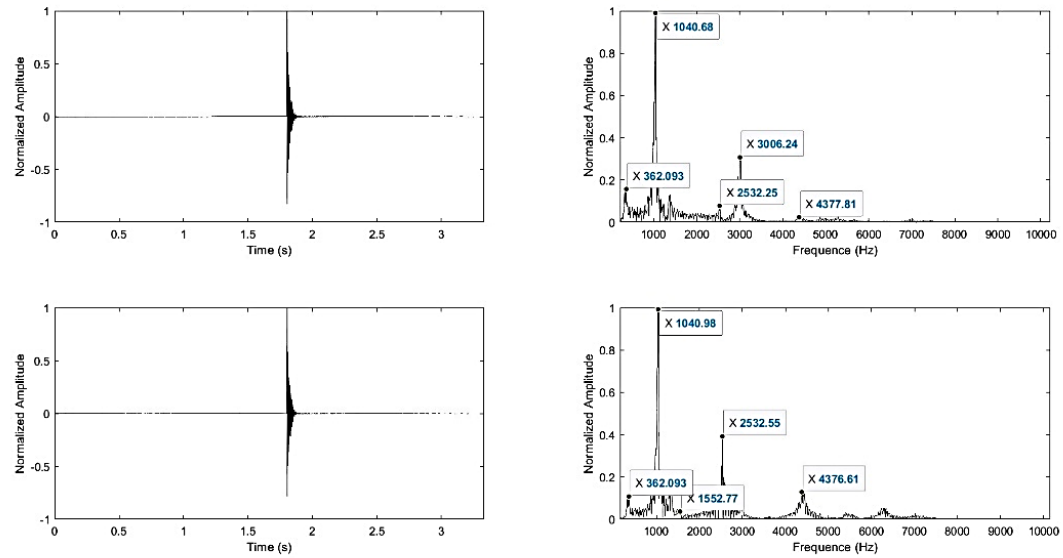

Figure 5.131 Vibration analysis results of the sample having 55- degrees filament wound, cured at 90°C and delamination in the middle

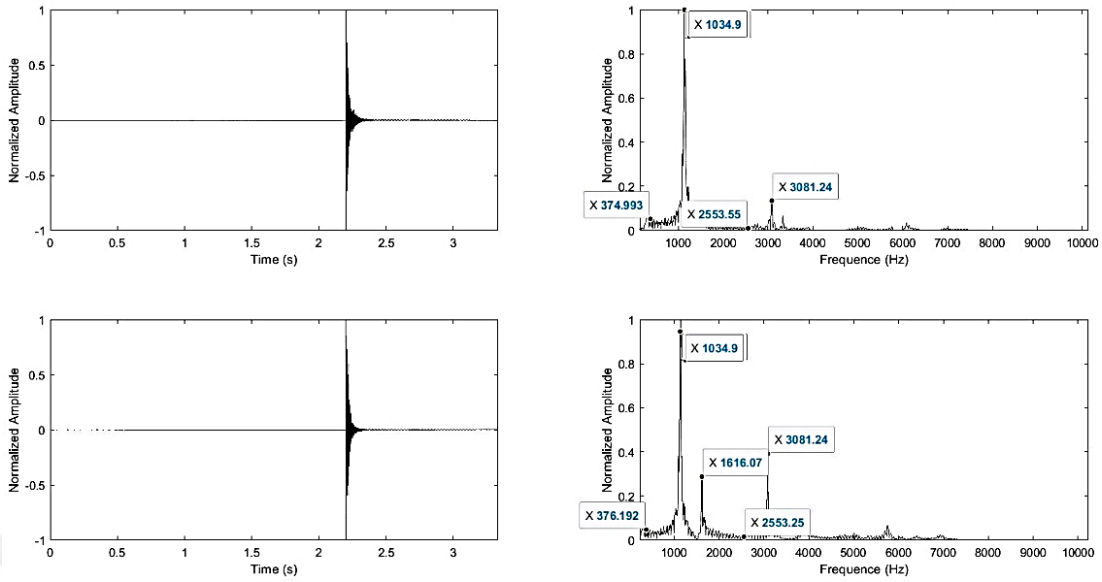

Figure 5.132 Vibration analysis results of the sample having 55- degrees filament wound, cured at 90°C and without delamination

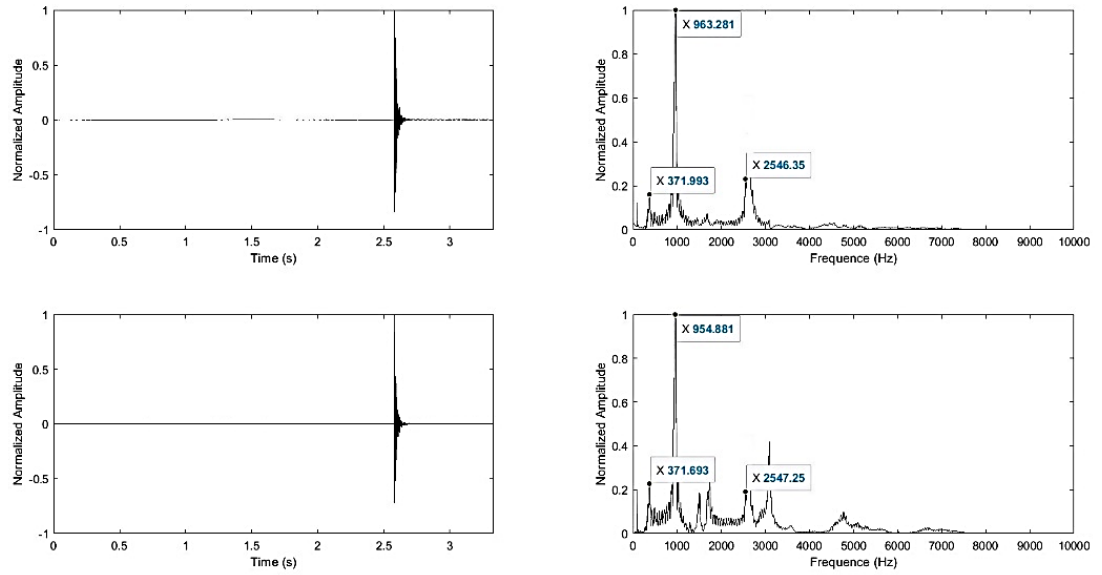

Figure 5.133 Vibration analysis results of the sample having 55- degrees filament wound, cured at 120°C and delamination at edge

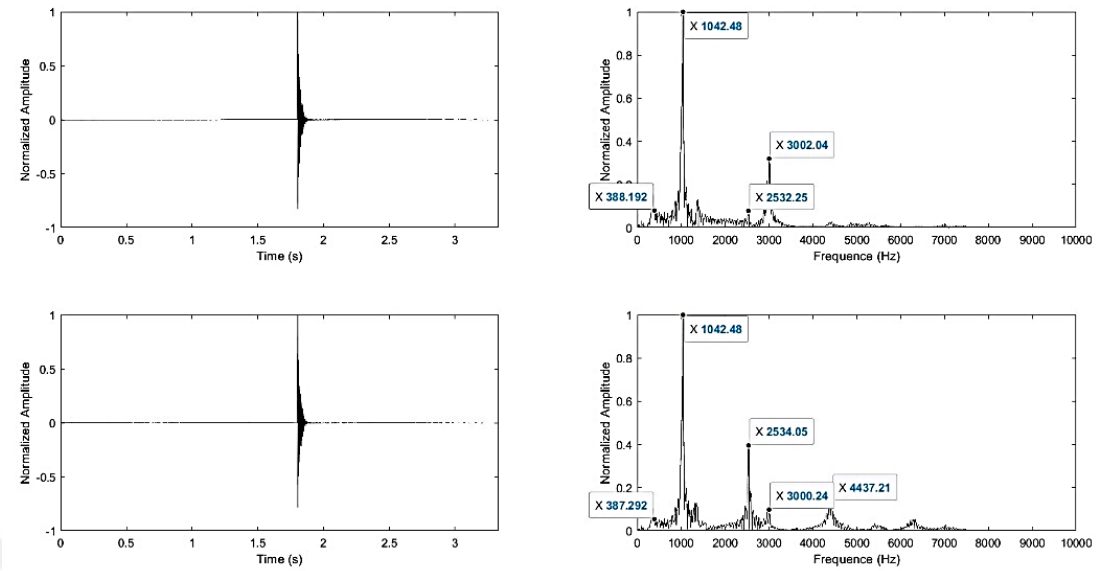

Figure 5.134 Vibration analysis results of the sample having 55- degrees filament wound, cured at 120°C and delamination in the middle

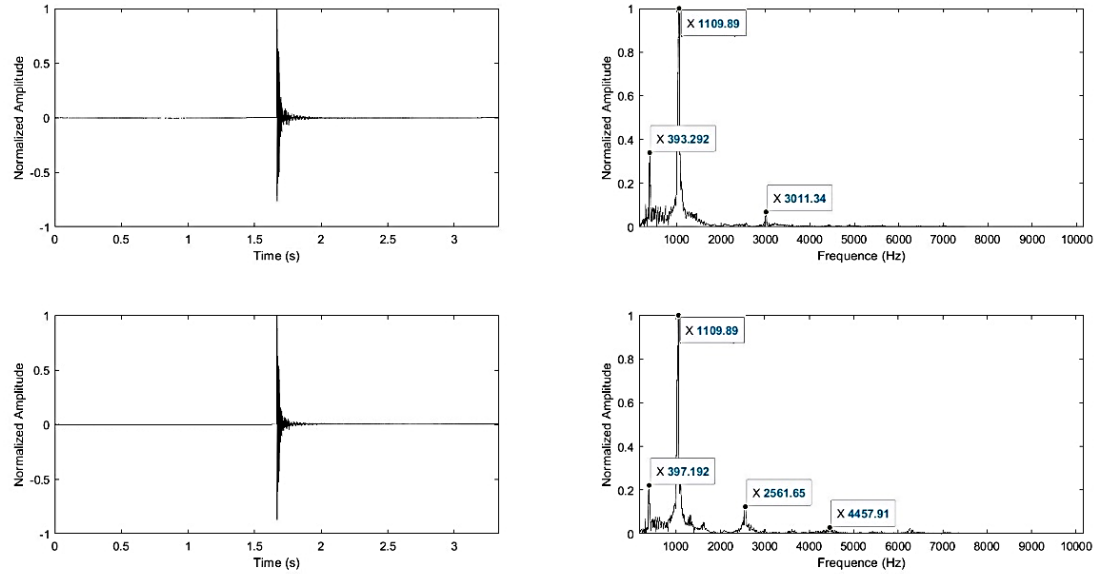

Figure 5.135 Vibration analysis results of the sample having 55- degrees filament wound, cured at 120°C and without delamination

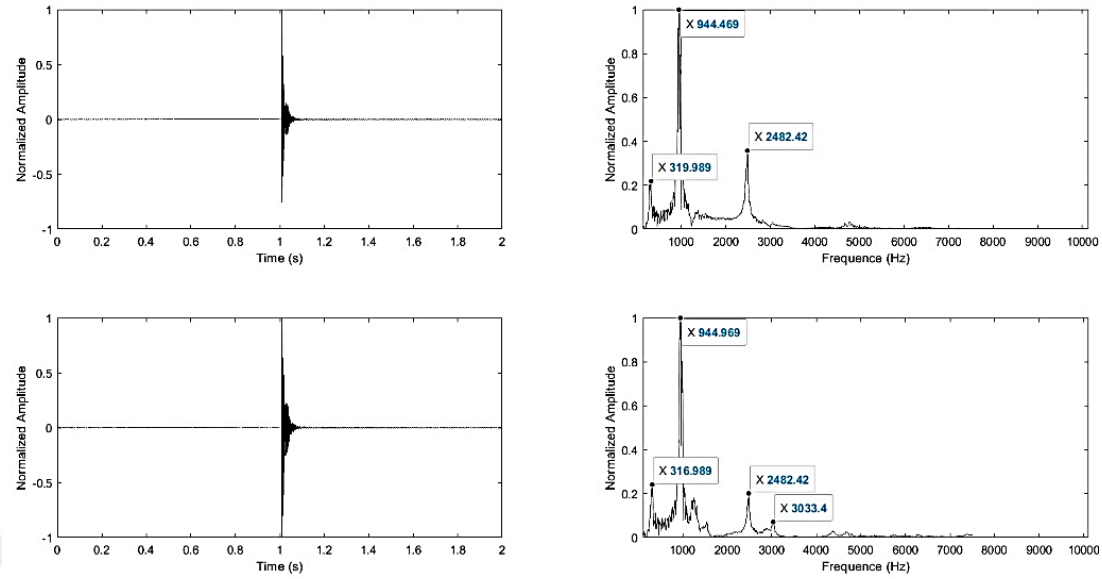

Figure 5.136 Vibration analysis results of the sample having 55- degrees filament wound, cured at 140°C and delamination at edge

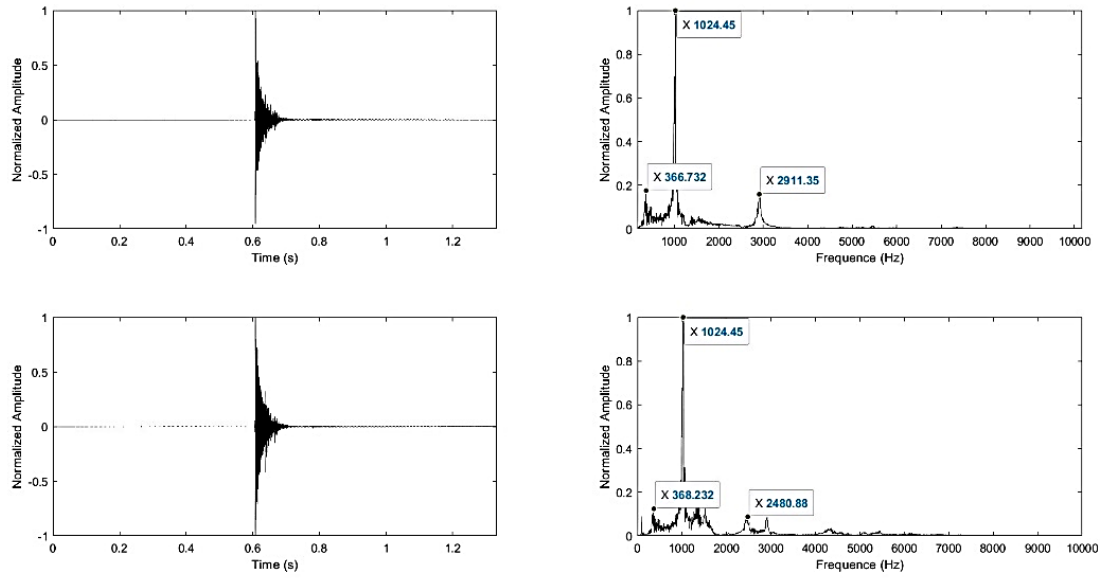

Figure 5.137 Vibration analysis results of the sample having 55- degrees filament wound, cured at 140°C and delamination in the middle

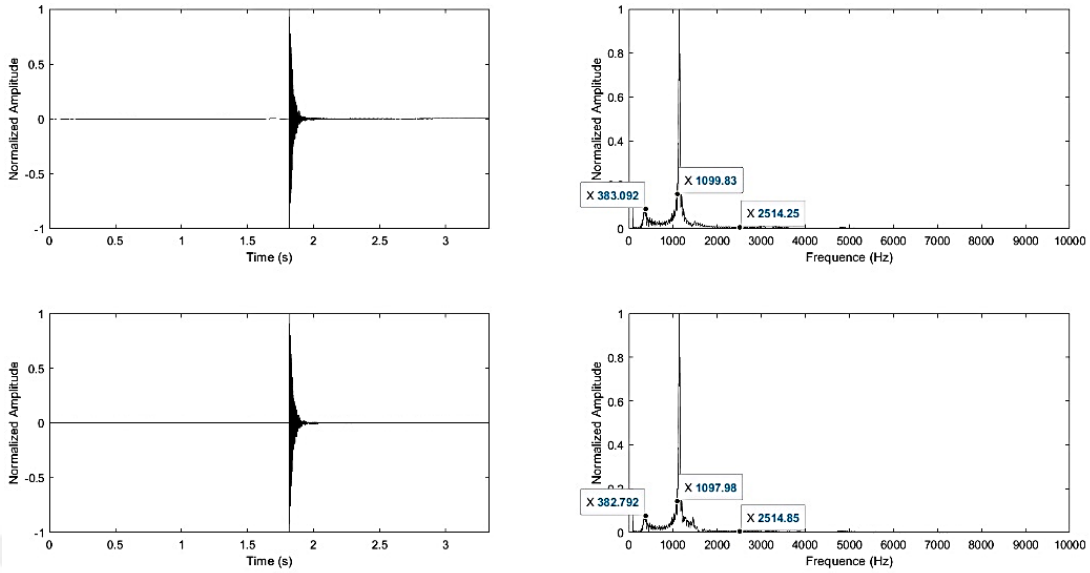

Figure 5.138 Vibration analysis results of the sample having 55- degrees filament wound, cured at 140°C and without delamination

In Figure 5.139-Figure 5.148, the variation of the first, second, and third natural frequencies regarding different 55 degrees filament wound, curing temperatures, delamination positions, and are shown.

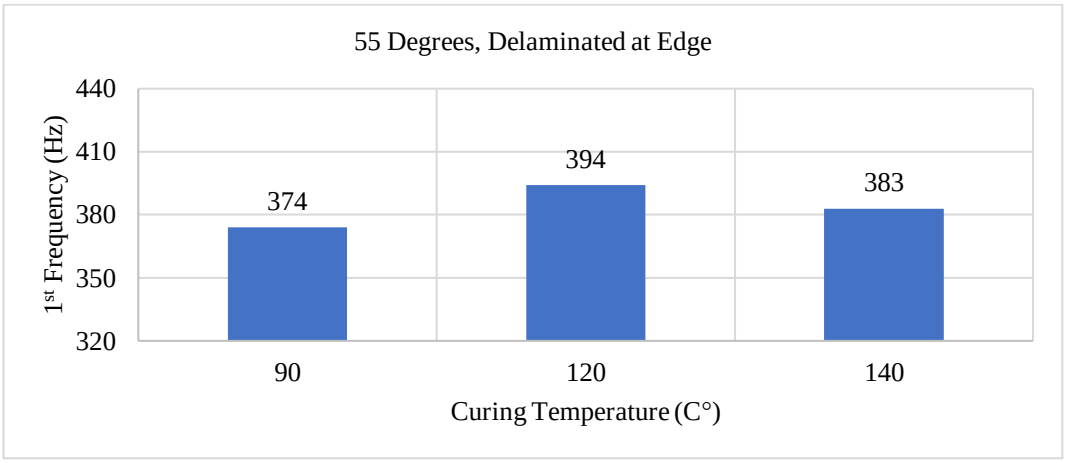

Figure 5.139 55 degrees filament wound, D++, for 1st natural frequency

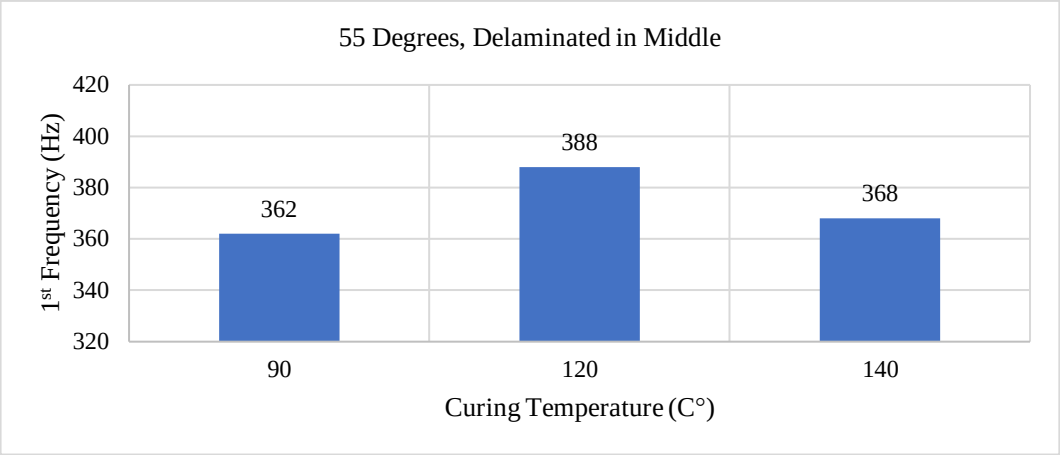

Figure 5.140 55 degrees filament wound, D+, for 1st natural frequency

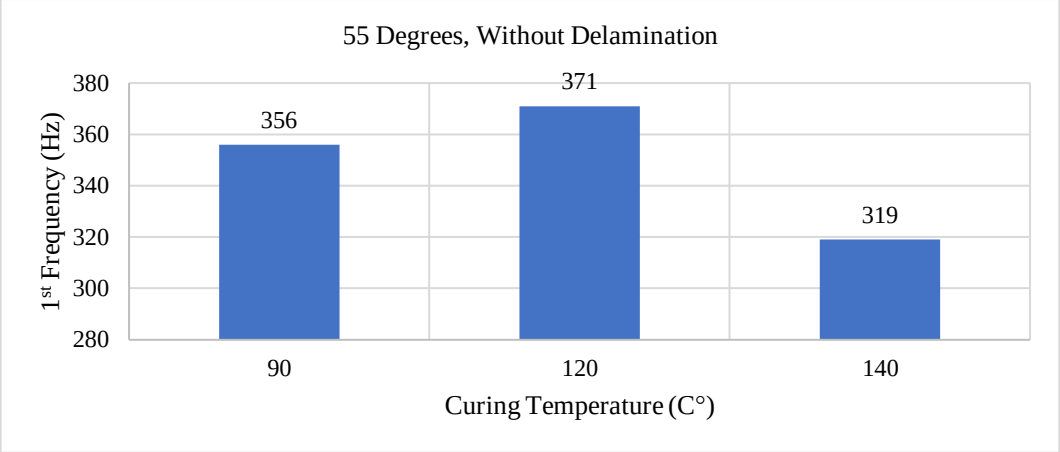

Figure 5.141 55 degrees filament wound, D-, for 1st natural frequency

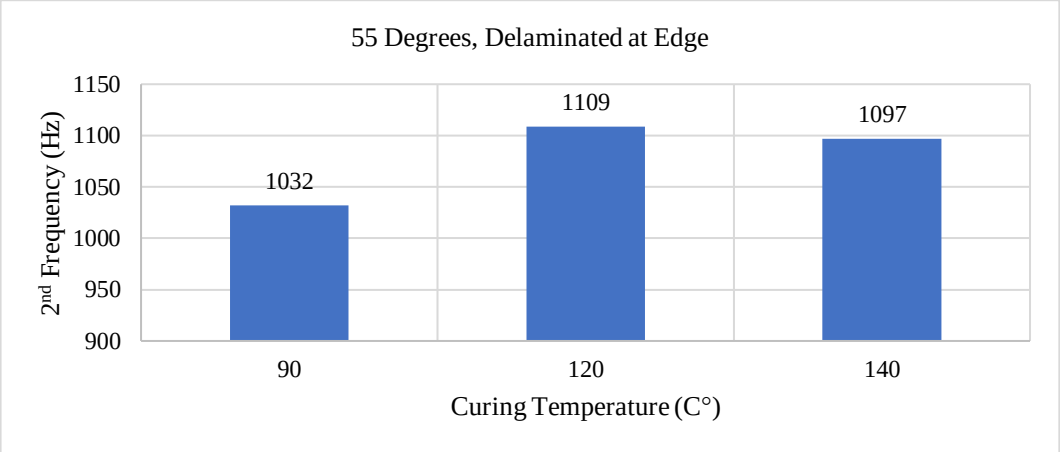

Figure 5.142 55 degrees filament wound, D++, for 2nd natural frequency

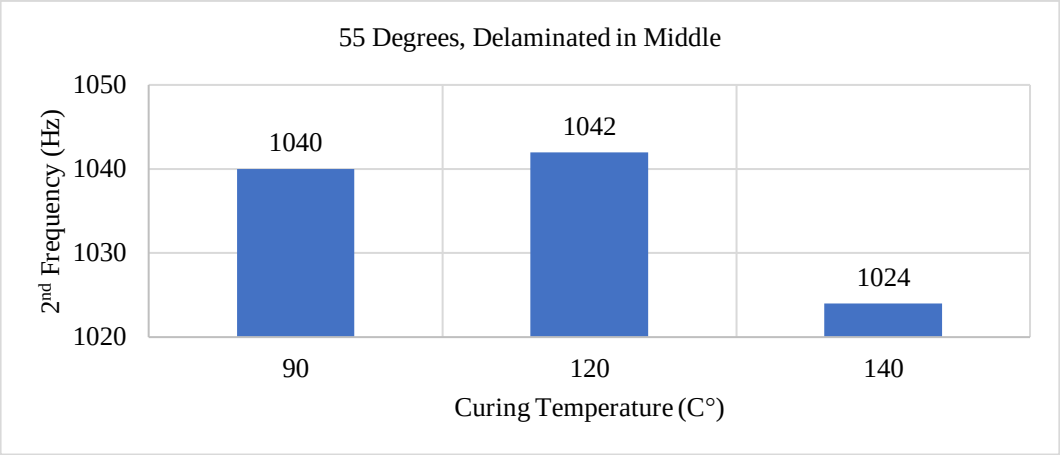

Figure 5.143 55 degrees filament wound, D+, for 2nd natural frequency

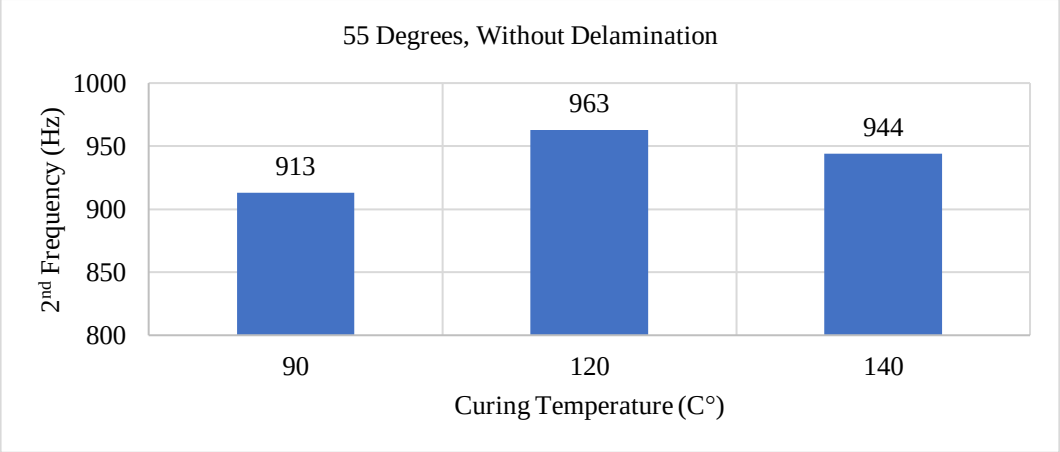

Figure 5.144 55 degrees filament wound, D-, for 2nd natural frequency

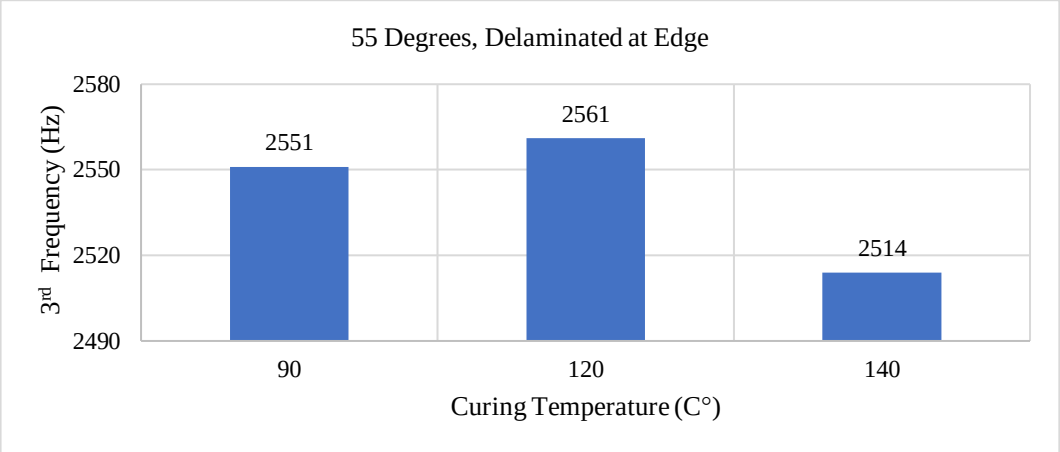

Figure 5.145 55 degrees filament wound, D++, for 3rd natural frequency

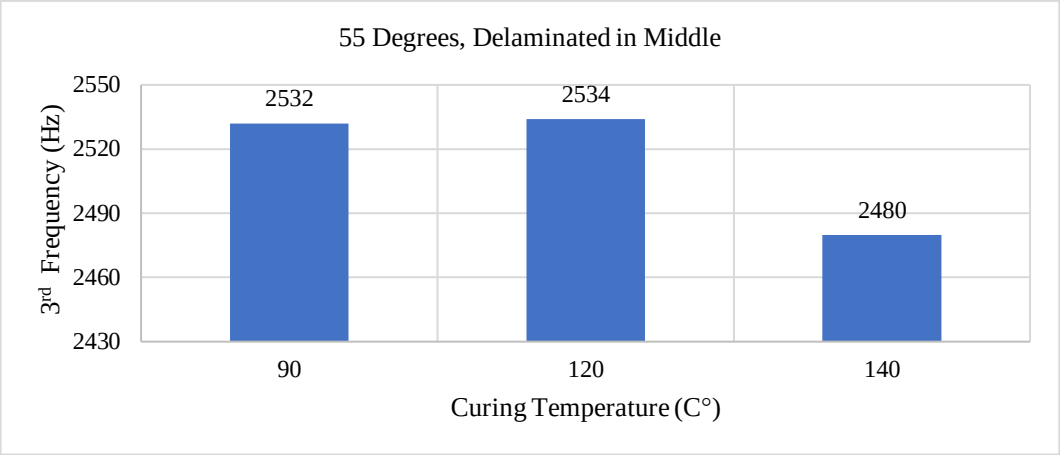

Figure 5.146 55 degrees filament wound, D+, for 3rd natural frequency

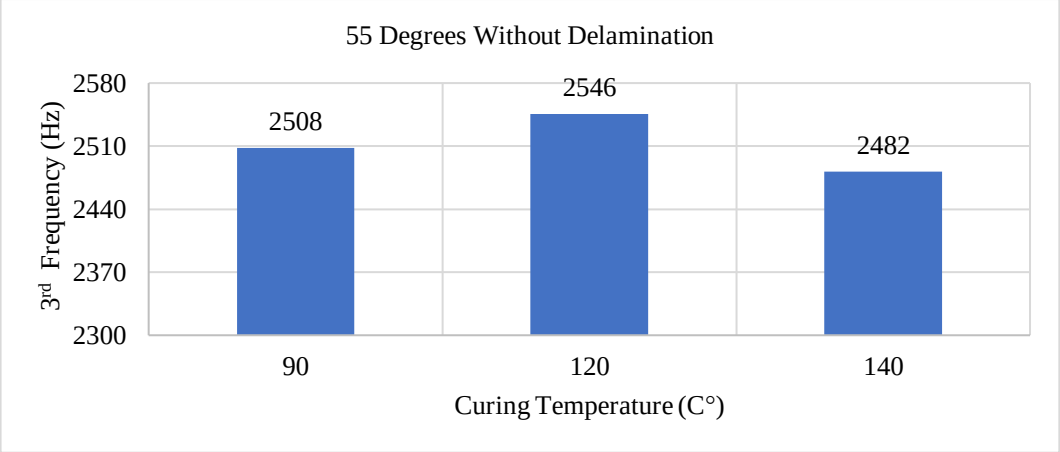

Figure 5.147 55 degrees filament wound, D-, for 3rd natural frequency

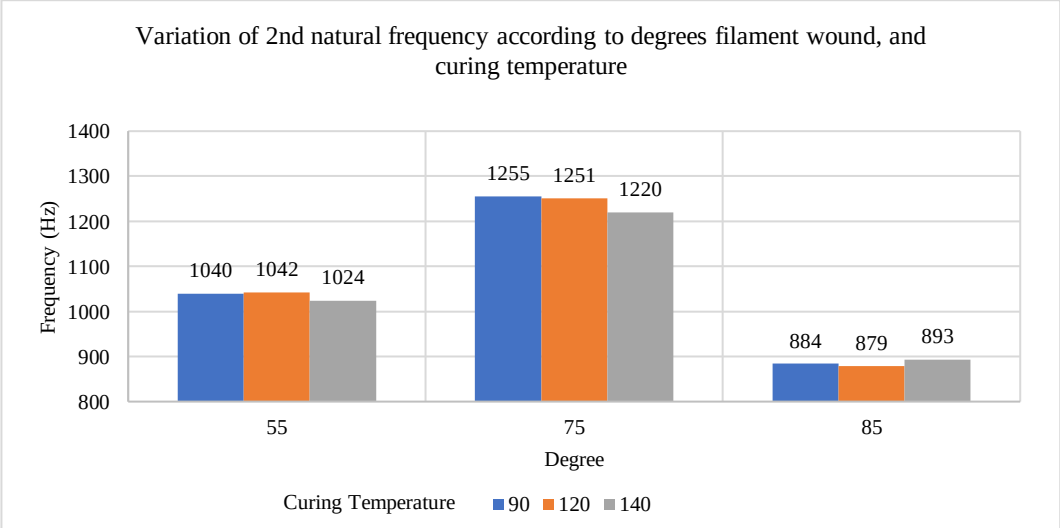

Figure 5.148 Variation of second natural frequency according to degrees filament wound, and curing temperature

In Figure 5.149, the comparison of the experiments for the fixed-free boundary condition with the analyzes made in the ANSYS program is shown. The experimental results of the samples produced with different laying angles are shown in the graphs as R55, R75 and R85. ANSYS results are seen as A55, A75 and A85 for each angle.

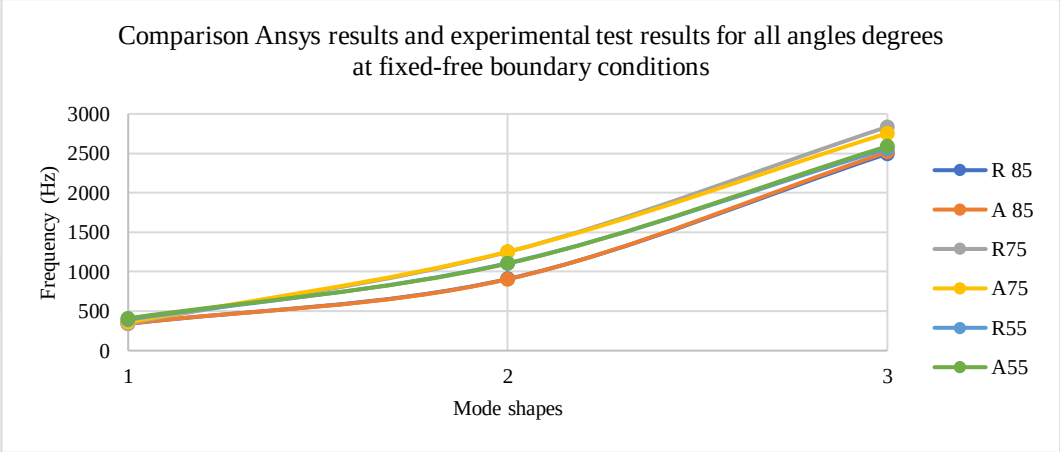

Figure 5.149 Comparison ANSYS results and experimental test results for all degrees at fixed-free boundary conditions

In Figure 5.150, the comparison of the experiments for the free-free boundary condition with the analyzes made in the ANSYS program is shown. The results of the samples produced with different laying angles are shown in the graphs as R55, R75 and R85. ANSYS results are seen as A55, A75 and A85 for each angle.

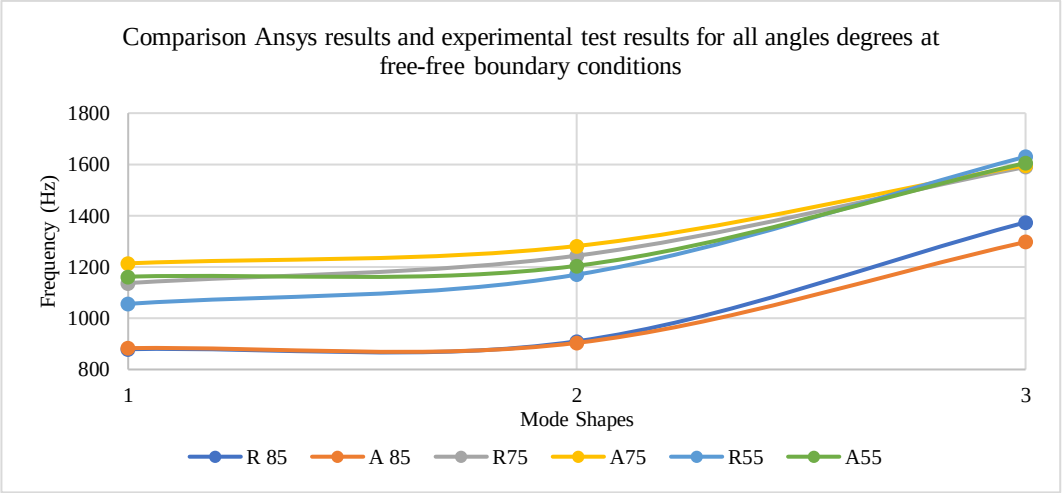

Figure 5.150 Comparison ANSYS results and experimental test results for all degrees at free-free boundary conditions

According to the data obtained from the literature review, the delamination located at the end of the structure lowers the natural frequency more than that located in the middle. Test results regarding the first and second natural frequencies were all as expected. For the third and fourth natural frequencies, the results of the sample with the delamination at the end were higher than the sample with the delamination in the middle.

The highest natural frequency results are obtained at a 75-degrees at all curing temperatures.

The lowest natural frequency was evaluated at 120°C degrees curing temperature in all delamination types according to the curing temperature in the sample produced with an angle configuration of 85 degrees.

The first and second natural frequencies of the products cured at 120°C degrees were found to be the highest in all delamination types according to the curing temperature in those produced with a 55-degrees angle configuration.

For all delamination types, the natural frequency decreased as the degrees increased for all delamination types produced with a 55-degrees angle configuration.

The natural frequency decreased as the degrees increased for all natural frequencies in all delamination types according to the curing temperature in the samples produced with a 75-degrees angle configuration.

ANSYS results show that the test results obtained in fixed-free boundary conditions converge more to the theoretical results than those obtained in free-free boundary conditions. The natural frequency values in the fixed free structure are lower than the free structure, this is due to geometry. Ghoneam et al. (2011) and Huang et al. (2018) in their studies, it was revealed that the natural frequency outputs of the tests performed under fixed-free boundary conditions for similar cylindrical geometries were the lowest.

5.6 Damping Ratio Results for Fixed-Free Boundary Condition

The damping ratio can be calculated using the logarithmic decrement method. In Figure 5.151-Figure 5.168, the variation of the damping ratio regarding different degrees filament wound, curing temperatures, and delamination positions are shown.

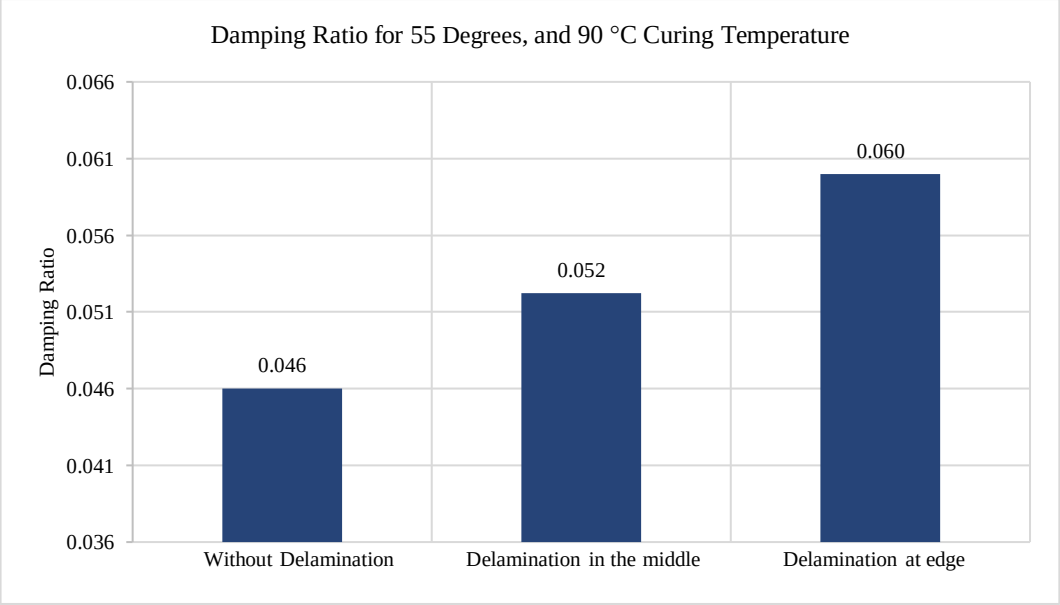

Figure 5.151 Damping ratio for 55 degrees filament wound, and 90 °C curing temperature

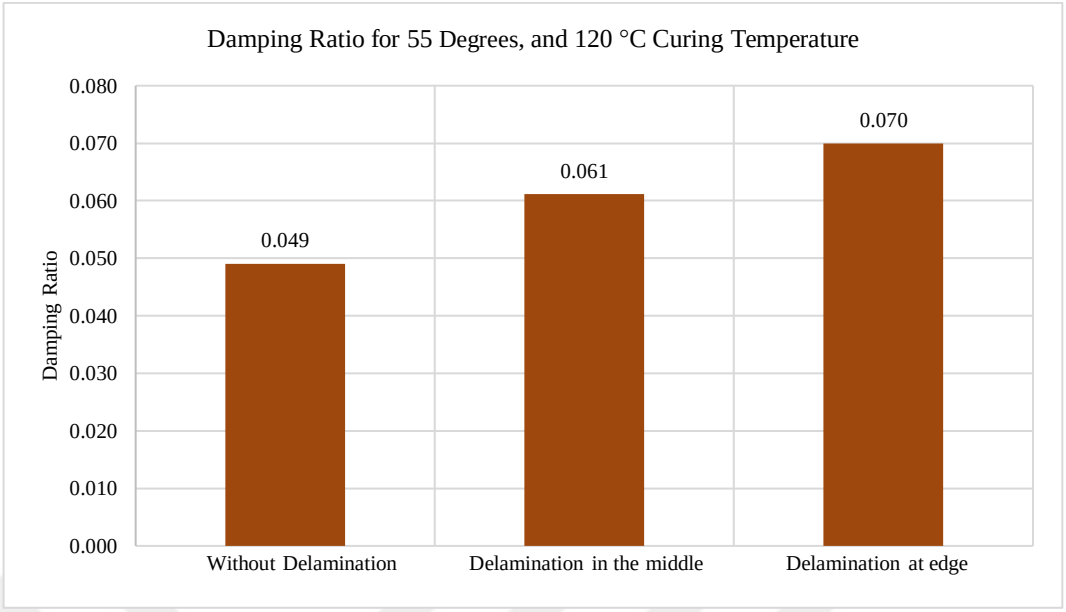

Figure 5.152 Damping ratio for 55 degrees filament wound, and 120 °C curing temperature

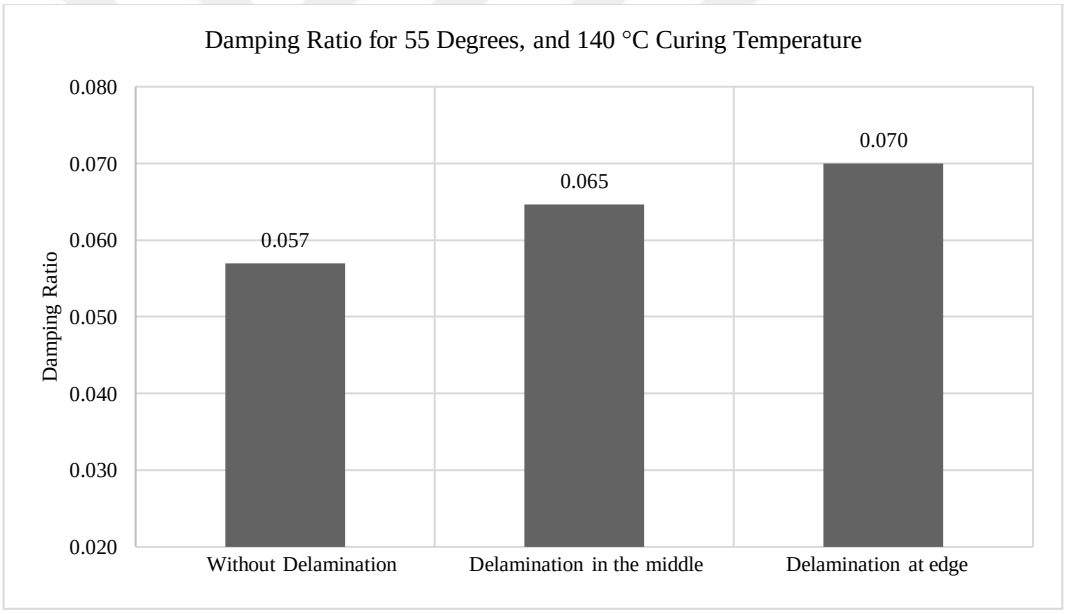

Figure 5.153 Damping ratio for 55 degrees filament wound, and 140 °C curing temperature

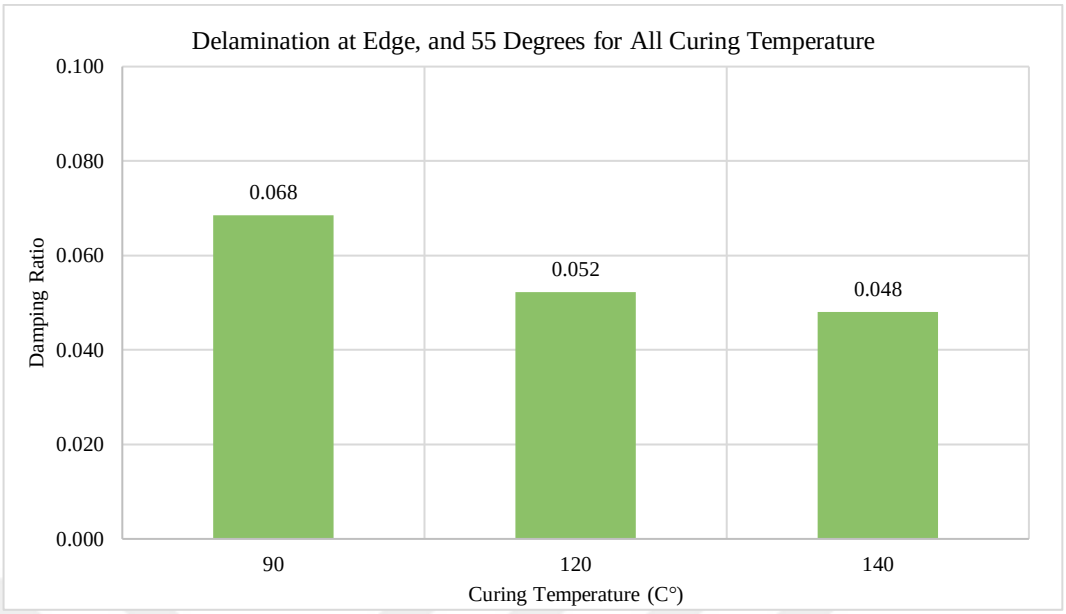

Figure 5.154 Damping ratio of the structure delamination at edge, and 55 degrees filament wound for all curing temperature

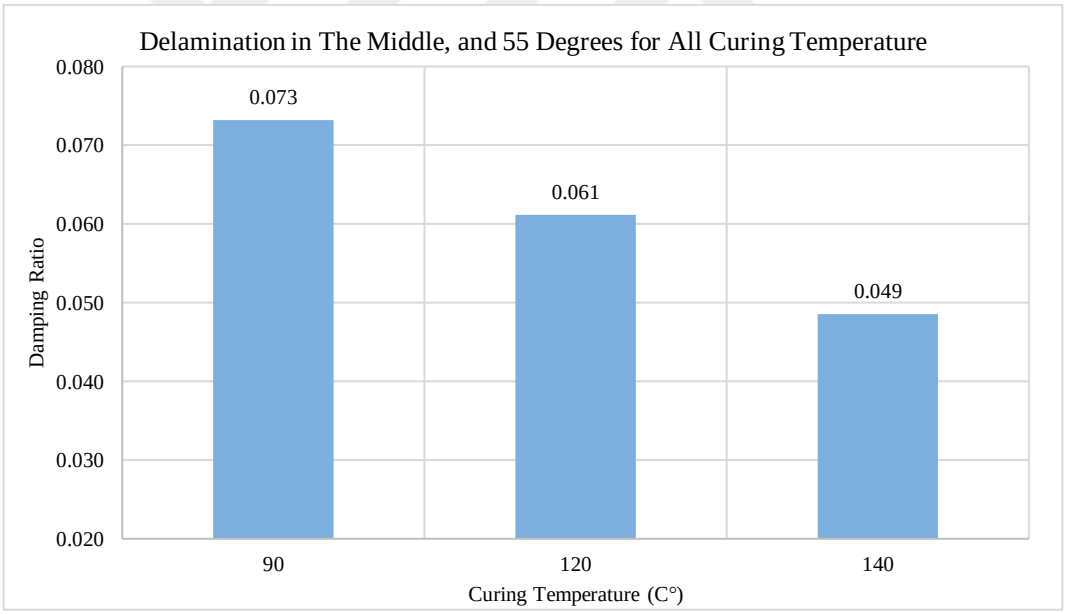

Figure 5.155 Damping ratio of the structure delamination in the middle, and 55 degrees filament wound for all curing temperature

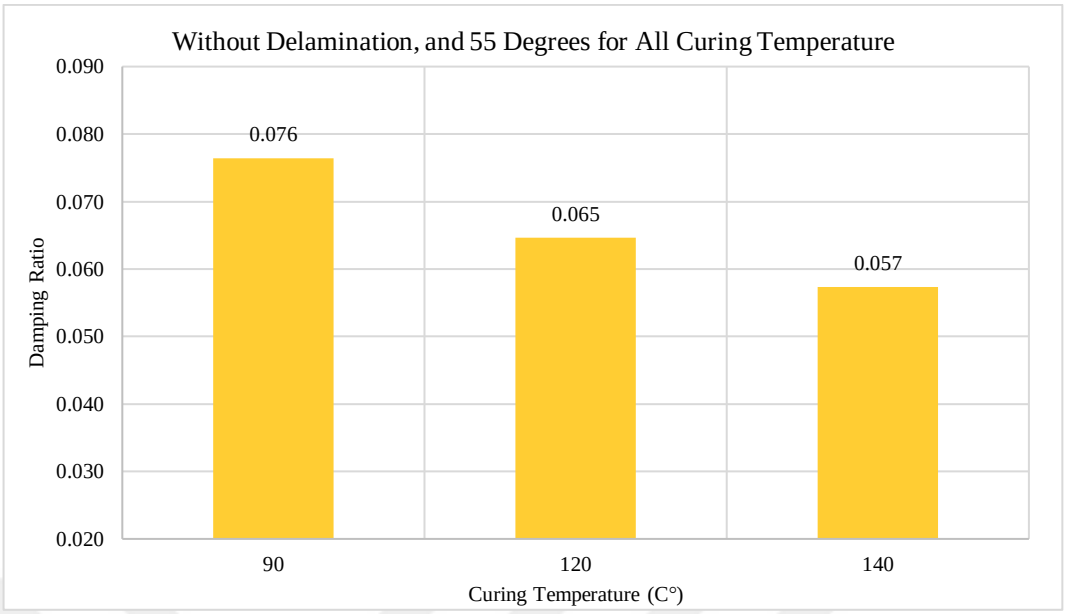

Figure 5.156 Damping ratio of the structure without delamination, and 55 degrees filament wound for all curing temperature

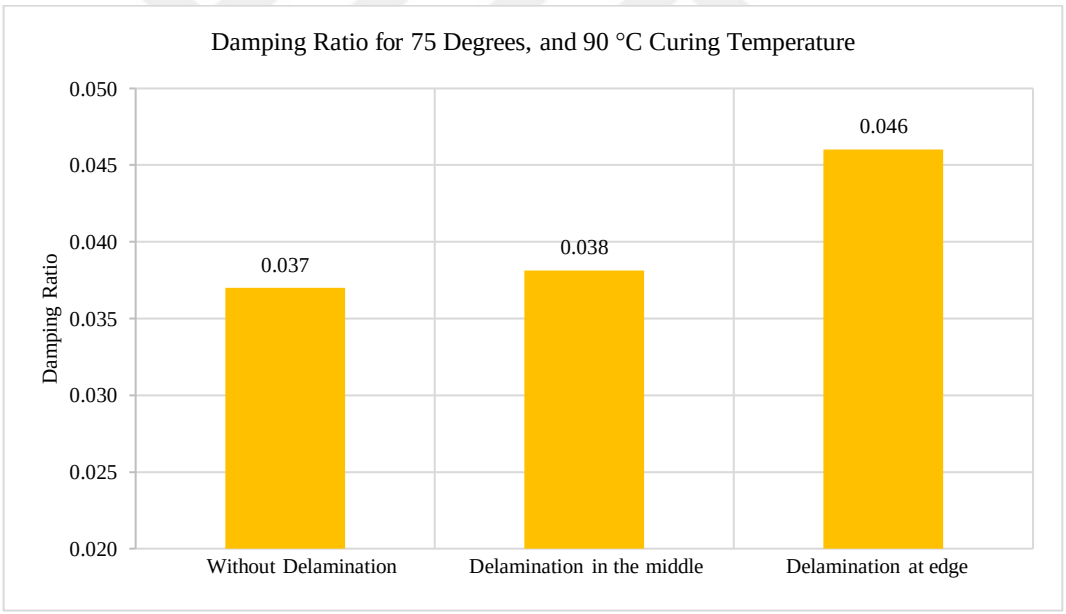

Figure 5.157 Damping ratio for 75 degrees filament wound, and 90 °C curing temperature

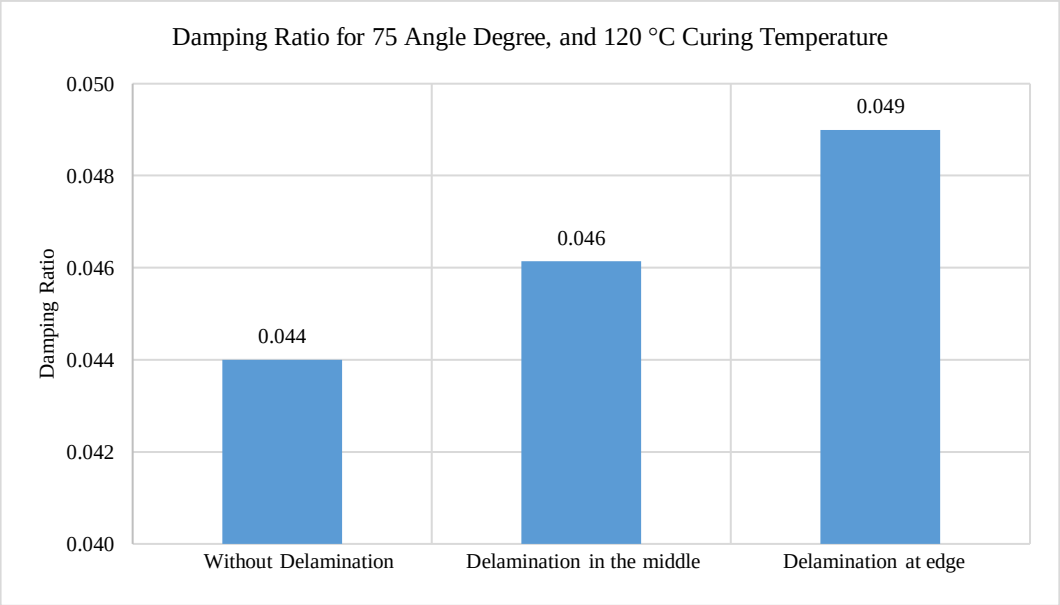

Figure 5.158 Damping ratio for 75 degrees filament wound, and 120 °C curing temperature

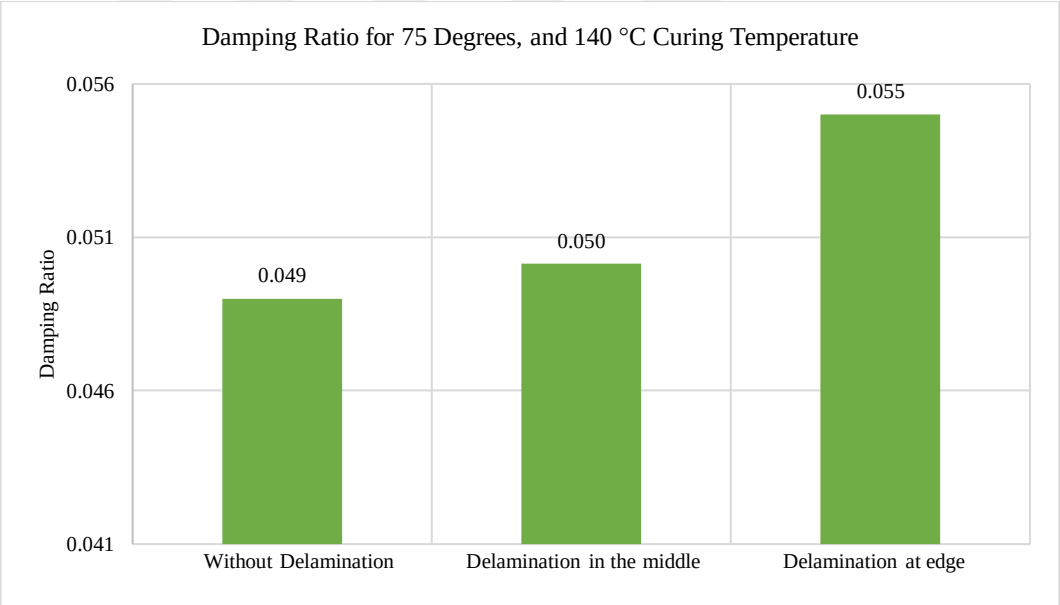

Figure 5.159 Damping ratio for 75 degrees filament wound, and 140 °C curing temperature

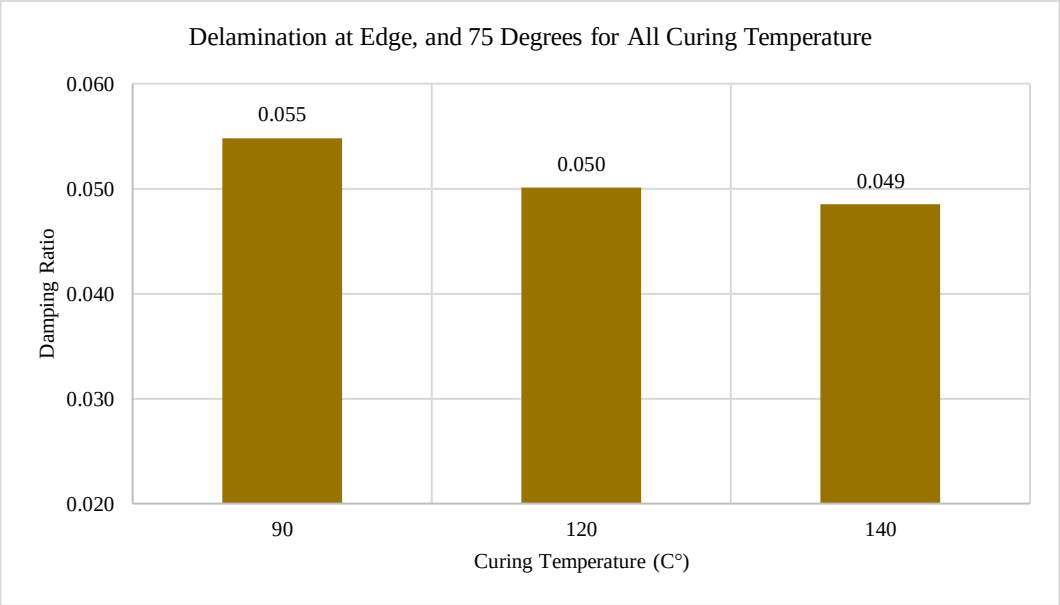

Figure 5.160 Damping ratio of the structure delamination at edge, and 75 degrees filament wound for all curing temperature

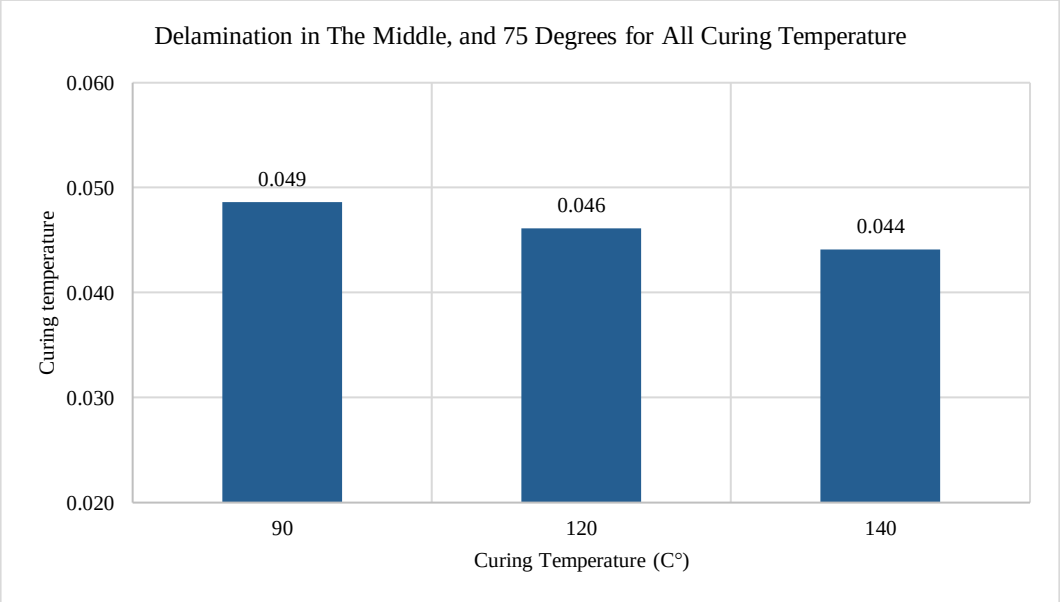

Figure 5.161 Damping ratio of the structure delamination in the middle, and 75 degrees filament wound for all curing temperature

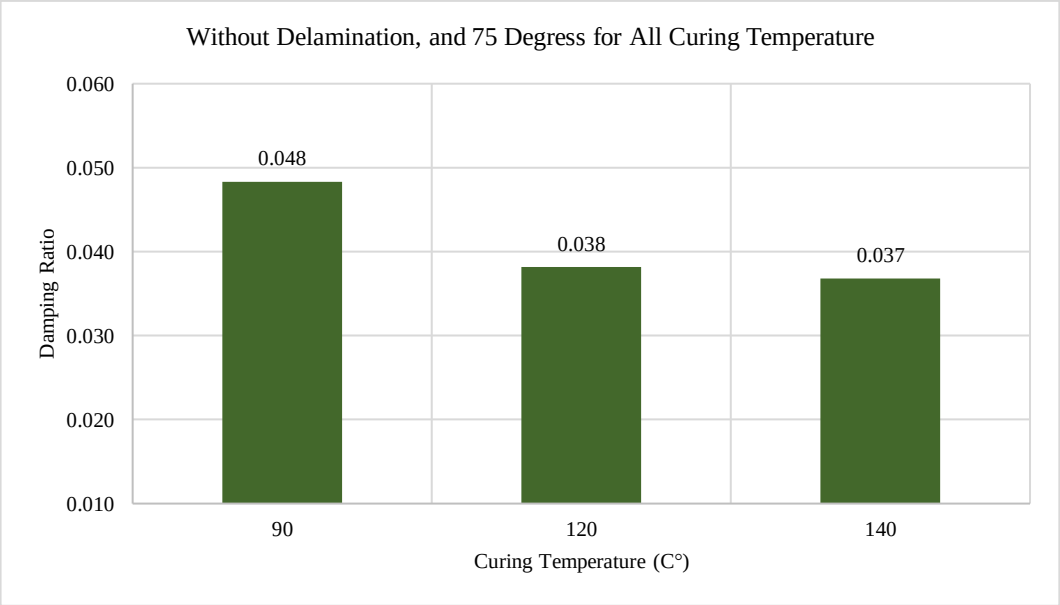

Figure 5.162 Damping ratio of the structure without delamination, and 75 degrees filament wound for all curing temperature

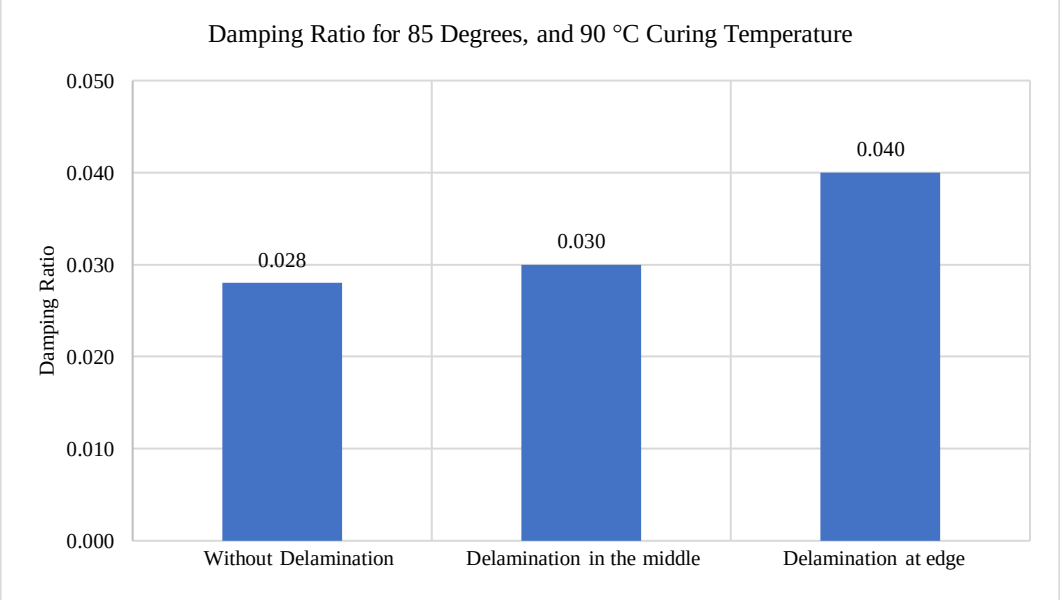

Figure 5.163 Damping ratio for 85 degrees filament wound, and 90 °C curing temperature

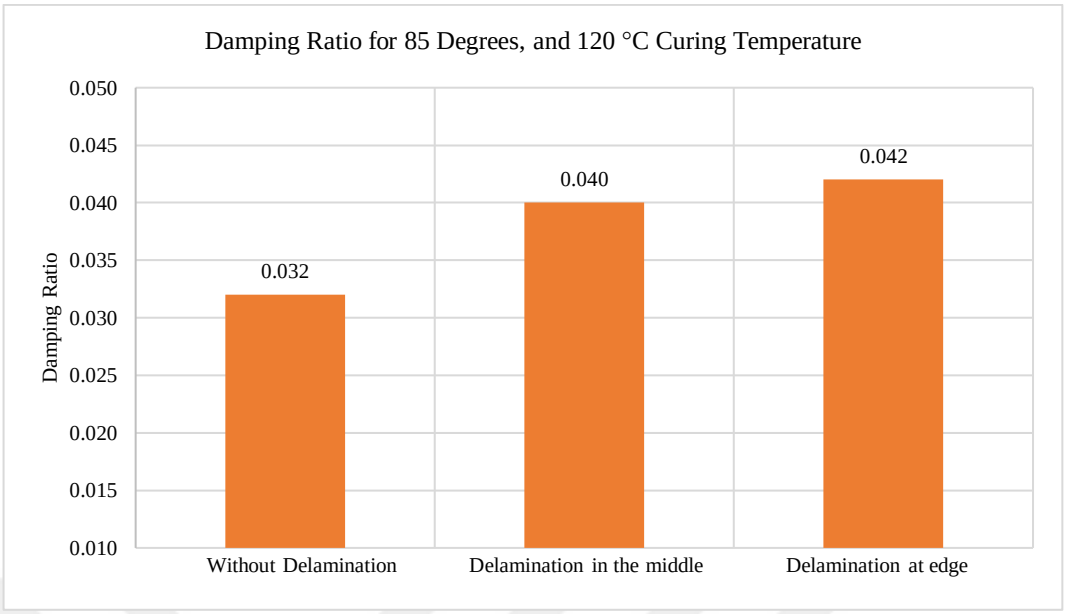

Figure 5.164 Damping ratio for 85 degrees filament wound, and 120 °C curing temperature

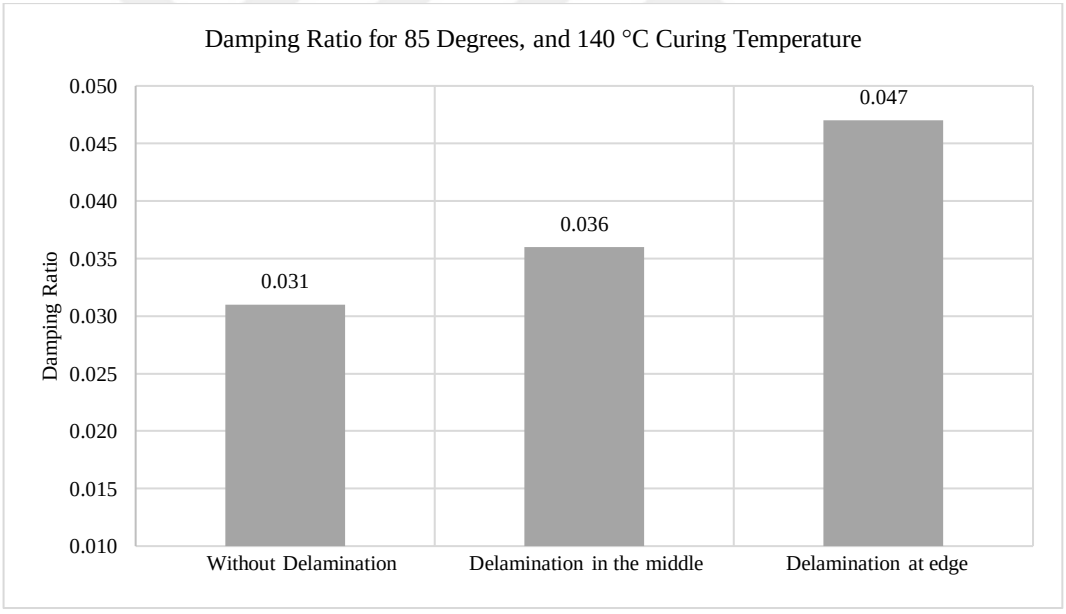

Figure 5.165 Damping ratio for 85 degrees filament wound, and 140 °C curing temperature

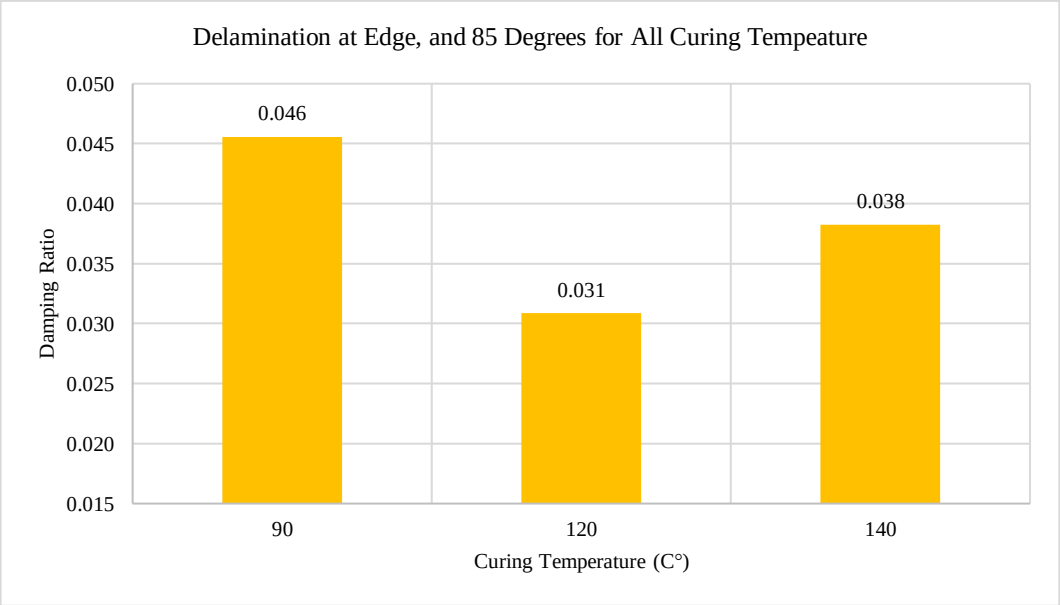

Figure 5.166 Damping ratio of the structure delamination at edge, and 85 degrees filament wound for all curing temperature

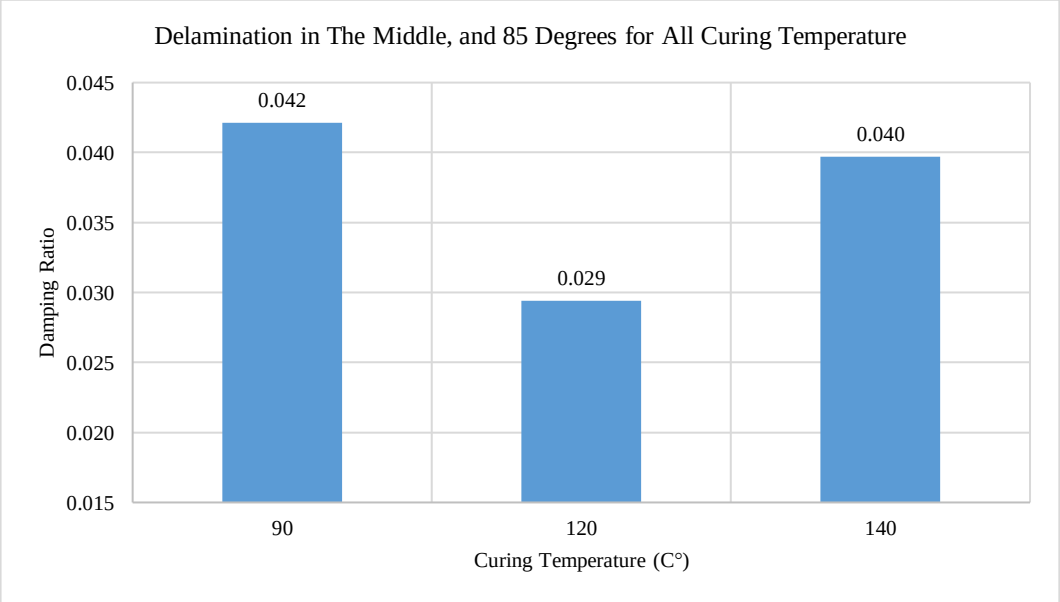

Figure 5.167 Damping ratio of the structure delamination in the middle, and 85 degrees filament wound for all curing temperature

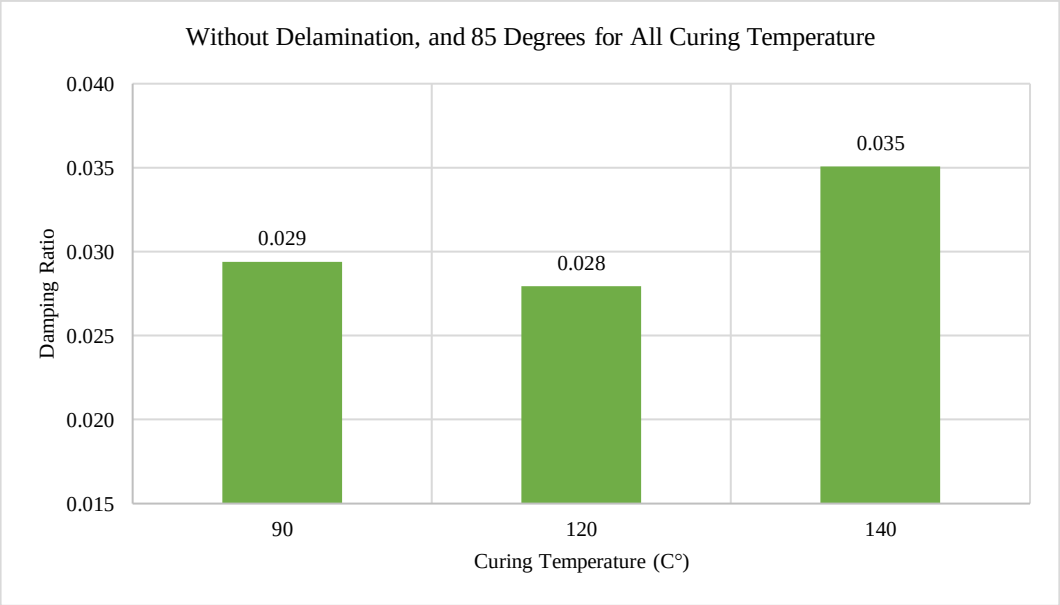

Figure 5.168 Without delamination, and 85 degrees filament wound for all curing temperature

The presence of delamination was compared with its location and presence in this study. The proximity of the delamination to the open end weakened the structure's stability. The delamination in the middle reduced the structure's stiffness less than it did at the end. The damping ratio was shown to rise as the delamination area increased. (He et at.,2019).

The stiffness matrices of the samples were affected by the variation in curing temperature by taking variable values based on the thickness and fiber laying angle for each sample. It is well known that as stiffness increases, so does the damping ratio (Kim et al.,1993). The fluctuation of the natural frequency in the samples as a function of temperature and the variation of the damping ratio as a function of temperature were found to be pretty similar.

Changing the boundary conditions obtained mode shape findings in this investigation. Because a change in boundary conditions has a direct effect on the system's equation of motion in terms of stiffness, it has resulted in damping ratio disparities between free-free and fixed-free. Comparisons demonstrate that when the global optimum is close to the boundary of the solution space, the unconstrained

boundary conditions are more efficient, and the damping boundary condition is more resilient and consistent (Fotsing et al.,2013).

The difference in damping was generally less than the shift in natural frequencies. The outcomes were often close. Damping outputs are less reliable than mod shape outputs (Brennan et al.,2005).

CHAPTER SIX
FINITE ELEMENT ANALYSIS OF COMPOSITE PRESSURE VESSEL

In this section, composite pressure vessels, another product produced by the filament winding method, are examined. Composite pressure vessels are lightweight and can operate at very high pressures. In this thesis, since the production and pressurization of composite pressure vessels are expensive, it is preferred to analyze them numerically rather than experimentally.

Classical lamination theory is used to determine the mechanical properties of composite materials. The theory assumes that the layers that make up the composite structure are orthotropic and homogeneous. The resin content of products with high engineering properties is less than fiber. At least a 60 percent fiber-to-resin ratio is provided in advanced composite materials. Resins are less durable than fibers. The matrix acts as an intermediary in the composite structure, transmitting the load between the fibers. The glass fiber-reinforced epoxy resin material's mechanical properties are calculated for a 60 percent fiber-to-resin ratio. The material data used for the experiment are given in Table 6.1 Material Data (Kaw, 2005).

Table 6.1 Material Data (Kaw, 2005)

Material Properties	
Density (kg/m^3)	2000
Modulus of Elasticity E_1 (GPa)	43
Modulus of Elasticity E_2 (GPa)	8.9
Major Poisson Ratio v_{12}	0.27
Minor Poisson Ratio v_{21}	0.06

When the composite structure testing free-free end condition boundary condition was used. The inner diameter of the composite pressure vessel is Ø 72 mm and shown in Figure 6.1 The boundary conditions, and the applied inner pressure is shown in Figure 6.2 , and Figure 6.3.

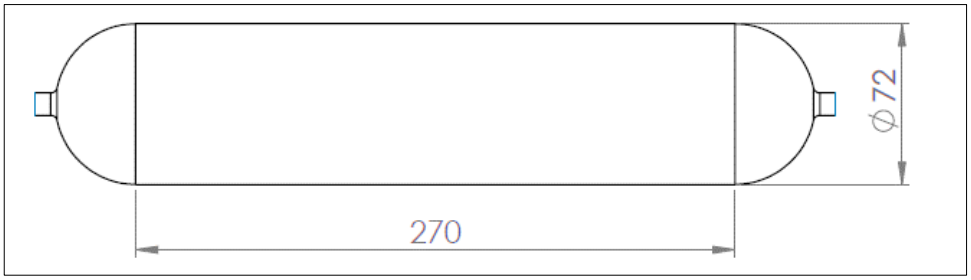

Figure 6.1 Dimension of composite pressure vessel

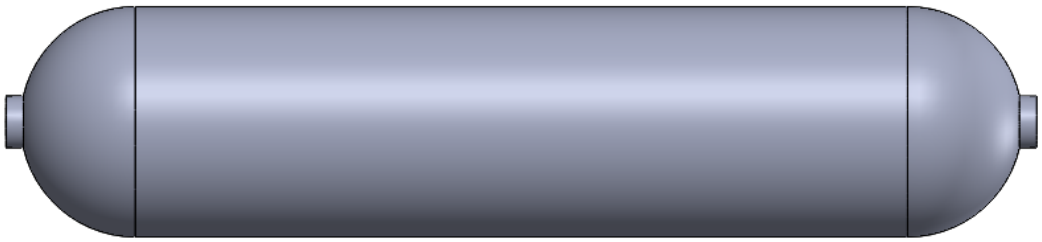

Figure 6.2 Free-free end boundary condition

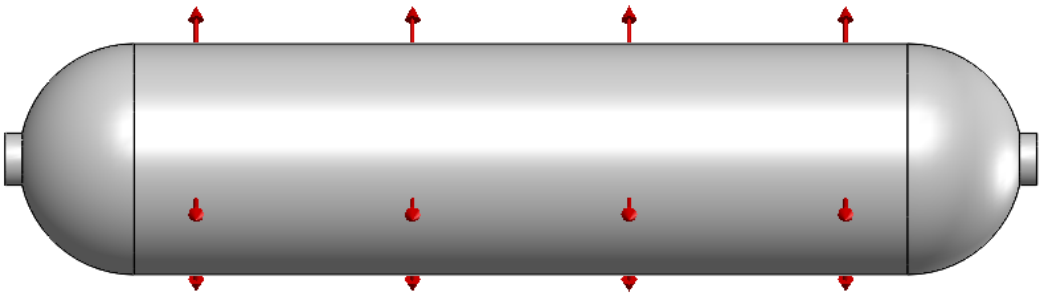

Figure 6.3 Inner pressure, and free-free end boundary condition

There are different experimental methods to find the damping matrix. In this study, the damping matrix was not calculated. Natural frequencies and mode shapes were found for the angled filament-wound tubes by using the mass and stiffness matrix.

The cylindrical composite structure was analyzed using the finite element method with the ANSYS program.

The filament winding process creates different layer thicknesses for different angles in accordance with its characteristics. To examine the impact of changes in angle, analyses were conducted with a constant layer thickness of 1 mm. In the next part, analyses with real layer thicknesses were carried out. Composite pressure vessels are forced by internal pressure during use. In the analysis, we examined composite pressure vessels operating in pressurized and unpressurized conditions and compared their ideal conditions together.

Table 6.2. Vibration analysis results of the pressure vessel having 55- degrees filaments wound and layer thickness of 1 mm

Mode Number	Free Vibration (Hz)	Under 2MPa Pressure (Hz)
1	955,75	1080,64
2	955,75	1084,18
3	1559,6	1564,31
4	1559,8	1566,40
5	1618,1	1707,51
6	1618,3	1712,37

In Figure 6.4, and Figure 6.5 show the first six natural frequencies of the vessel with 55 degrees of winding angle and 1mm layer thickness.

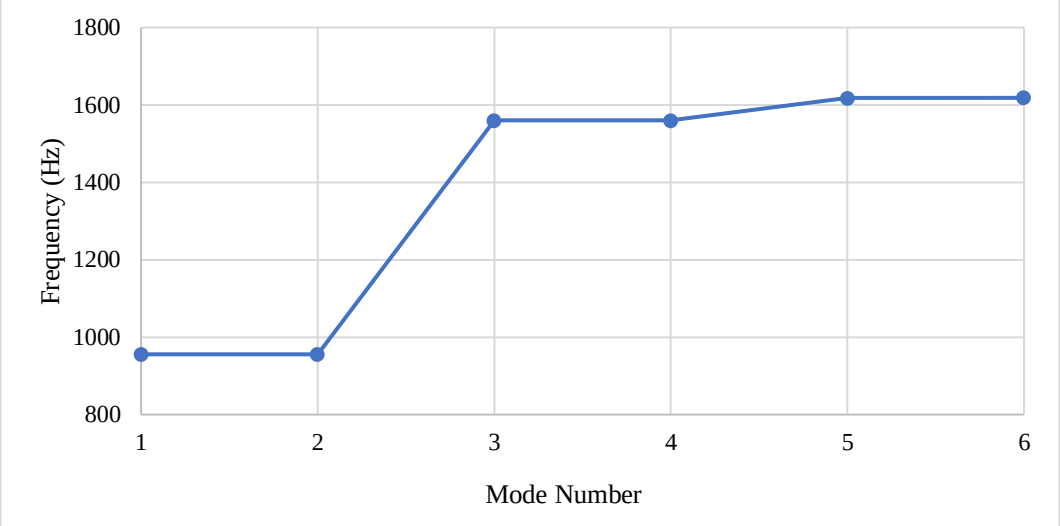

Figure 6.4 Natural frequencies for 55 degrees without pressure

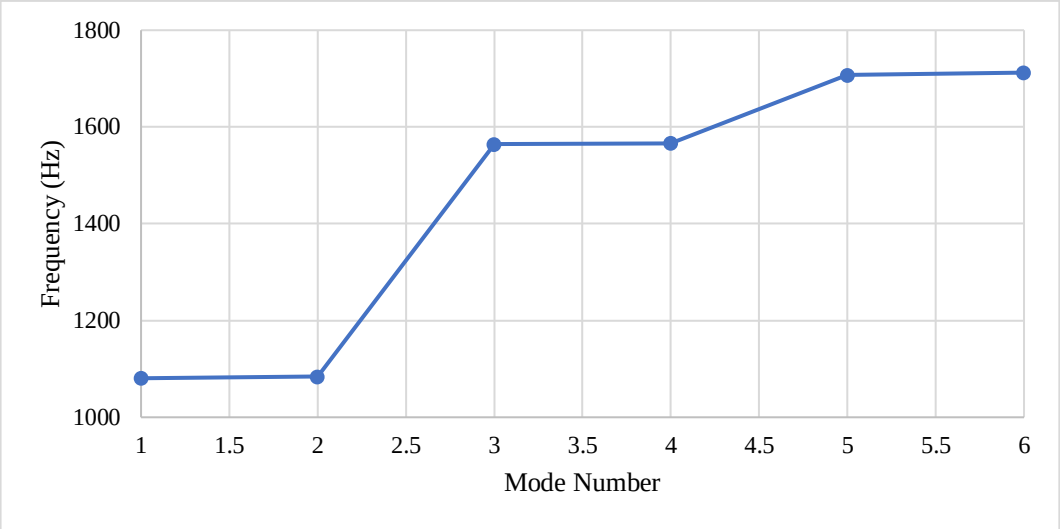

Figure 6.5 Natural frequencies for 55 degrees with pressure

The first six natural frequencies for pressurized at 2 MPa composite pressure vessels were higher than the first six natural frequencies for unpressurized pressure vessels wound at 55 degrees.

In Figure 6.6, and Figure 6.7 show the first six mode shapes of the non-pressurized and pressurized pressure vessel with 55 degrees filament wound and 1mm layer thickness.

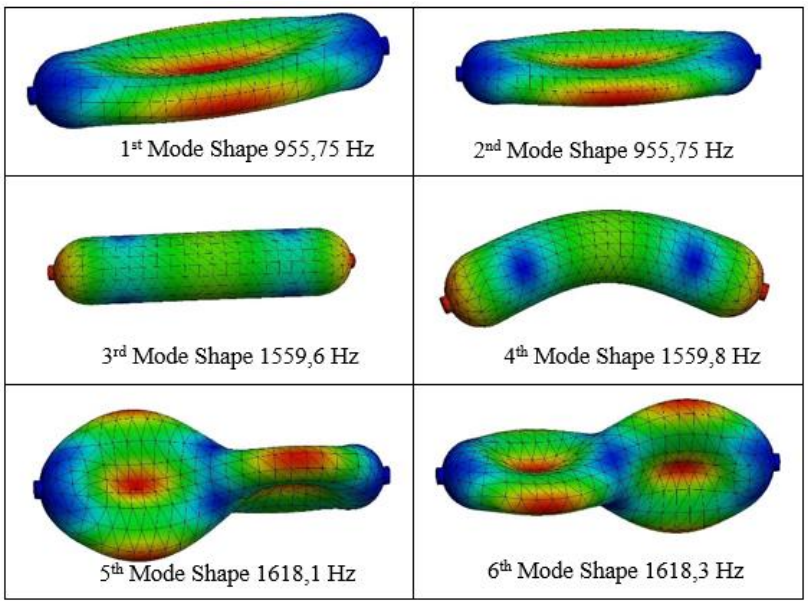

Figure 6.6 The first six mode shapes of the non-pressurized pressure vessel with 55 degrees wounding angle

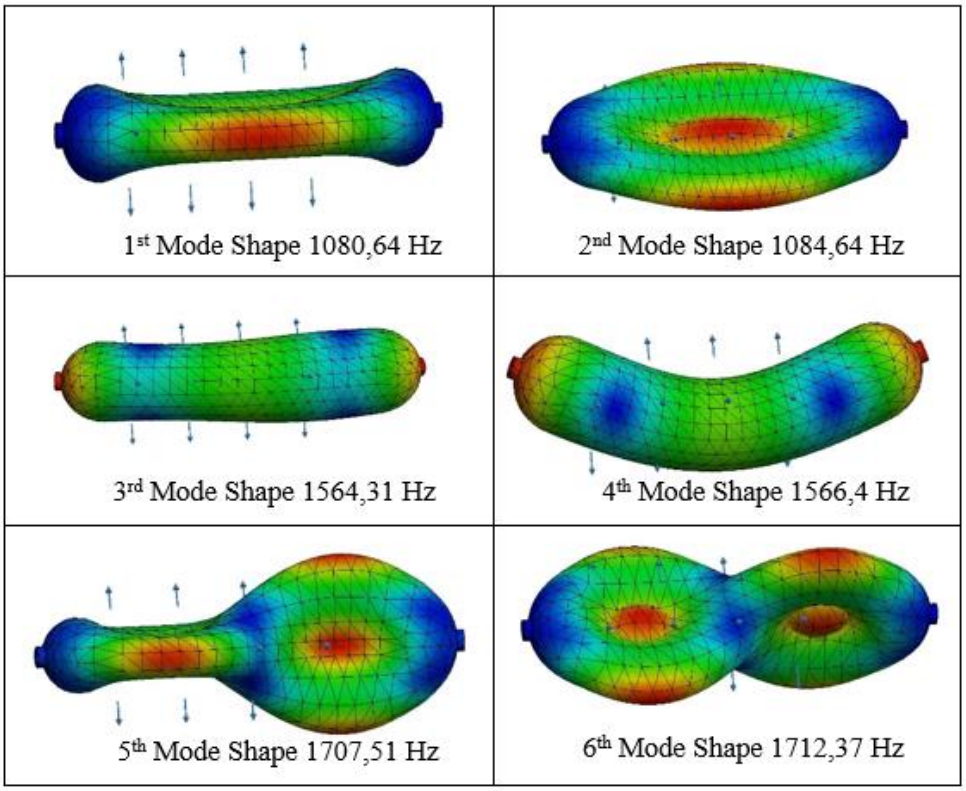

Figure 6.7 The first six mode shapes of the pressurized pressure vessel with 55 degrees wounding angle

Table 6.3 Vibration analysis results of the pressure vessel having 75- degrees filaments wound and layer thickness of 1 mm

Mode Number	Free Vibration (Hz)	Under 2MPa Pressure (Hz)
1	1299,9	1464,05
2	1300	1467,39
3	1527,7	1532,81
4	1529,2	1534,31
5	1758,3	1851,25
6	1759,7	1857,61

In Figure 6.8 and Figure 6.9 the first six natural frequencies of the vessel with 75 degrees filament wound and 1mm layer thickness.

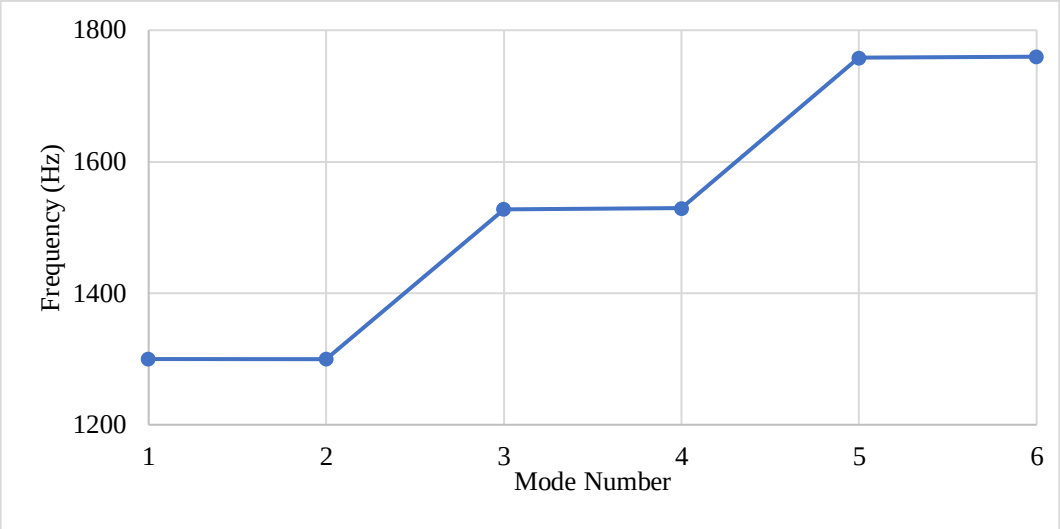

Figure 6.8 Natural frequencies for 75 degrees without pressure

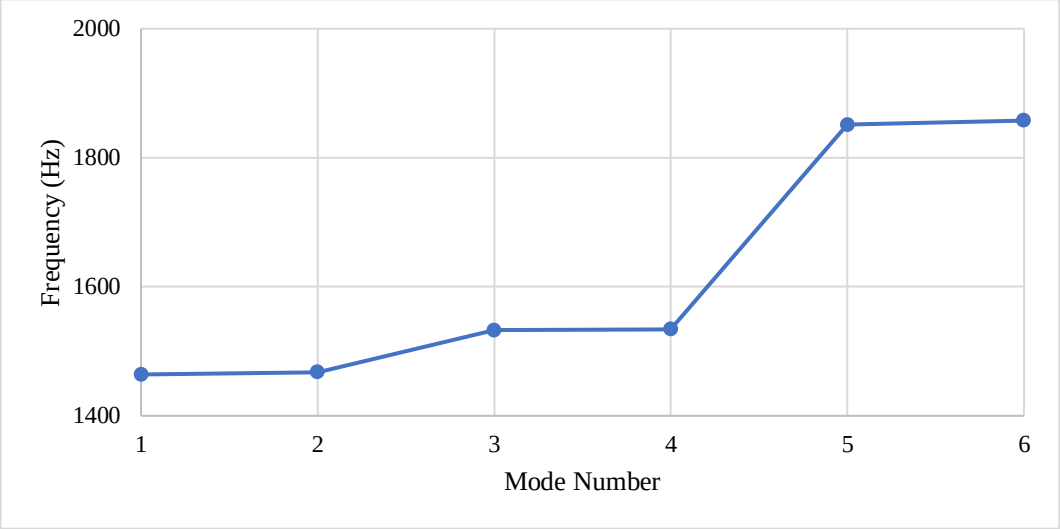

Figure 6.9 Natural frequencies for 75 degrees with pressure

The first six natural frequencies for pressurized at 2 MPa composite pressure vessels were higher than the first six natural frequencies for unpressurized pressure vessels wound at 75 degrees.

In Figure 6.10 and Figure 6.11 show the first six mode shapes of the non-pressurized and pressurized pressure vessel with 75 degrees filament wound and 1mm layer thickness.

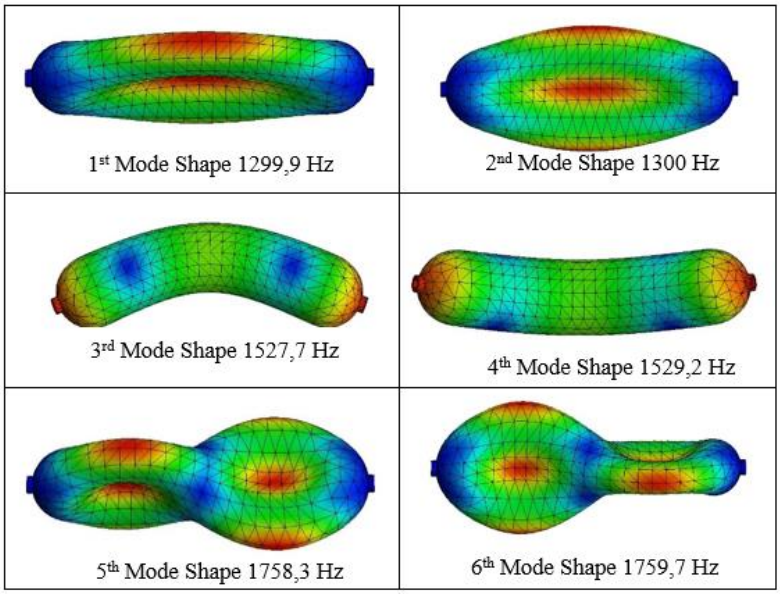

Figure 6.10 The first six mode shapes of the non-pressurized pressure vessel with 75 degrees wounding angle

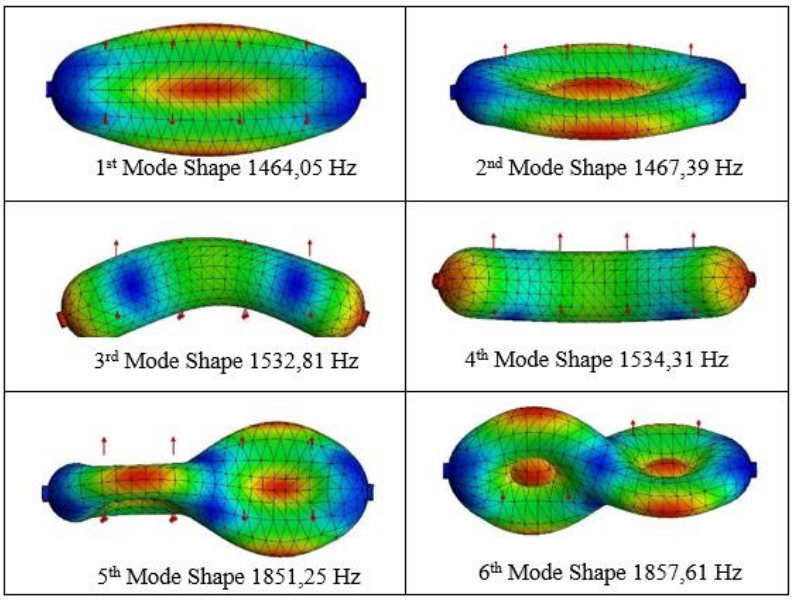

Figure 6.11 The first six mode shapes of the pressurized pressure vessel with 75 degrees wounding angle

Table 6.4 Vibration analysis results of the pressure vessel having 85- degrees filaments wound and layer thickness of 1 mm

Mode Number	Free Vibration (Hz)	Under 2MPa Pressure (Hz)
1	1497,7	1564,33
2	1501,3	1570,48
3	1589	1590,09
4	1589,4	1591,04
5	1959,4	1995,61
6	1962,1	2000,30

In Figure 6.12, and Figure 6.13 show the first six natural frequencies of the vessel with 85 degrees filament wound and 1mm layer thickness.

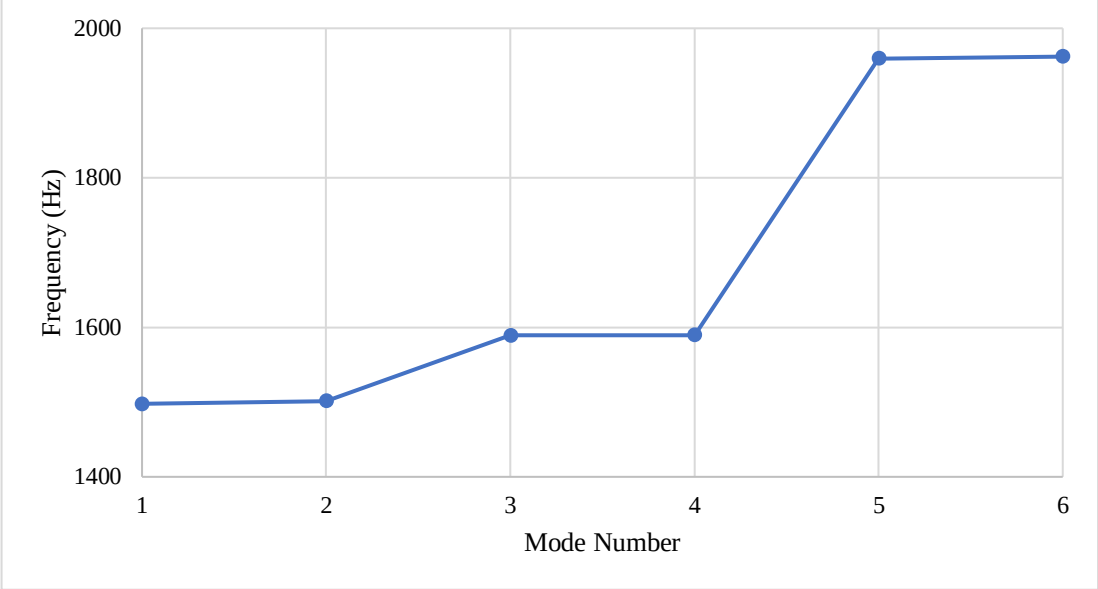

Figure 6.12 Natural frequencies for 85 degrees without pressure

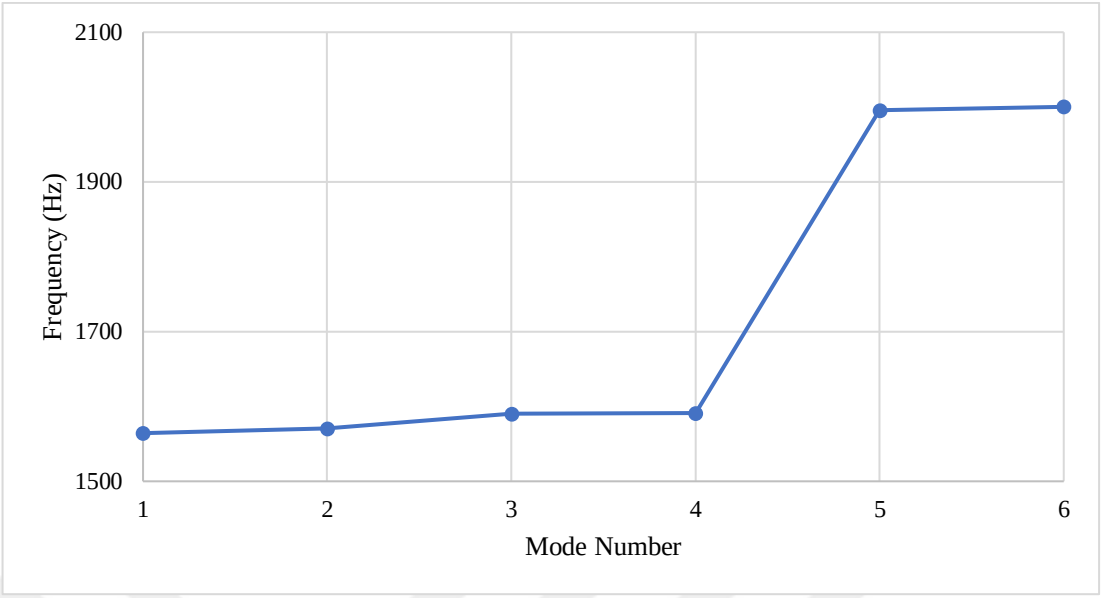

Figure 6.13 Natural frequencies for 85 degreess with pressure

Composite pressure vessels wound at 85 degrees have the highest natural frequency due to the advantage of angular orientation compared to other angles. The first six natural frequencies for pressurized composite pressure vessels at 2 MPa were higher than the first six natural frequencies for unpressurized pressure vessels wound at 85 degrees.

In Figure 6.14 and Figure 6.15 show the first six mode shapes of the non-pressurized and pressurized pressure vessel with 75 degrees filament wound and 1mm layer thickness.

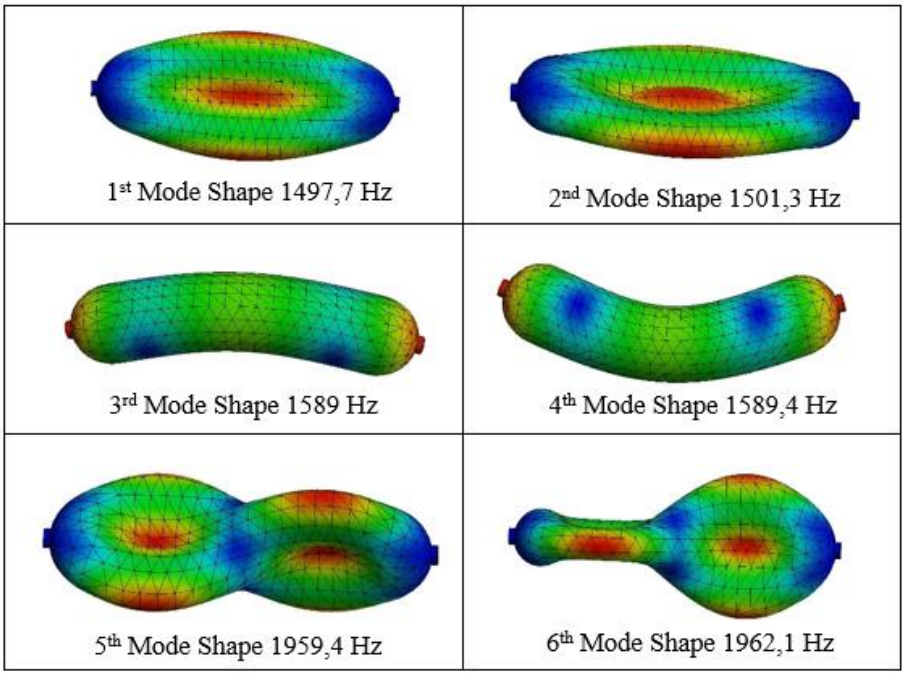

Figure 6.14 The first six mode shapes of the non-pressurized pressure vessel with 85 degrees filaments wound

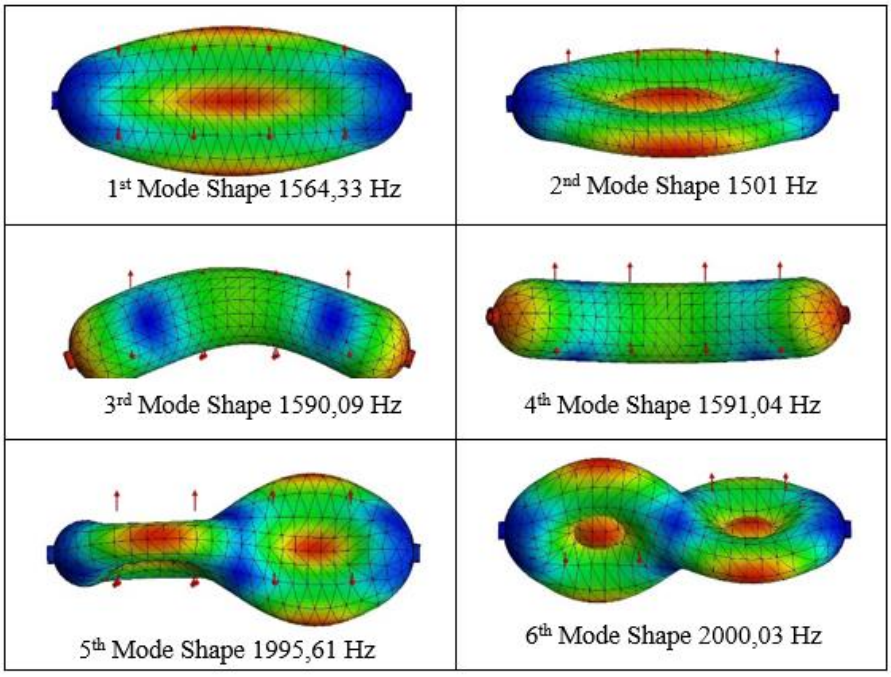

Figure 6.15 The first six mode shapes of the pressurized pressure vessel with 85 degrees filaments wound

In Figure 6.16 show the differences in the first six natural frequencies for all degrees filament wound without pressure and Figure 6.17 the differences in the first six natural frequencies for all degrees filament wound with pressure.

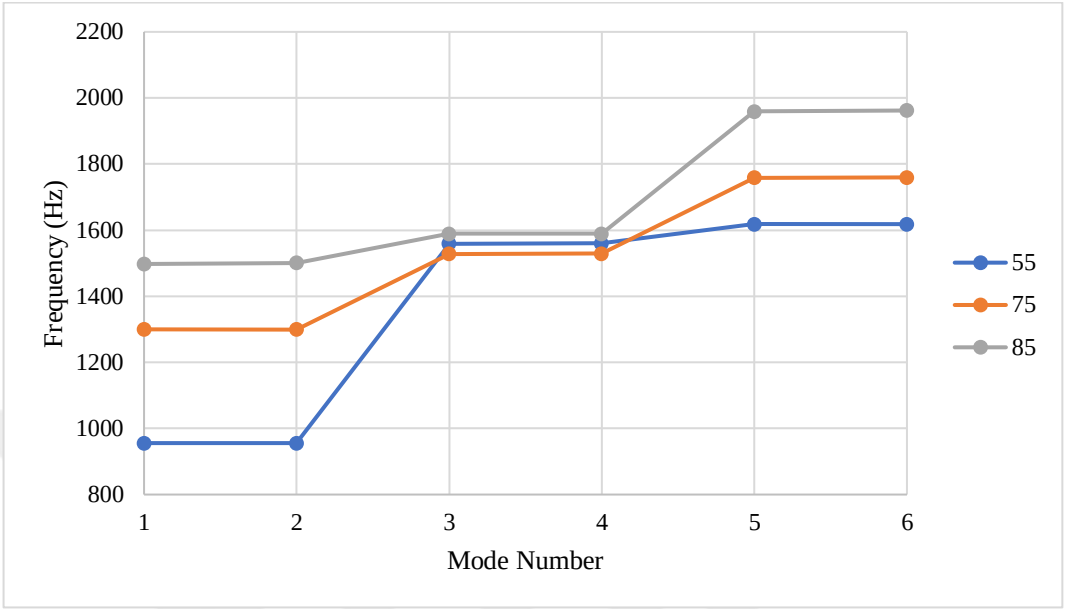

Figure 6.16 The differences in the first six natural frequencies for all degrees filaments wound without pressure

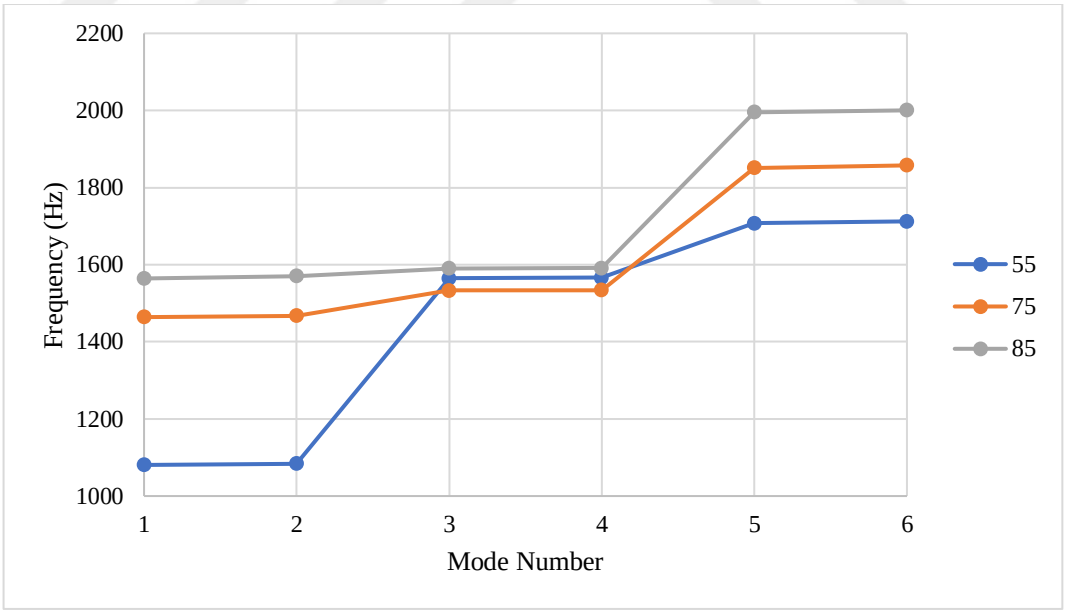

Figure 6.17 The differences in the first six natural frequencies for all degrees filaments wound with pressure

Composite pressure vessels produced at 85 degrees, which have the advantage of angular orientation when all thicknesses are equal, had the highest natural frequency.

The natural frequencies of composite pressure vessels wound at 55 degrees and pressurized at 2 MPa are lower than those of other angle orientations. Under pressure, due to the angular orientation disadvantage, it showed the greatest decrease in the natural frequency values.

Table 6.5 Vibration analysis results of the pressure vessel having 55- degrees filaments wound and layer thickness of 1.33 mm

Mode Number	Free Vibration (Hz)	Under 2MPa Pressure (Hz)
1	1244,6	1407,24
2	1244,6	1411,85
3	1599,8	1604,63
4	1600,1	1606,87
5	1771	1868,86
6	1771,2	1874,16

In Figure 6.18, and Figure 6.19 show the first six natural frequencies of the vessel with 55 degrees filament wound and 1.33 mm layer thickness.

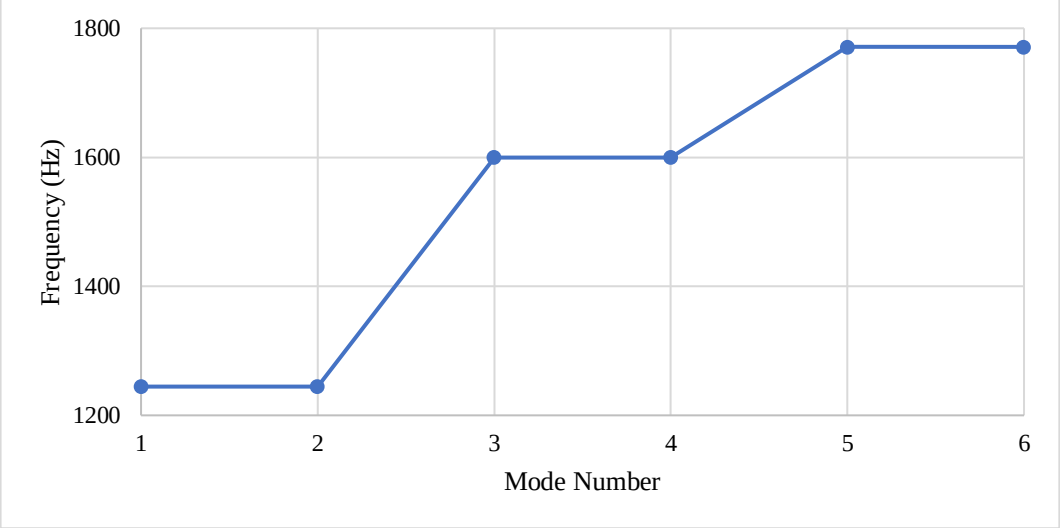

Figure 6.18 Natural frequencies for 55 degrees without pressure

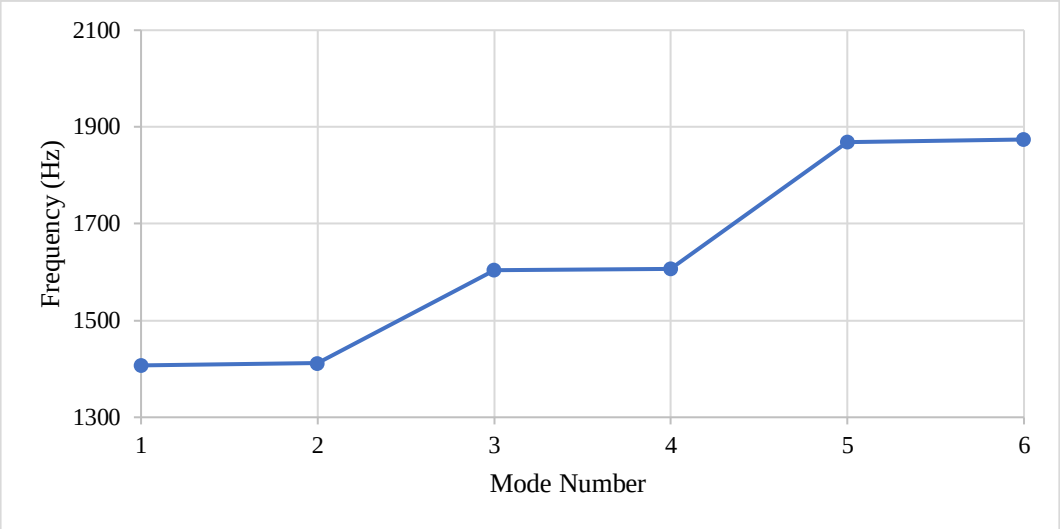

Figure 6.19 Natural frequencies for 55 degrees with pressure

The first six natural frequencies for pressurized at 2 MPa composite pressure vessels were higher than the first six natural frequencies for unpressurized pressure vessels wound at 55 degrees.

In Figure 6.20 and Figure 6.21 show the first six mode shapes of the non-pressurized and pressurized pressure vessel with 55 degrees filament wound and 1.33 mm layer thickness.

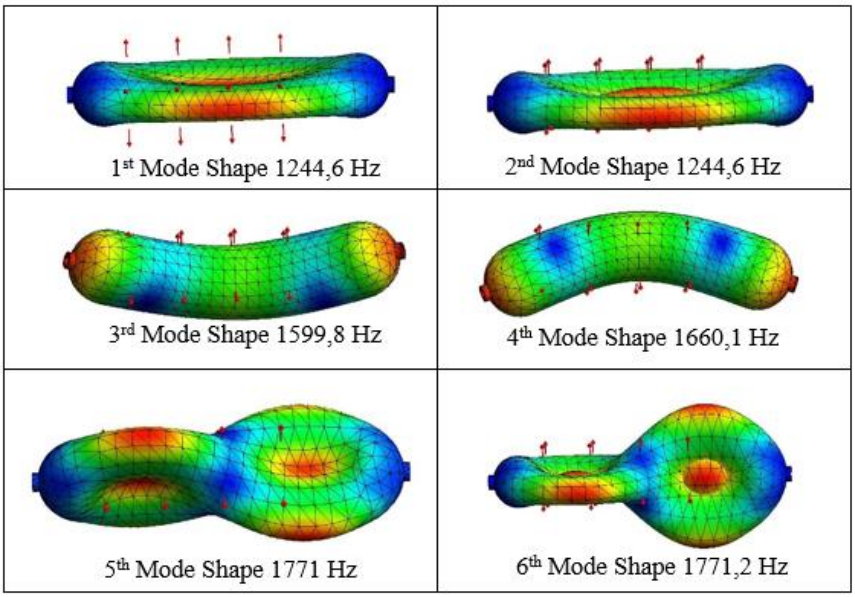

Figure 6.20 The first six mode shapes of the non-pressurized pressure vessel with 55 degrees filaments wound

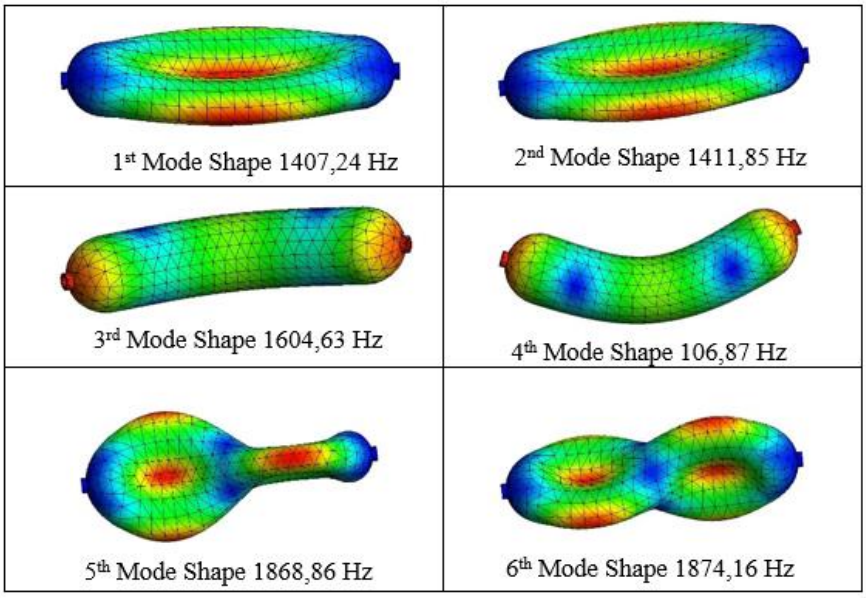

Figure 6.21 The first six mode shapes of the pressurized pressure vessel with 55 degrees filament wound

Table 6.6 Vibration analysis results of the pressure vessel having 75- degrees filaments wound and layer thickness of 1 mm

Mode Number	Free Vibration (Hz)	Under 2MPa Pressure (Hz)
1	1299,9	1464,05
2	1300	1467,39
3	1527,7	1532,81
4	1529,2	1534,31
5	1758,3	1851,25
6	1759,7	1857,62

In Figure 6.22, and Figure 6.23 show the first six natural frequencies of the vessel with 75 degrees filament wound and 1mm layer thickness.

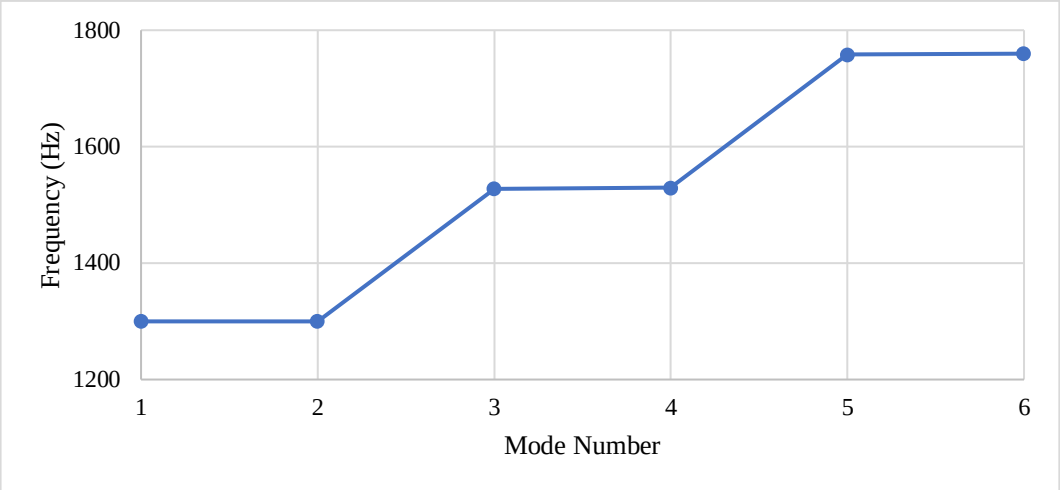

Figure 6.22 Natural frequencies for 75 degrees without pressure

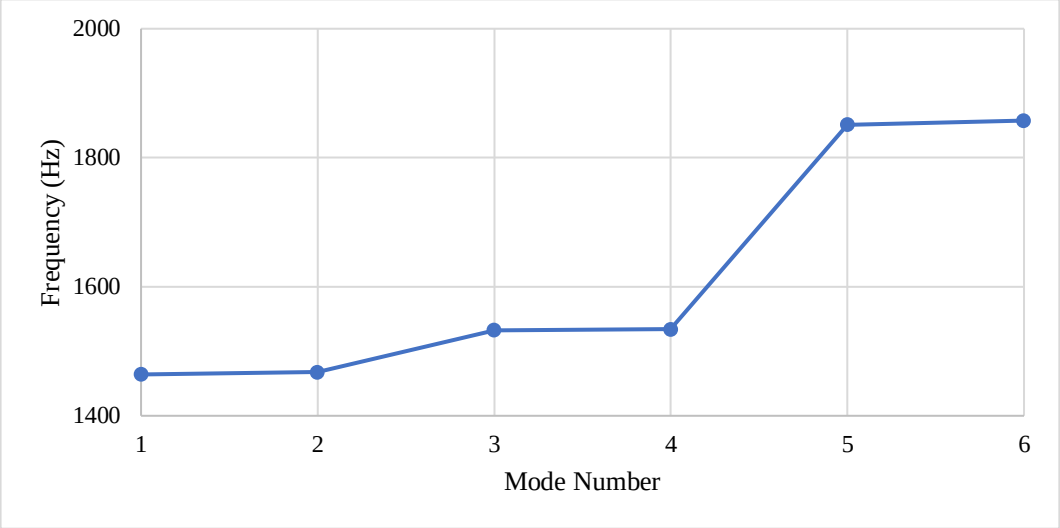

Figure 6.23 Natural frequencies for 75 degrees with pressure

The first six natural frequencies for pressurized composite pressure vessels at 2 MPa were higher than the first six natural frequencies for unpressurized pressure vessels wound at 75 degrees.

In Figure 6.24 and Figure 6.25 show the first six mode shapes of the non-pressurized and pressurized pressure vessel with 75 degrees filament wound and 1 mm layer thickness.

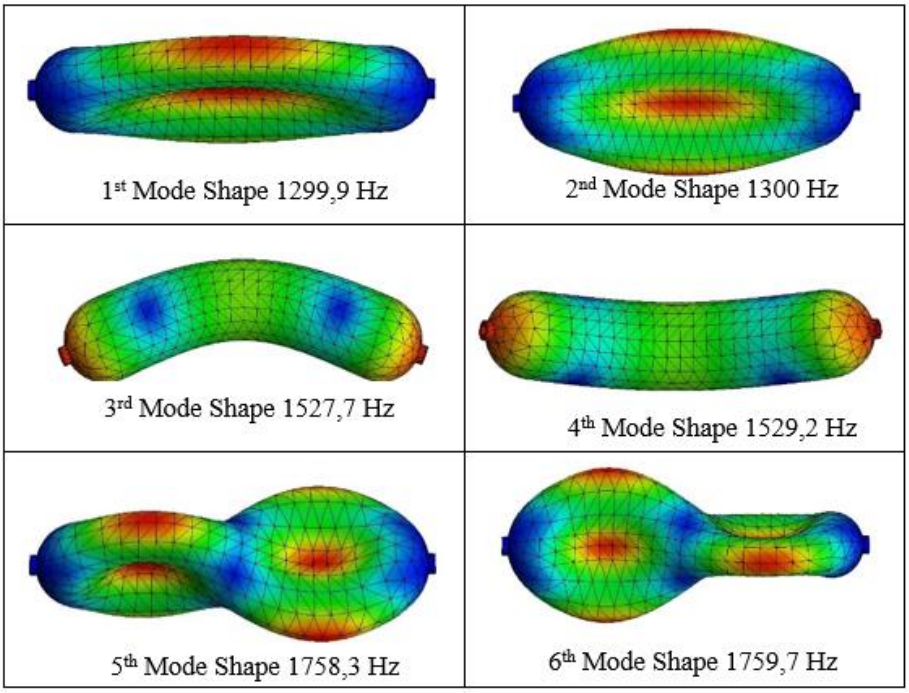

Figure 6.24 The first six mode shapes of the non-pressurized pressure vessel with 75 degrees filament wound

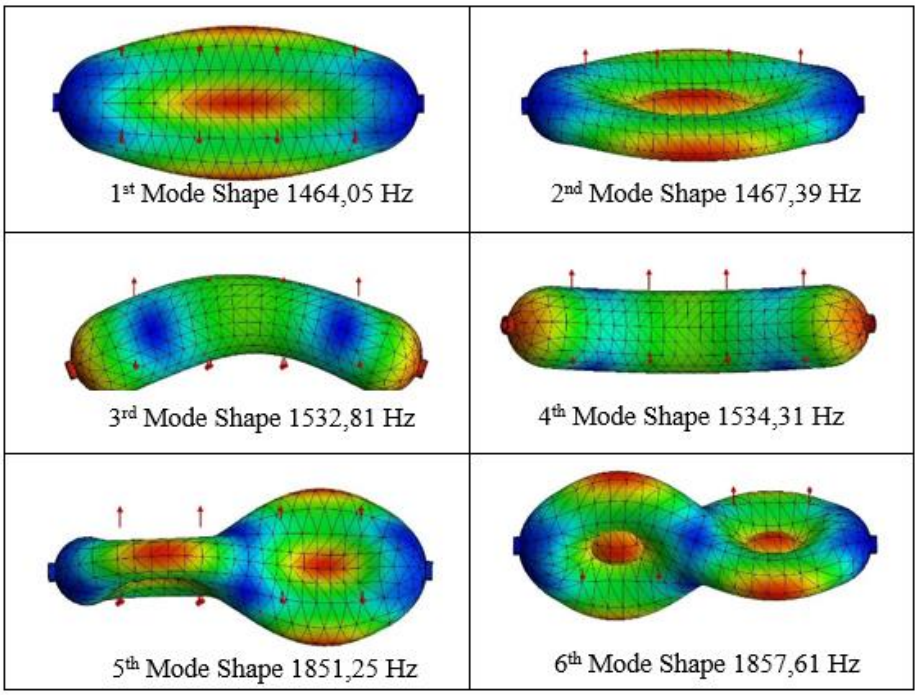

Figure 6.25 The first six mode shapes of the pressurized pressure vessel with 75 degrees filament wound

Table 6.7 Vibration analysis results of the pressure vessel having 85- degrees filament wound and layer thickness of 0.66 mm

Mode Number	Free Vibration (Hz)	Under 2MPa Pressure (Hz)
1	1070	1212,24
2	1070,3	1214,32
3	1515,9	1571,61
4	1519,6	1572,29
5	1557,6	1572,08
6	1559,9	1579,96

In Figure 6.26, and Figure 6.27 show the first six natural frequencies of the vessel with 85 degrees filament wound and 0.66 mm layer thickness.

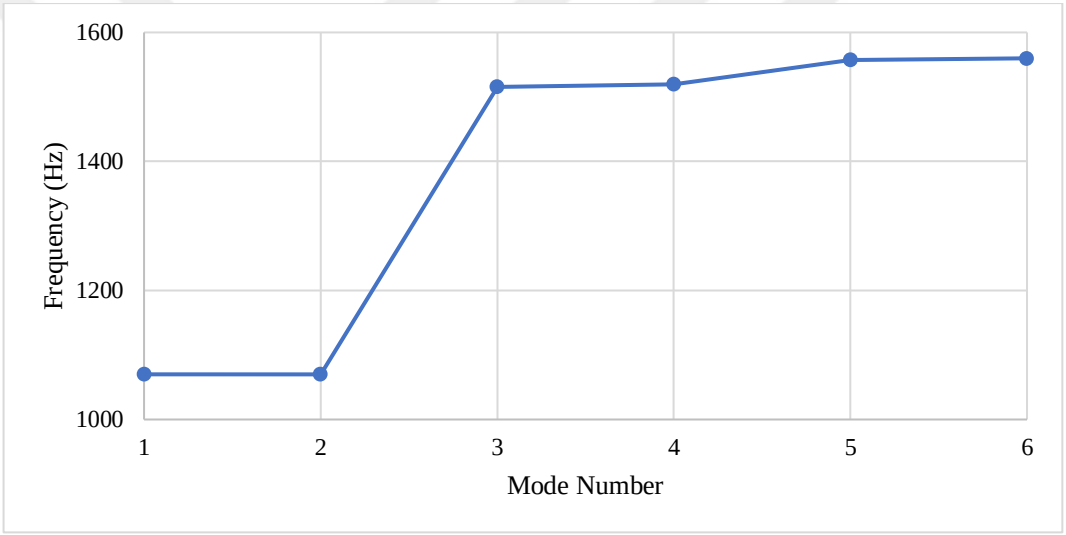

Figure 6.26 Natural frequencies for 85 degrees without pressure

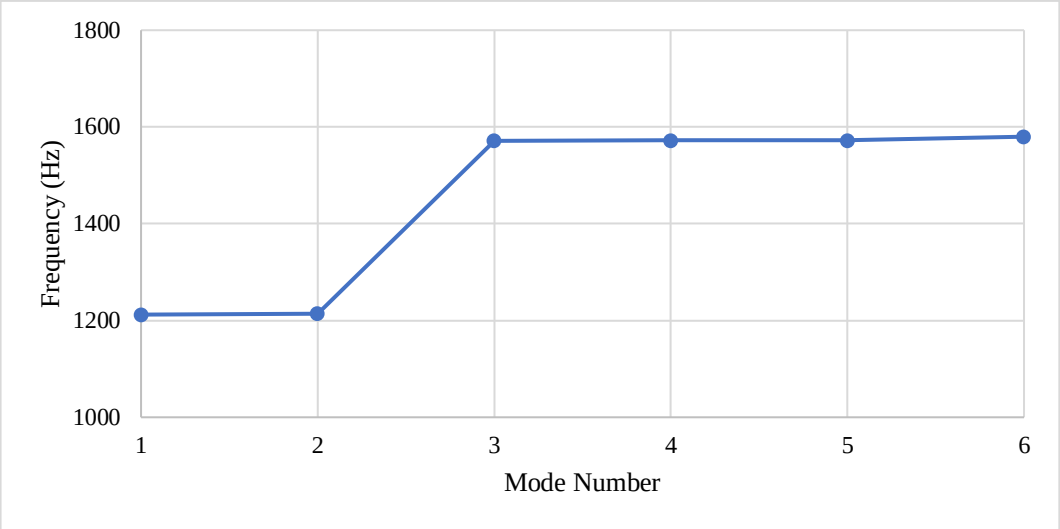

Figure 6.27 Natural frequencies for 85 degrees with pressure

The first six natural frequencies for pressurized composite pressure vessels at 2 MPa were higher than the first six natural frequencies for unpressurized pressure vessels wound at 85 degrees.

In Figure 6.28 and Figure 6.29 show the first six mode shapes of the non-pressurized and pressurized pressure vessel with 85 degrees filament wound and 0.66 mm layer thickness.

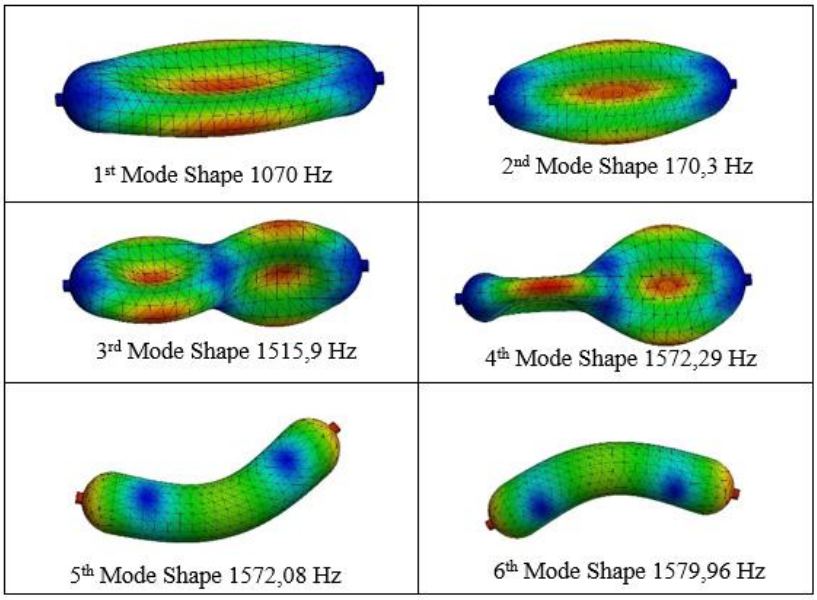

Figure 6.28 The first six mode shapes of the non-pressurized pressure vessel with 85 degrees filament wound

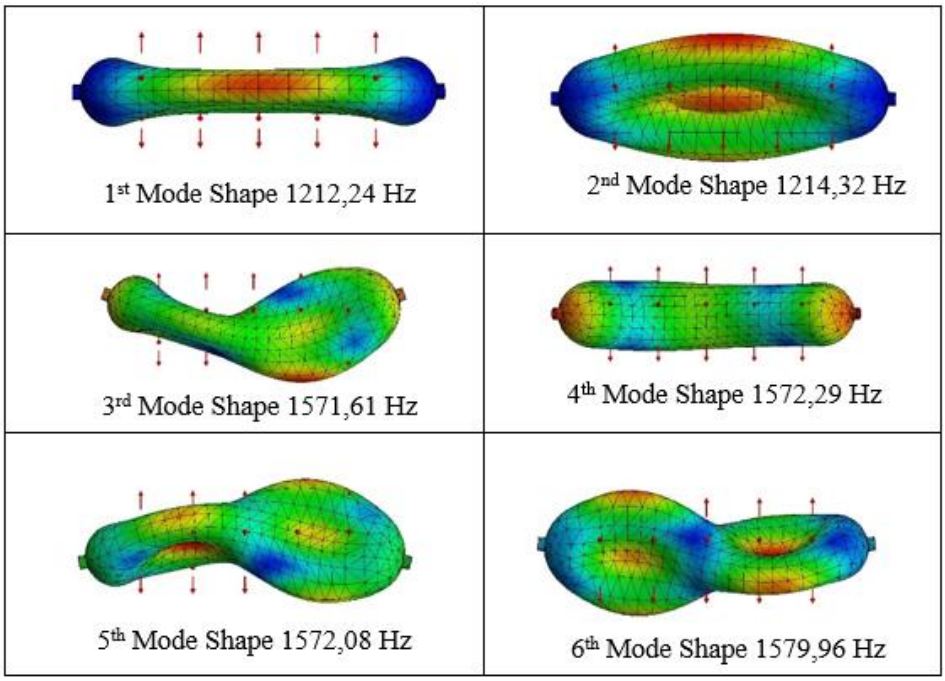

Figure 6.29 The first six mode shapes of the pressurized pressure vessel with 85 degrees filament wound

In Figure 6.30 shows the differences in the first six natural frequencies for all wounding angles without pressure and Figure 6.31 shows The differences in the first six natural frequencies for all degrees filaments wound with pressure.

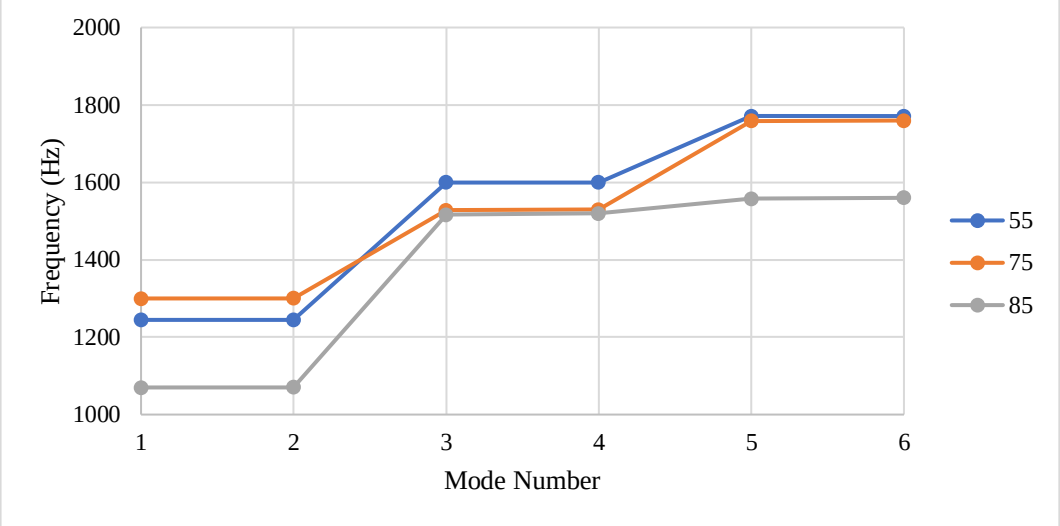

Figure 6.30 The differences in the first six natural frequencies for all degrees filaments wound without pressure

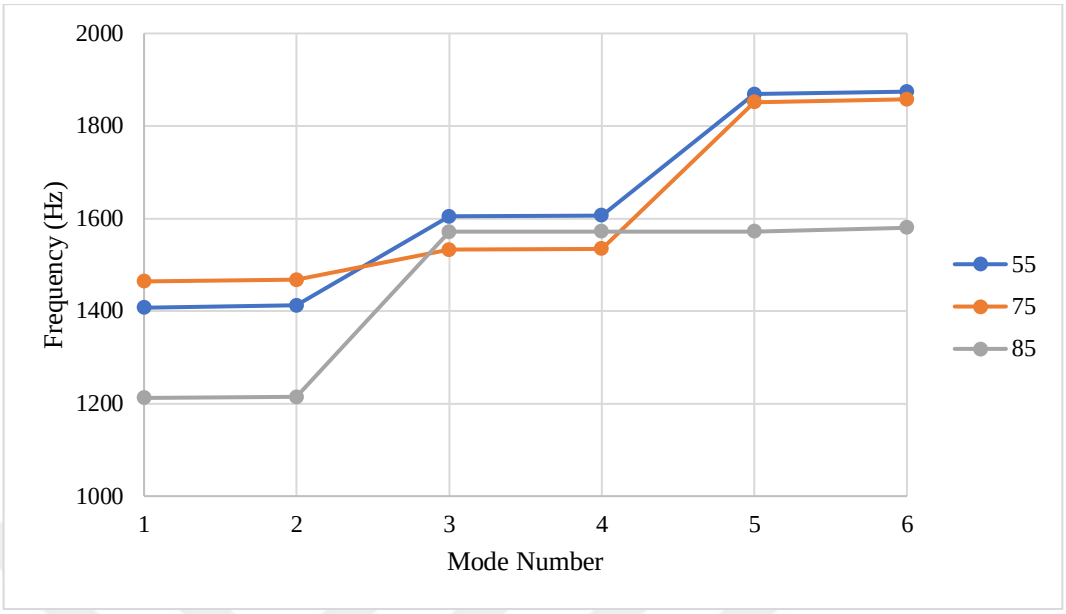

Figure 6.31 The differences in the first six natural frequencies for all degrees filaments wound with pressure

While the composite pressure vessels produced at 75 degrees at the first six natural frequencies have the highest natural frequency in pressure vessels under pressure, the composite pressure vessels produced at 85 degrees without pressure have the lowest natural frequency at the first six natural frequencies. Since the layer thickness of the vessel at 55 degrees is higher than the other angles, it is the angle for which the highest third, fourth, fifth, and sixth natural frequencies are obtained. But the second and third natural frequencies are increased for a 55- degrees filament wound.

CHAPTER SEVEN
CONCLUSION

In this study, the impact of curing temperature, delamination and winding angle on the natural frequencies and damping ratios of cylindrical FRP composites are investigated experimentally. Samples were produced using the reference curing temperature, as well as higher, and lower temperatures. Additionally, delamination is a common production issue what the layers do not adhere to each other. Samples were designed to include delamination factor in combination with the curing temperature. Together with the effect of different laying angles during production was also assessed.

When the samples are evaluated in terms of the effect of temperature, the products produced at 75 degrees and 55 degrees filaments wound show similar characteristics. The natural frequencies of the products cured at 90°C and 120°C are high and close to each other. The products were cured at 140°C, which is considered as a high temperature of natural frequency decrease. The products produced at 85 degrees filaments wound, curing at 90°C and 140°C give the approximately same natural frequency.

According to the ANSYS results, while the winding angles giving the highest natural frequency at the same layer thickness are 85, 75 and 55 respectively from the highest to the lowest. The increase in the winding angle causes increase the rigidity and the natural frequency of the material. The filament winding method creates different layer thicknesses for different angles, the outer diameters of the samples are different from each other for the samples wound at 85, 75 and 55 degrees. Each sample was produced in an equal number of layers to observe the effect of delamination. Therefore, the mass of specimens wound at 55 degrees is 1.5 times that of those wound at 85 degrees. In this case, the effect of the increase in mass on the natural frequencies are greater than the effect of the increase in the winding angle. However, this situation affected the damping ratio in the opposite way. Samples with the highest weight wound at 55 degrees have the highest damping ratio. Samples

wound at 75 degrees have the highest natural frequency by taking advantage of both thickness and winding angle.

Analysis for pressure vessels, is made for the different layer thicknesses condition in which the angles are formed by the filament winding method and considering a same layer thickness condition. The natural frequency is highest when the samples are wound at 85 degrees and have an equal layer thickness. For the different layer thicknesses condition the natural frequency is highest when the samples are wound at 75 degrees. The natural frequency of FRP composite pressure vessels increases as the pressure increases.

Delamination affected natural frequencies and damping ratios negatively. The existence of delamination natural frequencies is getting decreasing. The occurrence of delamination near the edges of the structure decreases the natural frequency more than that located in the middle parts.

Mode shape results from free-free and fixed-free boundary conditions were also examined separately and their compatibility with both the literature and ANSYS program outputs is observed. Due to the cylindrical shape of the samples, the natural frequencies result of free vibration test with free-free boundary conditions are higher than the fixed-free boundary conditions.

Regarding all the pressurized and non-pressurized vessels, the first-second and the third-fourth mode shapes are identical to each other. This phenomenon may be grounded in the free-free boundary conditions and the symmetrical shape of the structure. According to the analysis results, the structure vibrates in a surface-wise bending mode in the first two modes. In the next two modes, a different kind of bending mode is observed where the entire structure is subjected to bending, unlike in the first two modes. The vibration behavior of the vessel in the fifth and sixth are related to torsion. Although the displacement behaviors of those modes look similar to each other, they distinguish each other by having different torsion angles.

Damping ratio is calculated by using the logarithmic decrement method. The presence of delamination contributes to the damping ratio as it creates an atomic scale friction surface. Delamination at the open end of the samples also contributed to a higher damping ratio than the delamination in the middle. According to the temperature and winding angle, the damping ratio results of a sample is similar to the natural frequency results characteristic. Additionally, the damping ratio increased with the increase in the mass. The effect of increasing the mass is more dominant than the effect of increasing the winding angle. While choosing a product with a high damping ratio the mass will be the determining factor in the selection.

In this study, the mass criterion will be the determining factor in the selection of the winding angle for the products to be produced by the filament winding method. In the case where the natural frequency is desired to be high, keeping the winding angle decrease will increase the natural frequency with the increase in weight, and increasing the winding angle will cause a decrease in the natural frequency, although it will reduce the mass. As the winding angle and mass are important parameters, it is recommended to optimize the structure according to the operating and usage conditions.

Overall, the numerical, and experimental analysis results showed that the natural frequency of the composite material was affected by several variables, such as the curing temperature, delamination, degrees of filaments wound, and layer thickness.

For future studies, it will be more appropriate to perform tests on products with equal sample sizes to observe the effect of temperature. As seen in this study, the decrease in layer thickness may deteriorate the chemical structure of the polymer, the relationship between them can be evaluated by choosing the degrees with a high layer thickness. On the other hand, since only glass-fiber was used as the material in this study, carbon fiber, and aramid fiber can be used in future studies and can be examined and compared. In addition to boundary conditions, a fixed-fixed boundary condition can be used.

REFERENCES

Abdalla, F. H., Mutasher, S. A., Khalid, Y. A., Sapuan, S. M., Hamouda, A. M. S., Sahari, B. B., & Hamdan, M. M. (2007). Design, and fabrication of low-cost filament winding machine. *Materials & design*, 28(1), 234-239.

Abdurohman, K., Satrio, T., & Muzayadah, N. L. (2018, November). A comparison process between h, and lay-up, vacuum infusion, and vacuum bagging method toward e-glass EW 185/lycal composites. *In Journal of Physics: Conference Series* (Vol. 1130, No. 1, p. 012018). IOP Publishing.

Advani, S. G., & Sozer, E. M. (2002). *Process modeling in composites manufacturing*. CRC press.

Al-Salloum, Y. A., Elsanadedy, H. M., & Abadel, A. A. (2011). Behavior of FRP-confined concrete after high temperature exposure. *Construction, and Building Materials*, 25(2), 838-850.

Badawy, A. A. (2012). Impact behavior of glass fibers reinforced composite laminates at different temperatures. *Ain Shams Engineering Journal*, 3(2), 105-111.

Barbero, E. J. (2017). *Introduction to composite materials design*. CRC press.

Di Boon, Y., Joshi, S. C., & Bhudolia, S. K. (2021). Filament Winding and Automated Fiber Placement with In Situ Consolidation for Fiber Reinforced Thermoplastic Polymer Composites. *Polymers*, 13(12).

Bazli, M., & Abolfazli, M. (2020). Mechanical properties of fibre reinforced polymers under elevated temperatures: An overview. *Polymers*, 12(11), 2600.

Brennan, A. J., Thusyanthan, N. I., & Madabhushi, S. P. (2005). Evaluation of shear modulus and damping in dynamic centrifuge tests. *Journal of Geotechnical and Geoenvironmental Engineering,* 131(12), 1488-1497.

Campanelli, R. W., & Engblom, J. J. (1995). The effect of aminations in graphite/PEEK composite plates on modal dynamic characteristics. *Composite structures,* 31(3), 195-202.

Campbell, F. C. (2010). *Structural composite materials*. ASM international.

Carlone, P., & Palazzo, G. S. (2015). Unsaturated and saturated flow front tracking in liquid composite molding processes using dielectric sensors. *Applied Composite Materials,* 22(5), 543-557.

Chaowasakoo, T., & Sombatsompop, N. (2007). Mechanical and morphological properties of fly ash/epoxy composites using conventional thermal and microwave curing methods. *Composites science and technology,* 67(11-12), 2282-2291.

Chowdhury, E. U., Eedson, R., Bisby, L. A., Green, M. F., & Benichou, N. (2011). Mechanical characterization of fibre reinforced polymers materials at high temperature. *Fire technology,* 47(4), 1063-1080.

Costa, M. L., Rezende, M. C., & De Almeida, S. F. M. (2006). Effect of void content on the moisture absorption in polymeric composites. *Polymer-Plastics Technology and Engineering,* 45(6), 691-698.

Czaderski, C., Martinelli, E., Michels, J., & Motavalli, M. (2012). Effect of curing conditions on strength development in an epoxy resin for structural strengthening. *Composites Part B: Engineering,* 43(2), 398-410.

Fiore, V., & Valenza, A. (2013). Epoxy resins as a matrix material in advanced fiber-reinforced polymer (FRP) composites. *In Advanced Fibre-Reinforced Polymer (FRP) Composites for Structural Applications* (pp. 88-121). Woodhead Publishing.

Fotsing, E. R., Sola, M., Ross, A., & Ruiz, E. (2013). Lightweight damping of composite sandwich beams: Experimental analysis. *Journal of Composite Materials,* 47(12), 1501-1511.

Furtos, G., Silaghi-Dumitrescu, L., Moldovan, M., Baldea, B., Trusca, R., & Prejmerean, C. (2012). Influence of filler/reinforcing agent, and post-curing on the flexural properties of woven, and unidirectional glass fiber-reinforced composites. *Journal of Materials Science,* 47(7), 3305-3314.

Gadelrab, R. M. (1996). The effect of delamination on the natural frequencies of a laminated composite beam. *Journal of Sound, and Vibration,* 197(3), 283-292.

Ghoneam, S. M., Hamada, A. A., & El-Elamy, M. I. (2011, May). Dynamic analysis of a rotating composite shaft. In *International Conference on Aerospace Sciences and Aviation Technology* (Vol. 14, No. AEROSPACE SCIENCES & AVIATION TECHNOLOGY, ASAT-14–May 24-26, 2011, pp. 1-16). The Military Technical College.

Hamed, A. F., Khalid, Y. A., Sapuan, S. M., Hamdan, M. M., Younis, T. S., & Sahari, B. B. (2007). Effects of winding angles on the strength of filament wound composite tubes subjected to different loading modes. *Polymers, and Polymer Composites,* 15(3), 199-206.

He, Y., Xiao, Y., & Su, Z. (2019). Effects of surface contact on the dynamic responses of delaminated composite plates. *Composite Structures,* 229, 111378.

Hu, H. T., & Tsai, J. Y. (1999). Maximization of the fundamental frequencies of laminated cylindrical shells with respect to fiber orientations. *Journal of sound, and vibration*, 225(4), 723-740.

Huang, Y., Wang, T., Zhao, Y., & Wang, P. (2018). Effect of axially functionally graded material on whirling frequencies and critical speeds of a spinning Timoshenko beam. *Composite Structures,* 192, 355-367.

Kaw, A. K. (2005). *Mechanics of composite materials.* CRC press.

Kim, J., Palazzolo, A., & Gadangi, R. (1993). Dynamic Characteristics of TEHD Tilt Pad Journal Bearing Simulation Including Multiple Mode Pad Flexibility Model. *Journal of Vibration and Acoustics.*

Koushyar, H., Alavi-Soltani, S., Minaie, B., & Violette, M. (2012). Effects of variation in autoclave pressure, temperature, and vacuum-application time on porosity and mechanical properties of a carbon fiber/epoxy composite. *Journal of Composite Materials*, 46(16), 1985-2004.

Landesmann, A., Seruti, C. A., & Batista, E. D. M. (2015). Mechanical properties of glass fiber reinforced polymers members for structural applications. *Materials Research*, 18, 1372-1383.

Maxineasa, S. G., & Taranu, N. (2018). Life cycle analysis of strengthening concrete beams with FRP. In Eco-efficient Repair, and Rehabilitation of Concrete Infrastructures (pp. 673-721). Woodhead Publishing.

Munzke, D., Duffner, E., Eisermann, R., Schukar, M., Schoppa, A., Szczepaniak, M., & Mair, G. (2021). Monitoring of type IV composite pressure vessels with multilayer fully integrated optical fiber based distributed strain sensing. *Materials Today: Proceedings*, 34, 217-223.

Nele, L., Caggiano, A., & Teti, R. (2016). Autoclave cycle optimization for high performance composite parts manufacturing. *Procedia CIRP*, 57, 241-246.

Nguyen-Dinh, N., Zitoune, R., Bouvet, C., & Leroux, S. (2019). Surface integrity while trimming of composite structures: X-ray tomography analysis. *Composite Structures*, 210, 735-746.

Park, S. J., & Seo, M. K. (2011). *Interface science, and composites* (Vol. 18). Academic Press.

Peters, S. T. (Ed.). (2011). *Composite filament winding*. ASM International.

Reddy, J. N. (2003). *Mechanics of laminated composite plates and shells: theory and analysis.* CRC press.

Quanjin, M., Rejab, M. R. M., Kaige, J., Idris, M. S., & Harith, M. N. (2018, April). Filament winding technique, experiment and simulation analysis on tubular structure. In *IOP conference series: materials science and engineering* (Vol. 342, No. 1, p. 012029). IOP Publishing.

Rittweger, J., & Taiar, R. (2020). The physics of vibration. In *Manual of Vibration Exercise, and Vibration Therapy* (pp. 3-21). Springer, Cham.

Russo, S., Ghadimi, B., Lawania, K., & Rosano, M. (2016). Failure analysis using acoustic and energy emission assessment of fibre reinforced polymer material performance under severe conditions. *Journal of Reinforced Plastics and Composites.* https://doi.org/10.1177/0731684416638552.

Rosenow, M. W. K. (1984). Wind angle effects in glass fibre-reinforced polyester filament wound pipes. *Composites*, 15(2), 144-152.

Singh, J., Singh, S., & Dhawan, V. (2018). Effect of Curing Temperature on Mechanical Properties of Natural Fiber Reinforced Polymer Composites. *Journal of Natural Fibers*. https://doi.org/10.1080/15440478.2017.1354744.

Soden, P. D., Kitching, R., Tse, P. C., Tsavalas, Y., & Hinton, M. J. (1993). Influence of winding angle on the strength, and deformation of filament-wound composite tubes subjected to uniaxial, and biaxial loads. *Composites Science, and Technology,* 46(4), 363-378.

Thomsen, J. J., & Thomsen, J. J. (2003). Chaotic Vibrations. *Vibrations and Stability: Advanced Theory, Analysis, and Tools*, 225-286.

Thomson, W. T. (2018). *Theory of vibration with applications.* CrC Press.

Tse, F. S., Morse, I. E., & Hinkle, R. T. (1963). *Mechanical vibrations.* Boston: Allyn, and Bacon.